20 March 2009 | $10

Science

AAAS

EDITORIAL

NEWS OF THE WEEK

NEWS FOCUS

LETTERS

BOOKS *ET AL.*

POLICY FORUM

PERSPECTIVES

BREVIA

CONTENTS continued >>

page 1554 & 1578

page 1562

COVER

Movement trajectories, each recorded during a 1-hour time period, for rats with brain lesions that reduce dopamine signaling. These animals serve as a model of Parkinson's disease and display severe difficulty in initiating movements, as illustrated by the white trajectories (on black background) showing limited locomotion. Black trajectories (on white background) illustrate the recovery of locomotive activity induced by electrical stimulation of the dorsal columns of the spinal cord. See page 1578.

Photo illustration: Yael Kats/Science; images: Per Petersson

DEPARTMENTS

Published by AAAS

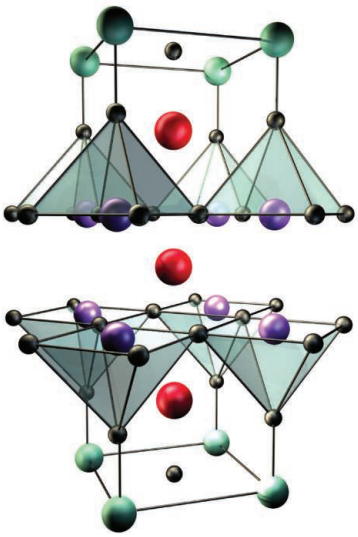

page 1570 & 1585

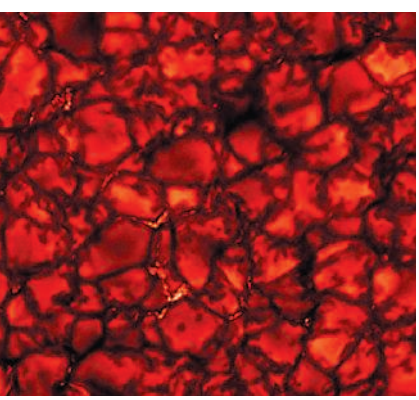

pages 1551 & 1582

pages 1550 & 1607

RESEARCH ARTICLES

REPORTS

Published by AAAS

SCIENCEONLINE

SCIENCEXPRESS
www.sciencexpress.org

The Disappearance of the Progenitors of Supernovae 1993J and 2003gd
J. R. Maund and S. J. Smartt

The presumed progenitor stars of supernovae are indeed absent in later images from these sites.
10.1126/science.1170198

Optical Deconstruction of Parkinsonian Neural Circuitry
V. Gradinaru et al.

The therapeutic effects of high-frequency stimulation of the subthalamic nucleus result from direct effects on afferent axons.
10.1126/science.1167093
>> *News story p. 1554; Research Article p. 1578*

Circadian Clock Feedback Cycle Through NAMPT-Mediated NAD^+ Biosynthesis
K. M. Ramsey et al.

A transcriptional-enzymatic feedback loop controls interactions between metabolism and circadian rhythms in mouse cells.
10.1126/science.1171641

γ-Secretase Heterogeneity in the Aph1 Subunit: Relevance for Alzheimer's Disease
L. Serneels et al.

Targeted knockout of only part of the γ-secretase complex lessens toxicity and still improves disease phenotypes.
10.1126/science.1171176

Benzothiazinones Kill *Mycobacterium tuberculosis* by Blocking Arabinan Synthesis
V. Makarov et al.

An enzyme required for cell-wall synthesis is a target for a possible alternative drug for tuberculosis treatment.
10.1126/science.1171583

SCIENCENOW
www.sciencenow.org
Highlights From Our Daily News Coverage

Southpaw Solar System
Meteorites might have seeded early Earth with 'left-handed' amino acids.

Oxygenated Oceans Go Way, Way Back
Seabed mineral suggests a much earlier start for photosynthesis.

A Hitch in Plans for 'Sunshade Earth'
Dusting the skies could help with global warming but harm solar power.

SCIENCESIGNALING
www.sciencesignaling.org
The Signal Transduction Knowledge Environment

RESEARCH ARTICLE: Obesity Increases Vascular Senescence and Susceptibility to Ischemic Injury Through Chronic Activation of Akt and mTOR
C.-Y. Wang et al.

Chronic activation of Akt and mammalian target of rapamycin (mTOR) link diet-induced obesity with cardiovascular disease.

PERSPECTIVE: Bacterial FIC Proteins AMP Up Infection
C. R. Roy and S. Mukherjee

A bacterial protein posttranslationally modifies and inactivates Rho family GTPases in host cells.

TEACHING RESOURCE: Measurement of Phosphorylated Extracellular Signal–Regulated Kinase 1 and 2 in an Undergraduate Teaching Laboratory with ALPHAscreen Technology
D. L. Hay

Students use a high-throughput assay to monitor cellular responses to receptor activation.

SCIENCECAREERS
www.sciencecareers.org/career_magazine
Free Career Resources for Scientists

Bringing Community Into Translational Research
S. Webb

Translational social scientists carry the lessons they learn in the community back to the lab.

Looking Up Your Career at the Library
L. Laursen

The work of a science librarian offers a mix of research, teaching, and interacting with people.

Tooling Up: The Informational Interview
D. Jensen

Landing an informational interview takes networking; making it pay off takes preparation.

SCIENCEPODCAST
www.sciencemag.org/multimedia/podcast
Free Weekly Show

Download the 20 March *Science* Podcast to hear about how the Sun's corona gets so hot, the power of neighborly advice, deep brain stimulation, and more.

ORIGINSBLOG
blogs.sciencemag.org/origins
A History of Beginnings

SCIENCEINSIDER
blogs.sciencemag.org/scienceinsider
Science Policy News and Analysis

SCIENCENOW
Dimmer future?

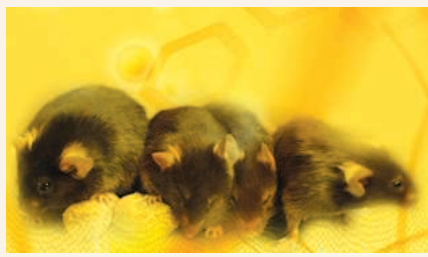

SCIENCESIGNALING
Obese mice have heart conditions.

SCIENCECAREERS
Careers for science librarians.

SCIENCE (ISSN 0036-8075) is published weekly on Friday, except the last week in December, by the American Association for the Advancement of Science, 1200 New York Avenue, NW, Washington, DC 20005. Periodicals Mail postage (publication No. 484460) paid at Washington, DC, and additional mailing offices. Domestic individual membership and subscription (51 issues): $146 ($74 allocated to subscription). Domestic institutional subscription (51 issues): $835; Foreign postage extra: Mexico, Caribbean (surface mail) $55; other countries (air assist delivery) $85. First class, airmail, student, and emeritus rates on request. Canadian rates with GST available upon request, GST #1254 88122. Publications Mail Agreement Number 1069624. **Printed in the U.S.A.**

Change of address: Allow 4 weeks, giving old and new addresses and 8-digit account number. **Postmaster:** Send change of address to AAAS, P.O. Box 96178, Washington, DC 20090–6178. **Single-copy sales:** $10.00 current issue, $15.00 back issue prepaid includes surface postage; bulk rates on request. The identification code for *Science* is 0036-8075. *Science* is indexed in the *Reader's Guide to Periodical Literature* and in several specialized indexes.

AAAS
ADVANCING SCIENCE, SERVING SOCIETY

Hello to *Hurdia* >>

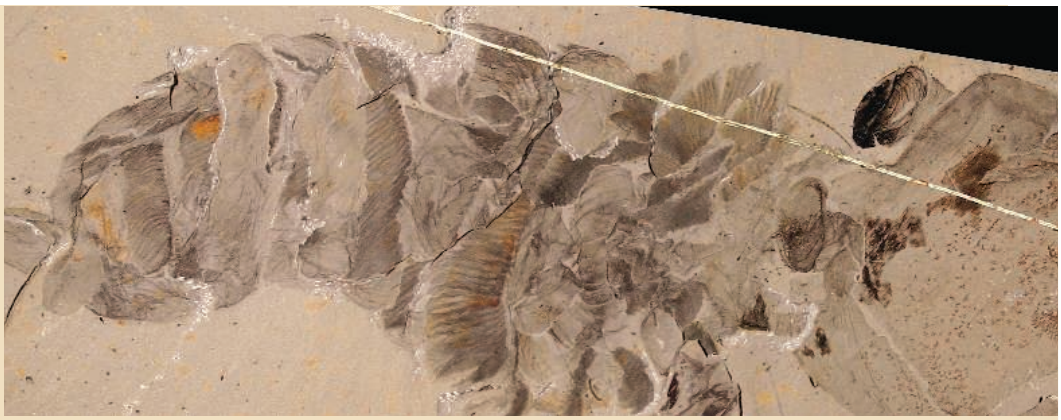

Anomalocaridids are among the most famous of all Cambrian organisms, and have been dubbed the "*T. rex* of the Cambrian" because of their large size and inferred predatory habits. *Hurdia*, described by **Daley *et al.*** (p. 1597), is the most common anomalocaridid in the Burgess Shale fossil beds in Canada. *Hurdia* has recently attracted interest because of its significance in arthropod evolution, yet it has remained effectively unknown because its fossil remains were misattributed among several other genera. *Hurdia,* with its unique and remarkable frontal carapace, provides critical new data on the gill structure of stem-group arthropods with a direct bearing on the recent debate about arthropod limb evolution.

Making Muscles Out of Materials

New materials are being investigated that can convert electrical, chemical, thermal, or photonic energy into mechanical energy. **Aliev *et al.*** p. 1575; see the Perspective by **Madden**) described the mechanical properties and electrostatic actuation of very low density multiwalled carbon nanotube sheets formed into aerogels. By electrostatically charging the sheets, a large expansion occurred in the direction perpendicular to the nanotube orientation, and a smaller contraction occurred parallel to the stretch direction. This work points the way to developing novel materials with highly directional mechanical properties.

Two-in-One Antibody

Textbook definitions of antibodies emphasize the exquisite specificity with which these proteins bind their target antigens. New research suggests that this "one antibody–one antigen" paradigm can be tweaked in the laboratory. Working with an engineered library of variants of Herceptin, a therapeutic monoclonal antibody targeting the breast cancer growth factor HER2, **Bostrom *et al.*** (p. 1610; see Perspective by **Parren and Burton**) successfully selected variants which had antibody-combining sites that simultaneously bound with high affinity to a second cancer-relevant antigen, vascular endothelial growth factor (VEGF). In preliminary assays of efficacy, the two-in-one antibodies inhibited HER2- and VEGF-mediated cell proliferation in vitro, as well as tumor growth in mice, thus indicating the feasibility of a single therapeutic for cancer treatment.

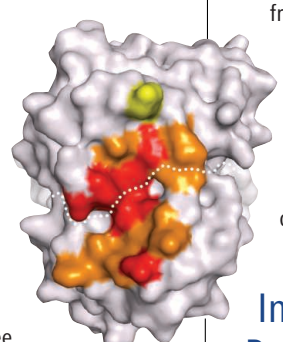

CREDITS (TOP TO BOTTOM): ALLISON C. DALEY; BOSTROM *ET AL.*

Ordered into Superconducting

In unconventional superconductors, such as the cuprates, electrons form Cooper pairs by mechanisms other than electron-phonon coupling. These systems have a high density of defects and are chemically doped, so it can be difficult to observe smooth transitions between the superconductor and the parent electronic state from which they form. **Takabayashi *et al.*** (p. 1585; see the Perspective by **Tosatti**) showed that a particular phase of the alkali fulleride superconductor Cs_3C_{60}, which is well-ordered and exhibits a body-centered cubic symmetry, transformed from a spin-1/2 antiferromagnetic insulator to a superconductor as pressure was applied. The transition was purely electronic, in that no structural changes or disordering occurred. The dependence of the transition temperature on pressure was not accounted for by the standard model for superconductivity.

Improving Parkinson's Treatment

Deep brain stimulation has become a popular procedure for the treatment of motor symptoms in Parkinson's disease. However, it is an invasive surgical technique and people have been trying to find alternative methods that carry less risk. **Fuentes *et al.*** (p. 1578; see the cover; see the news story by **Miller**) tested electrical stimulation of the spinal cord dorsal column as an alternative strategy in animal models of Parkinson's disease. They found that corticostriatal activity patterns preceded voluntary motor actions, which may offer some explanation for the mechanisms underlying volitional movements. Dorsal column stimulation markedly improved motor functions, and enhanced pharmacological treatment in the animals, and looks as if it holds considerable promise for the treatment of Parkinson's disease patients.

Heating the Solar Atmosphere

The temperature of the Sun increases markedly as one moves from its surface to the outer layers of its atmosphere. Types of plasma waves called Alfvén waves, that are hypothesized to be incompressible and driven by magnetic tension, are considered to be the best explanation for how energy is transported through the solar atmosphere, but their unambiguous detection is still in doubt. **Jess *et al.*** (p. 1582; see the news story by **Kerr**) obtained high-resolution images of the Sun and found oscillations that bear the signatures of torsional Alfvén waves and that carry sufficient energy to heat the solar atmosphere.

Meta Addition

Friedel-Crafts reactions are among the oldest adopted in modern organic chemistry and have been used for over a century to attach various atoms around benzene rings and create components of dyes, drugs, and a wide range of functional

Continued on page 1537

Published by AAAS

Continued from page 1535

materials. These reactions install incoming groups on the ring carbons adjacent to or diametrically opposite electron-donating substituents such as amines. Modifying the intermediate (or meta) sites, two carbons away from existing substituents, has been challenging. **Phipps and Gaunt** (p. 1593; see the Perspective by **Maleczka**) discovered a copper catalyst that selectively adds incoming phenyl groups to the meta positions of amide-substituted benzenes. This kind of catalysis opens the way to the development of novel agrochemicals and pharmaceuticals.

Methylation Rescue

Methylation of genomic DNA occurs with high frequency at transposons and repetitive DNA sequences to repress transcription of these potentially damaging genome features. Methylation patterns are normally inherited during cell division as the methylated parental DNA strand provides a template for the methylation of the daughter strand. But sometimes methylation marks are ablated and lost in all subsequent generations. **Teixeira *et al.*** (p. 1600, published online 29 January; see the Perspective by **Law and Jacobsen**) found that *Arabidopsis* recovered methylation marks in a process requiring meiosis and the RNA interference–dependent DNA methylation machinery. After one to three generations, original methylation levels were recovered. This mechanism not only helps to maintain genome stability, but might also permit adaptive responses in epigenetic inheritance.

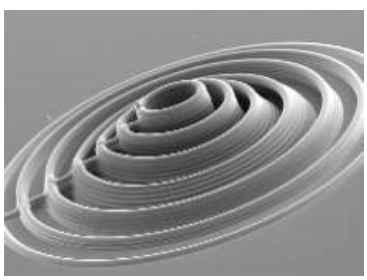

Conducting 3D Printing

One challenge to the development of more robust, flexible, or stretchable electronics is the printing of electrodes within devices and between devices. **Ahn *et al.*** (p. 1590, published online 12 February; see the Perspective by **Gates**) have formulated concentrated silver nanoparticle inks that can be printed in three dimensions. The electrodes are self-supporting and can be patterned in complex ways as planar or 3D forms on a wide variety of substrates. Once sintered at moderate temperatures, the colloidal particles fuse together to make wires with electrical resistivities that approach the value for bulk silver.

Sorting Light Receptors

In the retina, cyclic nucleotide gated (CNG) channels initiate the electrical response to light in the sensory cilia of the rods. The channels are exclusively localized to outer segments of the cilia, but how they are positioned has been largely unknown. Working on *Xenopus*, **Kizhatil *et al.*** (p. 1614) showed that the CNG-β subunit bound to ankyrin-G, a membrane scaffolding protein, is not only required for the post-Golgi transport of CNG channels, but is also required for rod outer segment development. A human mutation in the CNG-β subunit disrupts this targeting mechanism and is associated with retinitis pigmentosa. Similar ankyrin-G–based mechanisms may occur in olfactory cilia, in the sperm flagella, and other sites.

Take My Word for It

On issues of fact, such as whether the bus has just passed, we usually feel comfortable to accept information from a stranger; in situations where emotions are involved we are more likely to rely on our own feelings than what others report. **Gilbert *et al.*** (p. 1617) demonstrated that this confidence may be misplaced. In a speed-dating scenario, women were asked for their subjective evaluations before and after a 5-minute encounter with a single man. The women who had only been supplied with a man's profile and photograph fared significantly worse in predicting their after-the-fact reaction to their date than women who were supplied with an evaluation of a man from their predecessor.

Mother Knows Best

Gouldian finches have two color morphs that tend to mate true. **Pryke and Griffith** (p. 1605) showed that females forced to mate with males of the opposite morph have more sons and invest less effort in rearing them than if allowed to mate with their own type. But if the males are painted to resemble the females' preferred mates, the duped females will readjust their behavior and the sex ratio of the eggs. The results imply that female birds may be altering resource allocation to their female offspring in multiple ways.

CREDIT: AHN *ET AL.*

Published by AAAS

The Enlightenment Returns

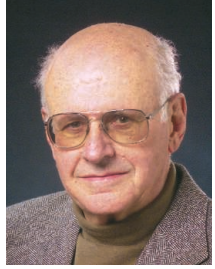

Kurt Gottfried is a cofounder of the Union of Concerned Scientists and chair of its board of directors. He is professor of physics emeritus at Cornell University.

Harold Varmus is president of the Memorial Sloan-Kettering Cancer Center, a cochair of the President's Council of Advisors on Science and Technology, and a former director of the National Institutes of Health.

The authors of the Declaration of Independence and the Constitution of the United States were children of the Enlightenment. They understood the power that flows from combining human reason with empirical knowledge, and they assumed that the political system they were creating would thrive only in a culture that upheld the values of the Enlightenment. And thrive it did, in large part because our people and government upheld those values throughout most of U.S. history. Recently, however, the precepts of the Enlightenment were ignored and even disdained with respect to the manner in which science was used in the nation's governance. Dogma took precedence over evidence, and opinion over facts. Happily, as was made clear by two policy announcements by President Barack Obama on 9 March 2009, the break in the traditionally harmonious relationship between science and government is now ending.

The first announcement, which dealt decisively with a single important and politically volatile issue, the funding of stem cell research, received the most attention. But the second, on scientific integrity, has greater breadth and at least equal significance. For as the president put it, "promoting science isn't just about providing resources—it is also about protecting free and open inquiry . . . free from manipulation or coercion, and listening to what [scientists] tell us, even when it's inconvenient—especially when it's inconvenient." In using the words "manipulation" and "coercion," the president was not speaking purely in the abstract; he was alluding to recent breaches of a code to which government must adhere if science is to play its proper role in advising the government on such complex issues as public health, climate change, or environmental protection. When the government systematically disregards this code, it undermines the historic role of science as a bulwark of an enlightened democracy.

In the president's Memorandum on Scientific Integrity last week, addressed to the heads of all executive departments and agencies, he directed those officials to neither suppress nor alter scientific and technological findings solicited in the process of policy formulation. He also asked that scientific information developed or used by the government be made readily available to the public. To put these directives in place, the president requested the director of the Office of Science and Technology Policy to develop, within 120 days, recommendations "designed to guarantee scientific integrity throughout the executive branch" and to ensure "that scientific data is never distorted or concealed to serve a political agenda."

The recommendations called for to sustain these bold ambitions would place scientific competence and integrity among the core principles of the government's science-based endeavors. For example, they should ensure that the selection of scientists for government positions is based on scientific qualifications and experience, establish means for addressing instances in which scientific integrity may be compromised, and provide protections for those who draw attention to possible assaults on the integrity of scientific advice. The need for these measures derives, in part, from the many well-documented cases in which scientific integrity was recently breached, as when political appointees shut government scientists out of critical decisions that hinged on scientific information, prevented the transmission of scientific reports to Congress, appointed unqualified individuals to scientific panels because of their ideological or political persuasion, or censored government reports dealing with climate change and species extinction.

The U.S. scientific community now has an opportunity to strengthen the president's initiative by informing students, colleagues, and fellow citizens about the issues at stake; by willingly offering professional advice to government either informally or when invited to serve on agency panels; by supporting and encouraging scientists who are considering careers in government; or by taking a turn in government service. The president has taken a large and inspiring step to restore the historically beneficial balance between science and government; we should all now offer to help with the enlightened effort just launched.

– Kurt Gottfried and Harold Varmus

10.1126/science.1173563

Published by AAAS

ECOLOGY

All Washed Up

Toxic algal blooms, or red tides, caused by dinoflagellates pose a danger for humans and many other vertebrates. In November 2007, a late red tide of *Akashiwo sanguinea* in Monterey Bay caused a mass stranding and high mortality of winter visiting seabirds. Jessup *et al.* report that the birds' plumage had become coated in a sticky green froth exuded from the algae that contained surfactant mycosporine-like amino acids, which acted like a detergent to strip the feathers of their natural waterproofing oils. Consequently, the soaking birds, already weakened from migration, became hypothermic, and many died. If the surviving birds were cleaned as if they had been caught in an oil spill, then most made a full recovery. The algae seemed to have no other toxic activity, although inhaling aerosolized green scum apparently caused lung pathology. With the major shifts currently affecting the marine environment that are favoring other types of red tides, this kind of algal hazard is likely to become a more widespread occurrence. — CA

PLoS ONE **4**, e4550 (2009).

CREDITS (TOP TO BOTTOM): SANFORD BERRY/VISUALS UNLIMITED, INC.; JESSUP *ET AL.*, *PLOS ONE* **4**, E4550 (2009); LESLIE *ET AL.*, *NAT. PHYS.* **5**, 231 (2009)

CHEMISTRY

Clicking onto Nanofibers

Vertically aligned carbon nanofibers—stacked "cups" of grapheme—are of interest for electrochemistry because they expose a high fraction of edge sites with much faster electron transfer rates than the basal plane sites that predominate on carbon nanotubes. For applications such as sensing, it would be useful to attach redox-active groups to the surface of these materials. Landis and Hamers report that copper click chemistry can be used to attach groups such as ferrocene. The carbon nanofiber surfaces were functionalized with azide groups, and ethynyl-substituted ferrocenes were then covalently attached through the Cu(I)-catalyzed cyclization reaction. The attachment was quite stable—the redox couple could be cycled at least 1500 times. The rates through this pi-bonded bridge were similar to those for ferrocene groups attached through saturated alkyl linkages, suggesting that electron transfer occurs through the aqueous solvent rather than the hydrocarbon bridges. — PDS

Chem. Mater. **21**, 724 (2009).

APPLIED PHYSICS

Circuit Training for Fluids

A nagging problem in microfluidic reactor design is the need for bulky external apparatus to control the pumping and directing of the fluid flows. To circumvent this issue, Leslie *et al.* tried to mimic passive electrical circuits—resistors, capacitors, and diodes. Capacitors store electrical charge, a function mimicked by bonding a deformable elastomeric film to a fluid microchannel, so that the film bulged to allow more fluid storage as the overall pressure increased. Diodes, which permit flow in only one direction, were fabricated by bonding a deformable film on top of a weir, thus allowing flow only when the pressure was above a critical value. Through a combination of these circuit elements, fluid flow could be predicted and controlled by modulating a pressure source with time through a selection of resistive channels and capacitors. More complex flows were achieved by creating branched streams that merged at the output channel. The flow from each branch was regulated by the frequency of the pressure oscillations, effectively rendering the device a bandpass filter. Diodes, with their nonlinear response to pressure, were used to convert oscillatory flow to steady flow, similar to the conversion of electrical current from ac to dc. — MSL

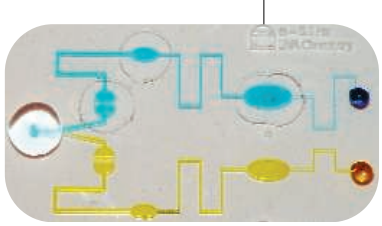

Microfluidic circuit.

Nat. Phys. **5**, 231 (2009).

MICROBIOLOGY

Do We Have a Quorum?

Bacteria can communicate with one another and act cooperatively as a group—a process known as quorum sensing (QS). However, such communication and cooperation can be exploited by "cheaters," who benefit from the shared metabolic or otherwise beneficial activities without contributing to them. In the case of the pathogenic bacterium *Pseudomonas aeruginosa*, the signal molecules that facilitate population-wide QS regulate important disease-related processes, such as biofilm formation, swarming motility, and the production of secreted virulence factors. Rumbaugh *et al.* demonstrate that this potentially deadly cocktail of activities can be undermined by mutant bacteria that cheat. In a burn injury model in mice, infection with QS *P. aeruginosa* leads to rapid death of the host; infection with QS mutant bacteria resulted in significantly less mortality. The mortality caused by QS bacteria was substantially diminished in the presence of the mutant bacteria, which, through their exploitation of the QS bacteria, were able to flourish at their benefactors' expense, reducing the overall virulence of the infection. Furthermore, the mutant bacteria, which cannot normally mount an effective systemic infection, were able to spread to the liver in the presence of the QS bacteria, presumably by piggy-backing on the social activities of the QS bacteria. QS mutants are known to arise in clinical settings and may thus affect the virulence and course of infections. — GR

Curr. Biol. **19**, 341 (2009).

www.sciencemag.org

Science

1200 New York Avenue, NW
Washington, DC 20005
Editorial: 202-326-6550, FAX 202-289-7562
News: 202-326-6581, FAX 202-371-9227
Bateman House, 82-88 Hills Road
Cambridge, UK CB2 1LQ
+44 (0) 1223 326500, FAX +44 (0) 1223 326501

Subscription Services For change of address, missing issues, new orders and renewals, and payment questions: 866-434-AAAS (2227) or 202-326-6417, FAX 202-842-1065. Mailing addresses: AAAS, P.O. Box 96178, Washington, DC 20090-6178 or AAAS Member Services, 1200 New York Avenue, NW, Washington, DC 20005

Institutional Site Licenses please call 202-326-6755 for any questions or information

Reprints: Author Inquiries 800-635-7181
Commercial Inquiries 803-359-4578

Permissions 202-326-7074, FAX 202-682-0816

Member Benefits AAAS/Barnes&Noble.com bookstore www.aaas.org/bn; AAAS Online Store www.apisource.com/aaas/ code MKB6; AAAS Travels: Betchart Expeditions 800-252-4910; Apple Store www.apple/eppstore/aaas; Bank of America MasterCard 1-800-833-6262 priority code FAA3YU; Cold Spring Harbor Laboratory Press Publications www.cshlpress.com/affiliates/aaas.htm; GEICO Auto Insurance www.geico.com/landingpage/go51.htm?logo=17624; Hertz 800-654-2200 CDP#343457; Office Depot https://bsd.officedepot.com/portalLogin.do; Seabury & Smith Life Insurance 800-424-9883; Subaru VIP Program 202-326-6417; VIP Moving Services www.vipmayflower.com/domestic/index.html; Other Benefits: AAAS Member Services 202-326-6417 or www.aaasmember.org.

science_editors@aaas.org	(for general editorial queries)
science_letters@aaas.org	(for queries about letters)
science_reviews@aaas.org	(for returning manuscript reviews)
science_bookrevs@aaas.org	(for book review queries)

Published by the American Association for the Advancement of Science (AAAS), *Science* serves its readers as a forum for the presentation and discussion of important issues related to the advancement of science, including the presentation of minority or conflicting points of view, rather than by publishing only material on which a consensus has been reached. Accordingly, all articles published in *Science*—including editorials, news and comment, and book reviews—are signed and reflect the individual views of the authors and not official points of view adopted by AAAS or the institutions with which the authors are affiliated.

AAAS was founded in 1848 and incorporated in 1874. Its mission is to advance science, engineering, and innovation throughout the world for the benefit of all people. The goals of the association are to: enhance communication among scientists, engineers, and the public; promote and defend the integrity of science and its use; strengthen support for the science and technology enterprise; provide a voice for science on societal issues; promote the responsible use of science in public policy; strengthen and diversify the science and technology workforce; foster education in science and technology for everyone; increase public engagement with science and technology; and advance international cooperation in science.

Information for Authors
See pages 807 and 808 of the 6 February 2009 issue or access www.sciencemag.org/about/authors

EDITOR-IN-CHIEF **Bruce Alberts**
EXECUTIVE EDITOR **Monica M. Bradford**
NEWS EDITOR **Colin Norman**
MANAGING EDITOR, RESEARCH JOURNALS **Katrina L. Kelner**
DEPUTY EDITORS **R. Brooks Hanson, Barbara R. Jasny, Andrew M. Sugden**

Editorial SENIOR EDITOR/PERSPECTIVES Lisa D. Chong; SENIOR EDITORS Gilbert J. Chin, Pamela J. Hines, Paula A. Kiberstis (Boston), Marc S. Lavine (Toronto), Beverly A. Purnell, L. Bryan Ray, Guy Riddihough, H. Jesse Smith, Phillip D. Szuromi (Tennessee), Valda Vinson; ASSOCIATE EDITORS Kristen L. Mueller, Jake S. Yeston, Laura M. Zahn; ONLINE EDITOR Stewart Wills; ASSOCIATE ONLINE EDITORS Robert Frederick, Tara S. Marathe; WEB CONTENT DEVELOPER Martyn Green; BOOK REVIEW EDITOR Sherman J. Suter; ASSOCIATE LETTERS EDITOR Jennifer Sills; EDITORIAL MANAGER Cara Tate; SENIOR COPY EDITORS Jeffrey E. Cook, Cynthia Howe, Harry Jach, Barbara P. Ordway, Trista Wagoner; COPY EDITORS Chris Filiatreau, Lauren Kmec; EDITORIAL COORDINATORS Carolyn Kyle, Beverly Shields; PUBLICATIONS ASSISTANTS Ramatoulaye Diop, Joi S. Granger, Jeffrey Hearn, Lisa Johnson, Scott Miller, Jerry Richardson, Jennifer A. Seibert, Brian White, Anita Wynn; EDITORIAL ASSISTANTS Carlos L. Durham, Emily Guise, Michael Hicks, Patricia M. Moore; EXECUTIVE ASSISTANT Sylvia S. Kihara; ADMINISTRATIVE SUPPORT Maryrose Madrid

News DEPUTY NEWS EDITORS Robert Coontz, Eliot Marshall, Jeffrey Mervis, Leslie Roberts; CONTRIBUTING EDITORS Elizabeth Culotta, Polly Shulman; NEWS WRITERS Yudhijit Bhattacharjee, Adrian Cho, Jennifer Couzin, David Grimm, Constance Holden, Jocelyn Kaiser, Richard A. Kerr, Eli Kintisch, Andrew Lawler (New England), Greg Miller, Elizabeth Pennisi, Robert F. Service (Pacific NW), Erik Stokstad; INTERN Jackie D. Grom; CONTRIBUTING CORRESPONDENTS Dan Charles, Jon Cohen (San Diego, CA), Daniel Ferber, Ann Gibbons, Robert Koenig, Mitch Leslie, Charles C. Mann, Virginia Morell, Evelyn Strauss, Gary Taubes; COPY EDITORS Linda B. Felaco, Melvin Gatling, Melissa Raimondi; ADMINISTRATIVE SUPPORT Scherraine Mack, Fannie Groom; BUREAUS New England: 207-549-7755, San Diego, CA: 760-942-3252, FAX 760-942-4979, Pacific Northwest: 503-963-1940

Production DIRECTOR James Landry; SENIOR MANAGER Wendy K. Shank; ASSISTANT MANAGER Rebecca Doshi; SENIOR SPECIALISTS Steve Forrester, Chris Redwood; SPECIALIST Anthony Rosen; PREFLIGHT DIRECTOR David M. Tompkins; MANAGER Marcus Spiegler

Art DIRECTOR Yael Kats; ASSOCIATE ART DIRECTOR Laura Creveling; ILLUSTRATORS Chris Bickel, Katharine Sutliff; SENIOR ART ASSOCIATES Holly Bishop, Preston Huey, Nayomi Kevitiyagala; ART ASSOCIATE Jessica Newfield; PHOTO EDITOR Leslie Blizard

***Science* International**

Europe (science@science-int.co.uk) EDITORIAL: INTERNATIONAL MANAGING EDITOR Andrew M. Sugden; SENIOR EDITOR/PERSPECTIVES Julia Fahrenkamp-Uppenbrink; SENIOR EDITORS Caroline Ash, Stella M. Hurtley, Ian S. Osborne, Peter Stern; ASSOCIATE EDITOR Maria Cruz; LOCUM EDITOR Helen Pickersgill; EDITORIAL SUPPORT Deborah Dennison, Rachel Roberts, Alice Whaley; ADMINISTRATIVE SUPPORT John Cannell, Janet Clements; NEWS: EUROPE NEWS EDITOR John Travis; DEPUTY NEWS EDITOR Daniel Clery; CONTRIBUTING CORRESPONDENTS Michael Balter (Paris), John Bohannon (Vienna), Martin Enserink (Amsterdam and Paris), Gretchen Vogel (Berlin); INTERN Sara Coelho

Asia Japan Office: Asca Corporation, Eiko Ishioka, Fusako Tamura, 1-8-13, Hirano-cho, Chuo-ku, Osaka-shi, Osaka, 541-0046 Japan; +81 (0) 6 6202 6272, FAX +81 (0) 6 6202 6271; asca@os.gulf.or.jp; ASIA NEWS EDITOR Richard Stone (Beijing: rstone@aaas.org); CONTRIBUTING CORRESPONDENTS Dennis Normile (Japan: +81 (0) 3 3391 0630, FAX +81 (0) 3 5936 3531; dnormile@gol.com); Hao Xin (China: +86 (0) 10 6307 4439 or 6307 3676, FAX +86 (0) 10 6307 4358; cindyhao@gmail.com); Pallava Bagla (South Asia: +91 (0) 11 2271 2896; pbagla@vsnl.com)

EXECUTIVE PUBLISHER **Alan I. Leshner**
PUBLISHER **Beth Rosner**

Fulfillment Systems and Operations (membership@aaas.org); DIRECTOR Waylon Butler; SENIOR SYSTEMS ANALYST Jonny Blaker; CUSTOMER SERVICE SUPERVISOR Pat Butler; SPECIALISTS Latoya Casteel, LaVonda Crawford, Vicki Linton, April Marshall; DATA ENTRY SUPERVISOR Cynthia Johnson; SPECIALISTS Eintou Bowden, Tarrika Hill, William Jones

Business Operations and Administration DIRECTOR Deborah Rivera-Wienhold; ASSISTANT DIRECTOR, BUSINESS OPERATIONS Randy Yi; MANAGER, BUSINESS ANALYSIS Michael LoBue; MANAGER, BUSINESS OPERATIONS Jessica Tierney; FINANCIAL ANALYSTS Priti Pamnani, Celeste Troxler; RIGHTS AND PERMISSIONS: ADMINISTRATOR Emilie David; ASSOCIATE Elizabeth Sandler; MARKETING DIRECTOR Ian King; MARKETING MANAGER Allison Pritchard; MARKETING ASSOCIATES Aimee Aponte, Alison Chandler, Mary Ellen Crowley, Julianne Wielga, Wendy Wise; MARKETING EXECUTIVE Jennifer Reeves; MARKETING/MEMBER SERVICES EXECUTIVE Linda Rusk; DIRECTOR, SITE LICENSING Tom Ryan; DIRECTOR, CORPORATE RELATIONS Eileen Bernadette Moran; PUBLISHER RELATIONS, eRESOURCES SPECIALIST Kiki Forsythe; SENIOR PUBLISHER RELATIONS SPECIALIST Catherine Holland; PUBLISHER RELATIONS, EAST COAST Phillip Smith; PUBLISHER RELATIONS, WEST COAST Philip Tsolakidis; FULFILLMENT SUPERVISOR Iquo Edim; FULFILLMENT COORDINATOR Laura Clemens; ELECTRONIC MEDIA: MANAGER Lizabeth Harman; PROJECT MANAGER Trista Snyder; ASSISTANT MANAGER Lisa Stanford; SENIOR PRODUCTION SPECIALISTS Christopher Coleman, Walter Jones; PRODUCTION SPECIALISTS Nichele Johnston, Kimberly Oster

Advertising DIRECTOR, WORLDWIDE AD SALES Bill Moran

Product (science_advertising@aaas.org); MIDWEST/WEST COAST/W. CANADA Rick Bongiovanni: 330-405-7080, FAX 330-405-7081; EAST COAST/E. CANADA Laurie Faraday: 508-747-9395, FAX 617-507-8189; UK/EUROPE/ASIA Roger Goncalves: TEL/FAX +41 43 243 1358; JAPAN Mashy Yoshikawa: +81 (0) 3 3235 5961, FAX +81 (0) 3 3235 5852; SENIOR TRAFFIC ASSOCIATE Deiandra Simms

Commercial Editor Sean Sanders: 202-326-6430

Project Director, Outreach Brianna Blaser

Classified (advertise@sciencecareers.org); INSIDE SALES MANAGER: MIDWEST/CANADA Daryl Anderson: 202-326-6543; INSIDE SALES REPRESENTATIVE Karen Foote: 202-326-6740; KEY ACCOUNT MANAGER Joribah Able; NORTHEAST Alexis Fleming: 202-326-6578; SOUTHEAST Tina Burks: 202-326-6577; WEST Nicholas Hintibidze: 202-326-6533; SALES COORDINATORS Rohan Edmonson, Shirley Young; INTERNATIONAL: SALES MANAGER Tracy Holmes: +44 (0) 1223 326525, FAX +44 (0) 1223 326532; SALES Susanne Kharraz, Dan Pennington, Alex Palmer; SALES ASSISTANT Louise Moore; JAPAN Mashy Yoshikawa: +81 (0) 3 3235 5961, FAX +81 (0) 3 3235 5852; ADVERTISING PRODUCTION OPERATIONS MANAGER Deborah Tompkins; SENIOR PRODUCTION SPECIALIST/GRAPHIC DESIGNER Amy Hardcastle; SENIOR PRODUCTION SPECIALIST Robert Buck; SENIOR TRAFFIC ASSOCIATE Christine Hall; PUBLICATIONS ASSISTANT Mary Lagnaoui

AAAS Board of Directors RETIRING PRESIDENT, CHAIR James J. McCarthy; PRESIDENT Peter C. Agre; PRESIDENT-ELECT Alice Huang; TREASURER David E. Shaw; CHIEF EXECUTIVE OFFICER Alan I. Leshner; BOARD Alice Gast, Linda P. B. Katehi, Nancy Knowlton, Cherry A. Murray, Julia M. Phillips, Thomas D. Pollard, David S. Sabatini, Thomas A. Woolsey

AAAS
ADVANCING SCIENCE, SERVING SOCIETY

Graphic Science

What's hotter than Harry Potter? In South Korea, at least, the answer is science—in comic-book form. The 50 titles in the English-titled *Why?* series have sold more than 20 million copies since 2001, outselling translations of J. K. Rowling's blockbuster series 3 to 2, according to publisher YeaRimDang.

Each 160-page, $6.50 book covers a different topic, including space, the sea, and puberty. These panels from *Why? Electricity and Electronics* explain how fuel cells combine hydrogen and oxygen to generate electricity, producing H_2O as a byproduct. The dog admonishes the fuel cell for "peeing all over the place." "It's just clean water," says the fuel cell. French, Russian, Chinese, and Thai translations have already appeared. Japanese and North American versions may soon follow.

Czar's Missing Children ID'd

On 17 July 1918, Czar Nicholas II of Russia, his wife, and five children were killed by the Soviets. A grave containing the remains of five family members was found in the 1970s, and in 1991, DNA testing established that the remains were those of the czar, his wife, and three of their children.

Now, researchers say they have definitively identified the missing children—the couple's hemophilic son, Alexei, and a girl—from bone fragments and teeth discovered near the original gravesite in 2007. Because the youngest daughters were only 2 years apart in age, the scientists couldn't be sure who the girl was.

A team led by Michael Coble of the DNA lab at the Armed Forces Institute of Pathology in Rockville, Maryland, made the matches by comparing mitochondrial and nuclear DNA from the remains with DNA from the earlier work and with Y chromosome markers from a living Romanov cousin, they reported 11 March in *PLoS ONE*.

At the same time, says Coble, researchers in Yekaterinburg, Russia, analyzed bloodstains from a shirt—stashed for decades in the Hermitage Museum in St. Petersburg—that Nicholas had been wearing when he was attacked while traveling in Japan in 1881. DNA from the blood showed "complete concordance" with DNA from one of Nicholas's teeth.

The newly discovered remains are now in a forensic lab in Yekaterinburg. Once the Russian Orthodox Church agrees that they are authentic, they can be buried with the rest of the family in a cathedral in St. Petersburg.

Giant Bug-Eater Descried

Plant explorers have discovered a giant new species of carnivorous pitcher plant on a mountaintop in the Philippines. At 30 cm long and 15 cm wide, the plant's pitchers may set a record for genus *Nepenthes*—the group that includes all 120-odd species of Old World pitcher plants.

The team spied the plant after scrambling up a 6-m waterfall to reach the summit of Mount Victoria on the island of Palawan, says Alastair Robinson, an independent field botanist formerly at the University of Cambridge, U.K. Dangling from long tendrils attached to a central stem, the trumpet-shaped pitchers are "akin to an open stomach" filled with milky digestive fluids and water, Robinson says. Insects attracted to the pitcher's nectar and color get trapped in the pool and drown. The new giant pitchers, whose ilk turned to carnivory because of the nutrient-deficient soils they live in, enjoy a varied diet: One contained several large green beetles, black beetles, bees, and wasps. Dubbed *N. attenboroughii*, the plant is described in the February *Botanical Journal of the Linnean Society*.

CREDITS (TOP TO BOTTOM): YEARIMDANG PUBLISHERS; POPPERFOTO/GETTY IMAGES; ALASTAIR ROBINSON

EDITED BY YUDHIJIT BHATTACHARJEE

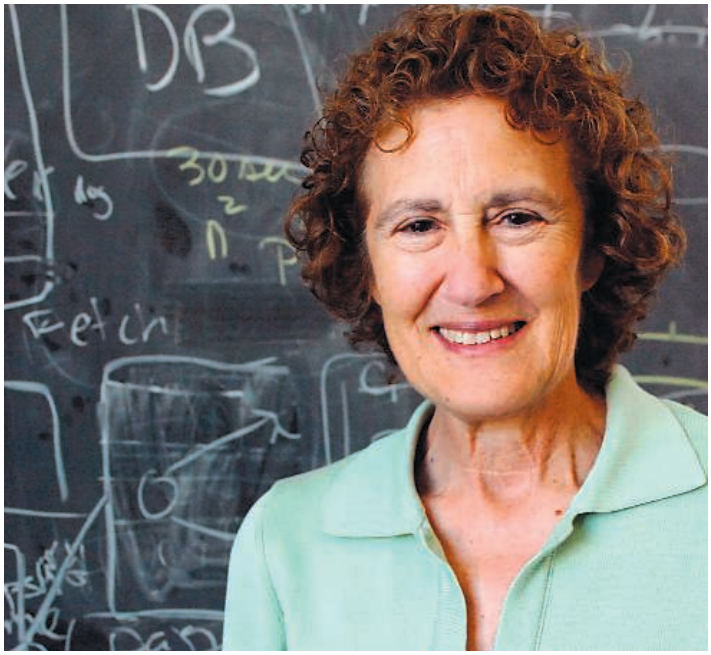

Awards

TURING AWARD. Barbara Liskov marvels at the technological gains in computer science in the 40 years since she earned her Ph.D. But progress on achieving gender equity has been much slower, says the first woman to earn a U.S. doctoral degree in the field.

This month, Liskov, 69, a professor at the Massachusetts Institute of Technology, received the 2008 A. M. Turing Award from the Association for Computing Machinery. The award, which comes with a $250,000 prize, recognizes her development of CLU and Argus, computer languages based on object-oriented programming. Her work laid the foundation for today's widely used programs Java and C++, which power most Internet software.

"I think we've made progress [in closing the gender gap], but I don't think we're where we want to be," says Liskov, who was one of only 10 women on the MIT faculty when she was hired in 1972. She's also associate provost for faculty equity, overseeing efforts to increase the number of women and minorities on the faculty.

NONPROFIT WORLD

NEW KAVLI HEAD. An engineer who has managed a venture-capital firm will be the next president of the Kavli Foundation. Robert Conn, a former dean of engineering at the University of California, San Diego, says his first task will be to preserve the foundation's endowment so it can continue to support its 15 university-based research centers. The foundation, started in 2000 by Norwegian-born businessman Fred Kavli, also awards biannual $1 million prizes in astrophysics, nanoscience, and neuroscience. Conn takes over next month from David Auston.

CHANGE AT MACARTHUR. Robert Gallucci, a military and foreign policy expert who served as the chief U.S. negotiator during the 1994 North Korean nuclear crisis, will be the next president of the John D. and Catherine T. MacArthur Foundation. Gallucci has held several jobs in the U.S. government and helped create the International Science and Technology Center in Moscow, which engages former Russian weapons scientists in nonweapons research. He's currently dean of the School of Foreign Service at Georgetown University in Washington, D.C.

MOVERS

FAVORITE SON. Eric Isaacs, the new director of Argonne National Laboratory, plans to make energy the Illinois lab's focus by expanding basic research already under way on storage, catalysis, alternative fuels, and combustion. For the condensed-matter physicist, energy conservation begins at home: An Argonne scientist since 2003 and deputy director since last May, Isaacs won't even need a moving van when he takes over in May for the outgoing director, Robert Rosner.

Simon Mochrie, a physicist at Yale University, predicts that Isaacs will be a good fit for the Department of Energy lab, which hosts the Advanced Photon Source synchrotron x-ray source. "Eric is a longtime user of x-ray facilities, and I think that will be a strength for Argonne," says Mochrie.

RISING STARS

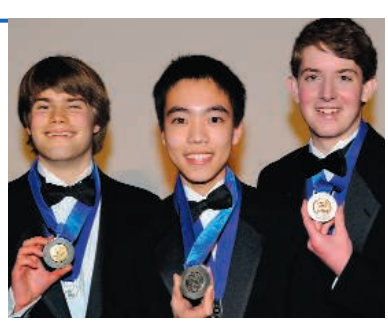

INTEL WINNERS. Eric Larson (left), a high school senior from Eugene, Oregon, has claimed the top prize—a $100,000 college scholarship—in the 2009 Intel Science Talent Search for his classification of new fusion categories, a type of algebraic structure with applications in string theory and quantum computation. Second- and third-place winners were William Sun, 17, of Chesterfield, Missouri, and Philip Streich, 18, of Platteville, Wisconsin.

Sun (middle) receives a $75,000 scholarship for researching the newly discovered molecule Golgicide A as a potential drug to treat bacterial infections and prevent Alzheimer's disease. Streich (right), a home-schooled student, earns a $50,000 scholarship for work demonstrating the solubility of carbon nanotubes; he and his mentor, chemist James Hamilton of the University of Wisconsin, Platteville, have filed for five patents.

CREDITS (TOP TO BOTTOM): DONNA COVENEY/MIT; MICHAEL DUNCAN/MIT; ROBIN WEINER/INTEL

Honors >>

TO SERVE. For physicist Mildred Dresselhaus, mentoring other women in science is simply emulating what Nobelist Rosalyn Yalow, then a young faculty member at Hunter College in New York City, did for her as an undergraduate there. It's also part of her credo: "Whenever I was asked to do something that would benefit others, I did it." Last week, the National Science Board, the oversight body for the National Science Foundation, honored her service and her accomplishments in carbon science with its Vannevar Bush Award.

A professor at the Massachusetts Institute of Technology since 1968, Dresselhaus has served as president of the American Physical Society and other societies including AAAS, which publishes *Science*. She also headed the U.S. Department of Energy's Office of Science from 2000–01.

At 78, Dresselhaus still begins work at 6 a.m. And she's lost none of her enthusiasm for research and mentoring. "You can do a lot by getting people excited about science. We don't do this for money, or awards, we do it for love."

Got a tip for this page? E-mail people@aaas.org

Published by AAAS

Science at FDA
1549

The slow domestication of rice
1550

Friendly climate. Danish Prime Minister Anders Rasmussen (*far right*) quizzed four climate scientists at the Copenhagen meeting.

GLOBAL WARMING

Projections of Climate Change Go From Bad to Worse, Scientists Report

COPENHAGEN—Meeting 2 years after the most recent report of the authoritative Intergovernmental Panel on Climate Change (IPCC), some 2000 scientists delivered a consistent if not unequivocal message here last week on the state of Earth's warming climate. "The worst-case IPCC projections, or even worse, are being realized," said the event's co-chair, University of Copenhagen biological oceanographer Katherine Richardson. Emissions are soaring, projections of sea level rise are higher than expected, and climate impacts around the world are appearing with increasing frequency, she told delegates in the opening session of the 3-day meeting.

The 11 universities that convened the Copenhagen Climate Congress hoped to provide a comprehensive picture of the status of world climate science before another set of delegates meets here in December to hammer out a follow-up to the 1997 Kyoto Accords, which expire in 2012. "This is our opportunity to get science back on the agenda," said climate modeler Vicky Pope of the U.K. Met Office. British Member of Parliament Colin Challen, who attended several sessions, said the update was crucial as nations are making plans "on data that's out of date."

Outside the conference center, a 75-m wind turbine reminded delegates of the promise, yet unfulfilled, of sustainable energy. And inside, the organizers definitely felt the wind at their backs. Unlike IPCC, which is affiliated with the United Nations and its member governments, last week's congress answered to no political bosses and, therefore, participants were free to make prescriptive statements at its conclusion. "Inaction is inexcusable" and "weaker [emissions] targets for 2020 increase the risk of crossing tipping points" were two of the six "messages" that organizers disseminated in a press release. Some scientists, however, felt that those messages suggested a false consensus among participants.

The meeting's 58 sessions were grouped into three general themes: physical climate science, prospects for mitigation, and impacts and adaptation. On the prognosis for the climate system, Richardson warned that there's "no good news." Some scientists criticized how the 2007 IPCC report addressed the loss of the world's ice sheets, because it explicitly omitted calculations of the movement of glaciers, which at the time was poorly understood (*Science*, 9 February 2007, p. 754). Two years later, the picture is clearer. Konrad Steffen of the Cooperative Institute for Research in Environmental Sciences in Boulder, Colorado, said that the loss of Greenland ice was accelerating, with the speedup of the glaciers contributing up to two-thirds of the loss.

Another question left unanswered by the last IPCC report was whether the Antarctic ice sheets were losing mass. University of California (UC), Irvine, glaciologist Eric Rignot said that more recent data from satellites and field studies "very clearly" show that the ice sheets are shrinking. Rignot said the accelerating movement of glaciers in Greenland and Antarctica would, on the current trajectory, lead to sea level rise of 1 m or more by 2100—flooding coastal residents around the world.

New modeling work presented by Jonathan Bamber of the University of Bristol, U.K., showed that a complete disintegration of the Greenland sheet would require a 6°C rise in global temperatures, double the conventional wisdom. But before the audience could digest what sounded like a rare piece of good news, Bamber added that a 15% loss to the sheet would translate into a 1-m rise in sea level. "[That] is a horrendous prospect whichever way you cut it," Bamber told *Science*.

Elsewhere, the science was just as gloomy. Ecologist Chris Field of the Carnegie Institution for Science, who is overseeing the next IPCC report's section on impacts, gave an update on his analysis of the behavior of carbon stocks in the soil, permafrost, and plants. It's a problem IPCC "underemphasized" 2 years ago, he said. The latest estimate of the amount of carbon in permafrost is 1.7 trillion tons, more than twice the 2007 estimate.

Scientists know that warming temperatures could unlock this carbon, making the yearly effort to cut the atmospheric concentration of carbon dioxide "that much tougher" in the coming decades, Field says. Modeling of carbon frozen in soils remains primitive, he said. But new findings from field studies suggest that a type of soil known as Yedoma sediments could be especially problematic because it decomposes easily and 30% of its emissions are methane, a potent greenhouse gas. Plus, he said, scientists have been unable to find evidence for the hypothesis that some natural carbon sinks like forests may be increasing their ability to take in CO_2 as the planet warms.

A number of sessions examined the frightening possibility that warming temperatures could trigger catastrophic tipping points,

CREDIT: LIZETTE KABRÉ/UNIVERSITY OF COPENHAGEN

Published by AAAS

Clues to how deep brain stimulation works
1554

20 years after the *Exxon Valdez*
1558

such as the loss of the Amazon rainforest through drought, which would create a vicious feedback. For example, modelers from the U.K.'s Met Office presented new data showing that even a global cessation of greenhouse gas emissions by 2050 could lead to a loss of up to 40% of the Amazon rainforest. "We thought we didn't need to worry till we got to 3°C of warming," says Pope (see graphic). Tim Lenton, an Earth systems scientist from the University of East Anglia, U.K., describes the change in looking at deforestation as going from "high-impact, low-probability events [to] high-impact, larger probability events." Atmospheric scientist Allan Gadian of the University of Leeds, U.K., says that the model "lacks credibility" because it fails to reproduce the current climate. But Chris Jones of the Met Office says the model closely replicates 20th century Amazon rain patterns.

The challenge of change

Although transforming the world energy economy poses what Ian Chubb, vice-chancellor of Australian National University in Canberra, calls "a diabolical policy problem," sessions on mitigating carbon emissions offered a mixed bag. UC Berkeley energy scientist Daniel Kammen explained how a Berkeley city employee had come up with a novel financing technique to fund residential energy-efficiency upgrades and solar panels. It's too early to assess the success of the 6-month-old program, which offers homeowners loans through a city bond. But a handful of U.S. cities have adopted it, he says, and officials in Lisbon and New York City are monitoring it. "Green growth is the answer to our climate problems and our economic problems," Danish Prime Minister Anders Fogh Rasmussen told the delegates during an appearance in which he quizzed a panel of scientists on what emissions cuts are required.

Nations like Denmark have shown the reliability of wind power. But one challenge has been getting businesses to work together. Danish engineering professor Erik Petersen of Risoe National Laboratory for Sustainable Energy in Denmark said that "surprisingly" turbulent wind conditions at sea have made the turbines less efficient but that scientists are having trouble studying the problem because the companies are concerned about giving their competitors an advantage by disclosing their data.

Scientists also examined how carbon-friendly mitigation techniques might cause other problems. Dozens of companies are developing new strains of algae to make biodiesel fuel, said Anthony Marchese of Colorado State University in Fort Collins, but his studies show that the resulting fuel can emit higher organic carbon or NO_x pollution levels than fossil fuels do when burned. "We have to consider issues like the emissions and health effects, not just how much oil bio algae fuel provides," he said.

Along similar lines, Australian geographer and ecologist Neville Crossman of the Australian Commonwealth Scientific and Industrial Research Organisation said that a carbon-trading system in Australia provided farmers with an incentive to plant certain native eucalyptus trees in dry areas. But the trees increase the demand on scarce water supplies. A better alternative would be to plant mixtures of species, he says, but that requirement is not included in the system.

The conference included dozens of sessions on how scientists are helping countries begin to adapt to climate impacts. "Adaptation is rapidly evolving as a new area of science," said Roger Street of the University of Oxford in the U.K. and an expert on impacts and adaptation. There's a lot to learn, however. Oxford plant ecologist Pam Berry showed how adaptation can hinder efforts to mitigate emissions and protect biodiversity. "We need triple wins," she said. A project to reroute streams to reduce the risk of flooding, for example, offered relatively cheap flood protection and increased aquatic biodiversity, she said. But the new ecosystem might feature additional sources of methane. Beach-restoration efforts to battle rising tides often involve the addition of sands, which have a chemical composition that can harm local species. Scientists are learning that climate change creates challenges more complicated than the "single stressor, single species" models that were used in the past, she said.

Attendees said that they appreciated the breadth of climate-related research presented at the meeting, which was much more political than the average scientific conference but far more scientific than a gathering of diplomats. Still, Field echoed the comments of several researchers in worrying about the stated message of the effort. Field said the scientists on stage in the final plenary session were overstating the level of support among climate scientists for the scientific validity of the 2°C target. Also troubling, he said, was that the organizers of the congress "were very unclear on the difference between [the messages] at the end of the meeting and the incredibly thorough, careful IPCC review and evaluation process."

Conference organizers plan to release a 30-page, peer-reviewed summary report of the conference findings in June. They hope the document will serve as a guide for this fall's negotiators of the evolving science.

–ELI KINTISCH

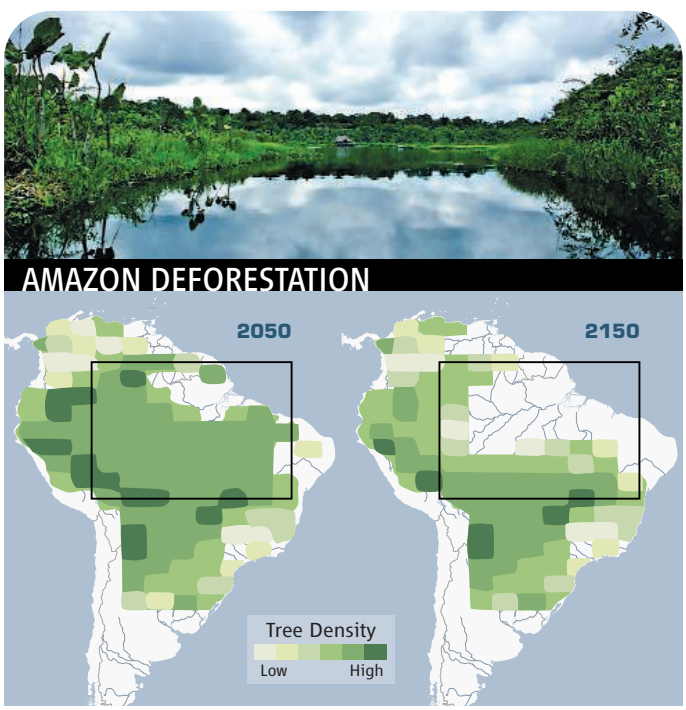

Emptying out. New models forecast that Amazonian forests could be decimated by 2150 even if greenhouse gas emissions fall to zero by 2050.

CREDITS (TOP TO BOTTOM): PHOTOS.COM; (SOURCE) MET OFFICE

Published by AAAS

MATHEMATICAL SCIENCES

Senate Majority Leader Hands NSF a Gift to Serve the Exceptionally Gifted

The budget of the National Science Foundation (NSF) has traditionally been free of congressional earmarks. But buried in the $410 billion federal spending measure enacted last week is a provision that gives NSF $3 million this year "to establish a mathematical institute devoted to the identification and development of mathematical talent." The directive, which is backed by Senate Majority Leader Harry Reid (D–NV), is aimed at serving supersmart children whose needs aren't being met in school.

As it happens, a proposal to create a national program along those lines has just been submitted to NSF as part of a competition to choose a new batch of university-based mathematical research institutes (www.mathinstitutes.org). A consortium that includes a group in Nevada is bidding to join a network, created in 2000, that is the biggest single activity within NSF's $212 million Division of Mathematical Sciences.

The seven current centers, with funding for up to 10 years, serve as user facilities for the mathematical community, providing jobs for graduate students and postdocs, temporary positions for senior professors, and a continuous stream of workshops, summer institutes, and public-outreach activities. Although each center also works with some precollege students and teachers, the focus is on exploring the frontiers of the mathematical sciences.

Last spring, NSF announced a new competition for up to six centers, with grants of $3 million to $5 million a year. (NSF provides a large majority of the operating budget for each center, and their directors say that life without NSF funding would be nearly impossible.) The deadline for applications was 27 February, and incumbents—including four whose funding ends next year—were eligible to apply. Although NSF won't disclose the number of applications it received, nor their identities, the four incumbents—at the Berkeley and Los Angeles campuses of the University of California, the University of Minnesota, and Ohio State University—have submitted proposals.

So did a team led by educational psychologist Susan Assouline of the University of Iowa's Belin-Blank International Center for Gifted Education and Talent Development. Linda Brody of Johns Hopkins University in Baltimore, Maryland, and Jill Adrian of the Davidson Institute for Talent Development in Reno, Nevada, are co-investigators on a proposal that Adrian describes as "a little bit out of the box."

The three researchers have spent decades working with the tiny population labeled "profoundly gifted." Assouline and Brody were postdocs together in the late 1980s on the renowned longitudinal exceptional talent study at Hopkins, which Brody now directs. The nonprofit Davidson Institute was created 10 years ago by education software developers Bob and Jan Davidson, who also support the Davidson Academy, a one-of-a-kind public school for exceptionally gifted students on the campus of the University of Nevada, Reno.

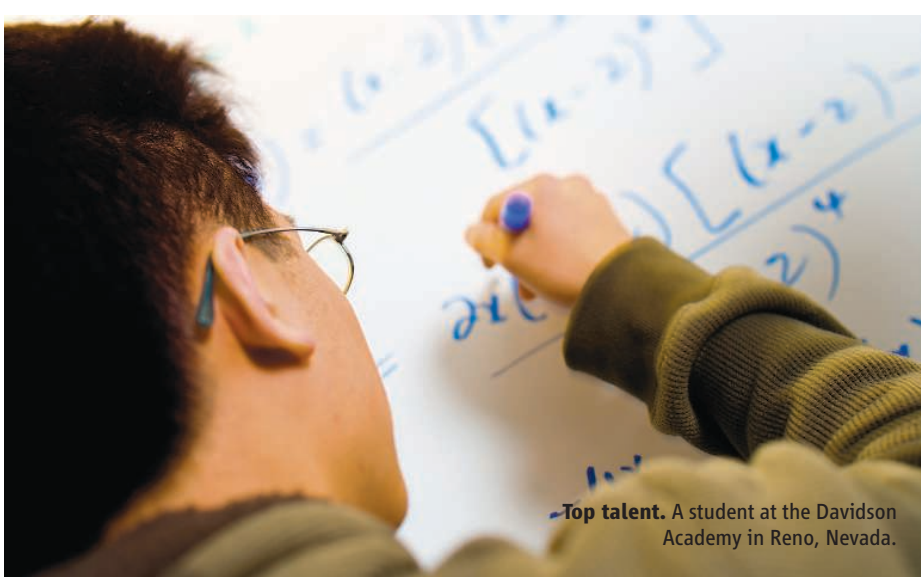

Top talent. A student at the Davidson Academy in Reno, Nevada.

CREDIT: JEFF DOW, COURTESY OF THE DAVIDSON ACADEMY

Assouline declined to describe the group's proposal in detail, citing the confidentiality of NSF's merit-review process. But a one-page project summary makes clear that the proposed National Institute for Mathematical Research would focus on prospective mathematicians—the youngest student at Davidson Academy is 9 years old—rather than the academic mathematicians—faculty members, postdocs, and graduate students—who populate the existing centers. It would likely expand the Davidson Institute's young scholars program, which provides counseling for students around the country and their parents, as well as offering some students a chance to work with professors on genuine research projects. Hopkins and Iowa would provide additional sites in what would otherwise be a largely virtual institute.

Although several states and local districts operate schools for high-end students, those with truly exceptional academic skills are usually left to fend for themselves, including home-schooling. "These kids need so much more than students in the average gifted and talented program, and not just with regard to academics," says Adrian. The goal, says Assouline, is to create "an integrated, national system." Assouline estimates that 10% of students at the new institute "will progress toward an active research agenda."

Assouline has a powerful friend in her corner in Reid. The $3 million in NSF's 2009 budget is not the narrowest type of earmark that requires an agency to give money to a particular entity in a legislator's district. But Peter March, head of NSF's math division, says the language constitutes "directed spending" of the sort that limits the agency's options.

Although March declined to discuss the matter further, *Science* has learned that he met several times with aides to Reid to talk about how NSF could do more for profoundly gifted students. Reid staffers were also in touch with the Davidson Institute as the proposal was being prepared. Aides to the senator declined repeated requests to explain the language in the spending bill and would say only that Reid "supported … the additional funding" for the NSF program.

Timing could be a touchy issue for NSF. The new centers aren't expected to be chosen until fall and will be funded out of NSF's 2010 budget. But the $3 million earmark is for the 2009 fiscal year, which ends on 30 September. Even if NSF doesn't fund Assouline's proposal as part of its current competition, it's a good bet that the needs of this special student population have moved up on the list of NSF priorities.

–JEFFREY MERVIS

Published by AAAS

PUBLIC HEALTH

Stronger Research Just One Item on Drug Agency's Wish List

The two public health veterans President Barack Obama has tapped to take charge of the U.S. Food and Drug Administration (FDA) face a daunting challenge. Margaret Hamburg, 53, and Joshua Sharfstein, 39, nominated to be FDA commissioner and deputy, respectively, will inherit an agency with fragmented authority and funding that has been stumbling from one crisis to the next.

Safe? FDA is scrutinizing a residue in plastic.

Their challenges stretch from fixing antiquated information technology systems to managing overseas inspections of food and drugs, but some of the biggest are scientific. In recent years, the agency has seen a flood of applications for novel medical therapies, such as those utilizing stem cells; at the same time it's been encouraging companies to develop personalized gene-based drugs. For monitoring and enforcement, FDA desperately needs new ways to quickly detect food-borne illnesses like salmonella.

Although FDA runs some in-house science efforts, including a sizable center for toxicological research in Arkansas, there's been political pushback to supporting extensive research in-house. The agency is "not funded or empowered to do basic drug research," says William Hubbard, a former FDA associate commissioner who spent nearly 30 years at the agency and recently retired. But while research is not its first priority, that doesn't mean FDA can let expertise pass it by: "You can ill afford to have reviewers that are not very well experienced in the most advanced technologies when in fact those technologies are being brought to the agency" for decisions, says Gail Cassell, vice president for scientific affairs at Eli Lilly in Indianapolis, who chaired a panel that issued a scathing report on FDA's science capabilities late in 2007 (*Science*, 7 December 2007, p. 1537).

Hamburg and Sharfstein may be well-placed to address some pressing issues. Both have headed big-city health departments: Hamburg in New York City during the 1990s, and Sharfstein as the current health commissioner of Baltimore. Both also have a long-standing interest in disease surveillance: for example, Hamburg served as an assistant secretary at the Department of Health and Human Services during the Clinton Administration, where she specialized in bioterrorism and planning a response to a potential flu epidemic.

Funding has been a big part of FDA's problem: Its $2.66 billion budget for the 2009 fiscal year, while a boost from the previous year, still falls short of what many say the agency needs. (Last year, FDA spent 6% of its budget on basic research.) In addition, scientist turnover at FDA is twice that of other federal agencies, Cassell's report noted. Philip Bushnell, a toxicologist at the Environmental Protection Agency who sat on an FDA subcommittee last fall that assessed the risks of bisphenol-A, a plastic found in baby bottles, says FDA officials at that review "were not up to speed" on the most current approaches to risk assessment.

It's clear that FDA needs more money, better morale, and improved leadership, says Garret FitzGerald, a pharmacologist at the University of Pennsylvania School of Medicine who sits on the agency's Science Board, a group of outside advisers. But "let's imagine all those things are fixed," he continues. That's still not enough, he believes, to provide FDA with the scientific expertise it needs.

To get that help, FitzGerald and others say, FDA needs to pursue more scientific collaborations. The agency has taken some steps in this direction—in 2006, it helped initiate a consortium with the Foundation for the National Institutes of Health, industry, and others to identify biomarkers for drug effectiveness and safety. A year ago, FDA appointed its first chief scientist, Frank Torti, a cancer biologist from Wake Forest University School of Medicine. Torti has been acting commissioner since January when FDA head Andrew von Eschenbach stepped down. He also launched an effort to bring 50 scientists to FDA for 2-year fellowship stints; the first class is there now.

Danielle Turley, who came to FDA as a fellow after a postdoc at Northwestern University, is trying to identify biomarkers in stem cells drawn from bone marrow to help predict how safe and potent they'll be. She is one of more than 1000 who applied for the first fellowships. Explaining why it's important for FDA to support this research, Turley says: "As you're reading an [investigational new drug application] and you're trying to understand the readouts and the tests, you have people on hand" who understand the technology.

While Cassell praises the fellowship program—her report urged FDA to bring in many more visiting scientists—several FDA watchers say more radical change is needed. FitzGerald wants to see FDA fund academics to conduct research it needs done—for example, in rapid detection or drug toxicology. He notes that even when clear concerns arise, staff may lack the means to explore them. With Vioxx, an anti-inflammatory drug pulled from the market in 2004 after being linked to numerous heart attacks, "there were people in the FDA who knew that there was a problem very early on, but they had no way of going to a neutral testing ground" not connected to the drug company. FitzGerald envisions FDA farming this work out to academics and allowing them to pursue research with unapproved drugs. The idea would ruffle long-standing conventions about protecting company secrets.

New blood. Margaret Hamburg has been nominated to be FDA commissioner; Joshua Sharfstein, to be her deputy.

But right now, FDA lacks the funds—and possibly the initiative—to regularly nurture collaborations like these. And the agency is accustomed to taking the back seat, Torti suggested in an interview with *Science* last month. He described seeing a poster on salmonella by FDA researchers and assumed the work was paid for by FDA. The response, he recalled: " 'Oh, we would never have the money to fund that—it was the Department of Homeland Security that felt sorry for us and gave us the money.' "

Whether Hamburg and Sharfstein can shift FDA's culture will depend partly on the whims and generosity of Congress and the Obama Administration—and partly on how people in the agency respond.

–JENNIFER COUZIN

CREDITS (TOP TO BOTTOM): PHOTOS.COM; LINDA A. CICERO/STANFORD NEWS SERVICE; STEVE BARRETT PHOTOGRAPHY

Published by AAAS

ARCHAEOLOGY

Recipe for Rice Domestication Required Millennia

Rice is delicious, nutritious, and the primary staple for about half of the world's population. Most researchers agree that humanity's close relationship with the grain (*Oryza sativa*) began thousands of years ago in China's Yangtze River valley, but they have sharply debated when prehistoric farmers began domesticating wild rice and how long they took to do it. On page 1607 of this issue, archaeologists argue that rice remains from a 7000-year-old site in the Yangtze delta point to a later and slower domestication than has often been claimed.

If correct, the findings suggest that the course of rice domestication paralleled that of cereal crops such as wheat and barley in the Near East, which apparently evolved only gradually into the domesticated plants we eat today (*Science*, 29 June 2007, p. 1830). "This is a very valuable and timely contribution to the sometimes heated debate about the dating and pace of rice domestication in China," says James Innes, a paleoecologist at Durham University in the United Kingdom. But archaeologists who have argued that rice farming began as early as 10,000 years ago in China are not convinced. "The interpretation of this paper is simplistic," says Yan Pan, an archaeobotanist at Fudan University in Shanghai, who says the debate cannot "be resolved by analyzing one single site."

The new data come from the site of Tianluoshan, just inland from Hangzhou Bay, south of Shanghai. Excavations between 2004 and 2007 revealed the wooden posts of buildings from a prehistoric village, along with boat paddles, stone axes, and thousands of plant remains. A team led by archaeologist Dorian Fuller of University College London and dig director Guo-Ping Sun of the Zhejiang Provincial Institute of Cultural Relics and Archaeology in the city of Hangzhou analyzed some 24,000 plant remains from the site, including about 2600 rice spikelets, which are attached to the stalk and carry the edible grain. In wild rice, the spikelets ripen and then fall to the ground naturally, allowing the plant to reproduce. But domesticated varieties require human action, such as threshing, to tear the spikelets from the stalk. Archaeologists can often tell the difference: The bases of wild spikelets have a smooth scar where they were attached to the plant, whereas domesticated spikelets have uneven scars from being torn off.

Early harvest. Prehistoric villagers at Tianluoshan cultivated wild rice, distinguished by its spikelets (*inset*), eventually leading to domestication of the grain.

The team focused on three archaeological levels spanning 6900 to 6600 years ago, based on radiocarbon dating of rice and other plant remains. (All dates are in calibrated calendar years.) Over that 300-year period, domesticated spikelets increased from 27.4% of the total to 38.8%; over the same time, rice increased from 8% to 24% of the total plant remains, which came from more than 50 species including wild acorns and water chestnuts. Fuller and his colleagues conclude that domestication was a slow process still under way 6600 years ago, and that the villagers of Tianluoshan relied heavily on wild plants—such as wild rice and acorns—at that late date.

The rise in domesticated spikelets over time shows that the villagers also cultivated wild rice: As they preferentially harvested and later replanted the grains that clung to the stalk longer, they inadvertently selected for mutants that separated less easily from the stalk. Evidence from other sites in the region suggests that early farmers often harvested wild rice when it was still immature to avoid losing the grains, and the team also found many immature spikelets at Tianluoshan. The team notes that a mix of wild and domesticated spikelets has also been found at the nearby 8000-year-old Yangtze Delta site of Kuahuqiao, suggesting that the full transition from wild to domesticated rice cultivation took at least 2000 to 3000 years.

Such a slow and late domestication clashes with the idea that rice domestication began 10,000 years ago in China. The most recent of such claims was made in a 2006 paper in *Antiquity* on the 10,000-year-old site of Shangshan, about 150 kilometers southwest of Tianluoshan. Archaeologists Leping Jiang of the Zhejiang Provincial Institute of Cultural Relics and Archaeology in China and Li Liu of La Trobe University in Melbourne, Australia, argued that some charred rice husks at the site were shorter and wider than those of wild rice. They said that rice at the site "probably was already in an early stage of domestication." But Fuller says detailed analysis, rather than simple eyeballing, is required for such a claim. The paper sparked a heated debate among Fuller, Jiang, Liu, Pan, and others in the pages of *Antiquity* and the journal *Holocene*, filling dozens of pages in 2007 and 2008.

Liu, Pan, and others say that Tianluoshan is not necessarily representative of the whole Yangtze River valley region or, certainly, the rest of China. Tianluoshan's late rice domestication does not invalidate the much earlier dates from Shangshan and several other sites, they say. Yongqiang Zong, a geoarchaeologist at the University of Hong Kong, agrees: "What Fuller *et al*. have reported is only representative of the area on the southern side of the Hangzhou Bay."

Even Fuller's opponents in the debate acknowledge the importance of Tianluoshan's new evidence, however. "The quality of the data is unprecedented," says Liu, who adds that the new study "is the most systematic and detailed" to date on rice domestication. The paper is unlikely to resolve the debate, Innes says, but "it is exactly the kind of focused research that is needed to improve our understanding of the complex rice-domestication process."

–MICHAEL BALTER

CREDITS: COURTESY OF DORIAN FULLER AND THE TIANLUOSHAN EXCAVATION TEAM

Published by AAAS

SOLAR PHYSICS

Unseen Link May Solve the Mystery Of the Sun's Superhot Corona

Why would the sun's faint, thin crown of ionized gas—so prominent during an eclipse—be at 1,000,000°C when the underlying surface is only 6000°C? Good question, solar physicists say. The energy ultimately comes from below, but how does it get to the corona? Researchers watching the sun from the ground in unprecedented detail think they have an answer: The energy is piped upward in the form of curious, twisty magnetic waves detected on the sun for the first time.

The new observations are "very exciting," says solar physicist Markus Aschwanden of Lockheed Martin's Solar and Astrophysics Laboratory in Palo Alto, California. "The measurements are getting better and better." Still, he adds, there are other explanations for what scientists are seeing, and most solar physicists remain unconvinced that it's anything fundamentally new.

On page 1582, solar physicist David Jess of Queen's University Belfast and colleagues explain how they peered into an apparently empty layer just above the sun's visible surface, or photosphere, looking for an energy connection to the corona. Both above and below the photosphere, the sun is nothing but ionized gas—plasma—permeated by powerful magnetic fields. Energy is flowing every which way in the form of waves and oscillations in the plasma and along the magnetic fields. The problem for solar physicists has been that none of the detectable energy flows looked big enough to heat the corona to a million degrees.

Jess and his colleagues took a closer look at one patch of the sun using the Swedish 1-m Solar Telescope on La Palma in the Canary Islands. Using adaptive optics to remove blurring due to Earth's turbulent atmosphere, they could resolve features as small as 110 kilometers and detect spectral shifts around the wavelength of the hydrogen-alpha absorption. Looking above a tight bunch of particularly bright spots on the photosphere, called a bright point group, they found distinctive oscillations in the motions of plasma revealed as Doppler shifts.

The group interprets the oscillations as Alfvén waves driven upward from the churning photosphere in the form of a flaring tube to the bottom of the corona 5000 kilometers above. Long hypothesized but never directly detected on the sun, Alfvén waves are twisting oscillations along magnetic field lines formed as if you could grab the ends of the field lines and twist them one way and then the other, sending your energy out in the twists propagating along the field lines. The group calculates that there are enough bright point groups on the sun for their Alfvén waves to heat the corona to its observed million degrees. "We have conclusive evidence that Alfvén waves do exist [on the sun], and they have the potential to transport all the needed energy," Jess says.

"There's definitely something there," Aschwanden says. "The question is whether Alfvén waves are the only way to interpret it. Theirs is one interpretation. Their measurements must stand the test of time." Most other solar physicists agree. Even if powerful Alfvén waves exist, they add, no one has explained how the waves break into the corona and dissipate their energy there. Many favor a different heating source, tiny but abundant solar nanoflares. Aschwanden's conclusion: "We need better measurements." **–RICHARD A. KERR**

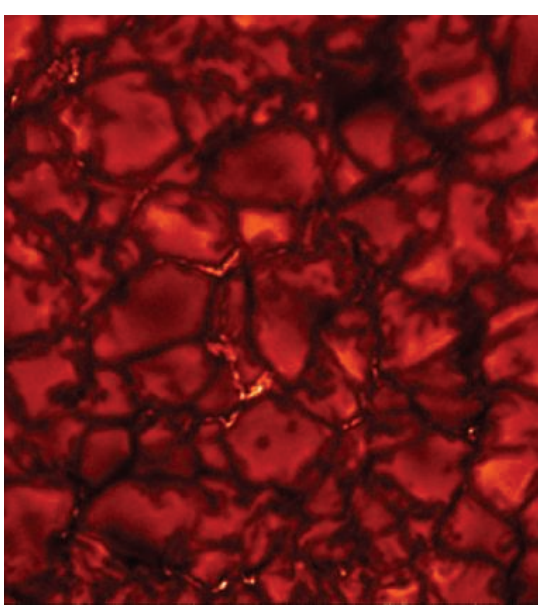

CREDITS (TOP TO BOTTOM): MICHAEL SINGER; D. B. JESS

Tiny but potent? Magnetic waves from bright specks on the sun (here in false color) may be heating the solar corona.

ScienceNOW.org

From *Science*'s Online Daily News Site

Split-personality superconductor. Researchers have long divided superconductors into two broad groups, depending on how they react to a magnetic field. Now, experiments by a group led by Victor Moshchalkov at the Catholic University of Leuven in Belgium show that one well-studied superconductor, magnesium diboride, actually belongs to both groups at the same time. That surprising finding suggests that superconductivity, which has already netted four Nobel Prizes, may be an even richer phenomenon that previously thought. The results will be published in *Physical Review Letters*.

Self-medicating caterpillars. Woolly bear caterpillars (*Grammia incorrupta*) like to dine on plants loaded with toxic pyrrolizidine alkaloids. Evolutionary ecologist Michael Singer of Wesleyan University in Middletown, Connecticut, and his colleagues surmised that the toxin may help the caterpillars overcome an infestation with the larvae of parasitic tachinid flies, a common scourge of these caterpillars. In the lab, the researchers provided infested and uninfested woolly bear caterpillars with either pyrrolizidine alkaloids or sugar. Infested caterpillars ate twice as much toxin as their uninfested brethren did, and the alkaloids increased their survival by 20%. This suggests that when the caterpillars feed on toxic plants, they are self-medicating, says Singer. It is believed to be the first time scientists have shown that an invertebrate can self-medicate when sick. The findings were published online in *PLoS ONE*.

Ancient lefties. Right-handed people may predominate here on Earth, but all of us are built from amino acids that are chemically "left-handed." Two NASA scientists studying meteorites older than our planet report in the *Proceedings of the National Academy of Sciences* that they have found a majority of left-handed amino acids, suggesting that our solar system has always had a preference for southpaws.

Read the full postings, comments, and more on **sciencenow.sciencemag.org**.

Published by AAAS

OBAMA EXECUTIVE ORDER

For Congress and NIH, Headaches Ahead on Stem Cells

With his long-awaited 9 March executive order lifting restrictions on federal funding for stem cell research, President Barack Obama has opened the door to some political fighting as nasty as any that has been seen so far on the subject of research with human embryonic stem (hES) cells.

As scientists hoped, Obama left all the details of the policy, which erased limits imposed 8 years ago by President George W. Bush, to be determined by the National Institutes of Health (NIH). The Bush policy restricted federal funding to work on hES cell lines created before 9 August 2001 from surplus embryos slated for discard by fertility clinics. NIH has until 7 July to put out a draft set of regulations, digest the tsunami of public comment expected, and establish a final set of guidelines on just what it will fund.

Scientists are thrilled that Obama is following their advice, but the new executive order leaves a void that, albeit temporary, is causing considerable anxiety in some quarters. At issue is the biological source of the hES cell lines now eligible for federal support. The question is whether work will still be limited to lines derived from surplus fertility clinic embryos or whether the government will approve the use of lines from embryos that have been created solely for research. Many scientists would like to work with lines created through research cloning, or somatic cell nuclear transfer (SCNT). This procedure—which has yet to be tried successfully—would enable a scientist to use a skin cell from a patient with Parkinson's disease, for instance, to reprogram an egg to generate an embryo so a particular disease could be studied in a test tube. Ultimately, some believe cell lines from such embryos could be used in genetically tailored cell therapies. The Dickey-Wicker Amendment prohibits federally funded scientists from harming embryos, which means they would not be allowed to derive the cell lines they work with regardless of the source. But there is no federal law governing cloning—either for research or for reproduction—so scientists could obtain cell lines from privately sponsored sources.

The stem cell community was expecting that as soon as Obama acted, Congress would codify the executive order by repassing a measure—twice vetoed by Bush—authorizing the government to support research, regardless of the date of derivation, on stem cell lines derived from excess embryos created for fertility treatments.

Now, however, with the source of eligible lines unspecified in the executive order, the bill's sponsors are heading back to the drawing board. A Senate staffer won't say whether they are thinking of eliminating the excess embryo restriction: "I think at this moment we are waiting to see what the NIH guidelines are going to be." On the House side, an aide to Representative Diana DeGette (D–CO) e-mailed *Science* that "in light of the president's Executive Order and in consultation with the experts, [sponsors of the bill] are reviewing past legislative efforts to assess what needs to be done going forward." Apparently, the sponsors were caught flat-footed. "The White House wouldn't tell us what was in the executive order before it was signed," says a staffer. While Congress wants to wait to see what NIH says, people at NIH would like to find out more about what Congress wants as they struggle to get draft guidelines ready before the end of April.

The traditional opponents of hES cell research are expecting the worst. Even with the derivation of new cell lines still banned, some fear the new policy will turn the federal government into an indirect supporter of cloning. The executive order "turned out to be far more extreme than [the] biggest proponents had hoped," said the Family Research Council. "With no clear policy from the White House, you and I could be footing the bill for research that clones embryos just to scavenge their parts." Psychiatrist and columnist Charles Krauthammer, a former member of the president's bioethics commission, said in an ▶

AUSTRALIA

Stem Cell Center Looks to Recast Itself in Supporting Role

MELBOURNE, AUSTRALIA—The Australian Stem Cell Centre (ASCC), a controversial experiment in speeding the commercialization of stem cell research, is slated for a radical overhaul. For the next 2 years, the center plans to turn away from its much-criticized commercial focus and recharge its research effort. Then in 2011, ASCC is likely to be transformed into an outfit that provides technical and licensing support for stem cell research.

The government-funded consortium of top stem cell researchers, which has received $75 million since it was founded in 2002, has long suffered from a clash of visions. One camp led by its former CEO, biotech entrepreneur Stephen Livesey, championed a model in which ASCC products would sustain the center after 2011, when public funding runs out. A second camp led by founder Alan Trounson, now leader of California's stem cell program (see p. 1564), argued that the time frame was unrealistic; the focus, he felt, should be on excellent research, and commercial spinoffs would follow. Trounson lost the battle and left in 2003. His departure did not ease tensions, which came to a head last August after a government review criticized ASCC's business plan. Livesey was sacked and the board purged (*Science*, 24 October 2008, p. 524).

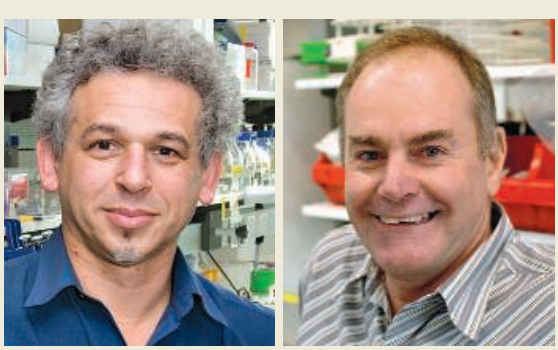

New map. Andrew Elefanty (*left*) and David Haylock are leading an effort to rethink stem cell research plans.

CREDITS: AUSTRALIAN STEM CELL CENTRE

With the clock ticking, ASCC scientists are reviewing research plans and scoping out alternative funding sources. The Australian government is expected to decide by June whether to endorse a new business plan and release the final 2 years of ASCC's public funding—or close it down early.

Andrew Elefanty, an embryonic stem cell researcher at Monash Univer-

Published by AAAS

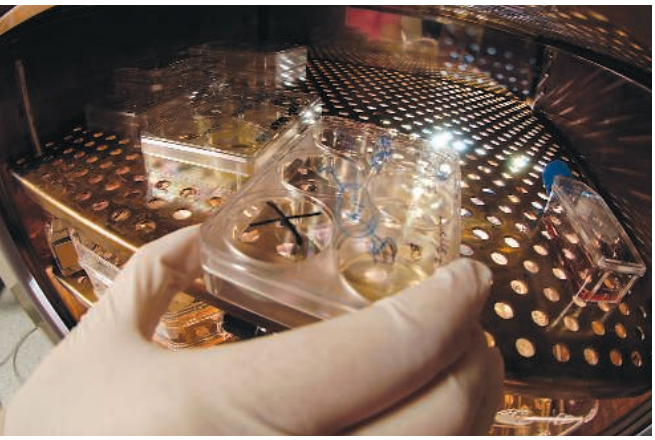

Supply lines. Obama has left it up to NIH and Congress to decide whether to restrict funding to cells derived from fertility clinic discards.

op-ed column that he does not oppose hES cell research but accused the president of "moral abdication" in leaving it up to scientists whether to create embryos solely for research.

On the contrary, says Harvard University's George Daley: "We need legislation that allows [such] decisions … to be left to scientists." Daley points out that guidelines hammered out in 2005 by a committee of the National Academy of Sciences (NAS) and regularly updated, as well as recommendations by the International Society for Stem Cell Research, do not specify what biological sources should be used but focus on informed consent procedures for obtaining eggs, sperm, or embryos, and proper scientific procedures.

So far, there's no available evidence that researchers anywhere are using lines other than from excess IVF embryos, says Willy Lensch, who works in Daley's lab at Harvard. In a survey of the literature, he has found references to at least 783 lines. "I've never encountered a report that IVF was used specifically to make a line of hES cells," he says.

University of Pennsylvania bioethicist Jonathan Moreno, a member of the NAS embryonic stem cell committee, says, "I would be surprised if NIH went beyond IVF discards" and opened the door to other embryo sources. But Daley says that even then, "the definition of 'excess embryos from IVF' is critical." Would lines derived only from frozen blastocysts be allowed, as was proposed in the last days of the Clinton Administration, or lines from fresh discarded embryos, like those made in Daley's lab, be included?

Out in the field, the executive order is lending new energy to efforts in some states to clamp down on hES cell research. The Georgia Senate on 12 March passed a bill introduced just that week with the support of Governor Sonny Perdue. It prohibits the creation of embryos for research—and covers not only SCNT but also parthenogenesis, in which nonviable embryos are generated from unfertilized eggs. **–CONSTANCE HOLDEN**

sity in Clayton, and hematologist David Haylock, whose lab studies adult stem cells at ASCC's administrative center in Monash, were appointed last October to head a committee to chart a new course. The duo has upended the former management's top-down approach—particularly its power to design projects and decide who should work with whom. "That's not the way collaborations work best," says Elefanty. "Right from the beginning, we were bleating: 'You can't force researchers to get into bed together.'"

Now ASCC researchers are masters of their destinies. "Previously, everything had to be aligned with commercial due-diligence decisions, which tended to hamper scientists getting together and doing what they do," says ASCC member Lars Nielsen, a biomedical engineer at the University of Queensland in St. Lucia. "Instead of a product pull, we now have a science push." Last month, all ASCC researchers were required to submit proposals to the center for projects over the next 2 years. That will better prepare them to compete for non-ASCC funding, says acting ASCC board chair Graham Macdonald.

Under a revised business plan that ASCC expects to deliver to the government by the end of April, ASCC would focus on licensing key technologies developed by the center, such as Haylock and Susie Nilsson's artificial niches for multiplying adult stem cells. ASCC would abandon attempts to commercialize a blood-cell product—the Holy Grail from its inception but a strategy that reviewers say was unattainable by 2011.

Beyond July 2011, ASCC would cease conducting its own research. Instead, it would provide services such as stem cell cultivation and commercialization expertise, with an eye toward joining the ranks of 12 other national infrastructure facilities. Its 130 scientists, meanwhile, would stay with their home institutions and seek research funding from traditional sources. **–ELIZABETH FINKEL**

Elizabeth Finkel is a writer in Melbourne, Australia.

CREDIT: JEFF MILLER/UNIVERSITY OF WISCONSIN, MADISON

*Science*Insider

From the *Science* Policy Blog

The FBI is investigating the 7 March firebombing of a UCLA neuroscientist's car by **animal-rights extremists**. It's the latest in a string of terror attacks on University of California scientists that goes back to 2006. The university and local authorities are offering a reward of $445,000 for information related to the incident. The targeted scientist was not identified by authorities.

*Science*Insider revealed that the **Defense Advanced Research Projects Agency** is looking into funding research on **geoengineering**, the deliberate tinkering with Earth's climate to combat global warming. The secretive and risk-taking agency sponsored a nonclassified meeting this week in Palo Alto, California, to explore the topic. But at least one climate scientist invited to the meeting feels that the military shouldn't be helping to develop such techniques.

A Washington, D.C., meeting was convened to brainstorm ways to help the **Iraqi academic and research enterprise** get back on its feet. Despite billions of dollars in aid to the war-torn nation since the U.S. invasion in 2003, presenters at the conference reported little progress in rebuilding the scientific infrastructure. Among the ideas floated were fellowships to encourage young Iraqi scientists to visit the United States, but participants fear that could result in a brain drain.

And in more sobering news from the **Copenhagen Climate Congress** (p. 1546), *Science*Insider blogged on alarming new results regarding **polar ice** shrinkage and the unappreciated threat of **soil carbon**. Researchers at the meeting also released a new scheme aimed at more fairly distributing **emissions allocation certificates** under a future greenhouse emissions cap, starting with the principle that every human should operate under the same emissions limit. And is **Denmark** really the green role model it advertises itself as?

For the full postings and more, go to **blogs.sciencemag.org/scienceinsider**.

Published by AAAS

Operation better mood. Doctors in Germany prepare to implant DBS electrodes in a man with severe depression.

Rewiring Faulty Circuits in the Brain

A wide range of neuropsychiatric disorders seems to respond to deep brain stimulation—but how does it work, and where will it lead?

For some patients with severe movement disorders like Parkinson's disease, years of struggle and frustration end with a flip of a switch that sends pulses of electric current through electrodes implanted deep inside the brain. Although it's considered only as a last resort for patients who've failed to respond to less invasive treatments, deep brain stimulation (DBS) has helped more than 55,000 people suffering from Parkinson's disease, essential tremor, or dystonia regain control of their bodies and their lives.

But despite the many success stories, remarkably little is known about how DBS works. Two studies in rodent models of Parkinson's disease published this week by *Science* provide some intriguing clues—and underscore how much remains to be figured out. One uses a sophisticated combination of genetic engineering and optics to investigate the mechanisms of DBS. The other suggests that stimulating the spinal cord—a far less invasive procedure—may have comparable benefits.

Even less is known about how DBS might help people with psychiatric conditions, yet its use in this area is mushrooming: Last month, the U.S. Food and Drug Administration (FDA) approved DBS for treating severe, intractable cases of obsessive-compulsive disorder (OCD), and in the past year, two clinical trials for major depression were launched. All told, DBS is being used or investigated as a treatment for at least a dozen disorders. "The bionic age is here," says Michael Okun, a neurologist and DBS researcher at the University of Florida in Gainesville. "Over the next 10 years, there's going to be several hundred thousand people worldwide with these devices for all sorts of different disorders."

All this progress makes even some proponents of DBS slightly uneasy. Haunted by the frontal lobotomies and other horrors of early 20th century psychosurgery, they insist that rules be developed to ensure that the errors of the past are not repeated. Fortunately, knowledge of the brain, not to mention ethical standards, have improved considerably since then. Even so, many researchers and clinicians agree that DBS should be an option only when it's backed by a strong scientific rationale and the fully informed consent of patients—not necessarily a trivial matter in those with severe mental disorders.

Moving forward

Parkinson's disease affects the basal ganglia, a neural circuit deep in the brain that plays a crucial role in regulating movement. When dopamine-releasing neurons in one part of the basal ganglia die off, the circuit malfunctions, resulting in the disease's hallmark tremor, rigidity, sluggish movement, and impaired balance. Drugs that restore dopamine help many patients but often stop working with time.

The rationale for DBS grew out of studies with animal models of Parkinson's disease that found that destroying certain nodes in the basal ganglia circuit reduced symptoms. Pulsing electrical current through thin wire electrodes placed in these brain regions had a similar effect, presumably by disrupting abnormal patterns of neural activity caused by the loss of dopamine. In people, DBS can reduce Parkinson's symptoms for years. But the exact mechanism is unclear, and researchers don't even agree on whether

CREDIT: THOMAS E. SCHLAEPFER/UNIVERSITY OF BONN

Published by AAAS

the benefits result from exciting or inhibiting neurons near the electrode's tip.

The answer may be neither, according to work reported online this week in *Science* (www.sciencemag.org/cgi/content/abstract/1167093) by researchers at Stanford University. Led by Viviana Gradinaru and Murtaza Mogri in the lab of Karl Deisseroth, the team used exciting new "optogenetics" methods (*Science*, 15 December 2006, p. 1674) to dissect the neural circuitry in a component of the basal ganglia that's a common target for DBS therapy, the subthalamic nucleus (STN). The researchers injected viruses into the STN of rats and mice to introduce genes encoding light-sensitive ion pumps and channels originally found in archaebacteria and algae. When neurons produce these proteins and stick them on their outer surface, their activity can be stimulated or inhibited—depending on the type used—by pulses of laser light delivered by an optical fiber inserted into the brain. By linking the pump or channel genes to stretches of regulatory DNA expressed only in certain cell types, the researchers could target them to just those cells. This approach is, in effect, a smarter form of DBS: Whereas the metal electrodes used in DBS create an electrical field that indiscriminately affects all nearby cells, the laser affects only the targeted cells.

In one experiment, the researchers inserted light-activated chloride pumps into the primary type of excitatory neuron in the STN. Pulses of laser light activated the pumps and squelched neural firing, enabling the researchers to test the popular hypothesis that turning off these neurons—and thereby dampening the overall level of neural activity in the STN—is the key to the therapeutic effect of DBS for Parkinson's disease. That doesn't appear to be the case. Turning off the excitatory STN neurons had no effect on movement abnormalities in Parkinsonian rats. Additional experiments failed to turn up evidence for a competing hypothesis: that DBS works by evoking rapid firing in the STN neurons, or for yet another proposal, that it works by activating nearby glial cells.

Instead, Deisseroth and colleagues suspect that the key may be manipulating axons that carry signals into the STN from other areas, including the primary motor cortex, a movement-control region on the surface of the brain. When they optically stimulated cortical neurons whose axons extend down into the STN in Parkinsonian mice, symptoms diminished as much as they did with standard DBS.

Online
sciencemag.org
Podcast interview with author Greg Miller.

The study demonstrates the power of optogenetics for dissecting the circuits involved in brain disorders, says Helen Mayberg, a neurologist and DBS researcher at Emory University in Atlanta, Georgia. When Deisseroth presented the work at psychiatry grand rounds at Emory a few weeks ago, Mayberg says, "people sat there with their mouths open in total awe of the possibilities." Mayberg and others think it might eventually be possible to develop optogenetics therapies for people. In principle, such treatments could maximize efficacy and minimize side effects, such as some of the mood and cognitive disturbances in some Parkinson's patients with DBS—but only if the method, particularly the genetic manipulation, proves safe to use in people.

In the meantime, a paper on page 1578 hints at the possibility of a simpler alternative to DBS. Romulo Fuentes, Per Petersson, and Miguel Nicolelis of Duke University and their colleagues report that stimulating electrodes placed on the surface of the spinal cord dramatically improved locomotion in mouse and rat models of Parkinson's disease. Nicolelis's team also monitored neural activity in the basal ganglia and motor cortex during spinal stimulation. These recordings suggested that spinal stimulation helps restore normal communication between these two brain regions by disrupting abnormal oscillations in neural firing caused by dopamine depletion. Nicolelis notes that the spinal electrodes stimulate fibers that convey tactile information to the brain, including the motor cortex, and he speculates that this indirect stimulation of cortex somehow breaks up the aberrant oscillations.

"If this were to be scalable to humans with Parkinson's disease, it would be a major achievement," says Andres Lozano, a neurosurgeon at Toronto Western Hospital in Canada. It's a much simpler and potentially safer procedure than implanting DBS electrodes in the basal ganglia, he says.

Both *Science* papers point to the cortex as an important player in the therapeutic effect of DBS for Parkinson's disease, says Cameron McIntyre, a biomedical engineer at the Cleveland Clinic in Ohio. That idea has gotten relatively little attention because researchers interested in the mechanisms have focused on neurophysiological effects within the basal ganglia, McIntyre says. "We need to start understanding more about what's happening at the cortical level," he says.

Mental stimulation

For all the questions remaining about DBS and movement disorders, even less is known about why electrodes implanted in the brain help many patients with severe psychiatric illness. The first such condition to be treated experimentally by DBS was OCD. In a 1999 pilot study in *The Lancet*, Belgian and Swedish researchers reported encouraging results in three of four OCD patients achieved by implanting electrodes in the anterior limbs of the internal capsule, an axon bundle deep in the brain. Destroying this part of the brain had been shown to help people debilitated by severe cases of OCD, and the Belgian team reasoned that electrodes that disrupt neural activity might provide similar benefits without the finality of destroying brain tissue.

Brain surgery may seem like an extreme intervention for OCD, but the worst cases are incredibly debilitating, says Wayne Goodman,

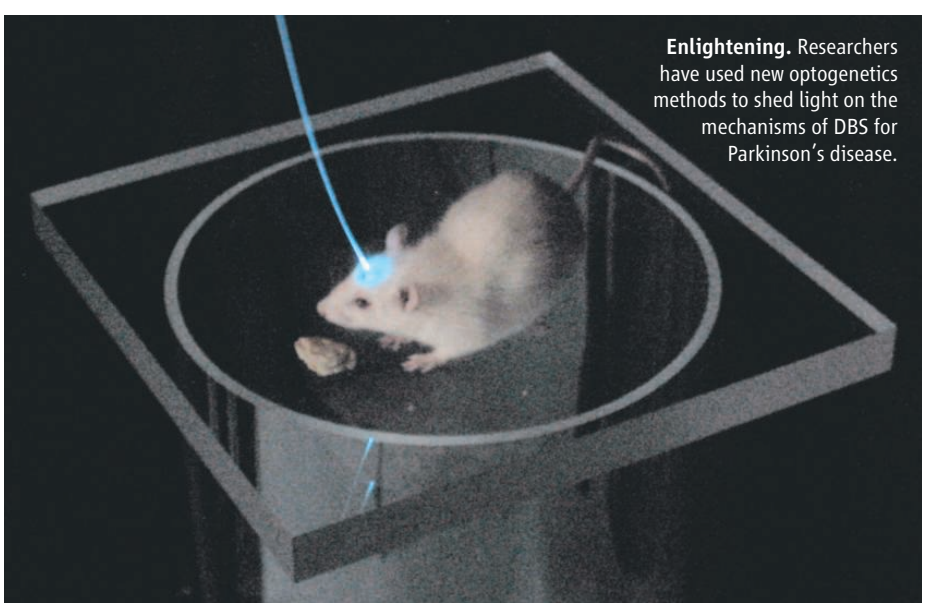

Enlightening. Researchers have used new optogenetics methods to shed light on the mechanisms of DBS for Parkinson's disease.

CREDIT: ALEX ARAVANIS AND KARL DEISSEROTH/STANFORD

director of adult translational research at the National Institute of Mental Health (NIMH) in Bethesda, Maryland, who helped develop the clinical scale that's used to assess the severity of OCD symptoms. Among other things, it considers the amount of time spent on obsessive thoughts. "For the patients who are candidates for DBS, we're talking more than 8 hours a day, and sometimes every waking minute being bombarded by thoughts and being driven to perform rituals over and over," Goodman says. "Their life is consumed by their illness."

Approximately 50 such patients have now received experimental DBS implants. Last year, researchers reviewed 26 cases in *Molecular Psychiatry* (Goodman and Okun were among the 20 co-authors). All had tried multiple courses of medication and behavioral therapy without success. With DBS, more than one-third of the patients went into remission, and about two-thirds were living more independently and functioning better at school or work. Based largely on these findings, in February 2009, the FDA granted DBS device manufacturer Medtronic Inc. of Minneapolis, Minnesota, a humanitarian device exemption for chronic, severe OCD. This type of limited approval applies to treatments for relatively rare conditions, and it marks the first approval of DBS for a psychiatric condition in the United States.

A far larger patient population that might benefit from DBS is people suffering from major depression. In a landmark 2005 *Neuron* paper, Mayberg, Lozano, and colleagues reported that electrodes implanted in the subcallosal cingulate gyrus and adjacent white matter caused remission in four of six patients who hadn't responded to drugs, psychotherapy, or electroconvulsive therapy. Neuroimaging studies indicate that this region is hyperactive in people with depression, and its anatomical connections suggest it is a hub in a network of brain regions involved in regulating emotion, Mayberg says. In 2008, she and her colleagues reported in *Biological Psychiatry* positive effects in 12 of 20 patients, and the device manufacturer St. Jude Medical began a multicenter trial to test the treatment.

In February, Medtronic announced it is starting its own trial to test DBS for depression, targeting the same region that proved useful for treating OCD. In the initial OCD studies, some patients reported elevated mood, and a pilot study funded by Medtronic and published in February in *Biological Psychiatry* found that eight of 15 patients with treatment-resistant depression improved with DBS and four met the criteria for remission. The clinical trial will ultimately enroll 200 patients and, like the St. Jude trial, will have a double-blind, placebo-controlled design in which some patients will not have the electrodes turned on immediately after implantation.

More research is needed to see which DBS target is most effective for depression, or whether different targets might work better for different patients, says Thomas Schlaepfer, a psychiatrist at the University of Bonn in Germany. He and colleagues have been investigating a third target, the nucleus accumbens, an integral part of the brain's reward circuitry. Until the advent of DBS, Schlaepfer says, psychiatrists had little to offer patients with the most resistant forms of depression and OCD beyond ever-changing combinations of drugs and ever-higher doses. "DBS is a new hope."

And not just for depression. Studies are under way to investigate its use for Tourette syndrome, epilepsy, and cluster headache, among other disorders. A smattering of case studies published in recent years hint at additional possibilities. In 2006, for example, researchers reported that electrodes implanted in the thalamus partially restored some cognitive function in a minimally conscious man with traumatic brain injury (sciencenow.sciencemag.org/cgi/content/full/2006/1016/1).

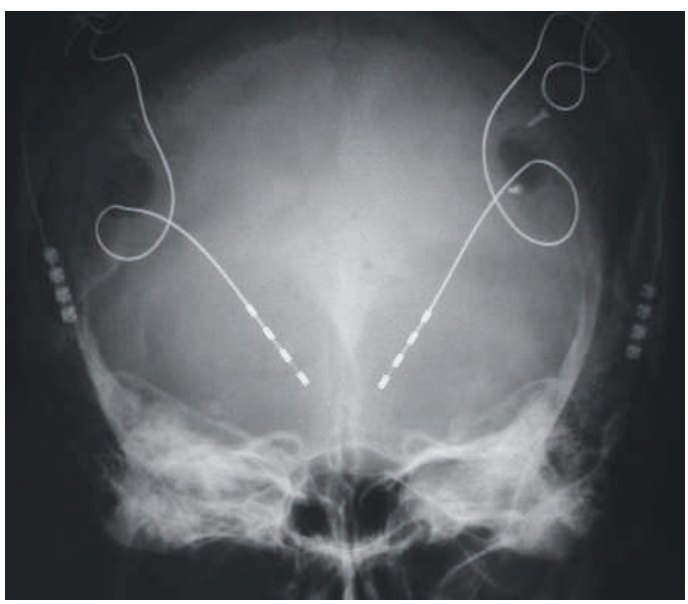

Shocking behavior. An x-ray image shows DBS electrodes implanted in a patient with severe OCD.

CREDIT: ALI REZAI/CLEVELAND CLINIC

And in 2007, Lozano and colleagues described the curious case of a 50-year-old man who'd received experimental electrode implants in his hypothalamus to try to treat morbid obesity. He didn't lose weight, but in the process of calibrating the electrodes, the researchers discovered that certain stimulation parameters evoked vivid memories from the man's youth and improved his performance on memory tests. Lozano suspects that the memory-enhancing effect resulted from the electrodes' proximity to the fornix, a bundle of axons conveying signals to and from the hippocampus, a crucial memory center. The serendipitous finding prompted the team to try a similar procedure in people with early stages of Alzheimer's disease. They have implanted electrodes in six people in hopes of staving off additional memory declines. "So far, we can tell you that it's safe and it's looking promising," says Lozano, who plans to submit the findings for publication later this year, after all six patients have had the implants for a full year.

In response to the growing interest in DBS, some researchers have called for guidelines to ensure that studies adhere to stringent ethical standards and employ placebo controls, long-term follow up, and other experimental designs that maximize their scientific value. In the checkered history of early 20th century surgical interventions for psychiatric illness, informed consent and scientific rigor were often lacking, Goodman and NIMH Director Thomas Insel note in a February editorial in *Biological Psychiatry*. "The clinical and scientific community must assure the public that the kind of mistakes made before are not repeated," they wrote.

Even if DBS is developed safely and ethically into a mainstream treatment, its very success might raise new quandaries. Would people with implants for obesity or addiction have the right to turn the stimulator off—and if so, would there be any point to the treatment? Could violent criminals be given implants to inhibit aggression in exchange for reduced sentences? Should healthy people be allowed to receive implants to boost their memory or other cognitive faculties? If the bionic age is indeed upon us, such questions may beg for answers sooner than we think.

–GREG MILLER

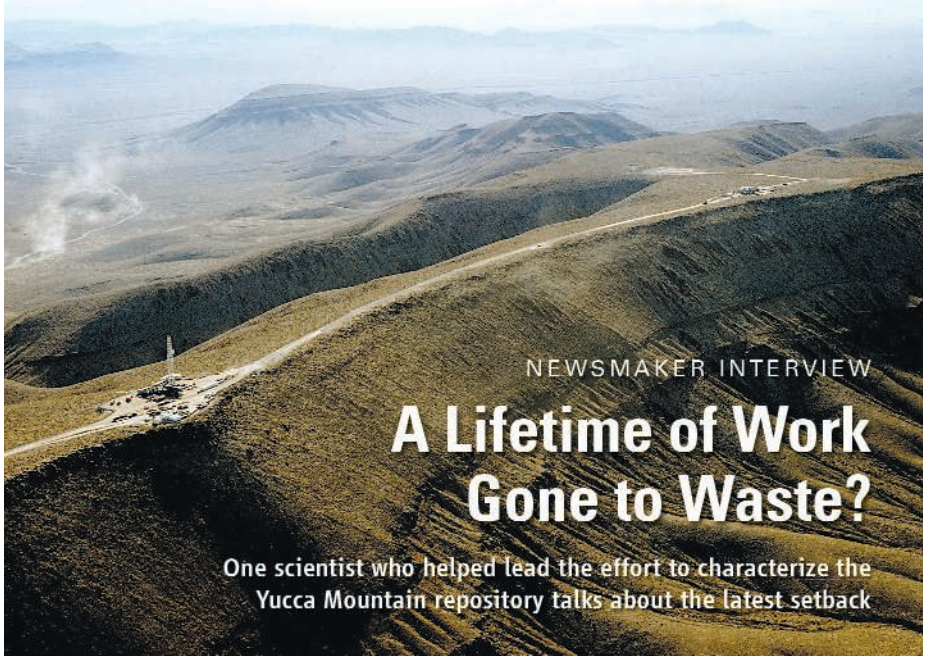

NEWSMAKER INTERVIEW

A Lifetime of Work Gone to Waste?

One scientist who helped lead the effort to characterize the Yucca Mountain repository talks about the latest setback

John Stuckless, a geochemist with the U.S. Geological Survey, spent 23 years probing the ancient history of Yucca Mountain, Nevada, and trying to predict its future. Working out of the survey's Denver, Colorado, office, he helped lead a large-scale scientific effort, costing hundreds of millions of dollars, to determine whether the site could safely store highly radioactive waste from nuclear power plants for thousands of years.

Last April, Stuckless, age 64, retired from the survey. Three months later, the Bush Administration formally applied for a license from the Nuclear Regulatory Commission to build a nuclear-waste repository at Yucca Mountain. Mission accomplished? Hardly.

The long and expensive search for a suitable disposal site appears far from over. Nevada politicians have fought the repository ever since Congress chose Yucca Mountain in 1987 over alternatives in Texas and the state of Washington. Their hand was strengthened 2 years ago when the state's senior senator, Democrat Harry Reid, became majority leader. They also have the support of President Barack Obama. Declaring that storing nuclear waste at Yucca Mountain "is not an option," the Administration's budget request for 2010 cuts funding for the repository. Instead, officials are promising "a new strategy toward nuclear-waste disposal."

The last word on Yucca Mountain probably hasn't been spoken. Many members of Congress still support the repository, and the Obama Administration has not withdrawn the government's application for a license. Even so, *Science* wanted to know what it feels like to have the rug pulled out from under a quarter-century of scientific work. Here's one man's answer. **–DAN CHARLES**

Q: What brought you into the project?
J.S.: It was the death of my wife. I had been working a lot internationally, and I had two small children. I wanted an assignment that didn't require travel.

Q: Was this considered a plum assignment, or was it something that people didn't particularly want to work on?
J.S.: That varied, depending with whom you spoke. A lot of the geologists did not like the idea of being directed in their research and [felt that the Department of Energy] really only wanted to know the favorable things. At least that was the perception. I don't think it was actually true.

Some of the people in the Geology Division weren't very happy about working for DOE, so they moved the whole thing into Water Resources. The Water Resources people tended to take a lot of assignments working for others—whom they called "cooperators."

Q: Is that because hydrology was the key?
J.S.: That's not what drove it, but hydrology was really the main question that needed to be solved. Because if radioactive waste does move, it'll be through water. But there also were scenarios involving major geologic things—volcanic eruptions and seismic activity.

A lot of the research was driven by somebody's belief that there was a problem. DOE would then direct us, or one of the national labs, to evaluate it.

Q: Was it interesting work?
J.S.: Yeah! I basically had to learn more areas of geology than I would ever have attempted to learn had I not been on this program. We did everything, including climatology, seismology, and volcanology. It was a very broadening experience.

Q: Was it worthwhile as a purely scientific exercise?
J.S.: Yes. Maybe not at the cost that we ended up with. But certainly we advanced the knowledge of geology of the unsaturated zone—the region above the water table—by orders of magnitude. We learned a lot about paleoseismology. We learned a tremendous amount about paleoclimate in the region. It really kicked off a lot of interest in that area.

We brought together paleontologists, chemists, geomorphologists. And I think we ended up with a much more complete picture than if these individuals had just been working on their own.

Q: Can you think of another project like this?
J.S.: No, I really can't. There's never been any reason to study any other point on the Earth to this degree.

Q: One of your colleagues called Obama's decision "a slap in the face to the energy and integrity of the scientists who have worked out there." How do you feel?
J.S.: I think it's very irresponsible. What it basically says is, they have no faith in the people who did the work, and they have no faith in the Nuclear Regulatory Commission to make a good decision. I mean, if there is something wrong with the work, the NRC will find it.

Decisions like that should be based on information, not on a gut feeling. The information we have is that there's basically nothing wrong with that site, and you're never going to find a better site.

Q: Does it leave you with a sense of wasted effort?
J.S.: No, because I'm moderately convinced that this is just a short-term hiccup in the road and that reason will prevail. But I don't know how long it will take.

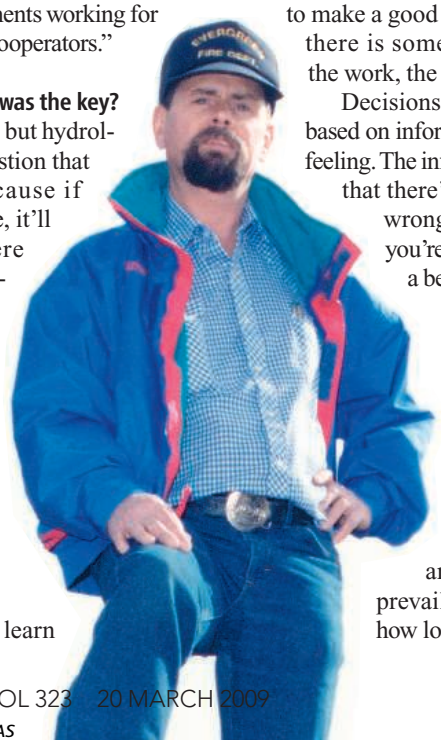

A mountain of data. John Stuckless (*below*) and the Yucca Mountain repository site.

CREDITS (TOP TO BOTTOM): DOE; COURTESY OF J. STUCKLESS AND USGS

Published by AAAS

CONSERVATION BIOLOGY

Exxon Valdez Turns 20

Twenty years ago this week, the worst oil spill in U.S. history struck Alaskan waters. Researchers are still asking: Has the ecosystem recovered?

Twenty years after the *Exxon Valdez* oil spill, little remains in Prince William Sound to remind the eye of 1989's striking images of oiled birds and sea otters, or of armies of workers in protective gear toiling to clean blackened beaches. Today, the waters of the sound are turquoise and the shorelines bristle with life, almost none of it human.

But researchers are still studying the spill's persistent aftereffects: Even as many species have recovered, others continue to struggle. Some may still come in contact with the oil that lingers, tucked away below the rocky surfaces of the beaches.

Scientists—some of whom have studied the spill for the entire 2 decades and are now looking to retire—are taking stock of their results and working to determine how (and whether) they might encourage further recovery of the ecosystem. This month, the *Exxon Valdez* Oil Spill Trustee Council, which oversees research and restoration, released its summary report. "It's not just research for the sake of research," says Catherine Boerner, a restoration specialist with the Trustee Council. The science now looks squarely at how to manage the injured species, she says, such as by opening a fishery or culling predators.

Before the incident, researchers had limited understanding of the long-term effects of a big spill. The *Valdez* studies are the largest, longest, and most expensive ever done. They suggest, for example, that oil may persist much longer than expected, affecting intertidal organisms, and that chronic exposure to low levels of oil can inflict subtle damage on wildlife. Many of the hundreds of scientific reports are "incredibly influential papers" that "will be cited for a long time," says marine chemist Christopher Reddy of Woods Hole Oceanographic Institution in Massachusetts, who did not work on the spill.

Despite the mountain of studies, government-funded and Exxon-funded scientists still clash over the spill's long-term effects and whether Exxon should pay the government an additional $92 million for yet more research. Government scientists say Exxon researchers don't accept good evidence, while Exxon scientists charge bias, too. Government-funded studies tend to be "bleak and negative," says Alan Maki, an environmental scientist who oversaw Exxon's research until he retired in late 2007. "This spill has not behaved much differently than what you would expect from studies of other spills," he says.

Some questions provoke less rancor but still may never be answered, such as why the Pacific herring populations crashed. In part, because of the complexity of the ecosystem, "we'll never know," says Stanley Rice, who manages research on the oil spill at the National Oceanic and Atmospheric Administration's (NOAA's) Auke Bay Laboratories in Juneau.

Aftermath of a disaster

The spill occurred just after midnight on 24 March 1989, when the supertanker *Exxon Valdez* ran aground on Bligh Reef in Prince William Sound. Forty million liters of crude oil ended up in the sea and on the beaches, making it the largest spill in U.S. waters. The immediate impact was dramatic: About 250,000 sea birds died, along with 22 killer whales, 2800 sea otters, 300 harbor seals, and untold numbers of fish eggs.

Scientists rushed to study the ongoing effects. Their efforts received a huge boost in 1991, when Exxon agreed to pay $900 million in a civil settlement with the U.S. and Alaskan governments to restore Prince William Sound. The Trustee Council has dedicated some $180 million to research, with the rest used to preserve land and reimburse cleanup expenses. The research efforts will continue indefinitely thanks to an endowment fund, currently about $100 million.

The company now known as ExxonMobil has sponsored its own research, and the scientists it funds have published or presented more than 400 peer-reviewed papers and talks. Over the years, their conclusions have often clashed with those of the government-funded researchers.

For example, one of the largest efforts has been to track the fate of the oil remaining in the sound years after the spill. In 2001, a team led by Jeffrey Short, a chemist then

CREDITS: PAOLO PETRIGNANI/STORIE DELLA TERRA

Published by AAAS

Digging for oil. Oil rises from below the surface on a Prince William Sound beach.

with NOAA, randomly sampled 91 beaches in the oiled parts of the sound, digging 9000 pits. Short estimated that 55,000 liters of oil remained, spread across and underneath 11 hectares of beaches.

David Page, an Exxon-funded chemist at Bowdoin College in Brunswick, Maine, insisted, after conducting his own sampling, that the government estimate was too high. Even though he later came to accept Short's results, he and others still questioned whether the lingering oil is affecting wildlife. They argue that other sources of hydrocarbon pollution outweigh what little oil remains from the 1989 spill. The remaining oil, says Page, is sequestered. "If it were available to be harming wildlife, it would have been long gone."

Government researchers challenge those claims. In 2005, Short's team resampled 10 of the beaches where oil remained in 2001. They reported in 2007 in *Environmental Science & Technology* that the oil was decaying at just 0% to 4% per year. "It will persist for decades up to a century," says Short, who retired from NOAA a few months ago and now works for Oceana, a marine conservation group. In another study reported last year in *Marine Environmental Research*, Short's team found that biologically active contaminants in the region were predominantly from the oil spill; he also thinks that biomarkers such as a particular liver enzyme reveal that organisms have been exposed to oil.

Swimming against the odds. One killer whale pod is slowly recovering from the oil spill, but another is headed for extinction.

These conflicting claims have fiscal consequences: The 1991 settlement contained a so-called reopener clause allowing the government to claim up to $100 million more if by 2006 unanticipated damages from the spill appeared. That year, the government asked Exxon for $92 million to find and remove the remaining oil, arguing that it was persisting longer than expected. Both sides have agreed to postpone negotiating the reopener until the government finishes more oil studies, perhaps 2 years from now, says Craig O'Connor, a lawyer with NOAA.

A pod dwindles

Scientists on both sides agree that many species have recovered in Prince William Sound, including bald eagles, cormorants, salmon, and river otters. But the oil, government scientists think, has had severe impacts on at least two photogenic animals: killer whales and sea otters.

The two pods of whales photographed and identified in the oil slick in 1989 each lost about 40% of their members around the time of the spill, says Rice. "That is just totally unprecedented," he says. One pod is recovering slowly, but the other, originally comprised of 22 whales, has lost all of its females of reproductive age and is down to seven or eight members. Eventually, Rice says, "they're going to become extinct."

Because the two unrelated pods declined so suddenly and at the same time, researchers argued last year in *Marine Ecology Progress Series*, the deaths were almost certainly caused by the spill when the whales breathed oil fumes or ate contaminated prey. But Exxon scientists say the deaths can't be conclusively linked to oil.

Meanwhile, sea otters have rebounded in most of the sound, but populations remain low in some heavily oiled areas where oil lingers in the intertidal zones. U.S. Geological Survey biologist James Bodkin fitted 16 otters with time-depth recorders and reported in February at a meeting of the Alaska Forum on the Environment that shallow intertidal digging represented about 18% of female sea otters' dives. "They're going to get exposure to oil," says Rice.

Most scientists do agree about the fate of at least one injured species: Pacific herring, whose populations are only 15% of their prespill numbers. In the late 1980s before the spill, the herring fishery in Prince William Sound was worth $12 million and the population was at a record high. The year after the spill, the population seemed high again—estimated at 120,000 tons—and the fishery opened. But then in 1993, the population crashed: Only 20,000 tons of herring appeared.

Was this due to the spill? Many scientists think not. A poor bloom of plankton in 1992 left the fish hungry and vulnerable to disease, says fish pathologist Gary Marty of the British Columbia Ministry of Agriculture and Lands in Canada, who has been studying the herring since the spill. He and Terrance Quinn of the University of Alaska, Fairbanks, developed a model that he says can "describe every blip in the population for the past 15 years."

But Richard Thorne, an acoustics researcher at the Prince William Sound Science Center, says hydroacoustic monitoring results suggest that the spill—and the subsequent 3 years of fishing—caused the population to crumble. In 1993, he started conducting annual hydroacoustic surveys, which use sonar to count fish. He and Gary Thomas, a fisheries scientist at the University of Miami, noted that the acoustic results correlate well with aerial surveys of herring spawn, which have been done every year for more than 30 years, and suggest the decline began in 1989.

Unfortunately, most herring studies stopped after 1990, so neither side in this debate has data about the critical precollapse years. As a result, researchers may never know for sure, says George Rose, a fisheries conservation expert at Memorial University in St. John's, Canada. "In a way, it doesn't matter," says NOAA's Rice. "We need to know why they don't come back."

That's where $2 million of this year's research has focused. With a better understanding of factors such as disease, predators, and climate change, researchers hope to help the fish rebound. Ideas include establishing a herring hatchery or targeted fishing for some of the herring's predators, like pollock. The best thing for the fish may simply be to protect them from fishing and other causes of mortality, Rose says: "In rebuilding natural systems, the main ingredient is patience and the other one is protection." Patience indeed is called for, many researchers agree. Two decades may span most of a scientific career, but they hardly register in the transformation of an ecosystem.

–LILA GUTERMAN

Lila Guterman is a science writer in Washington, D.C. With reporting by Jacopo Pasotti.

Published by AAAS

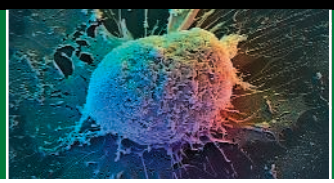

LETTERS

edited by Jennifer Sills

Pandemic Influenza: An Inconvenient Mutation

SEASONAL INFLUENZA AFFECTS 10% OF THE POPULATION ANNUALLY, KILLING UP TO ONE million persons worldwide. Pandemic viruses have even greater potential for mortality. We have several defenses, including personal and public health protective measures, vaccines immunologically matched to circulating strains, and two classes of antiviral drugs (neuraminidase inhibitors and adamantane ion-channel blockers). Our preventive options are limited by viral genetic diversity and a rapid viral mutation rate. Currently, two human influenza A subtypes (H1N1 and H3N2) and two influenza type B lineages cocirculate. About 425 million doses of trivalent influenza vaccine are produced annually, enough to protect less than 7% of the world's population. In the event of a pandemic, well-matched protective vaccines against a novel agent would not be available for at least several months, highlighting the importance of therapeutic options.

By 2009, however, 98% of circulating influenza A/H1N1 strains in North America have become resistant to the frequently prescribed and widely stockpiled neuraminidase inhibitor oseltamivir (Tamiflu), and 98% of A/H3N2 strains are resistant to the adamantanes. The alternative neuraminidase inhibitor zanamivir and the two approved adamantanes—amantadine and rimantadine—are all in short supply, and the adamantanes have substantial side effects. Influenza therapeutic options are clearly unraveling at a time when public health officials are appropriately concerned about pandemic emergence.

Preparing for a virus storm.

CREDIT: PAUL WEIN

The spread of high-level oseltamivir resistance in A/H1N1 strains is puzzling, as it appears to have occurred without antiviral selective pressure (*1*). Whether such levels of resistance will continue or diminish is unknown. Is high-level resistance an unfortunate byproduct of (still unknown) polygenic factors that confer viral fitness, such as balancing hemagglutinin and neuraminidase activity? Does resistance in influenza A/H1N1 imply a chance that resistance will develop in highly pathogenic avian A/H5N1 viruses, which bear the same neuraminidase subtype? Two past pandemic viruses (1957 and 1968) emerged after circulating human viruses reassorted with avian influenza viruses; emergence of a future pandemic strain by the same mechanism, but incorporating either an antiviral-resistant H1N1 neuraminidase or A/H3N2 matrix gene, is a possibility that cannot be ignored.

Pandemic planning envisions that if a virus with pandemic potential emerges, initial human-to-human transmission can be spotted quickly and contained by nonpharmaceutical interventions and by rapid community administration of antiviral agents and vaccines (*2*, *3*). If this strategy fails, a conceivable consequence, however unlikely, is accidental creation of a drug-resistant pandemic strain, a manmade analog of the feared naturally arising reassortant alluded to above.

Most national stockpiles have appropriately favored neuraminidase inhibitors (mainly orally administered oseltamivir) over ion-channel blockers (oral adamantanes) for pandemic preparedness, given the well-recognized rapid emergence of resistance to the latter when used in treatment (*4*). Now, as noted, transmissible oseltamivir resistance in human A/H1N1 strains makes this strategy problematic on many levels, including concern about efficacy in a pandemic, as well as emergence of a pandemic reassortant containing resistance genes (*1*). A complicating factor is increasing appreciation that secondary bacterial pneumonias have caused most deaths in past pandemics (*5*). Circulation of clinically aggressive community-acquired methicillin-resistant *Staphylococcus aureus* is an additional factor to be considered in planning for pandemic response. Taken together, these several developments suggest a need to continually examine and periodically reconfirm or update pandemic response strategies.

Whatever strategies are adopted, it is clear that additional anti-influenza therapeutics are urgently needed. So far, vaccines and antivirals have targeted three influenza envelope proteins: hemagglutinin, neuraminidase, and the matrix 2 ion channel protein. We need new classes of antivirals that interfere with other necessary viral processes (e.g., polymerase complex activity, interferon antagonist activity, and viral assembly). The desired outcomes of existing and future therapies (reduced severity, mortality,

Letters to the Editor

Letters (~300 words) discuss material published in *Science* in the previous 3 months or issues of general interest. They can be submitted through the Web (www.submit2science.org) or by regular mail (1200 New York Ave., NW, Washington, DC 20005, USA). Letters are not acknowledged upon receipt, nor are authors generally consulted before publication. Whether published in full or in part, letters are subject to editing for clarity and space.

Published by AAAS

Building in flexibility

1566

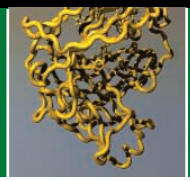

Closer to combination therapies

1567

viral shedding, and transmission) should be considered with respect to both seasonal and pandemic influenza.

The unpredictable nature of influenza presents a challenge for both research and pandemic preparedness planning. Our ability to anticipate pandemic events is poor, and our anti-pandemic armamentarium is weak. In an ever-shifting landscape of influenza evolution, we need to be farsighted and forceful in optimizing pandemic response capacity.

SCOTT P. LAYNE,[1]* ARNOLD S. MONTO,[2] JEFFERY K. TAUBENBERGER[3]

[1]Department of Epidemiology and Center for Rapid Influenza Surveillance and Research, University of California Los Angeles School of Public Health, Los Angeles, CA 90095, USA. [2]Department of Epidemiology, University of Michigan School of Public Health, Ann Arbor, MI 48109, USA. [3]Laboratory of Infectious Diseases, National Institute of Allergy and Infectious Diseases, National Institutes of Health, Bethesda, MD 20892, USA.

*To whom correspondence should be addressed. E-mail: scott.layne@ucla.edu

References and Notes

1. N. J. Dharan *et al*., *JAMA*, 10.1001/jama.2009.294, published online 2 March 2009.
2. M. E. Halloran *et al*., *Proc. Natl. Acad. Sci. U.S.A.* **105**, 4639 (2008).
3. A. S. Monto, *Clin. Infect. Dis*. **48**, 397 (2009).
4. The United States has stockpiled 81 million doses of oseltamivir—one dose each for 25% of the population.
5. D. M. Morens, J. K. Taubenberger, A. S. Fauci, *J. Infect. Dis*. **198**, 962 (2008).
6. This research was supported in part by the Intramural Research Program of the NIAID and the NIH.

Romanian Expatriates Face Career Obstacles

IN HIS NEWS FOCUS STORY "REACHING FOR the stars in Romania" (21 November 2008, p. 1183), M. Enserink gives a realistic description of some important problems of Romanian science. I would like to add another important issue: Successful expatriated Romanian scientists should be encouraged to return to Romania to hold important positions, and they should be appropriately compensated for doing so. In theory, expatriated scientists are encouraged to return and take leadership roles. In practice, these scientists have trouble securing their place in the applicant pool. To qualify for consideration, the expatriated scientists must demonstrate that the position they hold abroad is equivalent to the Romanian position immediately subordinate to the open position. The legal process to determine equivalency is cumbersome, and there is no definite authority who can certify equivalence. These ambiguous requirements often serve as an obstruction to expatriate scientists.

ZENO SIMON

Institute of Chemistry, Romanian Academy, Bd. Mihai Viteazul, 24, Timisoara 300223, Romania. E-mail: zsimon@acad-icht.tm.edu.ro

Reversible Exploration Not Worth the Cost

C. P. MCKAY ("BIOLOGICALLY REVERSIBLE exploration," Policy Forum, 6 February, p. 718) makes an impassioned case for so-called biologically reversible exploration of Mars. However, such a strategy will impose additional costs on an already strained program (*1*), and it is neither feasible in the context of a robust Mars exploration program nor necessary to ensure the fidelity of future in situ scientific endeavors. The concept of biologically reversible exploration is focused on potential effects of forward contamination—the transport of terrestrial microorganisms to other planetary bodies. Using real options theory (*2*), we can evaluate the ability to preserve future decision paths (such as the ability to "reverse" biological incursions) with present investments [such as spacecraft sterilization and constraints put in place on "special regions" (*3*)]. An accounting of present and future scientific costs and benefits must be made to critically assess this idea. In the near term, additional costs will result from spacecraft preparation regimes, compliance, and possibly reduced mission capability due to constraints on instrumentation and landing site restrictions. The suggestion that even human exploration should achieve "biological reversibility" will impose an enormous burden on such missions in terms of both direct costs and curtailed science from restrictions on access to the subsurface. In contrast, the supposed benefits are only potential benefits, mostly in the event of terraforming, and extremely long-term in nature. The exchange of meteorite material between Earth and Mars (*4*), the flotilla of existing landed missions, and the fleet of orbiters that will eventually crash into the surface already determine both the past and near-future two-way exchange of biological material between Earth and Mars. Special regions of scientific interest on Mars do call for prudent measures to reduce contamination, but the extreme measures advocated by McKay will not yield sufficient benefits to justify their high costs.

SAMUEL C. SCHON

Department of Geological Sciences, Brown University, Providence, RI 02912, USA. E-mail: samuel_schon@brown.edu

References

1. A. Lawler, *Science* **322**, 1618 (2008).
2. A. K. Dixit, R. S. Pindyck, *Investment Under Uncertainty* (Princeton Univ. Press, Princeton, NJ, 1994).
3. COSPAR, "Report on the 34th COSPAR Assembly," COSPAR Inform. Bull. No. 156, 24 (April 2003).
4. B. J. Gladman, J. A. Burns, M. Duncan, P. Lee, H. F. Levison, *Science* **271**, 1387 (1996).

CORRECTIONS AND CLARIFICATIONS

News of the Week: "NSF restores data on minority Ph.D.s" by J. Mervis (27 February, p. 1161). The National Science Foundation estimates that its new policy on reporting small numbers of minorities will suppress data on 3.7% of the new Ph.D.s in the Survey of Earned Doctorates. The original story incorrectly reported that 4% of the 280 subfields would be affected.

News Focus: "Tales of a prehistoric human genome" by E. Pennisi (13 February, p. 866). The story mischaracterized James P. Noonan's mouse experiment that used an enhancer showing human-specific activity. In that study (published in the 5 September 2008 issue of *Science*, p. 1346), the enhancer drove the expression of a reporter gene in the mice, but the researchers did not examine its effect on thumb development.

News Focus: "On the origin of art and symbolism" by M. Balter (6 February, p. 709). Ochre expert Ian Watts was cited as saying that there was little sign that ochre found at Twin Rivers, Zambia, was ground into powder, as needed for decoration. This incorrectly states Watts's view. Although only a small percentage of the approximately 300 pieces of ochre found at Twin Rivers show signs of grinding or other use, nearly all those that do are a dark, sparkly red. This leads Watts to conclude that they might have been preferentially chosen for symbolic purposes, although that is not certain.

Reviews: "Darwin's originality" by P. J. Bowler (9 January, p. 223). On page 226, reference 8 should read as follows: J. Browne, *Charles Darwin: The Power of Place* (Jonathan Cape, London, 2002). In reference 22, *Transmutation Notebook D* should have been *Notebook B*. Also in reference 22, two page numbers were missing: *Natural Selection*, p. 36, and *Charles Darwin's Notebooks*, p. 180.

Reports: "Observation of pulsed γ-rays above 25 GeV from the Crab pulsar with MAGIC" by The MAGIC Collaboration (21 November 2008, p. 1221). The e-mail address for N. Otte was incorrect. The correct address is nepomuk@scipp.ucsc.edu.

ENVIRONMENT AND HEALTH

Humans Need Biodiversity

David P. Mindell

The intimate connection between nature and human survival is indistinct for many people, especially the most affluent and intensive users of natural resources. The good news is that the notion of "living sustainably" seems to be gaining cachet and even a few adherents. The big challenge lies in moving beyond the blandishments of greenwashing to develop well-informed social, economic, and environmental policies—the three pillars of sustainability practice—to manage natural resource use and economic development.

Facts linking fossil fuel consumption with climate change are now well established, and development of alternative energy sources is at least under way. But the links between loss of species diversity in nature and the health of human populations are less well understood. Unlike fluctuating oil prices, declining species populations or outright extinctions do not have immediate, tangible impact on the cost of travel, food, or heat. Of course there are, and will be, substantial impacts from species loss, although our understanding of them is rudimentary. Handicapping our efforts, we still don't have a detailed inventory of Earth's organismal diversity. Probably less than 10% of the species on the planet have been described, and our knowledge of the ecosystem functions for the fraction of species that we do recognize is inadequate. These nontrivial functions include decomposition of waste, cycling of vital nutrients, and maintenance of healthy water, air, and soils.

For the want of bees. The extinction of bees in Maoxian County, China, has forced people to pollinate apple trees by hand.

At the same time, the number of known species considered to be threatened with extinction is increasing across nearly all taxonomic groups that have been evaluated, including roughly 12% of all bird species, 20% of all mammals, and a third of our fellow primates (*1*). Only two plant phyla have been assessed in this regard, conifers (25% threatened) and cycads (52%). The diversity of microscopic life forms (including viruses, archaea, bacteria, and small eukarya) are only recently coming to light, and their varieties, abilities, distributions, ecosystem functions, and conservation status are even more poorly known. These microscopic forms are important in all the nontrivial ways mentioned above, as well as in a broad range of symbiotic relationships critical to human health and disease.

In a comprehensive and compelling fashion, *Sustaining Life*, edited by Eric Chivian and Aaron Bernstein (physicians at Harvard University's Center for Health and the Global Environment), makes the case that the maintenance of biological diversity and human well-being are deeply entwined. Contributors synthesize efforts to circumscribe biological diversity and current threats to it and to reveal biodiversity's many functional roles in supporting healthy environments, in drug development and biomedical research, and in understanding infectious diseases and best practices for agriculture. Well researched and with stunning graphics, the volume could serve admirably as a college text or recommended reading for politicians, health and resource managers, and citizens at large. The authors place a primary focus on particular species or groups of species and how their activities contribute to ecosystems processes that influence water, air, and soil quality; erosion; climate change; and relative abundances of environmental toxins and human pathogens.

Sustaining Life
How Human Health Depends on Biodiversity
Eric Chivian and Aaron Bernstein, Eds.
Oxford University Press, New York, 2008. 566 pp. $34.95, £18.99.
ISBN 9780195175097.

For example, studies following the 2004 Southeast Asian tsunami illustrate the life-saving value of healthy mangrove forests, plant-covered sand dunes, and substantial coral reefs in reducing the force of storm waves and their devastation in densely populated coastal areas. Habitat changes associated with deforestation, agricultural development, climate change, and urbanization can increase diseases transmitted to people by displaced or redirected animal vectors. Archaea in the tongue-twisting families Methylococcaceae, Methylocystaceae, and Verrucomicrobiae break down the potent greenhouse gas methane, thus influencing local and regional climates. Some also detoxify chlorinated hydrocarbons, whether naturally occurring or from the pesticides widely used in agriculture and malaria control. Our digestive tracts are home to thousands of different kinds of archaea, bacteria, viruses, fungi, and microeukaryotes. Although we are mostly ignorant of their functions and taxonomies, the services of a few are known—e.g., *Bacteroides thetaiotaomicron* helps us digest starch and cellulose from plants, produces antimicrobial compounds (hydrogen peroxide, bacteriocins) that reduce bodily infections, and stimulates blood vessel growth necessary for nutrient absorption.

Going beyond the usual observation that the majority of prescribed medicines in the United States and as much as 80% of all medicines used in developing nations are derived from organismal species, the authors offer valuable discussions of particular groups of medicines, existing or in development, and their original sources. These include: painkillers from poppies (*Papaver*), cone snails (*Conus*), and frogs (*Dendrobates* and *Epipedobates*); anticancer medicines from sea squirts (Didemnidae), bryozoans (*Bugula*), sponges (*Discodermia* and *Luffariella*), and diverse plants (e.g., *Artemisia* and *Tabebuia*); and antiviral drugs from red algae (*Gigartina* and *Kappaphycus*) and sea cucumbers (Holothuroidea). People suffering from obesity could benefit from appetite suppressants modeled after aminosterols in dogfish sharks. After more than a decade of intense focus on combinatorial chemistry for drug development, it is clear that organisms,

The reviewer is at the California Academy of Sciences, 55 Music Concourse Drive, Golden Gate Park, San Francisco, CA 94118, USA. E-mail: dmindell@calacademy.org

CREDIT: FAROOQ AHMAD AND UMA PARTAP/INTERNATIONAL CENTRE FOR INTEGRATED MOUNTAIN DEVELOPMENT, NEPAL

having passed the tests of evolutionary time, still provide the best leads for compounds with medicinal value.

Our continuing dependence on organismal diversity within healthy ecosystems is clear. However, much more research and funding are needed to characterize all the species involved and to discover their complex interactions, impacts on humans, and responses to change. Further, raising public awareness and the political will to sustain biological diversity over time will require more than just science. We also need advocacy (which *Sustaining Life* ably serves) and greater legal and ethical commitments to conservation practices. Perhaps shining a bright light on the tight connections between sustainability practices and human survival could make conservation not only a practical concern but an ethical and moral one as well.

References

1. www.iucnredlist.org/documents/2008RL_stats_table_1_v1223294385.pdf.

10.1126/science.1170526

FUTUROLOGY

A Crystal Ball for Our Blue Planet

Giovanni F. Bignami

Wouldn't it be interesting to know what our ancestors 100 millennia ago thought would be happening about now? We can't, but *Surviving 1,000 Centuries* may be the next best thing. Roger-Maurice Bonnet (International Space Science Institute, Bern) and Lodewijk Woltjer (Observatoire de Haute Provence), two of the top astronomers in Europe, have the courage, intelligence, and culture to describe what the circumstances will be like on Earth circa 102,000 CE. One can look at this fascinating book as a mid-term report for the course "Civilization 101." Read it, and you will have a much better idea as to whether we will pass the final exam and survive.

Surviving 1,000 Centuries
Can We Do It?

by Roger-Maurice Bonnet and Lodewijk Woltjer

Springer, Berlin, in association with Praxis, Chichester, UK, 2008. 442 pp. $39.95, £20. ISBN 9780387746333.

A thousand centuries sounds like a lot of time, but it's only about one-fifty-thousandth of the age of our beloved planet and also, approximately, of life here. So the authors remind us at the beginning, in an illuminating crash course on the early history of Earth. They discuss why it ended up the way it did: very different from Mars and Venus, siblings born from the same protoplanetary disc around the same star but now either too hot or too cold, with too much atmosphere or not enough. Without a knowledge of Earth's history, we would be ignorant about its future.

That history has largely been shaped by Earth's oceans. They were a gift from heaven, rained down on the young planet in the form of watery cosmic debris (interstellar ice that might have carried who knows what else). Teeming with life, the oceans rid Earth of all that CO_2 in its ur-atmosphere, in the process making the Great Barrier Reef, the Dolomites, and Carrara marble (which sat patiently waiting for Michelangelo).

Of course, humanity's future could all end abruptly, as did that of the dinosaurs. We are fragile and can easily be wiped out by various cosmic catastrophes, from local supernovae to impacting asteroids to toxic volcanoes. (Personally, I vote for a nearby gamma-ray burst: think how more elegant it would be to go in a puff of gamma rays than to be done in by a rock falling from the sky.) Chances of that happening in 10^5 years may add up, but in our lifetime they are tiny—about the same as being eaten by a shark, averaged over the world population. In any event, life itself is very tough. Come what may, some bug is likely to hang on and be ready to start it all over again as soon as the skies clear.

As to what our planet and its biosphere will come to look like, a lot will depend on what we do this century. Although it may seem obvious, we are rightly reminded that we should leave enough space for wild fauna and flora and put an end to uncontrolled hunting, logging, and resource extraction. A species gone is lost forever, and from mammoths to dodos we have a very, very bad track record. The same concerns for conservation apply to our atmosphere. Let us make our response to the ozone hole a benchmark for future policy: recognize the danger, adopt world measures, and avoid disaster. Easier said than done, of course. And if we succeed in checking anthropogenic CO_2 production fairly soon, another ice age would be expected in about 50,000 years.

Alternatively, should the climate become inhospitable, would we leave Earth? And, if we decide to go, where to? Mars and Venus are close, but, as Bonnet and Woltjer (who should know) explain, to terraform them is not a realistic solution. To venture further aboard some autonomous but frighteningly lonesome Noah's Ark moving close to the speed of light remains, at least for the moment, a figment of science fiction. So far, humans have only gone one light-second away and have yet to invent something substantially better than the Semyorka rocket that put Sputnik in orbit. While we don't have the technology to emigrate, near-Earth, integrated space activities will have to be fully implemented if we are to manage our planet's future through monitoring and husbanding energy and inorganic resources as well as water and organic resources.

To find food for 11 billion people (the value at which the world population will stabilize) should be possible, we are told, even if we'll all be 3 meters tall and live to 130 years. Energy too shouldn't be an insurmountable problem, because we will have harnessed nuclear fusion. Inevitably, we will have installed a global governance, "an awful term but a vital concept," according to Javier Solana, Secretary General of the Council of the European Union.

One must be brave to predict the future. The physicist Charles Galton Darwin (grandson of Charles) offered a qualitative and sociological forecast of our world a million years on (*1*)—holding that forecasts for short timescales were difficult because of potential fluctuations introduced by individual events. Hats off to Bonnet and Woltjer, who manage to stay an order of magnitude closer to the present while being quantitative and learned yet amusing and daring.

References

1. C. G. Darwin, *The Next Million Years* (Hart-Davis, London, 1952).

10.1126/science.1172131

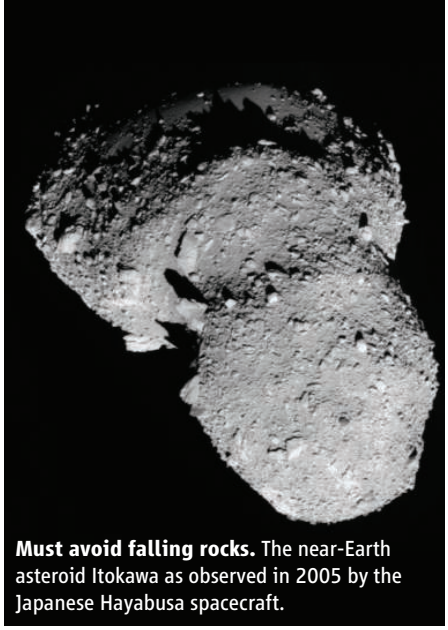

Must avoid falling rocks. The near-Earth asteroid Itokawa as observed in 2005 by the Japanese Hayabusa spacecraft.

CREDIT: JAPAN AEROSPACE EXPLORATION AGENCY

The reviewer is at the Istituto Universitario di Studi Superiori, Viale Lungo Ticino Sforza 56, 27100 Pavia, Italy, and the Accademia dei Lincei, Rome, Italy. E-mail: giovanni.bignami@gmail.com

MEDICINE

Monitoring and Regulating Offshore Stem Cell Clinics

Unverified medical treatments based on stem cells are proliferating and need oversight.

Sorapop Kiatpongsan[1,2,3] and Douglas Sipp[4,5]*

Traveling to another country in the hope of finding a stem cell–based treatment for a disease—"stem cell tourism"—has been the object of intense scrutiny in recent years, following reports of charlatanry, baseless claims, and adverse medical events (*1*). Providers of stem cell–based interventions vary widely in their assertions about the conditions that can be treated, the degree of improvement, and the cell types and protocols used (*2*), but there are many advertisements for medical procedures that have never been proven efficacious in appropriately designed clinical trials. To date, proven therapeutic applications for stem cells have been mainly for blood and immunological disorders. The scientific community and advocacy groups have begun to respond by formulating guidelines for physicians and scientists engaged in the clinical translation of stem cell research (*3*) and lists of questions for prospective patients to ask when considering an experimental stem cell treatment (*3*, *4*). Inaction and occasional complicity on the part of the government and medical establishment in some countries, however, have made enforcement, self-policing, and the maintenance of patient trust problematic.

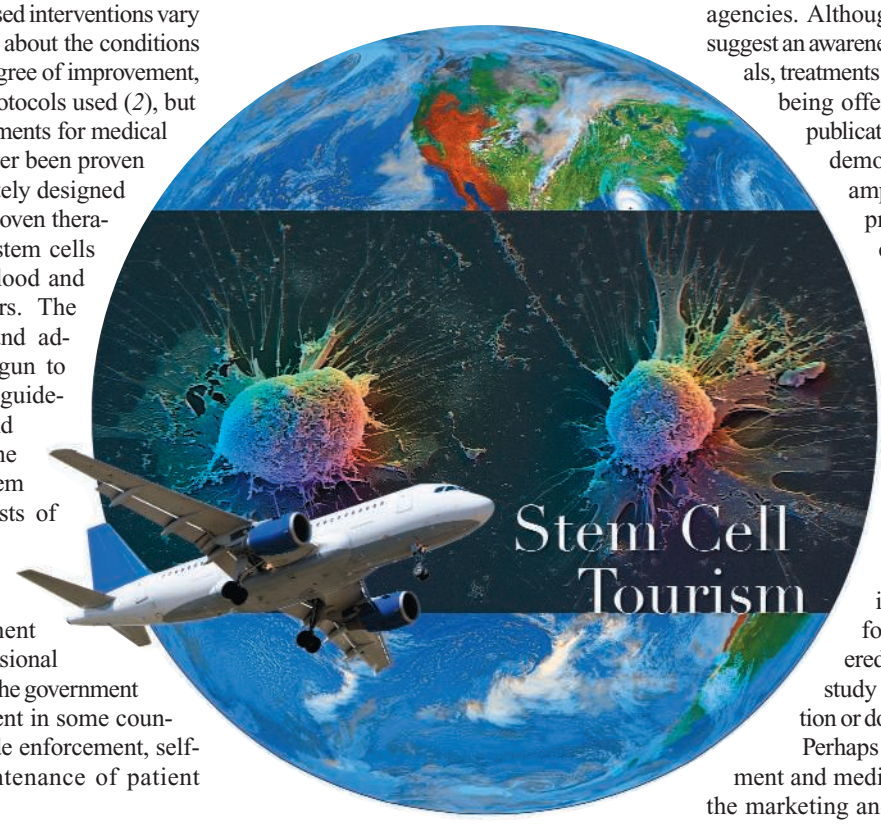

Controversies involving unverified medical treatments are not a new thing, but the adoption of protective laws and their vigorous enforcement has enabled many countries, including the United States, to rein in claims that can legally be made by providers or to relegate them to operating outside of their borders. The possibility of operating extraterritorially has meant that unapproved treatments could be had by those willing to travel abroad, but in the great majority of instances, this has meant to countries not known as leaders in biomedical research (e.g., despite more than 30 years of legal actions in the United States against purveyors of laetrile, a discredited cancer remedy, it remains readily available in places such as Mexico and the Bahamas).

The debate over human embryonic stem cell research in the United States under the George W. Bush administration not only opened the door to increased investment into stem cell research and its applications by Asian countries (*5*–*7*), but may have also distracted regulatory attention from the growing problem of unsubstantiated therapeutic claims involving adult stem cells. Nonetheless, several stem cell clinics have been closed by law enforcement or regulatory agencies in the United States (*8*), the Netherlands (*9*), and Ireland (*10*); others have been forced out of business (*11*) or prevented from opening by negative publicity (*12*, *13*).

Successful clinics that remain in business are sometimes supported by local medical associations, governments, and regulatory agencies. Although the company Web sites suggest an awareness of the need for clinical trials, treatments costing $20,000 or more are being offered in the absence of prior publication of peer-reviewed studies demonstrating efficacy. For example, TheraVitae has an impressive list of Thai physicians, including the current presidents of the Thai Heart Association and the Thai Atherosclerosis Society (*14*), and recognition from the Davos-based World Economic Forum as a 2006 Technology Pioneer (*15*). However, the peer-reviewed article listed by the company as "accreditation" for its therapeutic regime of adult stem cell therapy for heart disease was considered by the authors to be a safety study and did not use randomization or double-blind controls (*16*, *17*).

Perhaps as important as the government and medical establishment links are the marketing and patient recruitment strategies used by these companies. A number of companies, such as NuTech Mediworld, a human embryonic stem cell clinic, and Medra, Inc. (www.medra.com/), which uses human fetal cells, have enjoyed publicity in the form of published interviews, blogs, or YouTube videos describing subjective patient experiences following treatment (*18*, *19*). TheraVitae, and its associated companies VesCell (www.vescell.com/) and Regenocyte (www.regenocyte.com/), use online patient testimonials (*14*), blogging activity (*20*), and patient recruitment seminars held within the United States (*21*). Beike Biotechnology and other China-based treatment centers have a vocal proponent in the *China Stem Cells News*' Web site (www.stemcellschina.com/), which serves as an online portal highlighting

[1]Department of Obstetrics and Gynecology, Faculty of Medicine, Chulalongkorn University, Bangkok, Thailand 10330. [2]Vincent Center for Reproductive Biology, Vincent Obstetrics and Gynecology Service, Massachusetts General Hospital/Harvard Medical School, Boston, MA 02114, USA. [3]Science, Technology and Globalization Project/Science, Technology and Public Policy Program, Belfer Center for Science and International Affairs, John F. Kennedy School of Government, Harvard University, Cambridge, MA 02138, USA. [4]RIKEN Center for Developmental Biology, Kobe, 650-0047, Japan. [5]Center for iPS Research and Application, Institute for Integrated Cell-Materials Sciences, Kyoto University, Kyoto, 606-8501, Japan.

*Author for correspondence. E-mail: sipp@cdb.riken.jp

news and treatment experiences from local and foreign patients. The site lists dozens of subjective accounts of "successful" (typically defined as "some improvement") outcomes in people suffering conditions including autism, epilepsy, and stroke and includes a contact form for those with treatment inquiries.

Major research nations have also seen the appearance of stem cell clinics and therapeutics companies. Companies in Japan advertise stem cell–based treatments for conditions such as diabetes, Alzheimer's disease, and spinal cord injury (*22*–*25*). The X-cell Center (www.xcell-center.com/) in Cologne, Germany, offers to treat ailments ranging from erectile dysfunction to amyotrophic lateral sclerosis (ALS). Adult stem cells as a treatment modality have been championed with particular fervor by numerous groups in the United States, which commonly cite lists of many conditions that have been treated with adult cells (*26*, *27*). Such catalogs may introduce doubts and misunderstandings about the current state of the science.

Companies such as Medra, Stemedica (www.stemedica.com/), Stem Cell Biotherapy (www.stemcellbiotherapy.com/cn/index.php/lang/en), and Regenocyte have taken advantage of the resulting confusion and have occupied the current international regulatory vacuum. For example, Stem Cell Biotherapy and Regenocyte advertise procedures unavailable in the United States and arrange for patients to be sent to affiliated hospitals in other parts of the world. Of these, Medra became particularly notorious for the extraordinary claims made by its founder, psychiatrist William Rader, who has refused to share information on cell lines and techniques he claims can be used for treatment of conditions including spinal cord injury and Down syndrome (*28*).

There are several effective measures to prevent companies from going too far in their business practices. In the United States, the Food and Drug Administration provides clear rules governing the purity, potency, and quality of medical products (including stem cells) (*29*); the Federal Trade Commission oversees truth in advertising (*30*). Similar laws and authorities are in place in the European Union, and Thailand is now making moves to regulate stem cell therapies more tightly. A committee convened by the Thai Medical Council, which governs practice by licensed physicians, has drafted recommendations that call for stricter oversight of procedures involving stem cells in conditions other than blood disorders (*31*). These only came following a period of confusion as stem cells were seen as neither drug nor typical medical treatment, which put them for a time outside the purview of both the medical and drug-regulatory authorities. Such researcher-led efforts are to be encouraged and promulgated to regulatory agencies in other Asian countries as effective means of protecting patients as well as the national reputation.

Media reports can also play an important role. An *L.A. Times* feature on Biomark International (*32*) raised public doubts about the company. A series of BBC documentaries revealed a trade in which human fetuses from the Ukraine were sold to stem cell tourism clinics in the Caribbean, which resulted in the closing of at least one major clinic, the Institute for Regenerative Medicine in Barbados, owing to loss of its clients (*11*). To ensure the truly global dissemination of guidelines and patient information regarding stem cell–based clinical applications, the international research community, represented by organizations such as the International Society for Stem Cell Research, could provide local language translations or summaries of relevant documents and could use their members to distribute them to the press and government authorities. The World Health Organization could also contribute by releasing a consensus position on the clinical application of stem cell research.

Patient advocacy groups have begun to compile useful resources of physicians and hospitals offering stem cell procedures for conditions such as ALS (*33*). Although these serve only as anecdotal evidence, they tend to offer more balanced accounts, citing both positive and negative experiences, and may help to flag especially flagrant violators of patient trust. Stem cell and regenerative medicine research organizations might likewise consider steps toward identifying and dealing with members who have commercialized unproven treatments prematurely. Educational alliances between basic research, clinical, and patients groups, such as the Coalition for the Advancement of Medical Research, might prove to be an effective measure against the more egregious claims.

To ensure that the potential of stem cell research has the chance to develop unhampered by tragedy or fraud, members of the research community must work together to lobby their own local authorities to put proper regulations in place and must accept as their duty following the hard road to the truth, not the most expedient or profitable one. Given the current limits of international law and scientific diplomacy, a global ban on unapproved treatments seems unlikely to succeed, so for now, each government must take great care when granting funds and recognition to programs that fall short of ethical or professional standards. And ultimately, those who look to stem cells with hope for cures must also share in the obligation to protect this nascent field by becoming not only patient advocates, but also advocates of patience.

References and Notes

1. N. Amariglio *et al.*, *PLoS Med.* **6**, e29 (2009).
2. D. Lau *et al.*, *Cell Stem Cell* **3**, 591 (2008).
3. International Society for Stem Cell Research, *Guidelines for the Clinical Translation of Stem Cells* (ISSCR, Deerfield, IL, 4 December 2008); www.isscr.org/clinical%5Ftrans/.
4. Juvenile Diabetes Research Foundation International, *Participating in a Clinical Trial*; www.jdrf.org/index.cfm?fuseaction=home.viewPage&page_id=91EC2BF7-1321-C844-134D2E25FB931863.
5. B. Einhorn, J. Veale, M. Kripalani, *Business Week*, 10 January 2005, p. 34; www.businessweek.com/magazine/content/05_02/b3915052.htm.
6. J. Du *et al.*, *Stem Cell Mission to China, Singapore and South Korea* (for the U.K. Department of Trade and Industry, Pera Innovation, London, 2005); www.oti.globalwatchonline.com/online_pdfs/36206MR.pdf.
7. D. Sipp, *Stem Cell Report* **2**, 62 (2007).
8. M. Enserink, *Science* **313**, 160 (2006).
9. The Netherlands Health Care Inspectorate, Utrecht, 3 October 2006; www.igz.nl/uk/files/379598.
10. S. Boseley, *Guardian*, 1 May 2006; www.guardian.co.uk/society/2006/may/01/health.medicineandhealth.
11. S. Price, *Nation News* (Barbados), 26 November 2007; http://web.archive.org/web/20080128173958/http://www.nationnews.com/story/315095110731643.php.
12. "Stem cell firm drops Bermuda from website," *Royal Gazette*, 18 August 2008; www.theroyalgazette.com/siftology.royalgazette/Article/article.jsp?sectionId=60&articleId=7d8893730030003.
13. M. Ebbin, *Bermuda Sun*, 14 September 2007; www.bermudasun.bm/main.asp?SectionID=24&SubSectionID=270&ArticleID=34993.
14. TheraVitae, www.vescell.com/stem-cells-treating-physicians.php.
15. World Economic Forum, www.weforum.org/en/Communities/Technology%20Pioneers/SelectedTechPioneers/2006TechPioneers/index.htm.
16. Y. Porat *et al.*, *Br. J. Haematol.* **135**, 703 (2006).
17. K. V. Arom, P. Ruengsakulrach, V. Jotisakulratana, *Asian Cardiovasc. Thorac. Ann.* **16**, 143 (2008).
18. A. Boxtel, http://amandaboxtel.wordpress.com/.
19. R. Kilgore, http://jp.youtube.com/watch?v=kbozmOL1kSY.
20. J. Steele, *VesCell Adult Stem Cell Therapy Blog*, 19 December 2007; http://stem-cell-therapy.blogspot.com/2007/12/new-adult-stem-cell-blog.html.
21. Regenocyte, http://stem-cell-therapy.blogspot.com.
22. Elixcell, www.elixcell.com/.
23. Rejuvacell, http://rejuvacell-inc.com/Our%20Group.htm.
24. Stem Cell Sciences, www.stemcellsciences.com/.
25. Nichi-In Center for Regenerative Medicine, www.nichiin.org/.
26. D. Prentice, in *Monitoring Stem Cell Research: A Report of the President's Council on Bioethics* (President's Council on Bioethics, Washington, DC, 2004), Appendix K.
27. Repair Stem Cell Institute, www.repairstemcells.org/DiseaseTreated.php.
28. D. Ono, KABC-TV news, Los Angeles, 2007; http://abclocal.go.com/kabc/story?section=news/local&id=5283114.
29. D. G. Halme, D. A. Kessler, *N. Engl. J. Med.* **355**, 1730 (2006).
30. U.S. Federal Trade Commission, *Frequently Asked Advertising Questions: A Guide for Small Businesses*; www.ftc.gov/bcp/edu/pubs/business/adv/bus35.shtm.
31. Editorial, *Bangkok Post*, 22 June 2008; www.bangkokpost.com/220608_Perspective/22Jun2008_pers007.php.
32. A. Zarembo, *Los Angeles Times*, 20 February 2005; www.latimes.com/features/health/medicine/la-sci-stemcells20feb20,1,3062179,full.story.
33. S. Byer, B. Byer, ALS Worldwide, Madison, WI; www.alsworldwide.net.

10.1126/science.1168451

MATERIALS SCIENCE

Flexible Electronics

Inkjet printing of metal wires yields bendable electrical connections for use in flexible electronic devices.

Byron D. Gates

Organic polymers are the main components of most flexible electronic devices. These devices rely on the compliant physical properties of organic polymers to maintain electrical continuity when deformed. Electrical connections within these devices are a point of weakness and have limited the types of materials and processes that can be used. Although inorganic semiconductors and metals have high conductivity, these materials will not commonly sustain repeated bending or stretching. On page 1590 of this issue, Ahn *et al.* (*1*) show how metal can be added to components within flexible electronic devices, enabling conductivity to be maintained even after repeated deformation.

Connections between electronic structures have traditionally been designed with a planar architecture that is patterned through multiple fabrication steps (*2*, *3*). Much of the fabrication technology used in flexible electronics was initially borrowed from existing device fabrication platforms, such as those used to manufacture silicon-based thin-film transistors. These techniques largely depend on the selective liftoff or etching of materials, using process conditions that are not always compatible with organic polymers. Process techniques developed for the fabrication of flexible electronic devices must avoid large changes in temperature and pressure. These techniques must also minimize exposure to reagents that may degrade the conductivity, purity, or form of the organic polymer components in the device.

Inkjet printing has been used to pattern organic semiconductors (*4*), metal contacts on organic semiconductors (*5*–*7*), and metallic structures (*8*) that require minimal further processing. Ahn *et al.* have now used inkjet printing to create three-dimensional (3D) metallic connections between functional components of flexible devices (see the figure). The authors first fine-tuned a colloidal ink of silver nanoparticles by adjusting the uniformity of the particles, the viscosity of the ink, and the drying time of the solvents. They then extruded the ink through a nozzle that directed the selective deposition of silver particles onto the flexible substrate. After annealing at 250°C for ≤30 min, the printed wires exhibited an electrical resistivity nearing that of bulk silver. Annealing can also be done using light or microwaves (*9*, *10*). The resistivity of the printed silver wires is about two orders of magnitude lower than that of commonly used conductive organic polymers (*1*). This improvement translates into lower power consumption and a lower heat load on the surrounding environment for devices incorporating these printed wires.

Controlling the deposition of the colloidal silver ink is essential for fabricating free-standing wires that have both 2D and 3D components. The electrical connections demonstrated by Ahn *et al.* include springs and structures with built-in slack to accommodate the stretching and bending of a flexible device. The ability to form arched features is also essential for avoiding direct contact when one electrical connection crosses over another.

The authors further demonstrate the control provided by their technique by reporting silver wires with width-to-length ratios up to 1:1000. These wires can span gaps up to 1 cm wide. The narrow dimensions of the printed wires (from ~2 to ~10 μm) are an additional benefit of this fabrication process. These small dimensions minimize the footprint of the electrical contact lines, which decreases the impact of the wires on the optical quality of the device and increases the density of features in the device. Although inkjet printing is a serial process, Ahn *et al.* have demonstrated a wide range of benefits for this technology.

Flexible electronic devices compete with paper-based media as well as existing electronic media. It is desirable to find a technology platform that can be rolled or bent (as with paper), yet robust enough to be unfurled and reused. The end use of the device will depend on the functions incorporated into its architecture. Ahn *et al.* demonstrate a few features that might be desirable in a flexible device, including optical and optoelectronic components such as light-emitting diodes (LEDs) and solar cells. Tuning the optical properties of a flexible device is widely recognized as necessary, with research efforts directed toward both emissive and reflective properties (*2*, *3*, *11*). Other applications of flexible device technology include radio frequency identification (RFID) tags and antennas that can be incorporated into personal identification, as well as packaging and other forms of transferable media.

Traditional forms of print media, such as newspapers and books, have been prevalent in human lives for centuries. We have greatly benefited from the ease with which information can be efficiently distributed in print media. Entire industries have been created around the printing, distribution, and storage of paper articles. Overcoming our dependence on paper will require its replacement with a technology that is comparable to paper in its weight, flexibility, and ease of use. Key technologies are necessary to enable the manufacture of such an alternative form of media. The work of Ahn *et al.* is a transition from typical models of fabrication, providing possibilities

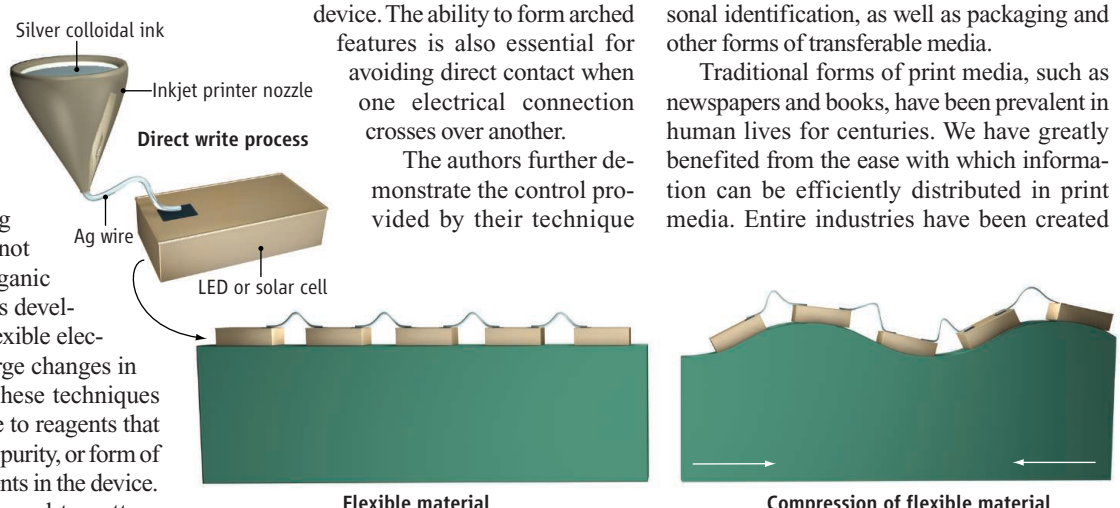

Flexible electrical metal connections. Wires connecting components within a flexible device can be fabricated by a direct-write process using inkjet printing of silver nanoparticles. As shown by Ahn *et al.*, the technique can be used to fabricate three-dimensional connections that span between components of a flexible device and that flex when the device is deformed.

Department of Chemistry, Simon Fraser University, Burnaby, British Columbia V5A 1S6, Canada. E-mail: bgates@sfu.ca

Published by AAAS

for incorporating multiple functions into a single flexible device.

Flexible electronic devices are becoming commonplace in our lives. Screens that can flex or otherwise distort have been incorporated into laptops, televisions, and mobile phones. Lightweight electronic display devices that can be rolled up for storage are being developed. The achievement of completely converting to a paperless society will be revolutionary in itself, but so are the technological advances necessary to make this new form of media commonplace in our daily lives.

References

1. B. Y. Ahn *et al.*, *Science* **323**, 1590 (2009); published online 12 February 2009 (10.1126/science.1168375).
2. S. R. Forrest, *Nature* **428**, 911 (2004).
3. E. Menard *et al.*, *Chem. Rev.* **107**, 1117 (2007).
4. H. Sirringhaus *et al.*, *Science* **290**, 2123 (2000).
5. Y. Nogucki, T. Sekitani, T. Yokota, T. Someya, *Appl. Phys. Lett.* **93**, 043303 (2008).
6. D. Kim, S. Jeong, H. Shin, Y. Xia, J. Moon, *Adv. Mater.* **20**, 3084 (2008).
7. S. Gamerith *et al.*, *Adv. Funct. Mater.* **17**, 3111 (2007).
8. J. E. Smay, J. Cesarano III, J. A. Lewis, *Langmuir* **18**, 5429 (2002).
9. J. Yun *et al.*, *Jpn. J. Appl. Phys.* **47**, 5070 (2008).
10. J. Perelaer, B.-J. de Gans, U. S. Schubert, *Adv. Mater.* **18**, 2101 (2006).
11. B. Comiskey, J. D. Albert, H. Yoshizawa, J. Jacobson, *Nature* **394**, 253 (1998).

10.1126/science.1171230

IMMUNOLOGY

Two-in-One Designer Antibodies

An antibody is engineered to recognize two different proteins with high affinity, opening the door to improved combination therapies for cancers and infections.

Paul W. H. I. Parren[1] and Dennis R. Burton[2]

Cancer and certain infectious diseases such as HIV-1/AIDS that are characterized by genetic heterogeneity are often difficult to treat with a single therapeutic agent. Combination therapies that target multiple disease-associated molecules are therefore widely deployed. For example, mixtures of antibodies are being tested for clinical use, despite high development, manufacturing, and treatment costs. The requirement for multiple antibodies is based on the prevailing one antibody-one antigen dogma. On page 1610 in this issue, Bostrom *et al.* (*1*) overthrow this dogma and describe a new "two-in-one" designer antibody concept in which the same binding site on an antibody is engineered to recognize two different antigens, both with high affinity.

The two antigens studied by Bostrom *et al.* are vascular endothelial growth factor (VEGF) and human epidermal growth factor receptor 2 (HER2), representing well-known tumor targets. VEGF promotes blood-vessel formation for the growing tumor and is targeted by the antibody bevacizumab (Avastin), commonly used to treat colorectal cancer. HER2 is highly expressed by some breast tumors and is targeted by the antibody trastuzumab (Herceptin). The authors show that an engineered antibody binds tightly to both antigens and inhibits the growth of both VEGF- and HER2-dependent tumors in animal models. The potential applications of the approach will need very careful exploration but will surely have far-reaching impact.

Bostrom *et al.* generated the two-in-one antibody by expressing the HER2-specific antibody trastuzumab on the surface of filamentous bacteriophage. Random nucleotide sequence was incorporated into the gene segments encoding the antigen-binding loops of the light chain to generate a large phage library. The library was selected for binding to HER2 and VEGF to generate a panel of two-in-one antibodies of varying affinity.

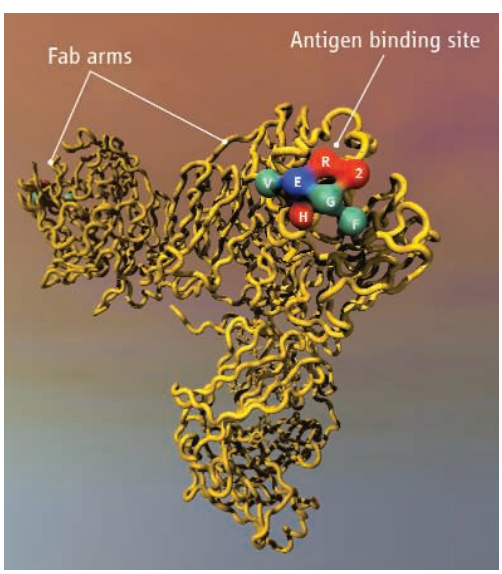

Two for the price of one. An antibody consists of four polypeptides, two heavy and two light chains, that form two "Fab arms." Each arm harbors an antigen binding site, formed by loops from the heavy and light chains. The binding site in the two-in-one antibody shown can interact with HER2 (red) and VEGF (green) through mostly unique, but also some shared (blue), elements. When affinity-matured, the antibody inhibits both HER2 and VEGF activity in vitro and in vivo. The source of the structure shown is antibody IgG1 b12 (*16*), RCSB PDB accession code 1HZH. The molecule was rendered using VMD software and further modeled with 3D software (Bryce 6.1). Refining and colors were done with Adobe Photoshop CS3.

High-resolution crystal structures of one of these antibodies in complex with either VEGF (dissociation constant K_d = 300 nM) or HER2 (K_d = 26 nM) were solved to elucidate the mechanism of "two-in-one" binding at the molecular level. The binding surface on the antibody for each antigen overlapped, but within the buried surface of each binding site, distinct amino acids contributed to the binding strength for each antigen: VEGF binding was primarily mediated by light-chain residues and HER2 binding by heavy-chain residues. The overlapping binding areas indicate that each antibody binding site cannot bind both antigens simultaneously (see the figure). The antibody binding sites in the two-in-one antibody are therefore selectively promiscuous; each can interact with two different partners, but will only bind to one at a time. For subsequent studies, an affinity improved two-in-one antibody (VEGF K_d = 3nM, HER2 K_d = 0.2 nM) was generated.

Approaches to generate antibody molecules with multiple binding moieties have been tried before, with varying success. Such molecules were engineered by "fusing" two or more antibody binding sites into a single molecule to increase binding avidity or bind multiple antigens (*2*, *3*). Antibodies binding two antigens can also be generated by Fab arm exchange, which occurs naturally in vivo for immunoglobulin G4 molecules (*4*), or can be created in vitro by cell fusion or antibody engineering (*5*). Antibodies in which two binding sites recognizing distinct antigens are connected to a single Fab arm represent another permutation (*6*). An example that is perhaps the closest comparable break with the one antibody–one antigen dogma comes from chemically

[1]Genmab, Yalelaan 60, 3584 CM Utrecht, Netherlands. [2]Department of Immunology and Microbial Science and IAVI Neutralizing Antibody Center, The Scripps Research Institute, La Jolla, CA 92037, USA. E-mail: p.parren@genmab.com, burton@scripps.edu

programmed antibodies in which antigen recognition is modified by the insertion of different ligands into the antibody binding site via a common reactive group (*7*). The beauty of the two-in-one molecule created by Bostrom *et al.* is its simplicity. For the first time, dual specificity has been engineered into a naturally occurring and stable antibody isotype that should pose no obstacles for manufacturing and that has been well validated for clinical use.

Two-in-one antibodies may replace combination therapies such as treatment of cancer with both bevacizumab and trastuzumab, which is currently in clinical trials. A practical limitation to this approach may be an inflexibility of dosing where optimal doses are discordant for the individual antigens targeted. A strong caveat comes from two recent studies that investigated the use of bevacizumab and chemotherapy in combination with either cetuximab (Erbitux) or panitumumab (Vectibix) [antibodies that inhibit epidermal growth factor receptor (EGFR)] for treating metastatic colorectal cancer (*8*, *9*). The studies showed that adding either of these antibodies to bevacizumab (plus chemotherapy) worsened clinical outcomes. These effects were unexpected because the antibody combinations had shown promise in the preclinical setting.

Two-in-one antibodies could also be used to target two nonoverlapping epitopes on the same antigen. Such antibodies would have a greater potential for aggregating targets than classical antibodies. For combinations of either EGFR or HER2 monoclonal antibodies (*10*, *11*), for example, such aggregation increases anti-tumor effects. The presence of two or more binding sites against distinct epitopes on a soluble antigen furthermore has the potential to increase binding avidity and in vivo potency (*12*).

The ability of antibodies to bind multiple antigens is, in itself, not a novel finding and has been described, for example, for the low-affinity binding of dissimilar peptides to distinct regions in a single antibody binding site (*13*). Indeed, by harboring multiple, spatially separated, binding sites in a single structure, antibodies may exploit a mechanism that has been recognized as a major source for multispecificity of proteins (*14*, *15*). The uniqueness of the work of Bostrom *et al.* is to show that promiscuous binding of antibodies is compatible with the high-affinity, pharmacologically relevant, binding of very different antigens. Promiscuous binding may even extend to natural immunity where it would represent a mechanism to maximally cover binding space by a given repertoire of antibodies. Cross-reactive antibodies, when isolated, are generally considered a nuisance and two-in-one antibodies may therefore have been overlooked. The increased availability of technologies for rapid and large-scale screening of antibody-antigen interactions should help identify promiscuous antibodies. The potential for high-affinity antibody binding of more than one antigen is intriguing and poses opportunities for future basic research and perhaps clinical development of antibody combination therapy.

References and Notes

1. J. Bostrom *et al.*, *Science* **323**, 1610 (2009).
2. P. J. Hudson, C. Souriau, *Nat. Med.* **9**, 129 (2003).
3. D. Neri, M. Momo, T. Prospero, G. Winter, *J. Mol. Biol.* **246**, 367 (1995).
4. M. van der Neut Kolfschoten *et al.*, *Science* **317**, 1554 (2007).
5. P. Carter, *Nat. Rev. Cancer* **1**, 118 (2001).
6. C. Wu *et al.*, *Nat. Biotechnol.* **25**,1290 (2007).
7. F. Guo *et al.*, *Proc. Natl. Acad. Sci. U.S.A.* **103**, 11009 (2006).
8. J. R. Hecht *et al.*, *J. Clin. Oncol.* **27**, 672 (2009).
9. J. Tol *et al.*, *N. Engl. J. Med.* **360**, 563 (2009).
10. M. Dechant *et al.*, *Cancer Res.* **68**, 4998 (2008).
11. T. Ben-Kasus, B. Schechter, S. Lavi, Y. Yarden, M. Sela, *Proc. Natl. Acad. Sci. U.S.A.* **106**, 3294 (2009).
12. A. Nowakowski *et al.*, *Proc. Natl. Acad. Sci. U.S.A.* **99**, 11346 (2002).
13. D. K. Sethi, A. Agarwal, V. Manivel, K. V. Rao, D. M. Salunke, *Immunity* **24**, 429 (2006).
14. R. A. Mariuzza, *Immunity* **24**, 359 (2006).
15. I. Nobeli, A. D. Favia, J. M. Thornton, *Nat. Biotechnol.* **27**, 157 (2009).
16. E. O. Saphire *et al.*, *Science* **293**, 1155 (2001).
17. P. Parren is part of the management team of Genmab, a public company that develops human therapeutic antibodies including those against Her2 and VEGF. He is a named inventor on patents issued by Genmab. Amgen, Inc. is among Genmab's partners.

10.1126/science.1172253

MOLECULAR BIOLOGY

Dynamic DNA Methylation

The methylation of DNA during plant development is a much more dynamic process than previously assumed.

Julie A. Law[1] and Steven E. Jacobsen[1,2]

The silencing of gene expression through the methylation of cytosine nucleotide bases in DNA is observed in a wide variety of eukaryotic organisms. It occurs mainly at repetitive elements of genomes, and plays a critical role in silencing transposable elements (transposons). Its heritability is a key aspect of DNA methylation as a stable epigenetic mark of gene repression. However, two studies, by Teixeira *et al*. on page 1600 in this issue (*1*) and Slotkin *et al*. (*2*), show that DNA methylation and gene silencing can be much more dynamic than previously thought.

In the model plant *Arabidopsis thaliana*, three different methylation systems maintain cytosine methylation in three different sequence contexts: CG [cytosine (C); guanine (G)], CHG [H is adenine (A), thymine (T), or cytosine (C)], and CHH (*3*). CG methylation is controlled by DNA METHYLTRANSFERASE 1 (MET1) and VARIANT IN METHYLATION 1 (VIM1) (*4*). The mammalian homolog of VIMI (UHRF1) recognizes hemimethylated CG DNA and facilitates its restoration to the fully methylated state (*5*, *6*). Another critical factor is the chromatin-remodeling protein DECREASED DNA METHYLATION 1 (DDM1), whose mutation causes massive losses of methylation (*7*), and reactivates transposons (*8*). CHG methylation is maintained by the plant-specific CHROMOMETHYLASE 3 (CMT3), and KRYPTONITE (SUVH4), a histone protein methyltransferase. CMT3 binds to methylated histones (chromatin-associated proteins) and KRYPTONITE binds to methylated CHG sites, thereby creating a feedforward loop for maintaining CHG methylation (*9*). CHH methylation is controlled by a third DNA methyltransferase, DOMAINS REARRANGED METHYLTRANSFERASE 2 (DRM2). DRM2 is guided to its DNA targets by 24-nucleotide small interfering RNAs (siRNAs) in a pathway called RNA-directed DNA methylation (*9*, *10*). In addition to maintaining CHH methylation, the RNA-directed DNA methylation pathway also controls the establishment of DNA methylation in all sequence contexts (*11*).

Although the details of these methylation systems are being quickly fleshed out, much less is known about the extent to which they are acting throughout plant development. Teixeira *et al*. show that some regions of the *Arabidopsis* genome can be efficiently

[1]Department of Molecular, Cell and Developmental Biology, University of California, Los Angeles, Los Angeles, CA 90095, USA. [2]Howard Hughes Medical Institute, University of California, Los Angeles, Los Angeles, CA 90095, USA. E-mail: jacobsen@ucla.edu

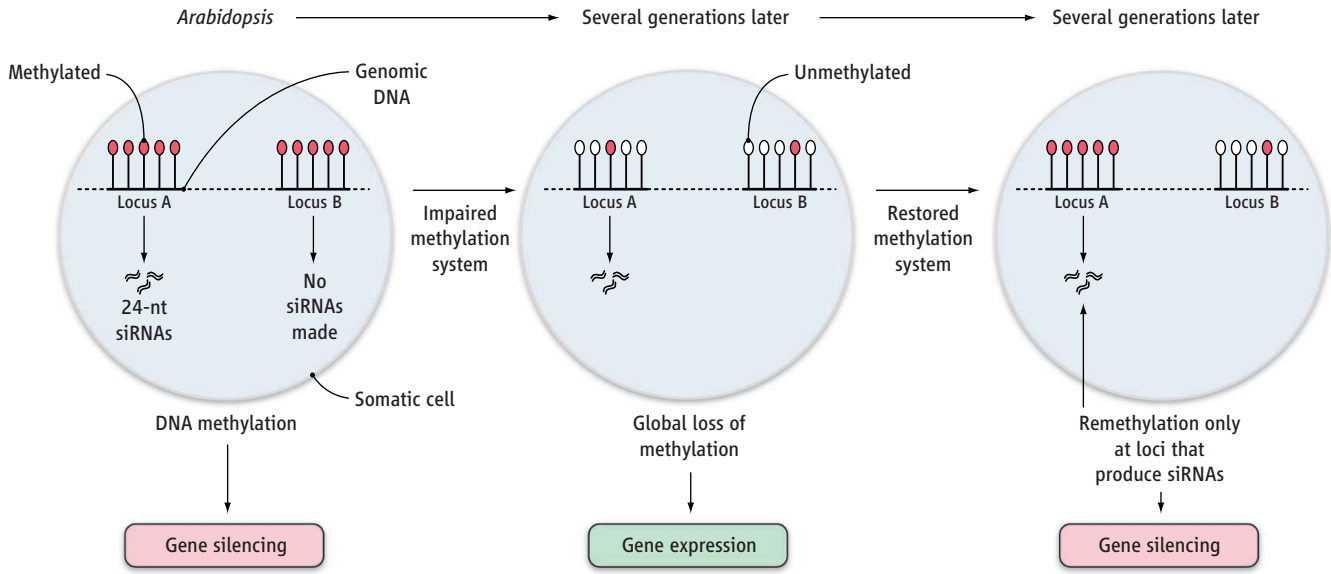

Silenced, again. DNA methylation that is lost in previous generations (for example, through mutation of a gene required for methylation) can be restored in subsequent generations when a gene encoding the wild-type version of the protein is reintroduced. However, remethylation is restricted to loci that produce siRNAs, and depends on the RNA-directed DNA methylation pathway. SiRNAs can thus selectively correct methylation defects to enforce silencing. nt, nucleotide.

remethylated if methylation was lost in previous generations. Using *ddm1* mutants, which display a global reduction in DNA methylation, the authors investigated whether DNA methylation can be restored after a wild-type *DDM1* is reintroduced. Roughly half the sequences they examined regained methylation, thus reestablishing gene silencing. Complete remethylation was observed only after several generations, consistent with the multigenerational nature of transgene silencing known for plants.

The loci that became remethylated were characterized by the presence of high amounts of siRNAs, whereas loci that remained unmethylated lacked siRNAs (see the figure). Furthermore, reestablishing methylation required RNA-DEPENDENT RNA POLYMERASE 2, a key component of the RNA-directed DNA methylation pathway. Most siRNAs correspond to transposons and other highly repetitive DNA, which if expressed could lead to genome instability. Thus, the ability to specifically remethylate these sequences is likely beneficial in a multigenerational manner to reinforce silencing and to correct defects in methylation patterning that might otherwise lead to transposon activation.

In mammals, DNA methylation is dynamic during development, and examples include gene-specific imprinting as well as genome-wide changes in some cell types (*12*). *Arabidopsis* and other flowering plants imprint specific genes by selective demethylation of promoters in the endosperm (nutritive tissue in seeds of plants) (*9*), but whether methylation patterns are altered globally in different plant tissues or cell types has been unclear. Slotkin *et al*. (*2*) report that the vegetative nucleus of *Arabidopsis* pollen cells shows a global loss of gene silencing, coupled with reactivation of transposon expression. Pollen contain three nuclei: the vegetative nucleus, which powers the cell; a sperm nucleus, which fertilizes the egg to form the zygote; and a second sperm nucleus, which fertilizes the central cell in the ovule to form the endosperm.

By comparing data from pollen with that of isolated sperm nuclei, Slotkin *et al*. (*2*) deduced that the vegetative nucleus was the location of transposon activation. Further, although new transposition events were detected in pollen, they were not inherited, again suggesting that transposon reactivation occurs in the vegetative nucleus, which does not contribute DNA to the zygote. Transposon reactivation was coupled with decreased expression of *DDM1*, and several genes that control RNA-directed DNA methylation, as well as reduced numbers of 24-nucleotide siRNAs. Interestingly however, a different class of transposon-related siRNAs (21 nucleotides in length) accumulates in pollen. The authors propose that these 21-nucleotide siRNAs, originating in the vegetative nucleus, may travel to the adjacent sperm cells to reinforce silencing, perhaps in a manner akin to that shown by Teixeira *et al*. for the remethylation of hypomethylated DNA in somatic tissue. Thus, only those transposons with the potential to be expressed (because they were expressed in the vegetative nucleus) would be targeted by siRNAs in sperm nuclei.

The results of Slotkin *et al.* raise the question of whether similar processes occur in the *Arabidopsis* female gametophyte—for instance, if loss of silencing in the central cell might cause reinforcement of silencing in the egg cell. There are also interesting parallels with the siRNA-mediated communication between nuclei seen in *Tetrahymena thermophila*, where small RNAs generated from the micronucleus target chromatin modifications (and eventually DNA deletion) to homologous genomic DNA sequences in the developing new macronucleus (*13*). In the future, it will be important to assess the extent to which the dynamic processes uncovered by these recent findings are utilized in other aspects of eukaryotic development.

References

1. F. K. Teixeira *et al.*, *Science* **323**, 1600 (2009); published online 29 January 2009 (10.1126/science.1165313).
2. R. K. Slotkin *et al.*, *Cell* **136**, 461 (2009).
3. S. W. Chan, I. R. Henderson, S. E. Jacobsen, *Nat. Rev. Genet.* **6**, 351 (2005).
4. H. R. Woo, O. Pontes, C. S. Pikaard, E. J. Richards, *Genes Dev.* **21**, 267 (2007).
5. M. Bostick *et al.*, *Science* **317**, 1760 (2007).
6. J. Sharif *et al.*, *Nature* **450**, 908 (2007).
7. A. Vongs, T. Kakutani, R. A. Martienssen, E. J. Richards, *Science* **260**, 1926 (1993).
8. H. Hirochika, H. Okamoto, T. Kakutani, *Plant Cell* **12**, 357 (2000).
9. I. R. Henderson, S. E. Jacobsen, *Nature* **447**, 418 (2007).
10. B. Huettel *et al.*, *Biochim. Biophys. Acta* **1769**, 358 (2007).
11. S. W. Chan *et al.*, *Science* **303**, 1336 (2004).
12. W. Reik, *Nature* **447**, 425 (2007).
13. K. Mochizuki, M. A. Gorovsky, *Curr. Opin. Genet. Dev.* **14**, 181 (2004).

10.1126/science.1172782

PHYSICS

Fullerides in a Squeeze

The superconducting behavior of very different materials—fullerides and cuprates—could have more in common than previously believed.

Erio Tosatti

Before the discovery of cuprate superconductors, superconducting metals and Mott insulators—would-be metals turned insulating by repulsion between electrons—seemed to have nothing to do with one another. Yet in cuprates, superconductivity popped up by simply doping Mott insulators with some impurities (see the figure, panels A and B), opening up perhaps the most controversial physics field of the past 25 years. As Takabayashi *et al.* show on page 1585 of this issue (*1*), pressure works very much the same feat in a completely different material: the hyperexpanded body-centered-cubic A15-structured fulleride Cs_3C_{60}, an insulator that is turned into a superconductor by giving it a light squeeze. What else, if anything, do cuprates and fullerides have in common? And if they do, could one of them teach us something about the other?

In fullerides, electron-donating alkali atoms are regularly interspersed in a lattice of C_{60} molecules (see the figure, panel C). The donated electrons are mobile between one C_{60} molecule and the next, turning the whole system into a metal. Upon cooling, these metallized fullerene crystals turn superconducting, and they do so at respectably high critical temperatures T_c of 20 to 30 K (*2*–*4*).

At first sight, this is no big deal, because superconductivity in fullerides appears similar in many ways to that of conventional superconductors and unlike that in cuprates. For example, the symmetry of electron pairs—whose condensation gives rise to superconductivity—is conventional (s-wave) in fullerides but unconventional (d-wave) in cuprates. In addition, the mechanism that glues the two electrons together to form the superconducting pair is conventional (phonon exchange) in fullerides (*3*, *4*), whereas an electronic and magnetic mechanism is more probable in cuprates, because electron correlations are strong in these systems (*5*).

However, according to proponents of the "strongly correlated superconductivity" theory, the difference between fullerides and cuprates may be more superficial than substantial (*6*, *7*). This theory identifies two basic elements that are common to fullerides and cuprates: First, the contiguity between a Mott insulating and a metallic phase; and second, some spin selective electron-electron interaction—be it phononic or electronic in origin—favoring singlet spin pairing in the insulating state.

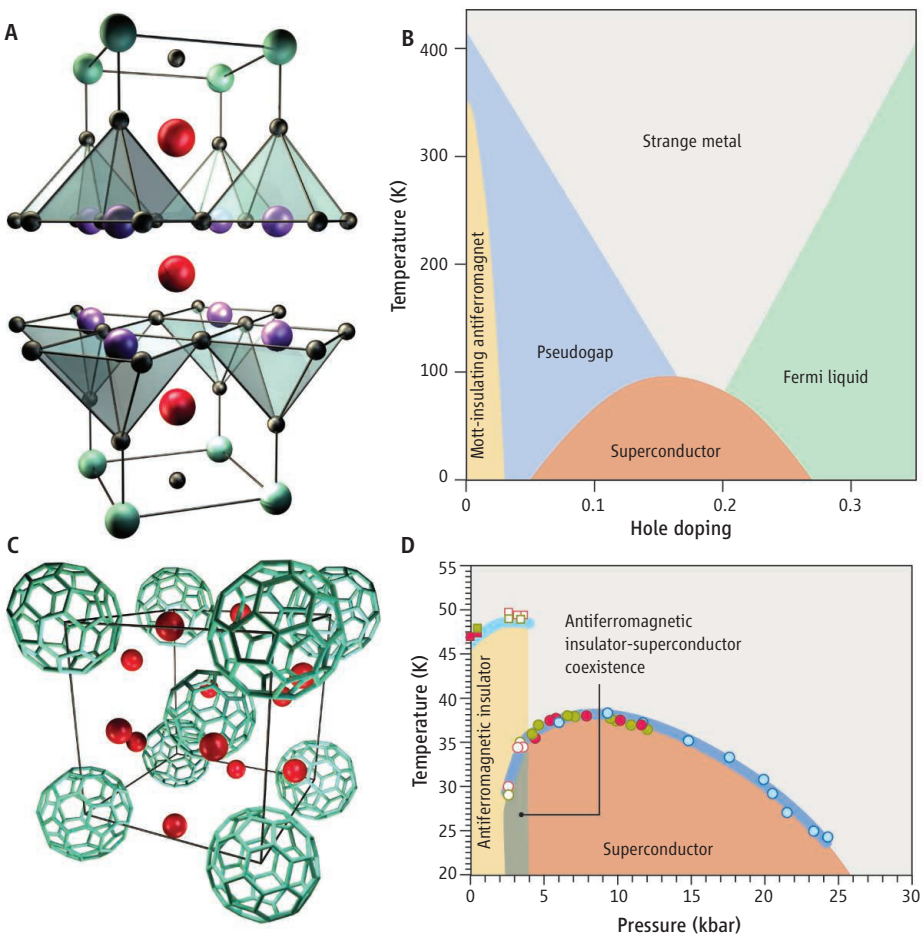

Different yet similar. Cuprates such as $Bi_2Sr_2CaCu_2O_8$+d (*13*) (**A**) show a bell-shaped dependence of superconducting transition temperature *Tc* on doping density (*14*) (**B**). Takabayashi *et al.* now report that in the fulleride A15 Cs_3C_{60} (**C**), a similar behavior can be induced through applying pressure (**D**).

It has been known for about a decade that fullerides can indeed be changed from metallic to Mott insulating by expanding the lattice. This was achieved in the past by inserting additional neutral molecules such as ammonia between the buckyballs; these molecules acted as spacers, exerting a kind of negative pressure and prying the lattice open. In these expanded compounds—exemplified by $(NH_3)K_3C_{60}$ (*8*)—theory has long shown how the role of electronic repulsion is enhanced by expansion, tilting the fine balance between metallic and Mott insulating state (*3*, *4*, *7*). The Mott insulating state is antiferromagnetic (nearest spins point opposite to one another), but the spin of each C_{60} site is only 1/2 instead of 3/2 as one might have expected for three electrons per molecule. The low spin state is due to coupling to phonon vibrations, known in molecular physics as the Jahn Teller effect. Under pressure, such a "Mott Jahn Teller" insulator (*9, 10*) should, according to theory, turn into a strongly correlated superconductor; and indeed it does (*11*). However, the lattice expansion caused by inserted molecules also changes the lattice symmetry and introduces disorder relative to the parent compound K_3C_{60}, introducing some ambiguity into the assessment of this insulator-superconductor transition.

International School for Advanced Studies and CNR-INFM Democritos National Simulation Center; and International Centre for Theoretical Physics, Trieste, Italy. E-mail: tosatti@sissa.it

Published by AAAS

The novel fulleride reported by Takabayashi *et al.* is born expanded, because the large Cs ions force the C_{60} lattice into a body-centered-cubic arrangement, which is more open than the face-centered-cubic structure of previous compounds (*12*). Takabayashi *et al*. show that the zero-pressure state of this fulleride is a true Mott Jahn Teller insulator; thus, it possesses both ingredients required by the strongly correlated theory. The insulating state is experimentally destroyed by a modest 2.5- to 4-kbar pressure—with no doping, no disorder, and no change of lattice symmetry. In the squeezed metal, magnetism disappears and is replaced by superconductivity below a T_c that rises from ~30 k at 2.5 kbar , peaks at ~38 k for 7 kbar, and then drops at higher pressure. This bell-shaped behavior (see the figure, panel D) is a general feature predicted by the strongly correlated theory (*7*) and is similar to that seen in cuprates upon doping (see the figure, panel B).

In this mapping between fullerides and cuprates, the superconducting A15 Cs_3C_{60} fulleride between 2.5 and 7 kbar corresponds to the "underdoped" cuprates (with a hole doping between 5 and 15; see the figure, panel B). Above T_c, the low-pressure fulleride normal state should, according to the strongly correlated theory, behave quite differently from the regular metal of conventional superconductors. For example, it should show a depression of electronic states near the Fermi level (a pseudogap) reminiscent of that of underdoped cuprates, and detectable, for example, through photoemission or tunneling spectroscopy.

What makes A15 Cs_3C_{60} particularly exciting is that it allows these and other predicted properties of a state claim to be akin to underdoped cuprates to be measured without the complications caused by doping, and that its properties seem easier to model and calculate than those of cuprates—and of other molecular superconductors, too (*13*). The hope is that we may finally make progress in grasping what is important and what is irrelevant in all strongly correlated superconductors, by scrutinizing and understanding the expanded fullerides.

References and Notes

1. Y. Takabayashi *et al.*, *Science* **323**, 1585 (2009).
2. A. P. Ramirez, *Superconductivity Rev.* **1**, 1 (1994).
3. O. Gunnarsson, *Rev. Mod. Phys.* **69**, 575606 (1997).
4. O. Gunnarsson, *Alkali-Doped Fullerides: Narrow-Band Solids with Unusual Properties* (World Scientific, Singapore, 2004).
5. P. W. Anderson, *Science* **235**, 1196 (1987).
6. M. Capone, M. Fabrizio, C. Castellani, E. Tosatti, *Science* **296**, 2364 (2002).
7. M. Capone, M. Fabrizio, C. Castellani, E. Tosatti, *Rev. Mod. Phys.*, in press; available at http://arxiv.org/abs/0809.0910.
8. O. Zhou *et al.*, *Phys. Rev. B* **52**, 483 (1995).
9. M. Fabrizio *et al.*, *Phys. Rev. B* **55**, 13465 (1997).
10. G. Klupp *et al.*, *Phys. Rev. B* **73**, 085415 (2006).
11. K. Prassides *et al.*, *J. Am. Chem. Soc.* **121**, 11227 (1999).
12. A. Y. Ganin *et al.*, *Nat. Mater.* **7**, 367 (2008).
13. K. Kanoda, *J. Phys. Soc. Japan* **75**, 051007 (2006).
14. B. Batlogg, C. M. Varma, *Physics World*, 33 (February 2000).
15. G.-H. Gweon *et al.*, *Nature* **430**, 187 (2004).

16. Sponsored by PRIN/Cofin 2006022847 and by the CNR-FANAS-AFRI-ESF project.

10.1126/science.1171840

MATERIALS SCIENCE

Stiffer Than Steel

A new material is as light as air and expands like rubber, yet is stiffer than steel by weight.

John D. W. Madden

The ultralow-density ribbons described by Aliev *et al* on page 1575 of this issue (*1*) have the strength and stiffness of steel by weight in one direction and are more compliant than rubber in the other two. When charged, two dimensions quickly and reversibly triple in size while the third contracts. This response is virtually the same from liquid-nitrogen temperatures up to the melting point of iron. The ribbons are also transparent and flexible, yet conductive. The work is an exciting example of how nanostructuring can lead to combinations of properties that are not possible in bulk materials.

Nature provides the best examples of the power of nanostructuring. For example, human hair is as strong as some steels (much stronger when scaled by density), and unlike steel can be stretched by 30% before breaking. These properties are enabled by the alignment and crosslinking of bundles of protein helices. Similarly, the use of micrometer- and nanometer-diameter fibers dramatically increases the strength of materials. Carbon fiber-reinforced plastics used in sports equipment and aircraft parts are both strong and light thanks to the incorporation of aligned fibers into a much less stiff epoxy resin. These composites can be about one hundred times as compliant perpendicular to the fiber axis as parallel to it.

Carbon nanotubes have attracted a lot of interest as reinforcing materials because individual tubes are almost as stiff as diamond, are low in density, and have a tensile strength that is far greater than any bulk material. Carbon nanotube-containing fibers are gradually approaching the stiffness and strength of their component tubes. Aliev *et al.* now show that

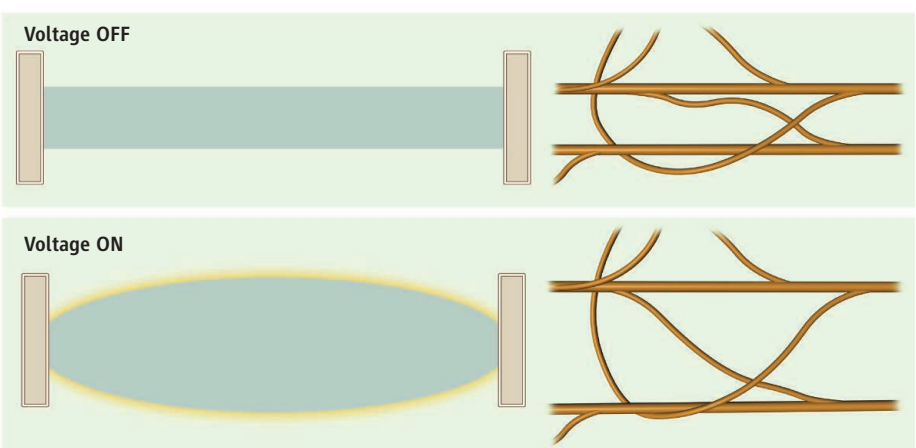

Intertwined tubes. Application of a voltage to ultralow-density carbon nanotube sheets produces a dramatic expansion in width and thickness (**left**). The sheets are highly compliant in the width and thickness directions, perhaps held together by the bending stiffnesses of intertwined nanotubes, enabling large deformations of the ribbon in these axes (**right**).

Department of Electrical and Computer Engineering, Advanced Materials and Process Engineering Laboratories, University of British Columbia, Vancouver, British Columbia V6T 1Z4, Canada. E-mail: jmadden@ece.ubc.ca

nanotubes also enable highly anisotropic material properties. The authors have grown forests of 11-nm-diameter carbon nanotubes and then pulled the entangled tubes into ribbons composed of oriented bundles. Their densities are extremely low—a little higher than that of air, and similar to that of the lightest materials known. The ribbons are very stiff for their weight in the stretch direction. Perpendicular to the stretch direction, they may be as much as one million times less stiff, and are far more compliant than rubber (*2*). This apparently unprecedented degree of anisotropy is akin to having diamond-like behavior in one direction and rubber-like behavior in the others. If the ribbons are stretched along the orientation axis, the other axes collapse dramatically—20 times as much as most materials do—leading to an overall shrinkage that is again unique in its magnitude and direction.

The nanotube ribbon's combination of the high stretch-direction modulus and low density is well suited for creating thin, stiff beams and plates for aerospace and other applications, in which minimizing mass is critical. The ribbons would require less than 10% of the mass needed by composites, wood, metals, or other materials, but are bulkier because of their extremely low densities (*3*).

The application of a voltage charges and expands the ribbons in milliseconds, as the repelling charges maximize the surface area by pushing apart loosely interconnected bundles (see the figure). Although carbon nanotube actuators have previously been activated by charging in an electrolyte, the resulting relative changes in length were much smaller. The large strains of the new actuation mechanism suggest that high electromechanical coupling and efficiency should be achievable. This is because large changes in the distance between charges lead to a substantial change in electrical potential energy that can be converted to work.

The actuators can deflect light, but are otherwise so compliant in their large strain axis that applications requiring large displacement and any appreciable force are excluded. This limitation might be overcome by greatly increasing the transverse stiffness of the ribbons by densification of the nanotube ribbons and increasing the degree of interconnection between adjacent fibres. When forces are increased, the ribbon artificial muscles will become candidates for use in medical devices, robots, and perhaps even implants.

How can a material that is so stiff in one direction be so compliant in the others? Entanglement of adjacent bundles might be expected to lead to a rubber-like elasticity, in which thermal agitations resist the uncoiling of weakly intertwined tubes. However, the nanotubes are much too stiff to bend due to thermal energy, and their response shows virtually no temperature dependence—the elasticity is "enthalpic" rather than entropic in origin. So what keeps the films together? Small bundles wind around and perhaps interconnect with the larger oriented fibers [supporting figure S10 in (*1*)]. These tiny but stiff wires may act as springs that bend to provide a restoring force when the ribbons are deformed (see the figure). If so, then altering the density and stiffness of interconnects should allow tuning of the mechanical properties of the ribbons.

The discovery of the stiff yet compliant, light yet strong, electrostatically deformable ribbons should inspire the development of new nanostructured materials whose stiff, long, and carefully arranged elements enable exquisite tailoring of material properties. For example, it may be possible to create custom materials with unique properties by assembling nanometer-thick beams into carefully designed three-dimensional structures. The beams in this case are stiff macromolecules or nanowires that can resist attractive surface forces from neighbors. Creating the desired property combinations is a challenge, but reports of engineered three-dimensional structures composed of stiffened DNA (*4*), zinc oxide ribbons, and other stiff materials suggest that it will ultimately be possible.

References and Notes

1. A. E. Aliev et al., *Science* **323**, 1575 (2009).
2. Aliev *et al.* do not report modulus in the compliant axes; I have estimated the modulus from the resonant frequency during actuation.
3. In such applications, prestrain may be needed because of the low initial modulus. Creep may also pose a problem.
4. N.C. Seeman, *Nature* **421**, 427 (2003).

10.1126/science.1171169

CHEMISTRY

Copper Puts Arenes in a Hard Position

Robert E. Maleczka Jr.

Copper catalysts enable substitution reactions on a benzene ring to occur at positions that normally are unfavorable.

As a professor of chemistry, I have written many letters of recommendation for nonchemistry majors. This task gives me the opportunity to ask what the students remember most from their year of organic chemistry. Electrophilic aromatic substitution—the replacement of hydrogen atoms on aromatic rings, or arenes, with substituents—often tops the list. With surprising regularity, students can recall the rules (or at least remember that rules exist) predicting whether substituted benzenes will react at their ortho, meta, or para positions (see the figure, panel A). A report by Phipps and Gaunt on page 1593 of this issue (*1*) might give my students pause. The authors show how ortho/para-directing amido groups can facilitate a difficult reaction, carbon-carbon (C–C) bond formation, at the less favored meta position, courtesy of a novel copper(I)/copper(III) catalytic sequence.

The problem addressed by Phipps and Gaunt is a long-standing one. Shortly after Faraday isolated benzene, chemists began to explore its reactivity. These studies soon revealed that benzene reacts in a way that replaces a hydrogen atom with a functional group such as NO_2 or Cl (*2*). Moreover, even before Kékulé suggested benzene's structure, a number of disubstitution reactions were known to yield three different isomers. Assigning the absolute structures of such isomers fell to Körner, who in 1869 introduced the terms ortho, meta, and para.

In 1877, Friedel and Crafts discovered reactions that formed C–C bonds at aromatic rings (*3*). By the turn of the 20th century, reliable predictions could be made of how substituent effects govern the reactivity and selectivity of reactions that would later be described as electrophilic aromatic substitutions (*4*).

A substituent on a benzene ring influences both where a second substituent will preferentially react and whether these reactions will be accelerated or inhibited. Benzene molecules bearing groups that release electron density into the ring, which include alkylbenzenes, as well as anilides and phenols, activate electrophilic aromatic substitution reactions and

Department of Chemistry, Michigan State University, East Lansing, MI 48824, USA. E-mail: maleczka@chemistry.msu.edu

favor substitution at the ortho or para positions, or both (see the figure). Halides also direct substituents to these positions, but because they pull electron density from the ring relative to H, the reactions are relatively slower. Lastly, benzenes bearing electron-withdrawing groups (such as NO_2) are deactivating and direct substituents to meta positions.

These "rules" made preparation of many arene substitution reactions predictable and also practical on an industrial scale. The benzene nucleus can be found in ~30% of all industrial chemicals and over half of the top 50 drugs (*5*). Unfortunately, arenes in which the substitution patterns do not fit these rules (and which are said to be contra-electronic) can be extremely difficult to prepare. For example, obtaining only ortho products in the presence of a para- or meta-directing group was long considered a challenge. Multistep syntheses, which tend to be time consuming, more expensive, and lower yielding, were often needed to achieve the desired substituted benzene.

In the 1980s, directed metalation chemistry, developed by Snieckus, emerged as a powerful tool for selective ortho substitution to certain functionalized groups, including some that are normally meta directors, such as carbamides (*6*). In this approach, an existing group guides a base to the nearby ortho proton. Acid-base chemistry leaves a metal such as lithium at the ortho position, which then exchanges with a nonmetal substituent. More recently, functional group–directed carbon-hydrogen (C–H) bond activation, especially with palladium catalysts in the Pd(II)/Pd(IV) oxidation states, has allowed the introduction of various atoms, such as carbon, oxygen, and halogens, at ortho positions (*1*, *7*).

The complementary problem of achieving selective substitution meta to ortho/para donors has been more aggravating to chemists. For example, one relatively simple and synthetically useful (*8*) molecule, 3-bromo-5-chlorophenol, has three ortho/para directors, two of which are deactivating, and all occupy meta positions with respect to the others. Thus, phenol and either halobenzene are poor starting materials—each would direct the next substituent to the wrong position. Until recently (*9*), the best effort at synthesizing this contra-electronic molecule was a 10-step procedure reported in the 1920s that used the explosive TNT (trinitrotoluene) as the starting material.

Partial solutions to this meta problem have relied on steric preferences, catalyst choice, acidity differences, and, most often, multistep syntheses (*1*, *10*). Some of these approaches

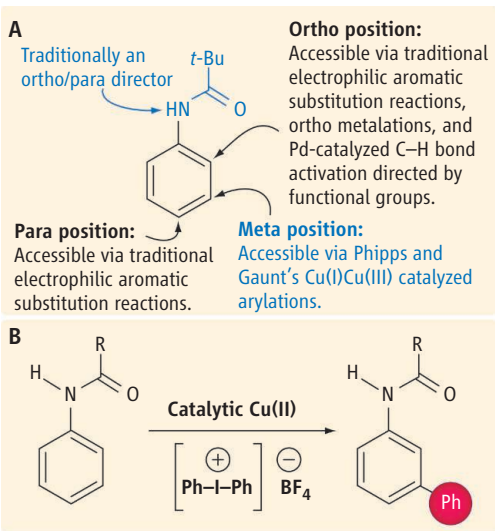

Location, location, location. (**A**) Many reactions readily add a second substituent to a benzene molecule at the positions across from the first substituent (para) or next to it (ortho), but addition at the remaining meta positions is usually slow and low in yield. The copper-catalyzed route described by Phipps and Gaunt forms carbon-carbon bonds to arene substituents at positions meta to an amide group; *t*-Bu is a tertiary butyl group. (**B**) The overall reaction; Ph is a phenyl group.

are quite clever, including Wilhem and Lautens' palladium-catalyzed alkylation hydride reduction sequence (*10*). Sterically guided iridium-catalyzed C–H borylations also afford meta-substituted products regardless of the electronic preferences (*11*). However, none of these methods could start with benzene bearing a single ortho/para donor and directly afford a single meta-substituted benzene.

Phipps and Gaunt changed that landscape by tapping into the electrophilicity of Cu(III) (see the figure, panel B). In their scheme, a Cu(III) species is generated from Cu(I) and a bisarylated hypervalent iodine (that has lost two electrons to form two bonds and developed a positive charge). That reagent apparently does not undergo traditional electrophilic aromatic substitution without the aid of the amide. The electrons on the basic amide oxygen attack the ortho position of the benzene. The ring electrons are effectively then pushed out to form the C–Cu bond, which breaks the ring's aromaticity in the process. Further reaction with base rearomatizes the ring, and then the aryl group, originally bonded to iodine, forms a C–C bond at the meta position occupied by the Cu(III) group. The Cu(I) is regenerated, and the whole process begins anew.

Cross-coupling reactions are among the most common C–C bond–forming reactions used for the preparation of drug candidates (*12*). Cross-coupling reactions that avoid the preparation of haloaromatics are among the aspirational reactions recently identified by the American Chemical Society Green Chemistry Institute Pharmaceutical Roundtable (*13*). The organocopper components of Phipps and Gaunt's reaction need not be isolated, nor do the anilides require a halogen to effect C–Cu bond formation, so this part of the method can be considered green.

Phipps and Gaunt's methodology also represents new advances in both C–H activation and Cu(III) chemistry. Although their approach builds on their previous studies on copper-mediated indole arylations, the work does open a new chapter in electrophilic aromatic substitution chemistry. The chapter is still being written; the authors' putative mechanism is speculative, and there are drawbacks to hypervalent iodides (such as availability, by-product formation, and cost). Relatively small changes to the reaction conditions can change the products (*14*). Moreover, the yield of an anilide disubstituted with a deactivating meta director was a disappointing 11%.

Nonetheless, this study inspires the imagination. What besides aryl groups can be transferred? Can the approach be used in combination with other Cu(III) methods (*15*)? Finally, the role of Cu(III) in biological systems suggests that there may be biochemical or biosynthetic implications to these findings.

References

1. R. J. Phipps, M. J. Gaunt, *Science* **323**, 1593 (2009).
2. D. Astruc, Ed., *Modern Arene Chemistry: Concepts, Synthesis, and Applications* (Wiley-VCH, Weinheim, 2002), pp. 1–16.
3. R. M. Roberts, A. A. Khalaf, *Friedel-Crafts Alkylation Chemistry: A Century of Discovery* (Dekker, New York, 1984).
4. A. F. Holleman, *Chem. Rev.* **1**, 187 (1925).
5. *Chemical and Engineering News* (2005); http://pubs.acs.org/cen/coverstory/83/8325/8325list.html.
6. V. Snieckus, *Chem. Rev.* **90**, 879 (1990).
7. L. V. Desai, K. J. Stowers, M. S. Sanford, *J. Am. Chem. Soc.* **130**, 13285 (2008).
8. S. Höger, K. Bonrad, A. Mourran, U. Beginn, M. Mölle, *J. Am. Chem. Soc.* **123**, 5651 (2001).
9. R. E. Maleczka Jr., F. Shi, D. Holmes, M. R. Smith III, *J. Am. Chem. Soc.* **125**, 7792 (2003).
10. T. Wilhem, M. Lautens, *Org. Lett.* **7**, 4053 (2005).
11. A. M. Norberg, L. Sanchez, R. E. Maleczka Jr., *Curr. Opin. Drug Discov. Dev.* **11**, 853 (2008).
12. J. S. Carey, D. Laffan, C. Thomson, M. T. Williams, *Org. Biol. Chem.* **4**, 2337 (2003).
13. D. J. C. Constable *et al.*, *Green Chem.* **5**, 411 (2007).
14. G. Evindar, R. A. Batey, *J. Org. Chem.* **71**, 1802 (2006).
15. L. M. Huffman, S. S. Stahl, *J. Am. Chem. Soc.* **130**, 9196 (2008).

10.1126/science.1172298

Flagellum Mediates Symbiosis

Takefumi Shimoyama,[1,2] Souichiro Kato,[1,3] Shun'ichi Ishii,[1,4] Kazuya Watanabe[1,2,3]*

Prokaryotes perform a wide variety of cooperative behaviors (*1*); for example, the anaerobic biodegradation of organic matter is achieved by cooperative catabolism of diverse bacteria and archaea (*2*). With only a few exceptions [e.g., quorum sensing (*1*)], however, little is known of molecular mechanisms underlying these complex interactions. We have investigated syntrophy (symbioses based on nutritional cooperation) between fermentative bacteria (syntrophs) and methanogenic archaea (methanogens) that leads to the conversion of volatile fatty acids to methane in anaerobic environments (*2*). In such interactions, reducing equivalents (e.g., H_2) produced by syntrophs need to be rapidly consumed by methanogens (*2*), and close physical proximity between them is necessary for efficient H_2 transfer (*3*). Previous work suggested that unidentified extracellular filaments are important for *Pelotomaculum thermopropionicum* (syntroph) and *Methanothermobacter thermautotrophicus* (methanogen) to initiate syntrophy (*3*).

Inspection of the genomes of *P. thermopropionicum* and *M. thermautotrophicus* showed that putative gene clusters for flagellum and pilus occur in the bacterium (figs. S1 and S2), and similar extracellular filaments were observed in *P. thermopropionicum* monocultures (*3*). Differential centrifugation and gel electrophoresis showed that a partially purified fraction of the filaments in monoculture contained one major protein of about 55 kD (fig. S3), which was identified as FliC flagellin (PTH_2102, the major component of a bacterial flagellum) by N-terminal sequencing (fig. S3). However, we could not purify filaments from cocultures, probably because they mostly adhered to *M. thermautotrophicus* cells. We hence raised an antiserum against a recombinant FliC protein and identified that the filament in a coculture was the flagellum of *P. thermopropionicum* (Fig. 1A). We also used recombinant FliC and/or FliD (the flagellar cap protein) in an assay to test their binding specificities (fig. S4 and table S1) and found that, in addition to *M. thermautotrophicus*, these proteins adhered only to cells of *Methanosaeta thermophila* (fig. S4), an acetoclastic methanogen also known to form syntrophic association with *P. thermopropionicum*.

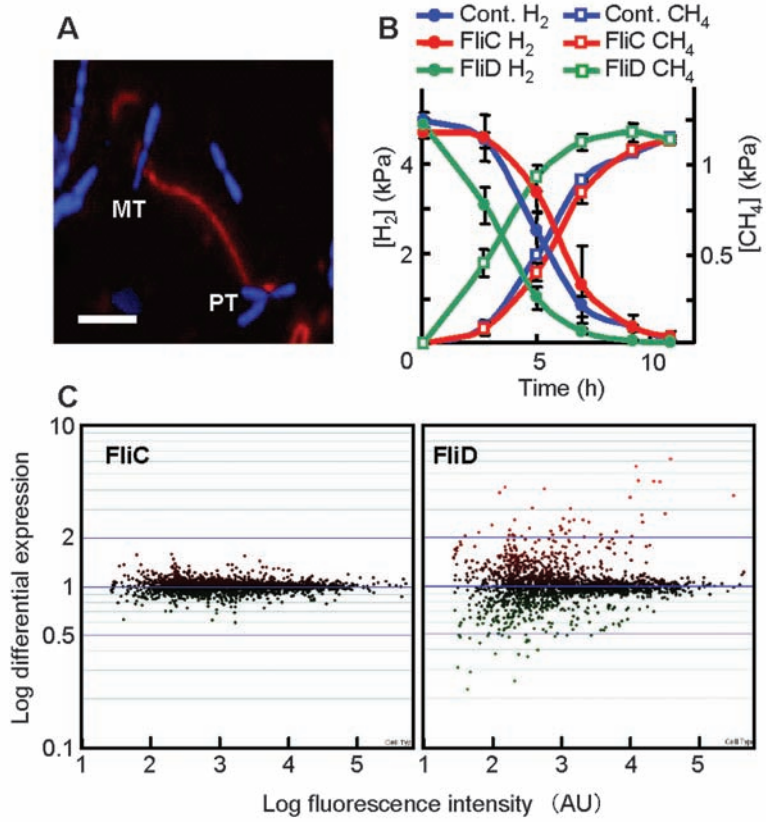

Fig. 1. Roles of the *P. thermopropionicum* flagellum in the syntrophic interaction with *M. thermautotrophicus*. (**A**) Fluorescence micrograph of *P. thermopropionicum* (PT) and *M. thermautotrophicus* (MT) connected by a flagellum. Cells were stained with DAPI (4′,6′-diamidino-2-phenylindole, blue), whereas filaments were stained with an anti-FliC serum and Texas red–labeled secondary antibody (red). *P. thermopropionicum* cells are short rods, whereas *M. thermautotrophicus* cells are cylindrical, slender, and longer than *P. thermopropionicum* cells. Scale bar indicates 2 μm. (**B**) Changes in headspace hydrogen (solid circle) and methane (open square) partial pressures in *M. thermautotrophicus* monocultures supplemented with FliC (red) or FliD (green). In the control (blue), neither FliC nor FliD was supplemented. Error bars indicate SD (n = 3). (**C**) Scatter plots of microarray data for FliC- and FliD-supplemented cultures by reference to the control culture (1868 spots in one plot). AU indicates arbitrary units.

Mammal immune cells perceive flagellins of pathogens by using Toll-like receptors and activate intercellular signaling pathways for innate immunity (*4*). In the case of *M. thermautotrophicus*, the onset of methanogenesis was not affected by the presence of the FliC flagellin (Fig. 1B) but was accelerated by FliD [$P < 0.01$, Student's t test (at time point 2.7 hours)]. Comparison of transcriptome patterns showed that after 2 hours FliD binding altered the expression of over 50 genes [exceeding the threshold values (>2 or <0.5), $P < 0.05$] (Fig. 1C) (*5*). FliC had no effect. FliD up-regulated genes for enzymes in methanogenesis, adenosine triphosphate synthase, and hydrogenases (table S2), indicating that *M. thermautotrophicus* perceives FliD of *P. thermopropionicum* to prepare for syntrophy.

We identified a role of a bacterial flagellum in maintaining a symbiosis between prokaryotes, not only to ensure proximity between specific partners but also to synchronize their metabolism. The liaison between *P. thermopropionicum* and *M. thermautotrophicus* represents a protein-mediated communication system that has specifically evolved for interspecies interactions.

References and Notes

1. L. Keller, M. G. Surette, *Nat. Rev. Microbiol.* **4**, 249 (2006).
2. B. Schink, *Microbiol. Mol. Biol. Rev.* **61**, 262 (1997).
3. S. Ishii, T. Kosaka, K. Hori, Y. Hotta, K. Watanabe, *Appl. Environ. Microbiol.* **71**, 7838 (2005).
4. S. Akira, K. Takeda, *Nat. Rev. Immunol.* **4**, 499 (2004).
5. Microarray data were deposited in the ArrayExpress database under accession numbers E-MEXP-1362 and E-MEXP-1971.
6. We thank K. Nealson for the critical reading of the manuscript, T. Kosaka for microarray setup, and F. Numazaki and M. Sato for technical assistance. This work was supported by the New Energy Development Organization of Japan, JST, and the Japan Society for Promotion of Science.

Supporting Online Material

www.sciencemag.org/cgi/content/full/323/5921/1574/DC1
Materials and Methods
Figs. S1 to S4
Tables S1 and S2
References

22 December 2008; accepted 12 February 2009
10.1126/science.1170086

[1]Laboratory of Applied Microbiology, Marine Biotechnology Institute, 3-75-1 Heita, Kamaishi, Iwate 026-0001, Japan. [2]Research Center for Advanced Science and Technology, The University of Tokyo, Komaba, Meguro-ku, Tokyo 153-8904, Japan. [3]Hashimoto Light Energy Conversion Project, Exploratory Research for Advanced Technology, Japan Science and Technology Agency (JST), Hongo, Bunkyo-ku, Tokyo 113-8656, Japan. [4]J. Craig Venter Institute, 10355 Science Center Drive, San Diego, CA 92121, USA.

*To whom correspondence should be addressed. E-mail: watanabe@light.t.u-tokyo.ac.jp

Giant-Stroke, Superelastic Carbon Nanotube Aerogel Muscles

Ali E. Aliev, Jiyoung Oh, Mikhail E. Kozlov, Alexander A. Kuznetsov, Shaoli Fang, Alexandre F. Fonseca, Raquel Ovalle, Márcio D. Lima, Mohammad H. Haque, Yuri N. Gartstein, Mei Zhang,* Anvar A. Zakhidov, Ray H. Baughman†

Improved electrically powered artificial muscles are needed for generating force, moving objects, and accomplishing work. Carbon nanotube aerogel sheets are the sole component of new artificial muscles that provide giant elongations and elongation rates of 220% and (3.7×10^4)% per second, respectively, at operating temperatures from 80 to 1900 kelvin. These solid-state–fabricated sheets are enthalpic rubbers having gaslike density and specific strength in one direction higher than those of steel plate. Actuation decreases nanotube aerogel density and can be permanently frozen for such device applications as transparent electrodes. Poisson's ratios reach 15, a factor of 30 higher than for conventional rubbers. These giant Poisson's ratios explain the observed opposite sign of width and length actuation and result in rare properties: negative linear compressibility and stretch densification.

Actuator materials and mechanisms that convert electrical, chemical, thermal, or photonic energy to mechanical energy have been sought for over a century. Electrostatic attraction and repulsion between two nanotubes was used for cantilever-based nanotweezers (*1*) and mechanically based switches and logic elements (*2*, *3*). On the macroscale, electrically powered (*4*–*6*) and fuel-powered (*7*) nanotube actuators provided up to a few percent actuator stroke and a hundred times higher stress generation than natural muscle. Demonstrated large-stroke pneumatic nanotube actuators used electrochemical gas generation within nanotube sheets (*8*). Carbon nanotube composites with organic polymers provided photoresponsive (*9*), shape memory (*10*, *11*), and electromechanical (*12*) actuators.

Carbon nanotube aerogel sheets. We have developed carbon nanotube actuators from aerogel sheets that are drawn from forests of carbon multiwalled nanotubes (MWNTs). They typically have a density of ~1.5 mg/cm^3, an areal density in the sheet plane of ~1 to ~3 μg/cm^2, and a thickness of ~20 μm (*13*, *14*). The sample dimension in the sheet draw direction is the sheet length (L), and the orthogonal sheet dimensions are the sheet width (W) and the sheet thickness (H), which have initial values L_o, W_o, and H_o before actuation. Liquid-based densification of the aerogel sheets can decrease sheet thickness ~400-fold to typically 50 nm, which is useful for decreasing actuator volume. These nanotube aerogel sheets can be drawn from forests at above 2 m/s and a gram of sheet could cover over 30 m^2 (fig. S1). The aerogel sheets act as a low-modulus rubber when stretched in the sheet-width direction by up to 300%, which is important for accommodating large-stroke actuation.

The Alan G. MacDiarmid NanoTech Institute, University of Texas at Dallas, Richardson, TX 75083, USA.

*Present address: Department of Industrial Engineering, Florida State University, Tallahassee, FL 32306, USA.

†To whom correspondence should be addressed. E-mail: ray.baughman@utdallas.edu

Actuation in sheet width and thickness directions. Actuation results from applying a positive voltage to a nanotube sheet electrode with respect to a counter electrode, which is usually a distant ground plane. Figure 1, A to C, demonstrate width-direction actuator strokes of about 220%, as well as actuation from ambient to 1500 K. Figure 1D shows that electrically produced actuation of ~3× can be permanently frozen by laying the electrically expanded sheet on a substrate and using van der Waals bonding between nanotubes and substrate to prevent return to the initial nonexpanded state. This freezing of electrically driven actuation enables tuning of areal density and related properties for transparent electrode applications. The consequence of "ballooning" in the width direction, from 0% at the sample grips to about 220% at the center of the nanotube strip, is periodic corrugation in the width direction during nanotube sheet cycling (Fig. 1, E and F). Corrugation formation can be avoided by either increasing the length-to-width ratio of the sheets, so that strains in the width direction become more uniform, or decreasing the applied potential.

The observed voltage dependence of actuator stroke in the width direction at length center, normalized to the initial width to provide generated strain $\varepsilon_w = \Delta W/W_o$, is shown in Fig. 2A for single and stacked aerogel ribbons having the same L_o/W_o ratio. Although ε_w increases approximately quadratically with applied voltage V, a crossover occurs at higher voltages to a weaker dependence, $\sim V^{2/3}$. A similar transition in the voltage dependence of lateral deflection has been observed and explained for a charged single nanotube that is clamped at both ends (*15*). At relatively low applied voltage (260 V), the observed width-direction actuation (fig. S5) was 14% for a sheet strip having L_o/W_o = 13.9 (*14*). Movie S1 shows width-direction actuation during cycling at high applied voltage, as well as simultaneously recorded changes in optical diffraction from the sheet.

This crossover in voltage dependence from $\sim V^2$ to $\sim V^{2/3}$ results from ballooning caused by end clamping. In this geometry, width-direction expansion requires stretch in the high-modulus nanotube orientation direction, and this elonga-

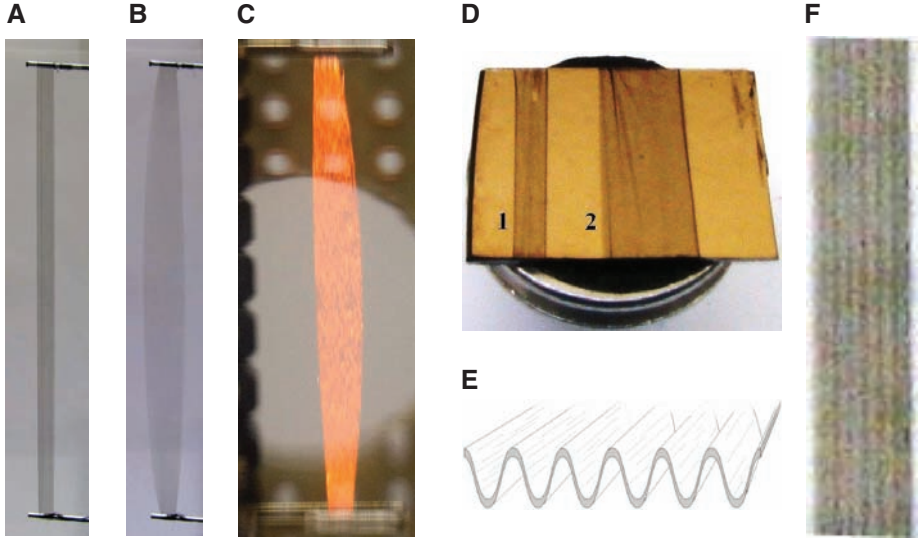

Fig. 1. (**A** and **B**) Photograph of a rigidly end-supported 50-mm-long by 2-mm-wide nanotube sheet strip (A) and the same sheet strip expanded in width by applying 5 kV with respect to ground (B). (**C**) Photograph of a 25-mm-long nanotube sheet strip actuated at 1500 K by applying 3 kV, where the color of incandescence is not correctly captured by the camera. (**D**) Picture of identical-dimension nanotube sheet strips of (A) and (B) that were contacted with a Au-coated Si substrate while in un-actuated (1) and actuated (2) states and subsequently densified on the substrate by absorption and evaporation of ethanol. (**E** and **F**) Schematic representation (E) and optical micrograph (F), taken at ~45° to the sheet-width direction to enhance visibility, of the periodic corrugation in the width direction that results from periodic cycling under the inhomogeneous strains caused by sheet strip ballooning.

tion provides the dominant elastic energy term at the large strokes produced at high applied voltages. The charge-injection–generated force needed to provide strain ε_w is approximately $F = A\varepsilon_w + B\varepsilon_w^3$, where A and B are coefficients proportional to elastic stiffness in the width and nanotube orientation directions, respectively. The ε_w term is just the ordinary linear dependence of force on elastic strain in the width direction. The ε_w^3 term arises from combination of the ε_w^2 dependence of fractional elongation of the bowed nanotubes and the ε_w dependence of the projection of the resulting restoring force onto the width direction.

Because the electrostatic repulsive force F producing ε_w depends quadratically on injected charge and the injected charge is CV, where C is the sheet capacitance, the combination of linear and cubic terms in ε_w for F leads to the correct prediction that ε_w increases as $\sim V^2$ when ε_w is small and as $\sim V^{2/3}$ when ε_w is large. The crossover voltage and the ε_w obtained at high voltage should increase with increasing L_o/W_o, which is experimentally confirmed (fig. S4).

The Fig. 2A data on the voltage dependence of ε_w can be reduced to a universal curve (Fig. 2A, inset) that is independent of the number N of stacked sheets (between N = 1 and 8), by plotting ε_w versus $V^2 S_N$, where $S_N = (N^{-1} - R)/(1 - R)$ and where R is a fitting parameter (0.095). We theoretically derived this normalization factor S_N using a simple mechanical model. The average charge-induced stress in the width direction scales as $1/N$, while the average stress in the thickness direction is largely independent of N (*14*). If charge-injection–generated stress in the thickness direction had no effect on width-direction strain, R would be zero and ε_w would therefore be a function of only V^2/N. The N-independent stress in the thickness direction upon charge injection will decrease width-direction strain as a result of sufficiently strong elastic cross-coupling between these parameters, thereby giving rise to a finite R. Although use of S_N as a normalization factor accurately predicts the dependence of actuation strain on voltage over an eightfold change in sheet thickness, it becomes unreliable for thicker sheet stacks having low actuation strains at all voltages. The decrease in width-direction stroke by a factor of about 3.7 upon densification of an eight-sheet stack (Fig. 2A) is consistent with the increase in nanotube-nanotube interconnects and the corresponding increase in specific stiffness (*16*) as a result of densification.

The average actuation rate in the width direction was determined in air (*14*) for a high–aspect ratio single sheet (L_o/W_o = 36) by measuring the time delay (5 ms) between applying 5 kV to the nanotube sheet and subsequent 180% width expansion (fig. S6). This average actuation rate was a notable (3.7×10^4)%/s, as compared with the maximum 20%/s achieved rate for other electrically driven carbon nanotube yarn or sheet actuators and the 50%/s maximum rate of natural muscle (*17*). A comparable average actuation rate $(3.4 \times 10^4$ %/s) was obtained for artificial muscles based on silicon elastomers, but this rate was obtained for electrical drive at resonant frequency where the actuator stroke was about 12% (*17*, *18*).

Resonant actuation in vacuum caused large strokes in the width direction at low applied voltages because of a surprisingly high observed quality factor Q (fig. S7). Applying 1 V_{RMS} (root mean square voltage) ac drive voltage to a 25-by-1.8–mm single sheet resulted in a resonant frequency of 1089 Hz and a Q of 455, which markedly decreased (fig. S8) when air was in-

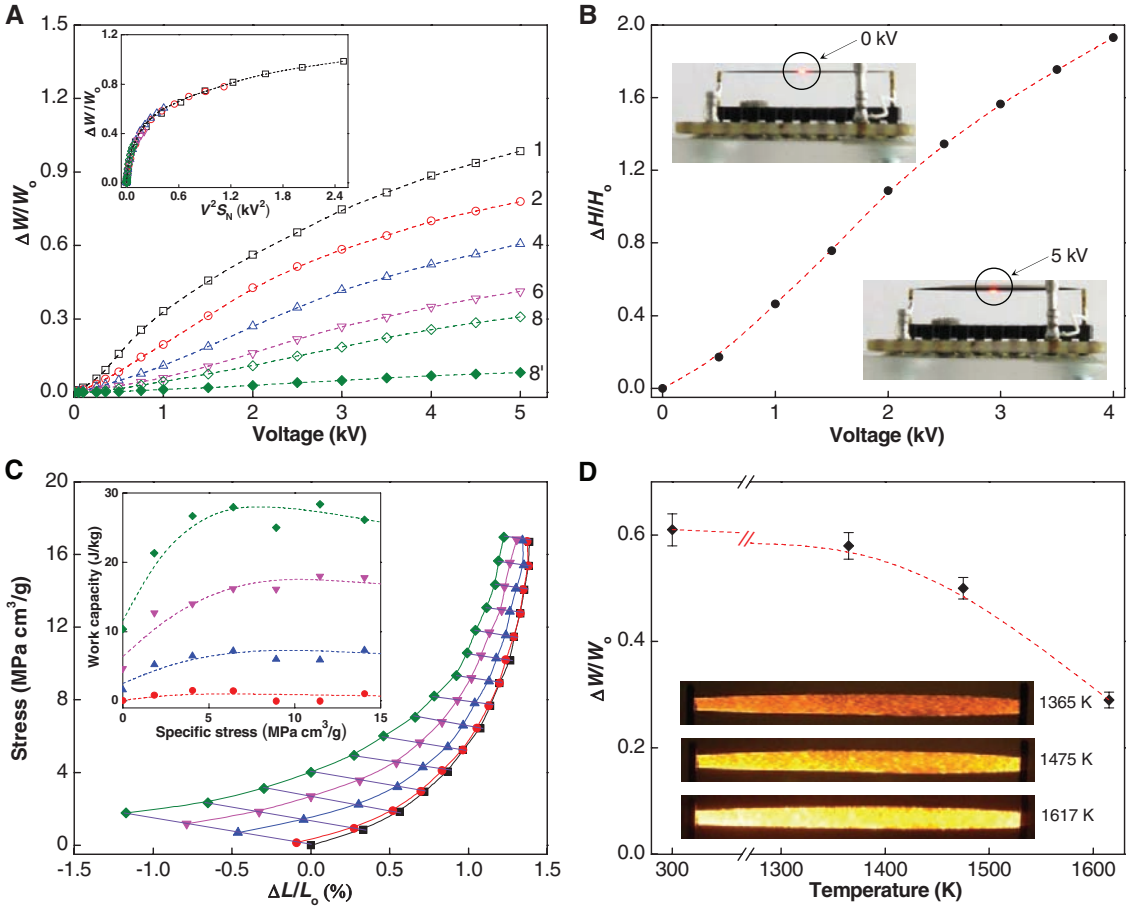

Fig. 2. (**A**) Width-direction actuation strain, $\Delta W/W_o$, versus applied voltage for N = 1 to 8 stacks of single aerogel sheets and for a densified eight-sheet stack, labeled 1 to 8 and 8′, respectively, having L_o = 25 mm and W_o = 2 mm. The universal curve in the inset for this aspect ratio (12.5) shows results for undensified nanotube sheet stacks that are normalized with a single-fit parameter R, where the normalization factor is $S_N = (N^{-1} - R)/(1 - R)$. (**B**) Actuation-generated thickness-direction strain versus applied voltage for an eight-layer sheet strip with the above L_o and W_o and H_o = 0.3 mm. The insets are edge-view photographs of the sheet strip in the sample jig of fig. S2 before (top) and after actuation (bottom), showing at midpoint the laser beam used for thickness measurement. (**C**) Specific stress versus length-direction strain at constant applied voltage (curves rising to the right) and for increasing voltage for a given tensile stress applied before actuation (lines rising to left), where the squares, circles, up triangles, down triangles, and diamonds correspond to applied voltages of 0, 0.4, 0.8, 1.2, and 1.6 kV, respectively. The investigated single sheet was 14.3 mm long and 0.55 mm wide and the sample jig of fig. S3 was used. The inset provides corresponding specific work capacity as a function of initially applied specific stress for different applied voltages. (**D**) Width-direction actuator strain for a single nanotube sheet strip (25 mm by 1 mm) on switching between 0 and 3 kV at the indicated temperatures. The insets picture the actuated sheets at incandescent temperatures. All results are for length-end supported nanotube sheets; measurements of $\Delta W/W_o$ and $\Delta H/H_o$ were made midway between these supports, and provided lines are guides for the eye.

troduced (*14*). The high mechanical quality factor in vacuum, as well as the high quality factor for electronic resonance (due to the largely capacitive nature of electronic load of nanotube sheet and cables), enabled an observed ±30% oscillatory actuation to be driven at high frequency by a 10 V_{RMS} ac power supply (fig. S9). The trick here is to place a small inductor coil between the power supply and the nanotube sheet, where the inductance of the coil and the capacitance of the sheet and associated leads provide an electronic resonant frequency that is close to the mechanical resonance frequency of the nanotube sheet (*14*). The electronic resonance increased the 10 V_{RMS} voltage applied to the inductor to a measured 150 V_{RMS}, which combined with mechanical resonance enhancement to provide this ±30% oscillation at 1100 Hz.

Because charge-injection–based forces act only at the sides of a conductor sheet, sheet deformation during actuation is expected to be uniform on the macroscale across sample width, as long as large sheet aspect ratio ensures that width constraints at end supports are unimportant. Optical measurements demonstrate strain uniformity in the sheet-width direction on dimensional scales where sheet mechanical properties achieve bulk values (*14*). The expected increase in charge density close to sheet boundaries (figs. S10 and S11) was evident from potential measurements using a Kelvin probe attached to an atomic force microscope (*14*).

Charge-induced actuation in the sheet thickness is much like that for sheet width: Actuator strokes in the thickness direction are also giant (~200%), and the voltage dependence of this actuation again switches from approximately a V^2 dependence to close to a $V^{2/3}$ dependence as applied voltage increases (Fig. 2B). A likely reason for this similarity in actuator stroke for sheet thickness and width directions is the approximate structural equivalence of these directions.

Actuation in the sheet-length direction. Large-stroke actuation by expansion in sheet width during charge injection is accompanied by contraction of a few percent in sheet length, where modulus and strength are much higher than for other directions. Length-direction actuation generates an isometric specific stress of up to 4.0 MPa cm^3/g (corresponding to the data point for $\Delta L/L_o = 0$ and 1.6 kV in Fig. 2C). Because electrostatically generated stress is proportional to $1/H$, densification of the sheet by decrease in sheet thickness H leaves the isometric specific stress unchanged. Hence, a densified sheet strip with a density of 0.8 g/cm^3 has an isometric stress–generation capability of 3.2 MPa, which is about 32 times as high as the maximum sustainable stress-generation capability of natural skeletal muscle (*17*). The actuator stroke for a specified change in applied potential decreases with increasing initially applied stress, because the Young's modulus increases with strain, so the specific work per cycle reaches a plateau, where there is little sensitivity to the initially applied stress. The maximum achieved work per cycle (Fig. 2C, inset) is ~30 J/kg, compared with the maximum capability of ~40 J/kg for natural muscle (*17*).

Actuation at extreme temperatures. The data in Fig. 2D show that width direction actuator stroke does not significantly change upon increasing temperature from 300 to 1365 K by resistively heating the sample. Considering the high-temperature changes and the possibility that permanent modulus changes will occur because of irreversible annealing, it is also surprising that the nanotube sheets can be repeatedly cycled between 300 K and at least 1500 K without causing substantial change in actuation at either temperature (*14*). Also, no change in actuator stroke was observed in going from 300 K to the lowest observation temperature (80 K).

Because essentially constant electrostatically generated stresses are acting against the elastic modulus to provide the actuator stroke, the observed near-temperature-invariant actuator stroke indicates that the nanotube sheet modulus is largely temperature independent. This is a signature of enthalpic elasticity and contrasts with the highly temperature-dependent modulus of ordinary entropic rubbers. Single MWNT and MWNT bundle rigidity explains the absence of a noticeable entropic contribution to rubber elasticity. The ~12-nm-diameter, approximately nine-wall MWNTs used have very high bending modulus, and further modulus increase results from MWNT bundling (providing an average of ~25 nanotubes in a bundle) (*14*). The ability of these bundles to act as rigid rods is described by the persistence length, which equals the ratio of the bending modulus to k_BT, where k_B is the Boltzmann constant and T is the absolute temperature. Assuming that walls in the MWNTs can easily slip with respect to each other, and making the same approximation for MWNTs in a bundle, a lower-limit estimate of the bending stiffness of the MWNT bundles is obtained as the product of the number of MWNTs in a bundle and the sum of the known bending stiffnesses of single nanotube walls in a MWNT (*19*). The thereby obtained persistence length of the MWNT bundles is so long (about a meter at 1900 K) that stress-induced change in entropy cannot appreciably contribute to rubberlike elasticity (*14*).

Giant Poisson's ratios and their effects on actuation. Giant Poisson's ratios are observed, which are important both for actuation and for possible use of nanotube sheets and sheet strips for strain amplifiers. This ratio of percent lateral contraction to the percent applied tensile elongation was measured optically (*14*) for stretch in the length direction to provide a width-direction Poisson's ratio of 9.5 ± 2.0 for sheet stacks with between 1 and 15 layers and strains up to 2%. The corresponding measured Poisson's ratio in the thickness direction was even larger (15 for a 30-layer sheet stack). A similarly giant Poisson's ratio (−12), but of opposite sign, has been observed for nanoporous polytetrafluoroethylene (*20*). These large Poisson's ratios indicate that the nanotube sheets can function as previously sought strain amplifiers (*21*), which amplify strain over an order of magnitude without providing the added bulk and frequency limitations associated with conventional lever systems (*14*). Because both the width- and thickness-direction Poisson's ratios are so large, a percent extension in the nanotube sheet direction would produce a ~23.5% decrease in sheet volume. This property of decreasing volume when stretched, called "stretch densification," is extremely rare (*22*) and implies that the aerogel will have a negative linear compressibility in the length direction, meaning that it will expand in this direction when hydrostatically compressed without infiltration.

Because of the giant Poisson's ratios for length-direction stretch, confinement of sheet length by rigid end supports substantially reduces actuation in width and thickness directions. The overall width (or thickness) change during actuation for a length-confined nanotube sheet is approximately equal to the sum of those for a two-step process: actuation in the absence of length constraint followed by applied stretch to return the length to its initial value. Correspondingly, for a 2% contraction in length for an unconfined sheet during actuation and the above Poisson's ratios, length confinement using rigid end supports decreases actuation strain in the width and thickness direction by about 19 and 30%, respectively.

Why does the nanotube sheet contract in the length direction during charging, when repulsive interactions between injected charges are normally expected to produce expansion in all directions? The explanation has the same structural origin as the giant Poisson's ratios for length-direction stretch. Because injected charge can freely move in the electrically conducting aerogel to eliminate internal electric fields, except very near the sheet surfaces, the actuator strokes arise from electrostatically generated tensile stresses σ_L, σ_W, and σ_H applied in the length, width, and thickness directions, respectively (*14*). The elastic compliance coefficients S_{LL}, S_{LW}, and S_{LH} then provide a length direction strain of $\varepsilon_L = S_{LL}\sigma_L + S_{LW}\sigma_W + S_{LH}\sigma_H$. Because diagonal terms like S_{LL} must be positive as a requirement for structural stability and σ_L must be positive when σ_L is electrostatically generated, the first term would produce an expansion in the length direction. Even though $\sigma_L > \sigma_W >> \sigma_H > 0$ (*14*), the contributions from the other terms (with S_{LW} and S_{LH} negative, corresponding to the observed positive Poisson's ratios) must be sufficient to reverse the sign of ε_L. Support for this is provided by the giant positive observed Poisson's ratio in width (ν_{LW}) and thickness directions (ν_{LH}) for length-direction stretch: $\nu_{LW} = -S_{LW}/S_{LL}$ and $\nu_{LH} = -S_{LH}/S_{LL}$. The existence of a contraction for electrostatically generated stresses implies the existence of a negative linear compressibility, because increase of the tensile stresses in the width and thickness direction to equality with σ_L would further increase the shrinkage in the length direction for the resulting negative hydrostatic pressure,

and reversal of this negative hydrostatic pressure to a positive value would result in a corresponding pressure-induced expansion in the length direction for positive hydrostatic pressure.

Application possibilities. In addition to extending the capabilities of artificial muscles to giant strokes and strain rates at extreme temperatures, the present actuator mechanism provides other application possibilities that relate to the structural change of the nanotube sheets during large-stroke actuation. The nanotubes diffract light perpendicular to the alignment direction, which can be dynamically modulated at over kilohertz frequencies for optical applications (*14*) (movie S1). The ability to tune the density of nanotube sheets and then freeze this actuation is being used for optimizing nanotube electrodes for organic light-emitting displays, solar cells, charge stripping from ion beams, and cold electron field emission.

References and Notes

1. P. Kim, C. M. Lieber, *Science* **286**, 2148 (1999).
2. T. Rueckes *et al*., *Science* **289**, 94 (2000).
3. V. V. Deshpande *et al*., *Nano Lett.* **6**, 1092 (2006).
4. R. H. Baughman *et al*., *Science* **284**, 1340 (1999).
5. U. Vohrer, I. Kolaric, M. H. Haque, S. Roth, U. Detlaff-Weglikowska, *Carbon* **42**, 1159 (2004).
6. S. Gupta, M. Hughes, A. H. Windle, J. Robertson, *J. Appl. Phys.* **95**, 2038 (2004).
7. V. H. Ebron *et al*., *Science* **311**, 1580 (2006).
8. G. M. Spinks *et al*., *Adv. Mater.* **14**, 1728 (2002).
9. S. V. Ahir, E. M. Terentjev, *Nat. Mater.* **4**, 491 (2005).
10. H. Koerner, G. Price, N. A. Pearce, M. Alexander, R. A. Vaia, *Nat. Mater.* **3**, 115 (2004).
11. P. Miaudet *et al*., *Science* **318**, 1294 (2007).
12. S. Courty, J. Mine, A. R. Tajbakhsh, E. M. Terentjev, *Europhys. Lett.* **64**, 654 (2003).
13. M. Zhang *et al*., *Science* **309**, 1215 (2005).
14. See supporting material on *Science* Online.
15. S. Sapmaz, Ya. M. Blanter, L. Gurevich, H. S. J. van der Zant, *Phys. Rev. B* **67**, 235414 (2003).
16. Specific strength (strength normalized to density), and corresponding specific Young's modulus and work capacity, are used because of their fundamental and practical importance, as well as ease of reliable determination from force and weight-per-length measurements.
17. J. D. W. Madden *et al*., *IEEE J. Oceanic Eng.* **29**, 706 (2004).
18. R. Pelrine, R. Kornbluh, Q. Pei, J. Joseph, *Science* **287**, 836 (2000).
19. B. I. Yakobson, L. S. Couchman, *J. Nanopart. Res.* **8**, 105 (2006).
20. K. E. Evans, A. Alderson, *Adv. Mater.* **12**, 617 (2000).
21. R. H. Baughman, *Nature* **425**, 667 (2003).
22. R. H. Baughman, S. Stafström, C. Cui, S. O. Dantas, *Science* **279**, 1522 (1998).

23. We thank T. Mirfakhrai, J. D. W. Madden, and V. M. Agranovich for their contributions. Supported by Air Force Office of Scientific Research grant FA9550-05-C-0088, NSF grant DMI-0609115, Office of Naval Research MURI grant N00014-08-1-0654, Robert A. Welch Foundation Grant AT-0029, Honda Corporation, Lintec Corporation, and the Brazilian agency CNPq (Conselho Nacional de Desenvolvimento Científico e Tecnológico). A provisional patent for nanofiber actuators and strain amplifiers has been filed by the authors (Patent Office Provisional Filing No. 61089275).

Supporting Online Materials

www.sciencemag.org/cgi/content/full/323/5921/1575/DC1
Materials and Methods
SOM Text
Figs. S1 to S11
References
Movie S1

10 November 2008; accepted 30 January 2009
10.1126/science.1168312

Spinal Cord Stimulation Restores Locomotion in Animal Models of Parkinson's Disease

Romulo Fuentes,[1]*† Per Petersson,[1,2]* William B. Siesser,[3] Marc G. Caron,[1,3] Miguel A. L. Nicolelis[1,4,5,6,7,8]

Dopamine replacement therapy is useful for treating motor symptoms in the early phase of Parkinson's disease, but it is less effective in the long term. Electrical deep-brain stimulation is a valuable complement to pharmacological treatment but involves a highly invasive surgical procedure. We found that epidural electrical stimulation of the dorsal columns in the spinal cord restores locomotion in both acute pharmacologically induced dopamine-depleted mice and in chronic 6-hydroxydopamine–lesioned rats. The functional recovery was paralleled by a disruption of aberrant low-frequency synchronous corticostriatal oscillations, leading to the emergence of neuronal activity patterns that resemble the state normally preceding spontaneous initiation of locomotion. We propose that dorsal column stimulation might become an efficient and less invasive alternative for treatment of Parkinson's disease in the future.

Patients suffering from Parkinson's disease (PD) experience chronic and progressive motor impairment (*1*). The main cause of PD is basal ganglia dysfunction, resulting from degeneration of neurons in the dopaminergic nigrostriatal pathway (*2*). Dopamine replacement therapy, through administration of the dopamine precursor 3,4-dihydroxy-L-phenylalanine (L-dopa), effectively ameliorates symptoms associated with PD and remains the treatment of choice to date (*3*). Unfortunately, L-dopa pharmacotherapy has proven less efficient in the long term and is associated with several complications (*4*). Additional therapeutic strategies, employed in conjunction with pharmacological treatment, have thus attracted considerable attention. In particular, improved techniques for electrical stimulation of the basal ganglia—referred to as deep-brain stimulation (DBS)—are effective for treatment of motor symptoms in PD (*5*). Furthermore, DBS permits a reduction of L-dopa dosage in PD patients (*6*). However, a disadvantage of DBS is the requirement of a highly invasive surgical procedure, as well as the crucial dependence on accurate targeting of very small brain structures (*7*). Hence, it is desirable to identify a less invasive method to electrically stimulate neuronal circuits to obtain beneficial effects similar to those of DBS.

Some clues for new PD therapies may come from epilepsy studies. In both animal models and in epilepsy patients, stimulation of peripheral nerve afferents is effective in desynchronizing aberrant low-frequency neural oscillatory activity, thereby reducing the frequency and duration of seizure episodes (*8*–*10*). Aberrant low-frequency neural oscillations are well documented in patients (*11*, *12*) and in animal models of PD (*13*). These findings led us to hypothesize that stimulation of afferent somatic pathways could alleviate motor symptoms of PD by disrupting aberrant low-frequency oscillations.

Dopamine, akinesia, and synchrony. The first set of experiments was carried out using an inducible mouse model of PD, first in wild-type animals and then in dopamine-transporter knockout (DAT-KO) mice (*14*). Through pharmacological inhibition of dopamine synthesis, we induced acute dopamine depletion in both types of animals (*2*, *13*, *14*). In patients, the cardinal symptoms of idiopathic PD have been reported to be clinically apparent after degeneration of 60 to 70% of the dopaminergic neurons of the substantia nigra pars compacta, which results in a 30 to 50% reduction of striatal dopamine levels (*15*, *16*). By means of two intraperitoneal injections (250 mg/kg) of the tyrosine hydroxylase inhibitor alpha-methyl-para-tyrosine (AMPT) during a 6-hour period (*15*, *16*), we achieved acute pharmacological dopamine depletion slightly below the levels observed in PD patients in wild-type C57/BL6J mice (69% reduction of striatal dopamine levels; mean ± SD = 4.5 ± 2.0 ng dopamine per mg

[1]Department of Neurobiology, Duke University Medical Center, Durham, NC 27710, USA. [2]Department of Experimental Medical Science, Neuronano Research Center, Lund University, BMC F10, 221 84 Lund, Sweden. [3]Department of Cell Biology, Duke University, Durham, NC 27710, USA. [4]Center for Neuroengineering, Duke University, Durham, NC 27710, USA. [5]Department of Biomedical Engineering, Duke University, Durham, NC 27710, USA. [6]Department of Psychology and Neuroscience, Duke University, Durham, NC 27710, USA. [7]Edmond and Lily Safra International Institute of Neuroscience of Natal (ELS-IINN), Natal RN 59066060, Brazil. [8]Ecole Polytechnique Fédérale de Lausanne, Lausanne 1015, Switzerland.

*These authors contributed equally to this work.
†To whom correspondence should be addressed. E-mail: fuentes@neuro.duke.edu

tissue in depleted animals compared with 14.4 ± 3.3 in controls; $P < 0.005$ Mann-Whitney, $n = 6/6$) (fig. S1). Equivalent symptoms of main clinical motor manifestations in PD patients were found in AMPT-injected mice (figs. S2 and S3). In particular, locomotive activity was significantly reduced [average locomotion scores in nondepleted and depleted animals were (mean ± SEM) 3.7 ± 0.1 and 0.4 ± 0.02 mm/s, $n = 11$ and 14, respectively], and a preferential reduction of faster movements indicated bradykinesia in the depleted state (fig. S2) (*17*, *18*).

Neuronal activity patterns of dorsolateral striatum and primary motor cortex (MI) were also significantly altered. Differences were found both on the population level, through inspection of local field potentials (LFP) and in the firing patterns of single cortical and striatal neurons (*13*). Figure 1A shows an example of LFP spectrograms recorded in MI during two 5-min periods before and after dopamine depletion (second row, left and right, respectively). Spectral analysis revealed particularly powerful oscillations ~1.5 to 4 Hz and in the lower beta range (10 to 15 Hz), whereas the power of oscillations >25 Hz was decreased in relation to baseline conditions (standardized spectrograms, Fig. 1A, third and fourth row, and fig. S6).

Important differences in single- and multi-unit activity were also found. The firing rates of a majority of 52 striatal and cortical neurons, which were positively identified after a 6-hour depletion period, showed significant differences (70.0% in motor cortex and 75.0% in striatum, $\alpha = 0.001$) when we compared the more active nondepleted state and the immobile depleted condition (see activity raster plots shown for a few units in Fig. 1A, bottom row). During dopamine depletion, a higher proportion of neurons tended to discharge phase-locked to LFP oscillation, in effect resulting in increased synchronicity [52.7% (64/129) in depleted versus 37.0% (44/127) in nondepleted state; $\alpha = 0.001$] (see fig. S6 for details).

DCS alleviates akinesia and synchrony. The effect of dorsal column stimulation (DCS) was next evaluated in mice before and after acute pharmacological dopamine depletion. DCS was achieved by chronic implantation of custom-

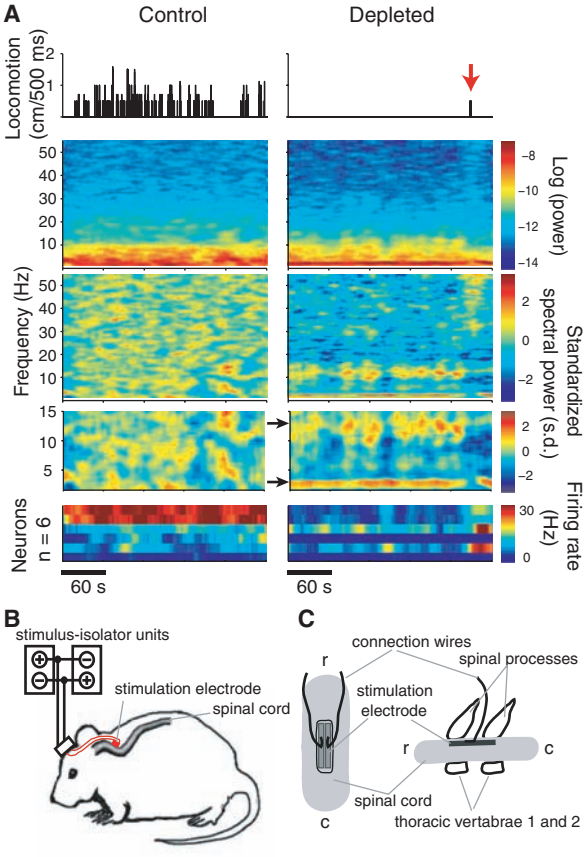

Fig. 1. Acute inhibition of dopamine synthesis produces a Parkinsonian state. (**A**) Examples of LFP spectrograms and firing-rate plots recorded in MI during two 5-min periods before and after dopamine depletion. Top row: Locomotion during recording periods. Second row: LFP power. Third row: LFP power standardized to the nondepleted 5-min period. Fourth row: Close-up of low-frequency range shown in third row. Note the increased power in low frequencies in the depleted state (black arrows) and the relative normalization of spectral power upon locomotion (red arrow). Bottom row: Average firing per second for 6 MI units. (**B**) Set-up for electrical stimulation of dorsal columns. The stimulation electrode (red) is implanted above the spinal cord, and connection wires are passed subcutaneously to a connector attached to the skull. Two stimulus-isolator units provide biphasic constant-current pulses at desired frequency and intensity. (**C**) Schematic dorsal (left) and sagittal (right) views of the implanted electrode. *r*, rostral; *c*, caudal.

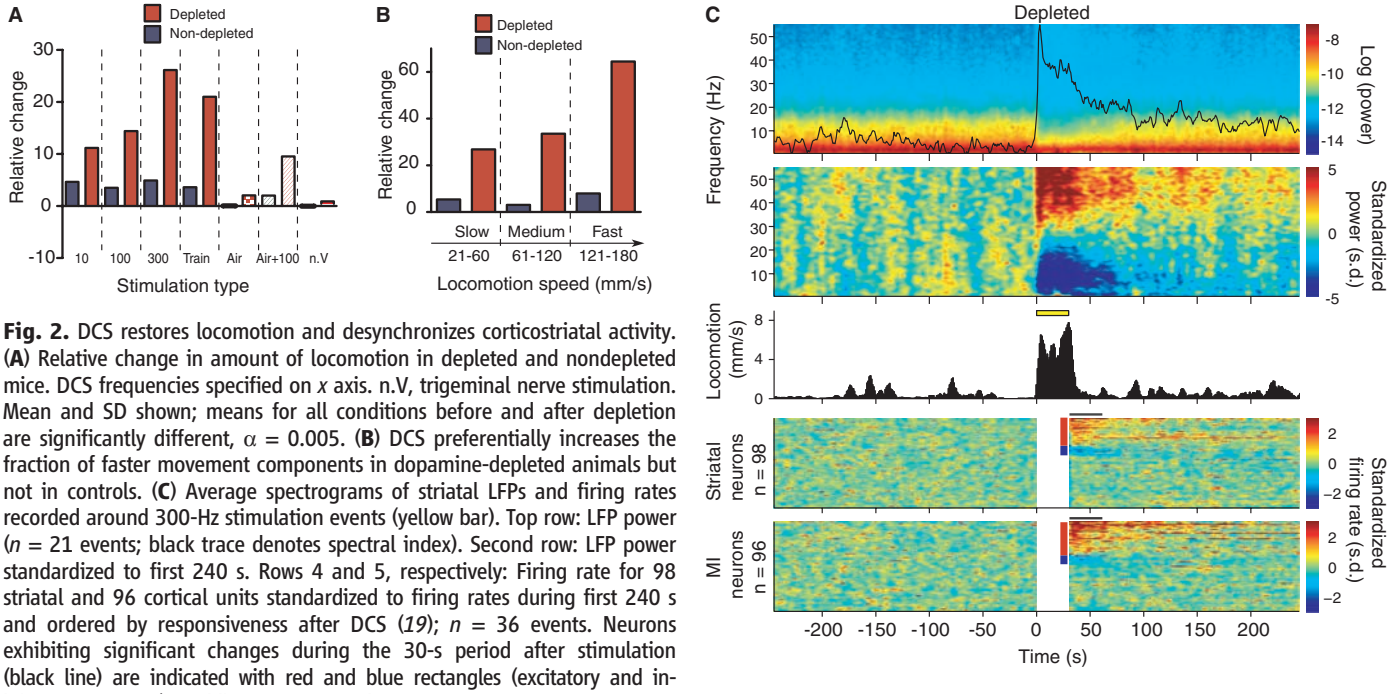

Fig. 2. DCS restores locomotion and desynchronizes corticostriatal activity. (**A**) Relative change in amount of locomotion in depleted and nondepleted mice. DCS frequencies specified on *x* axis. n.V, trigeminal nerve stimulation. Mean and SD shown; means for all conditions before and after depletion are significantly different, $\alpha = 0.005$. (**B**) DCS preferentially increases the fraction of faster movement components in dopamine-depleted animals but not in controls. (**C**) Average spectrograms of striatal LFPs and firing rates recorded around 300-Hz stimulation events (yellow bar). Top row: LFP power ($n = 21$ events; black trace denotes spectral index). Second row: LFP power standardized to first 240 s. Rows 4 and 5, respectively: Firing rate for 98 striatal and 96 cortical units standardized to firing rates during first 240 s and ordered by responsiveness after DCS (*19*); $n = 36$ events. Neurons exhibiting significant changes during the 30-s period after stimulation (black line) are indicated with red and blue rectangles (excitatory and inhibitory responses). Middle row: Average locomotion; $n = 36$ events.

made flat bipolar platinum electrodes positioned epidurally above the dorsal columns of the spinal cord at the upper thoracic level (Fig. 1, B and C).

DCS had a dramatic effect on the amount of locomotion displayed during stimulation periods in the dopamine-depleted animals. This effect was strongest for 300-Hz stimulation; on average, the amount of locomotion during stimulation periods was more than 26 times as high as during the 5-min period before stimulation (Fig. 2A and Movie S1). DCS had a smaller, albeit clear, effect, using lower stimulation frequencies. In contrast, control experiments using air puffs or trigeminal nerve stimulation were not effective (Fig. 2A and fig. S5). DCS caused increased locomotion also during nondepleted conditions, but this increase was moderate (4.9 times prestimulus values at 300 Hz) in comparison to that in depleted animals (Fig. 2A. Locomotion was normally initiated a few seconds after the onset of DCS, with a slightly longer delay in depleted animals (median = 3.35/1.35 s, interquartile range = 2.22/1.22 s, $P = 0.023$, Mann-Whitey, in depleted/nondepleted animals at 300 Hz). In addition, a small residual effect was found after high-frequency stimulation in depleted, but not in nondepleted, animals (3.4 and 0.95 times prestimulus values, respectively for the 30 s after 300-Hz DCS). DCS also proved efficient for alleviation of bradykinesia as indicated by the relatively larger increase in the amount of fast-movement components in depleted animals (Fig. 2B).

Analysis of LFP recordings during DCS in both MI and in striatum showed a shift in spectral power from lower to higher frequencies (average spectrograms from a total of 21 events of DCS at 300 Hz obtained from nine animals are shown in Fig. 2C). The spectral shift was maintained throughout the stimulation period and lasted for ~50 s after the end of stimulation. To condense the spectral shift into a single measure, a spectral index was computed by dividing the spectral range analyzed into an upper and lower half and calculating the ratio of the summed power of the frequencies in the two intervals [(25 to 55 Hz)/(1.5 to 25 Hz)]. The spectral index (black trace in Fig. 2C) illustrates the rapid spectral shift induced by DCS and the prolonged effect after DCS had ceased.

DCS also affected the firing patterns of individual neurons. To avoid interference from stimulation artifacts, the 30-s stimulation periods were excluded from the analysis of spike data. Even during the period following stimulation, though, numerous neurons showed significantly altered firing rates (47.9% in MI and 41.8% in striatum, $\alpha = 0.01$; Fig. 2C, rows 4 and 5, respectively). The fraction of units entrained to LFP dropped notably (from 42.7/38.8% in MI/striatum the 30 s before DCS to 24.5/24.0% the 30 s after DCS, $\alpha = 0.01$).

Although the onset of locomotion was delayed a few seconds, changes in the neural activity were detected almost immediately after DCS onset (mean ± SD evoked potential latency = 44 ± 5 ms), perhaps indicating that the electrophysiological changes have a permissive rather than a directly instructive role for the initiation of locomotion.

A brain state permissive of locomotion. During the relatively rare instances when the depleted animals displayed locomotion, low-frequency oscillations were diminished (Fig. 1A). This situation bears an obvious resemblance to the DCS-induced state. Thus, a certain decrease of low-frequency oscillations may be required to initiate locomotion. We analyzed the detailed temporal patterns of shifts in oscillatory LFP activity during spontaneous locomotion events in nondepleted (115 events in 10 animals) and depleted (51 events in 5 animals) mice (Fig. 3, A and B). In both states, significant spectral shifts from lower to higher frequencies, assessed by spectral index changes ($P < 0.01$) (*19*), were detected a number of seconds before the initiation of locomotion (nondepleted: mean ± SD =

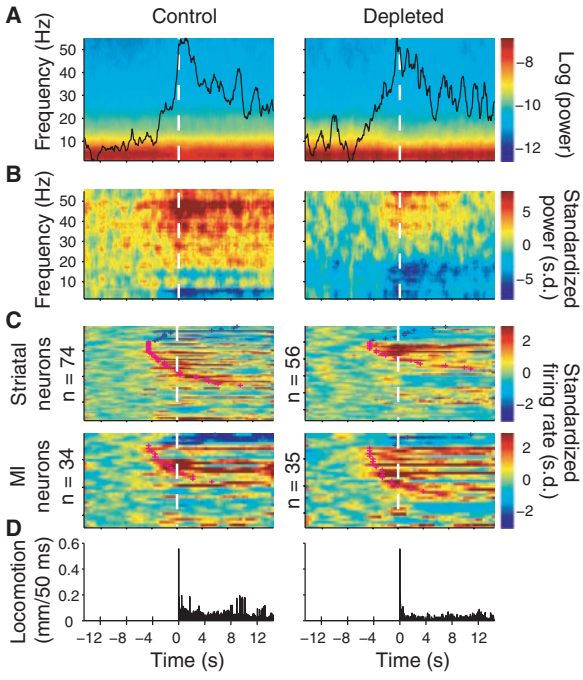

Fig. 3. Activity patterns during spontaneous locomotion. (**A**) Average spectrogram of striatal LFP aligned to the onset of spontaneous locomotion in control ($n = 115$ events) and dopamine-depleted condition ($n = 51$ events). The gradual shift from lower to higher frequencies indicated by the average spectral index (black trace) starts before locomotion onset (dashed white line). (**B**) Standardization of spectrogram relative to directly preceding nonlocomotion periods (collected between 20 and 10 s before locomotion onset from 112 stationary 10-s periods). (**C**) Firing rate (binned at 0.5 s) of striatal and MI units around the onset of spontaneous locomotion. Significant changes in firing rate (as compared to stationary period) are indicated with magenta (excitatory response) and blue (inhibitory response) crosses. (**D**) Average locomotion during recorded events.

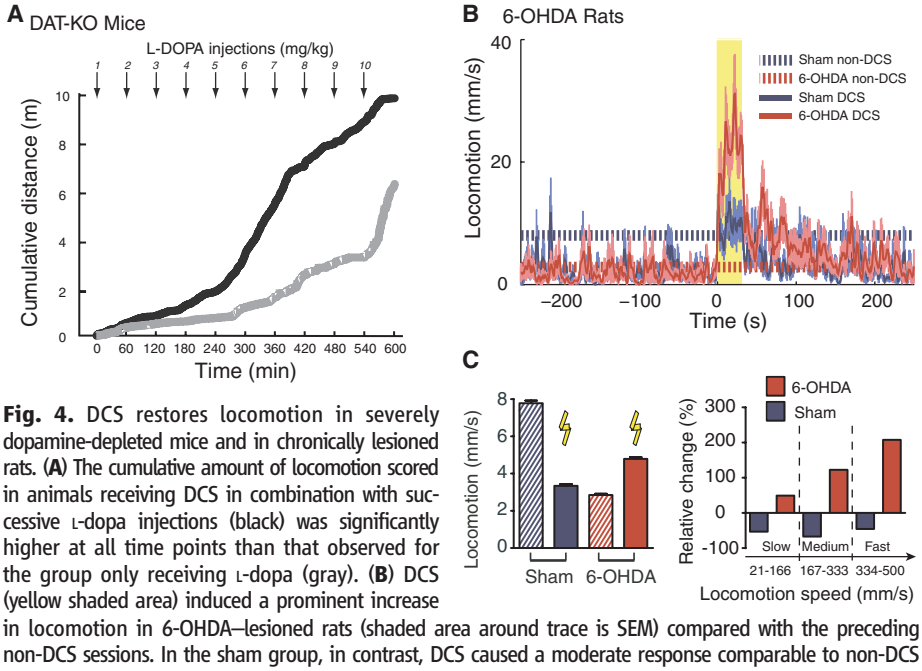

Fig. 4. DCS restores locomotion in severely dopamine-depleted mice and in chronically lesioned rats. (**A**) The cumulative amount of locomotion scored in animals receiving DCS in combination with successive L-dopa injections (black) was significantly higher at all time points than that observed for the group only receiving L-dopa (gray). (**B**) DCS (yellow shaded area) induced a prominent increase in locomotion in 6-OHDA–lesioned rats (shaded area around trace is SEM) compared with the preceding non-DCS sessions. In the sham group, in contrast, DCS caused a moderate response comparable to non-DCS sessions (mean ± SEM, $n = 64$ stimulation and 64 control sessions for both sham-treated and lesioned rats). (**C**) (Left) DCS specifically increases locomotion in 6-OHDA–lesioned rats (mean and SEM shown; all means are significantly different from the others, $P < 0.001$, Kruskal-Wallis and Dunn's multiple comparison test; flashes indicate DCS sessions). (Right) A preferential relative increase of faster movement components locomotion was found in the 6-OHDA–lesioned group reflecting alleviation of bradykinetic symptoms. Relative changes in amount of locomotion in three speed intervals (DCS/non-DCS sessions) are shown.

2.9 ± 1.7 s, range 0.1 to 5.5 s, n = 88, MI and striatal LFP; depleted: 3.0 ± 1.7, range 0.2 to 5.5 s, n = 48, MI and striatal LFP). Yet, there were also important differences, most notably below 25 Hz. A more differentiated decrease in power of oscillations below 8 Hz and an increase above 17 Hz was observed in nondepleted animals, whereas the spectral power in a broader range between 5 and 25 Hz was decreased in depleted animals. Because these different patterns occurred before the onset of locomotion, it is unlikely that they were due to differences in locomotion between the two groups. Instead, they could be part of the explanation of why depleted animals moved slower and for shorter time periods.

On the single-neuron level, the same type of firing rate changes after DCS also occurred in conjunction with spontaneous locomotion events. From a total pool of 193 neurons (from nine control and five dopamine-depleted recording sessions in 11 animals), 111 modulated their firing rate during locomotion and, unexpectedly, 59 of these neurons showed a pattern of early activation, 2.9 ± 1.4 s (mean ± SD) before actual locomotion onset (range = 0.5 to 4.5 s, n = 59 striatal and MI units from depleted and nondepleted conditions) (Fig. 3C).

DCS in combination with L-dopa treatment. To find the minimum dose of L-dopa (alone or combined with 300-Hz DCS) required to restore locomotion, DAT-KO mice were used. These mice have <5% of normal striatal content of dopamine (*14*). Dopamine can be further decreased to virtually undetectable levels by injecting AMPT (250 mg/kg intraperitoneally), resulting in a completely akinetic animal model (*14*). By gradually increasing dopamine levels through repeated L-dopa injections every hour, we tested the locomotion thresholds. In the group receiving only L-dopa injections (n = 6 sessions from 4 mice), locomotion typically first occurred after the fifth injection (5 mg/kg dose, corresponding to a total dose of 15 mg during the first 5 hours). When L-dopa treatment was combined with DCS, the same amount of locomotion was displayed after the second injection (2 mg/kg dose, corresponding to a total dose of 3 mg in the first 2 hours) (n = 10 experiments from seven mice (Fig. 4A). That means that in combination with DCS, one-fifth of the L-dopa total dose was enough to produce equivalent locomotion to L-dopa alone. There was also a general increase in the amount of locomotion displayed in the L-dopa+DCS group over the entire range studied. Thus, L-dopa+DCS seems to be superior to L-dopa alone in terms of the ability to rescue locomotive capability after severe dopamine depletion. Finally, animals in the L-dopa+DCS group consistently showed higher values of spectral index than the L-dopa only group. This suggests that DCS facilitates locomotion, even in severely depleted animals, through similar mechanisms (fig. S7).

DCS is effective after chronic lesions. Although the acute dopamine depletion model employed in the first set of experiments could reproduce all the main symptoms of PD, it was important to confirm the effectiveness of DCS in an animal model that also involves loss of nigrostriatal dopaminergic connections. Chronic dopaminergic denervation of the striatum was achieved using bilateral 6-OHDA lesions in rats (n = 4), resulting in progressive deterioration of motor function and sustained weight loss, both cardinal signs of successful lesioning (*20*, *21*). When placed in the open field, lesioned rats displayed reduced locomotion compared with controls (n = 4), which received vehicle injections in identical sites in the striatum (mean ± SEM = 2.85 ± 0.068 and 7.78 ± 0.144 mm/s on average, respectively). Quantification of immunohistochemical staining of the dopamine-synthesizing enzyme tyrosine hydroxylase indicated that lesioned rats had only ~20% of the immune signal found in sham-lesioned animals (fig. S8).

Rats were tested during two 1-hour sessions in the open field, the first hour without stimulation and the second with DCS applied for 30 s every tenth minute. In the lesioned group, DCS resulted in remarkably increased amounts of locomotion compared to the first hour, whereas sham animals actually moved less during DCS sessions than during non-DCS sessions (Fig. 4C). Hence, there were specific improvements of motor function in the Parkinsonian state compared with controls. In lesioned rats, DCS not only alleviated hypokinesia during stimulation but also caused an increase in locomotion after the stimulation period. This residual effect lasted ~100 s (Fig. 4B).

The effect of DCS on bradykinesia in 6-OHDA–lesioned rats was also evaluated. Lesioned animals showed a relative increase in the number of scored locomotion events for all movement speeds, but this effect was more pronounced for faster movements, indicating a specific effect on bradykinetic symptoms in addition to the general improvement in the overall amount of locomotion (Fig. 4D).

Discussion. We demonstrated that stimulation of the dorsal column pathways using epidural implanted bipolar electrodes—a simple, easy-to-perform, semi-invasive method—can restore locomotive capability in two animal models of PD symptoms: acutely dopamine-depleted mice and rats with dopaminergic neuronal loss. In parallel with the behavioral improvements, DCS shifted activity patterns in the primary motor cortex and in the dorsolateral striatum into a state closely resembling that found before and during spontaneous initiation of locomotion in normal and depleted animals. This suggests that DCS helps motor-related brain areas shift into a state permissive of the initiation of movements.

What could be the mechanisms through which DCS allows a shift into a locomotion-permissive state? The first possible explanation could be that DCS, in addition to stimulating specific somatosensory pathways, may also recruit brainstem arousal systems, leading to sufficient cortical and striatal desynchronization required for voluntary initiation of movements (*8*). Such a possibility can be raised when the phenomenon of paradoxical kinesia is considered, that is, rare events in which PD patients, aroused by frightening situations, exhibit sudden and transient improvement in motor function (*22*, *23*). Here, the increase by a factor of 4.9 in locomotion produced by DCS in control animals, albeit much less than that observed in dopamine-depleted animals, could in theory support such an arousal hypothesis. Yet, a variety of observations suggest that this may not be the main mechanism accounting for DCS-induced locomotion. First, neither air puffs alone nor stimulation of trigeminal nerve afferents, both potent somatosensory arousal stimuli, induced locomotion in either control or dopamine-depleted animals. Secondly, in control experiments carried out in both awake and lightly anesthetized animals, DCS produced only a minimal arousal response when compared with other tactile, proprioceptive, and nociceptive stimuli (fig. S9, A and B). This is in line with a previous study that demonstrated that dorsal column recruitment produces no significant arousal effect (*24*). Overall, these data suggest that DCS may increase locomotion behavior primarily through direct modulation of lemniscal/thalamic pathways. However, more experiments will be required to settle this issue.

Our electrophysiological data suggest possible mechanisms for the success of DCS in restoration of locomotion, based on existing theories of basal ganglia pathology in PD and specifically considering the circuitry known to be involved in initiating voluntary locomotion (*25*). The command to the spinal cord to initiate locomotion, via reticulospinal pathways, is issued by the diencephalic and mesencephalic locomotor regions. For these midbrain structures to become active and trigger locomotion, they must be relieved from the tonic inhibition exerted by the output nuclei of the basal ganglia. This is accomplished by activation of striatal medium spiny neurons projecting to the output nuclei of the basal ganglia (*26*, *27*). Under normal circumstances, the cortex has a powerful excitatory influence on the striatum. In contrast, with reduced striatal dopamine levels, the activation threshold of the projection neurons from the striatum is significantly increased (*25*), making it less likely that cortical input to the striatum will be conveyed through this pathway. As a consequence, brainstem motor regions remain under tonic inhibition, and the initiation of goal-directed locomotion and other types of volitional motor activity become impaired. DCS may exert its effect by activating large cortical areas, increasing the cortical and thalamic input to the striatum. This may, in turn, promote the depolarization and, consequently, facilitate the activation of striatal projection neurons. Another consequence of the reduced cortical control of striatum at low dopamine levels is that both thalamic and internally driven striatal low-frequency oscillations become more prominent (*28*, *29*). These oscillations may lead to increased synchronicity because the generation of action potentials tends to occur at more distinct phases of the LFP oscillation (*13*, *30*). This was confirmed in our experiments in which both motor cortex and striatum showed excessive low-frequency synchronized oscillatory activity

in dopamine-depleted animals and an increased entrainment of spikes to low-frequency components of the LFPs. Such synchronous activity interferes with normal information processing in these circuits and should likely be considered pathogenic in PD (*12*). Our data show that DCS effectively abolishes aberrant synchronous low-frequency oscillations. It is, therefore, tempting to speculate that the suppression of low-frequency oscillations is particularly important for amelioration of motor symptoms in PD (*31*).

Finally, the combined effect of L-dopa and DCS allowed for recovery of motor function at significantly lower doses of L-dopa in severely dopamine-depleted animals. The considerably less invasive nature of the epidural DCS electrode compared with DBS electrodes suggests that DCS could be a complement for treatment of symptoms of PD in earlier stages of the disease. We therefore propose that DCS should be investigated further in extensive experiments employing primate models of PD, preferably over longer time periods, to evaluate the potential viability of this new procedure as a treatment for Parkinsonian patients.

References and Notes

1. S. Fahn, *Ann. N.Y. Acad. Sci.* **991**, 1 (2003).
2. A. Carlsson, *Acta Neurol. Scand. Suppl.* **51**, 11 (1972).
3. O. Hornykiewicz, *Amino Acids* **23**, 65 (2002).
4. K. M. Shaw, A. J. Lees, G. M. Stern, *Q. J. Med.* **49**, 283 (1980).
5. A. L. Benabid, *Curr. Opin. Neurobiol.* **13**, 696 (2003).
6. J. S. Perlmutter, J. W. Mink, *Annu. Rev. Neurosci.* **29**, 229 (2006).
7. P. Plaha, Y. Ben-Shlomo, N. K. Patel, S. S. Gill, *Brain* **129**, 1732 (2006).
8. E. E. Fanselow, A. P. Reid, M. A. Nicolelis, *J. Neurosci.* **20**, 8160 (2000).
9. C. M. DeGiorgio, A. Shewmon, D. Murray, T. Whitehurst, *Epilepsia* **47**, 1213 (2006).
10. M. S. George *et al*., *Biol. Psychiatry* **47**, 287 (2000).
11. P. Brown *et al*., *J. Neurosci.* **21**, 1033 (2001).
12. C. Hammond, H. Bergman, P. Brown, *Trends Neurosci.* **30**, 357 (2007).
13. R. M. Costa *et al*., *Neuron* **52**, 359 (2006).
14. T. D. Sotnikova *et al*., *PLoS Biol.* **3**, e271 (2005).
15. D. J. Brooks, P. Piccini, *Biol. Psychiatry* **59**, 908 (2006).
16. K. G. Lloyd, L. Davidson, O. Hornykiewicz, *J. Pharmacol. Exp. Ther.* **195**, 453 (1975).
17. X. Drouot *et al*., *Neuron* **44**, 769 (2004).
18. K. Sakai, D. M. Gash, *Brain Res.* **633**, 144 (1994).
19. Materials and methods are available as supporting material on *Science* Online.
20. M. A. Cenci, I. Q. Whishaw, T. Schallert, *Nat. Rev. Neurosci.* **3**, 574 (2002).
21. C. Winkler, D. Kirik, A. Bjorklund, M. A. Cenci, *Neurobiol. Dis.* **10**, 165 (2002).
22. I. Schlesinger, I. Erikh, D. Yarnitsky, *Mov. Disord.* **22**, 2394 (2007).
23. M. Glickstein, J. Stein, *Trends Neurosci.* **14**, 480 (1991).
24. P. D. Wall, *Brain* **93**, 505 (1970).
25. S. Grillner, P. Wallen, K. Saitoh, A. Kozlov, B. Robertson, *Brain Res. Brain Res. Rev.* **57**, 2 (2008).
26. S. M. Brudzynski, M. Wu, G. J. Mogenson, *Can. J. Physiol. Pharmacol.* **71**, 394 (1993).
27. M. R. DeLong, *Trends Neurosci.* **13**, 281 (1990).
28. Y. Smith, D. V. Raju, J. F. Pare, M. Sidibe, *Trends Neurosci.* **27**, 520 (2004).
29. C. J. Wilson, *Neuron* **45**, 575 (2005).
30. J. D. Berke, M. Okatan, J. Skurski, H. B. Eichenbaum, *Neuron* **43**, 883 (2004).
31. A. A. Kuhn *et al*., *Brain* **127**, 735 (2004).

32. We thank W. M. Chan, G. Lehew, and J. Meloy for outstanding technical assistance; R. Gainetdinov, S.-C. Lin, H. Zhang, and K. Dzirasa for valuable comments; and S. Halkiotis for proofreading the manuscript. This work was supported by the National Institute of Neurological Disorders and Stroke (NINDS) R33NS049534 and the International Neuroscience Network Foundation to M.A.L.N., R01NS019576 and R01MH073853 to M.G.C., Ruth K. Broad Postdoctoral Award to R.F., and NRC and Knut and Alice Wallenberg Foundation to P.P. The content is solely the responsibility of the authors and does not necessarily represent the official views of the NINDS or the National Institutes of Health. M.A.L.N. dedicates this paper to Lily Safra for her continuing support and to the memory of his grandfather, Angelo Nicolelis, who suffered from Parkinson's disease. M.A.L.N. acknowledges a visiting professorship, Chaire Blaise Pascal, from the Région Ile de France at the Ecole Supérieure de Physique et de Chimie Industrielles, Paris.

Supporting Online Material

www.sciencemag.org/cgi/content/full/323/5921/1578/DC1
Materials and Methods
Figs. S1 to S9
Movie S1
References

20 August 2008; accepted 10 December 2008
10.1126/science.1164901

REPORTS

Alfvén Waves in the Lower Solar Atmosphere

David B. Jess,[1,2]* Mihalis Mathioudakis,[1] Robert Erdélyi,[3] Philip J. Crockett,[1] Francis P. Keenan,[1] Damian J. Christian[4]

The flow of energy through the solar atmosphere and the heating of the Sun's outer regions are still not understood. Here, we report the detection of oscillatory phenomena associated with a large bright-point group that is 430,000 square kilometers in area and located near the solar disk center. Wavelet analysis reveals full-width half-maximum oscillations with periodicities ranging from 126 to 700 seconds originating above the bright point and significance levels exceeding 99%. These oscillations, 2.6 kilometers per second in amplitude, are coupled with chromospheric line-of-sight Doppler velocities with an average blue shift of 23 kilometers per second. A lack of cospatial intensity oscillations and transversal displacements rules out the presence of magneto-acoustic wave modes. The oscillations are a signature of Alfvén waves produced by a torsional twist of ±22 degrees. A phase shift of 180 degrees across the diameter of the bright point suggests that these torsional Alfvén oscillations are induced globally throughout the entire brightening. The energy flux associated with this wave mode is sufficient to heat the solar corona.

Solar observations from both ground-based and spaceborne facilities show that a wide range of magneto-acoustic waves (*1*, *2*) propagate throughout the solar atmosphere. However, the energy they carry to the outer solar atmosphere is not sufficient to heat it (*3*). Alfvén waves (pure magnetic waves), which are incompressible and can penetrate through the stratified solar atmosphere without being reflected (*4*), are the most promising wave mechanism to explain the heating of the Sun's outer regions.

However, it has been suggested that their previous detection in the solar corona (*5*) and upper chromosphere (*6*) is inconsistent with magneto-hydrodynamic (MHD) wave theory (*7*, *8*). These observations are best interpreted as a guided-kink magneto-acoustic mode, whereby the observational signatures are usually swaying, transversal, periodic motions of the magnetic flux tubes (*7*, *9*). Numerical simulations (*10*) show that subsurface acoustic drivers and fast magneto-sonic kink waves (*11*, *12*) can convert energy into upwardly propagating Alfvén waves, which are emitted from the solar surface. These numerical simulations are also in agreement with current analytical studies. In particular, it has been shown that footpoint motions in an axially symmetric system can excite torsional Alfvén waves (*13*). Other Alfvén wave modes may exist, although these are normally coupled to magneto-sonic MHD waves (*14*). In the solar atmosphere, magnetic field lines clump into tight bundles, forming flux tubes. Alfvén waves in flux tubes could manifest as torsional oscillations (*7*) that create simultaneous blue and red shifts, leading to the non-thermal broadening of any isolated line profile, and should thus be observed as full-width half-maximum (FWHM) oscillations (*15*). A promising location for the detection of Alfvén waves is

[1]Astrophysics Research Centre, School of Mathematics and Physics, Queen's University, Belfast, BT7 1NN, Northern Ireland, UK. [2]Solar Physics Laboratory, NASA Goddard Space Flight Center, Code 671, Greenbelt, MD 20771, USA. [3]Solar Physics and Space Plasma Research Centre, University of Sheffield, Hicks Building, Hounsfield Road, Sheffield, S3 7RH, England, UK. [4]Department of Physics and Astronomy, California State University Northridge, 18111 Nordhoff Street, Northridge, CA 91330, USA.

*To whom correspondence should be addressed. E-mail: d.jess@qub.ac.uk

in the lower solar atmosphere, where they can be generated by the overshooting of convective motions in the photosphere (*16*). Here, we report the detection of substantially blue-shifted plasma and FWHM oscillations originating in a large conglomeration of magnetic bright points.

We used the Swedish Solar Telescope (SST) to image a 68-by-68–arc sec region on the solar surface positioned near the disk center. Using the Solar Optical Universal Polarimeter (SOUP) (*17*) and high-order adaptive optics (*18*), we obtained narrowband images across the Hα absorption profile centered at 6562.8 Å. We observed with a cadence of 0.03 s to obtain 89 min of uninterrupted data. Because SOUP is tunable, we sampled the complete Hα line profile using seven discrete steps. The wavelength intervals we chose became increasingly narrow toward the line core in order to enable an accurate determination of the line characteristics, such as Doppler velocities, FWHMs, and intensities. Our images have a sampling of 0.068 arc sec per pixel, which corresponds to ≈110-km resolution (two pixels) on the solar surface.

By using the multi-object multi-frame blind deconvolution (MOMFBD) (*19*) image restoration technique to remove the small-scale atmospheric distortions present in the data, we achieved an effective cadence of 63 s for a full line profile. We acquired 85 complete scans across the Hα line profile in addition to 595 simultaneous continuum images. For each of the 85 profile scans, every pixel of the 1024-by-1024–pixel^2 charge-coupled device contains information acquired at a particular wavelength position. Therefore, we obtained a total of 8.9×10^7 individual Hα absorption profiles, covering the full 68-by-68–arc sec field of view, during the 89-min duration of the data set. We fit a Gaussian distribution to each of the observed Hα profiles to obtain values for the integrated intensity and FWHM. To determine the line-of-sight velocity, we compared each measured central wavelength position with the rest-frame Hα profile core at 6562.8 Å. We created time series for intensity, line-of-sight velocity, FWHM, and wavelength-integrated data cubes and used fast Fourier transform and wavelet routines to analyze them.

The SST field of view shows a range of features, including pores, exploding granules, and a multitude of bright points (Fig. 1), a large conglomeration of which is located at heliocentric coordinates (–10 arc sec, 10 arc sec) or N07E01 in the solar north-south–east-west coordinate system. We selected a 10-by-10–arc sec box surrounding the bright-point group (BPG), which occupies an area of 430,000 km^2, for

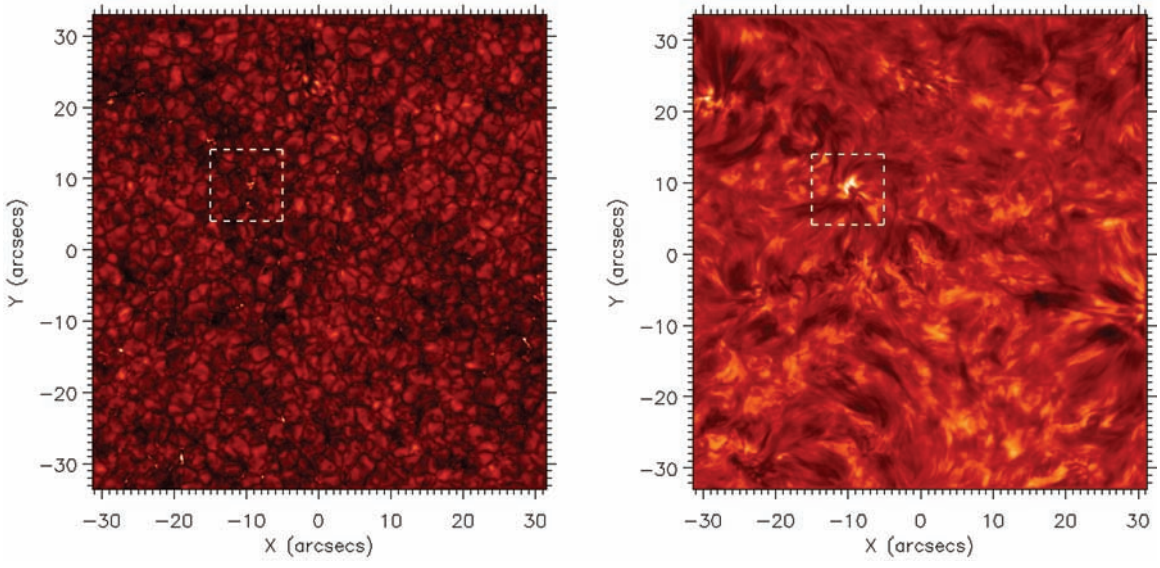

Fig. 1. Simultaneous images in the (**left**) Hα continuum (photosphere) and (**right**) Hα core (chromosphere) obtained with the SST. The conglomeration of bright points within the region we investigated is denoted by a square of dashed lines. The scale is in heliocentric coordinates where 1 arc sec ≈ 725 km.

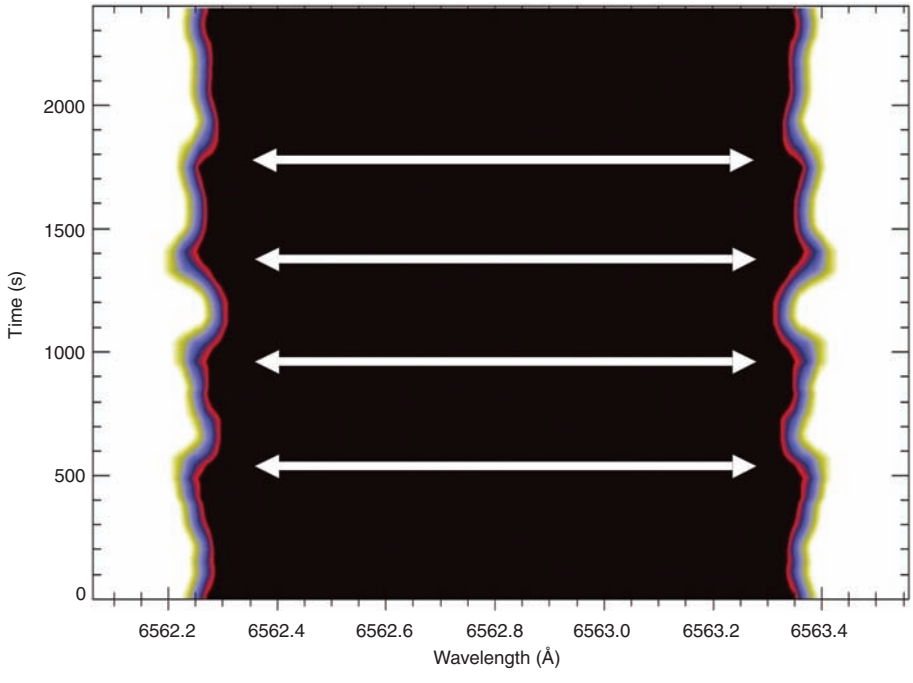

Fig. 2. A wavelength-versus-time plot of the Hα profile showing the variation of line width at FWHM as a function of time. The arrows indicate the positions of maximum amplitude of a 420-s periodicity associated with the bright-point group located at (–10 arc sec, 10 arc sec) in Fig. 1. The torsional motion of the Alfvénic perturbations creates nonthermal broadening that is visible in the Hα line profile. The peak-to-peak velocity is ≈3.0 km s^{-1} (≈65 mÅ). For an inclination angle of 35°, the absolute velocity amplitude is ≈2.6 km s^{-1}.

further investigation. The line-of-sight Doppler velocities associated with this BPG show blue shifts with an average value of 23 km s^{-1}. There is no evidence of periodic trends in either intensity or line-of-sight velocity; the intensity of the BPG is constant, with minimal variation during its 53-min lifetime.

Wavelet analysis shows that FWHM oscillations with significance levels exceeding 99% occur within the spatially averaged BPG (Fig. 2). We detected FWHM oscillations as low as the Nyquist period (126 s) throughout the duration of the data set, with the strongest detected power originating in the 400-to-500-s interval. These oscillations are located directly above the large BPG, encompassing a near-circular shape that is cospatial with the detected Doppler velocities, and are apparent in all FWHM time series. This shows that powerful coherent periodicities are present throughout the surface of the BPG. We detected oscillations until the BPG fragmented into a series of smaller bright points after 3150 s.

Numerical simulations based on three-dimensional magnetoconvection show that the bright points that were observed in the wing of the Hα line profile correspond to magnetic field concentrations measured in kilogauss in the photosphere (*20*). The canopy structure seen in the Hα core images reveals a wealth of flux-tube structures, with many securing anchor positions in the photosphere directly above the BPG (Fig. 1). The coincidence of bright-point structures with high magnetic field concentrations implies that MHD waves are likely to be present (*21*). However, the chromospheric brightening is of much larger physical size than the underlying photospheric BPG. Because the observations were made very close to the center of the solar disk, an increase in physical size between the photosphere and the chromosphere can be interpreted as an expansion of the photospheric flux-tube bundle as a function of atmospheric height (*22*). A comparison of the maximum diameter of the bright point at each height in the atmosphere suggests an expansion of ~1300 km; a height separation of ≈1000 km and a symmetric expansion around the bright-point center suggest a flux-tube expansion angle of ≈33°. Additionally, an offset of ≈700 km between the centres of the BPG at photospheric and chromospheric heights suggests a magnetic flux-tube tilt angle of ≈35° from the vertical.

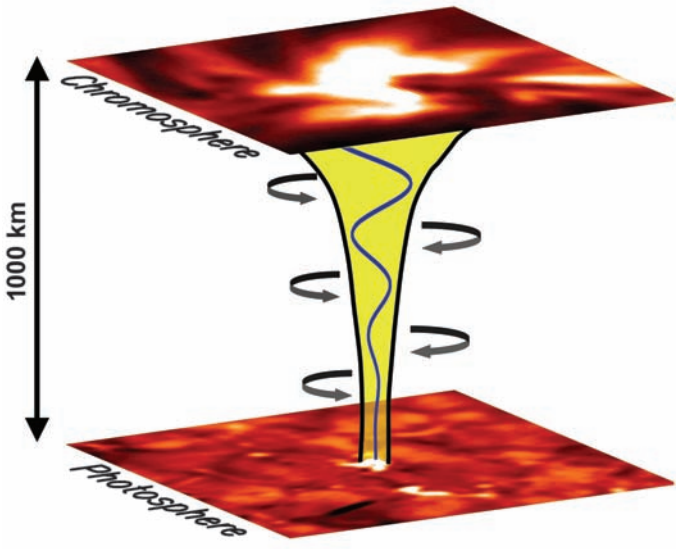

Fig. 3. Expanding magnetic flux tube sandwiched between photospheric and chromospheric intensity images obtained with the SST, undergoing a torsional Alfvénic perturbation and generating a wave that propagates longitudinally in the vertical direction. At a given position along the flux tube, the Alfvénic displacements are torsional oscillations that remain perpendicular to the direction of propagation and magnetic field outlining constant magnetic surfaces. The largest FWHM will be produced when the torsional velocity is at its maximum (at zero displacement from the equilibrium position). The figure is not to scale.

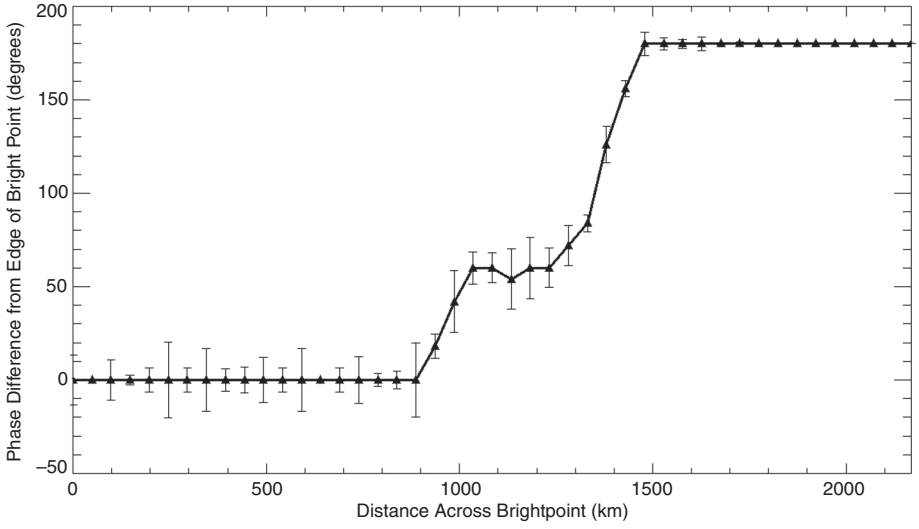

Fig. 4. Average phase difference of FWHM oscillations plotted as a function of distance across the diameter of the bright point. The triangles denote the locations where a measurement is made, and the error bars indicate the phase variance in the temporal domain. The phase at 0 km is used as a reference, with all other phases plotted relative to this value. Spatial coherence of FWHM oscillations across the BPG ranges between 90 and 100%, suggesting that the BPG is acting as a coherent waveguide. The phase difference increases around the midpoint of the BPG with opposite sides of the waveguide, indicating out-of-phase oscillatory phenomena, which is as predicted for a torsional Alfvénic perturbation.

Alfvénic fluxes are predicted to be at their strongest in the regime of high magnetic field strength and moderately inclined waveguides (*10*). Because of their incompressibility, they exhibit no periodic intensity perturbations. Thus, the observational signature of a torsional Alfvén wave propagating with a velocity component along the observer's line of sight will arise from its torsional velocities on small spatial scales (*8*). These torsional velocities are responsible for the FWHM oscillations we observed (Fig. 3). The line-of-sight velocity amplitude of ≈1.5 km s^{-1} and the inclination angle of ≈35° indicate an absolute Alfvénic perturbation amplitude of ≈2.6 km s^{-1}. Because the circumference of the photospheric bright point [where torsional Alfvén waves are believed to be generated (*16*)] is on the order of 2800 km (55 pixels), a torsional twist of ±22° is sufficient to generate the observed wave motion.

The moderate inclination angle of the flux tubes, coupled with the detection of substantially blue-shifted material and strong FWHM oscillations, is evidence of the presence of torsional Alfvén waves. For a typical photospheric internal waveguide electron density (*23*) of $n_e^i \approx 10^{16}$ cm^{-3} and a magnetic field strength (*20*) of 1000 G, the Alfvén speed within a cylindrical flux tube is estimated (*14*) to be ≈22 km s^{-1}. This value is above the speed of sound in the upper photosphere/lower chromosphere (*24*) and is consistent with the blue-shift velocity we determined.

We took a slice through the center of the bright point and analyzed the stability of opposite edges of the BPG as a function of time. This was performed by examining any displacements of the BPG from its initial position at the start of the observing sequence (fig. S1). The bright point moves less than one pixel during the first 3150 s. As the BPG begins to fragment after 3150 s, the motions of the bright-point edges increase substantially. However, we did not find periodic motions of the bright point, particularly during the initial 3150 s when the FWHM oscillations were detected. A magneto-acoustic wave mode would produce ob-

servable periodicities in intensity, similar to those caused by the periodic contractions when viewed along the flux tube, that are associated with sausage-mode waves (*25*). A sausage-mode wave is caused by the axially symmetric expansion and contraction of magnetic flux tubes (*14*). Kink-mode oscillations are generated through a bulk motion, whereby the whole flux tube is displaced from its original position in a periodic fashion. Therefore, magneto-acoustic waves cannot explain our observations.

A torsional Alfvénic perturbation should produce a FWHM oscillation that is 180° out of phase at opposite boundaries of the waveguide (*8*). The relative time-averaged oscillatory phase as a function of distance across the ≈2200-km diameter of the bright point shows that opposite sides of the bright point display oscillatory phenomena that are indeed 180° out of phase (Fig. 4). This is consistent with current torsional Alfvénic wave models (*26*).

We estimated the energy flux of the observed waves using $E = \rho v^2 v_A$, where ρ is the mass density of the flux-tube, v is the observed velocity amplitude, and v_A is the Alfvén speed (*6*). For a mass density of $\rho \approx 1 \times 10^{-6}$ kg m^{-3}, derived from a quiet-Sun chromospheric model (*23*), the energy flux in the chromosphere is $E \approx 15000$ W m^{-2}. At any one time, it is estimated (*27*) that at least 1.6% of the solar surface is covered by BPGs similar to that presented here. Thus, combining the energy carried by similar BPGs over the entire solar surface produces a global average of 240 W m^{-2}. Alfvén waves with an energy flux of ≈100 W m^{-2} are believed to be vigorous enough to heat the localized corona or to launch the solar wind when their energy is thermalized (*6*, *28*). Therefore, a transmission coefficient of ≈42% through the thin transition region will provide sufficient energy to heat the entire corona. Regions containing highly magnetic structures, such as bright points, should possess even higher mass densities (*29*). In this regime, the energy flux available to heat the corona will be substantially higher than the minimum value required to sustain localized heating.

References and Notes

1. Magneto-acoustic waves, normally classified as fast and slow, are waves of acoustic origin whose properties are modified by the presence of a magnetic field.
2. V. M. Nakariakov, E. Verwichte, *Living Rev. Sol. Phys.* **2**, 3 (2005).
3. A. Fossum, M. Carlsson, *Nature* **435**, 919 (2005).
4. L. Ofman, *Astrophys. J.* **568**, L135 (2002).
5. S. Tomczyk *et al.*, *Science* **317**, 1192 (2007).
6. B. De Pontieu *et al.*, *Science* **318**, 1574 (2007).
7. R. Erdélyi, V. Fedun, *Science* **318**, 1572 (2007).
8. T. Van Doorsselaere, V. Nakariakov, E. Verwichte, *Astrophys. J.* **676**, L73 (2008).
9. V. Kukhianidze, T. V. Zaqarashvili, E. Khutsishvili, *Astron. Astrophys.* **449**, L35 (2006).
10. P. S. Cally, M. Goossens, *Sol. Phys.* **251**, 251 (2008).
11. M. Goossens, I. Arregui, J. L. Ballester, T. J. Wang, *Astron. Astrophys.* **484**, 851 (2008).
12. W. J. Tirry, M. Goossens, *Astrophys. J.* **471**, 501 (1996).
13. M. S. Ruderman, D. Berghmans, M. Goossens, S. Poedts, *Astron. Astrophys.* **320**, 305 (1997).
14. P. M. Edwin, B. Roberts, *Sol. Phys.* **88**, 179 (1983).
15. T. V. Zaqarashvili, *Astron. Astrophys.* **399**, L15 (2003).
16. J. Vranjes, S. Poedts, B. P. Pandey, B. De Pontieu, *Astron. Astrophys.* **478**, 553 (2008).
17. A. M. Title, W. J. Rosenberg, *Opt. Eng.* **20**, 815 (1981).
18. G. B. Scharmer, P. M. Dettori, M. G. Lofdahl, M. Shand, *Proc. SPIE* **4853**, 370 (2003).
19. M. van Noort, L. H. M. Rouppe van der Voort, M. G. Lofdahl, *Sol. Phys.* **228**, 191 (2005).
20. J. Leenaarts, R. J. Rutten, P. Sütterlin, M. Carlsson, H. Uitenbroek, *Astron. Astrophys.* **449**, 1209 (2006).
21. W. Kalkofen, *Astrophys. J.* **486**, L145 (1997).
22. S. K. Solanki, W. Finsterle, I. Ruedi, W. Livingston, *Astron. Astrophys.* **347**, L27 (1999).
23. J. E. Vernazza, E. H. Avrett, R. Loeser, *Astrophys. J. Suppl.* **45**, 635 (1981).
24. B. Sánchez-Andrade Nũno, N. Bello González, J. Blanco Rodriguez, F. Kneer, K. G. Puschmann, *Astron. Astrophys.* **486**, 577 (2008).
25. V. M. Nakariakov, V. F. Melnikov, V. E. Reznikova, *Astron. Astrophys.* **412**, L7 (2003).
26. P. Copil, Y. Voitenko, M. Goossens, *Astron. Astrophys.* **478**, 921 (2008).
27. D. S. Brown, C. E. Parnell, E. E. Deluca, L. Golub, R. A. McMullen, *Sol. Phys.* **201**, 305 (2001).
28. A. Verdini, M. Velli, *Astrophys. J.* **662**, 669 (2007).
29. D. Pérez-Suárez, R. C. Maclean, J. G. Doyle, M. S. Madjarska, *Astron. Astrophys.* **492**, 575 (2008).

30. D.B.J. is supported by a Northern Ireland Department for Employment and Learning studentship and thanks NASA Goddard Space Flight Center for a Co-operative Award in Science and Technology studentship. R.E. thanks M. Kéray for encouragement and is grateful to NSF, Hungary (Országos Tudományos Kutatási Alapprogram, ref. no. K67746), for financial support. F.P.K. is grateful to the Atomic Weapons Establishment–Aldermaston for the award of a William Penney Fellowship. The SST is operated on the island of La Palma by the Institute for Solar Physics of the Royal Swedish Academy of Sciences in the Spanish Observatorio del Roque de los Muchachos of the Instituto de Astrofísica de Canarias. These observations have been funded by the Optical Infrared Coordination network, an international collaboration supported by the Research Infrastructures Programme of the European Commission's Sixth Framework Programme. This work is supported by the Science and Technology Facilities Council, and we thank L. H. M. Rouppe van der Voort for help with MOMFBD image processing.

Supporting Online Material

www.sciencemag.org/cgi/content/full/323/5921/1582/DC1
Fig. S1

18 November 2008; accepted 27 January 2009
10.1126/science.1168680

The Disorder-Free Non-BCS Superconductor Cs_3C_{60} Emerges from an Antiferromagnetic Insulator Parent State

Yasuhiro Takabayashi,[1]* Alexey Y. Ganin,[2]* Peter Jeglič,[3] Denis Arčon,[3,4] Takumi Takano,[5] Yoshihiro Iwasa,[5] Yasuo Ohishi,[6] Masaki Takata,[6,7] Nao Takeshita,[8] Kosmas Prassides,[1]† Matthew J. Rosseinsky[2]†

The body-centered cubic A15-structured cesium fulleride Cs_3C_{60} is not superconducting at ambient pressure and is free from disorder, unlike the well-studied face-centered cubic A_3C_{60} alkali metal fulleride superconductors. We found that in Cs_3C_{60}, where the molecular valences are precisely assigned, the superconducting state at 38 kelvin emerges directly from a localized electron antiferromagnetic insulating state with the application of pressure. This transition maintains the threefold degeneracy of the active orbitals in both competing electronic states; it is thus a purely electronic transition to a superconducting state, with a dependence of the transition temperature on pressure-induced changes of anion packing density that is not explicable by Bardeen-Cooper-Schrieffer (BCS) theory.

Superconductivity requires an attractive interaction between electrons to form Cooper pairs, which form a condensate that can move without electrical resistance. In simple metals and alloys, the Bardeen-Cooper-Schrieffer (BCS) theory explains how electron-phonon coupling overcomes the repulsion between negatively charged electrons (*1*). In high-temperature superconductors, such as the copper oxides and iron oxyarsenides, the origin of the attraction is less clear. Beyond the theoretical challenges, the experiments are complicated by imperfections within the materials, such as structural disorder, low symmetry and dimensionality, and variations in chemical valence at the electronically active sites. Here we show that in the cubic alkali metal fulleride Cs_3C_{60}, which is completely ordered and for which precise valences can be assigned, the 38 K superconducting state (*2*) emerges directly from a localized electron antiferromagnetic insulating (AFI) state with the application of pressure as the anion packing density increases. This transition maintains the threefold degeneracy of the active orbitals in both competing electronic states, and is thus a purely electronic transition to a superconducting state. The transition temperature T_c depends on the anion packing density in a way that is not explicable within a simple BCS approach.

In systems where the bands in which the electrons move are narrow, there are electron-electron correlation energies associated with inter-electron repulsion, which are comparable to the electronic bandwidth. These electron correlation effects (*3*) need to be taken into account in understanding the mechanisms for formation of the Cooper pairs (*4*). These concepts have been developed primarily in d-electron–based systems

such as the cuprates and iron oxyarsenides, where doping, with the associated structural disorder and distribution of metal charge states and d-electron counts within the material, is required to produce superconductivity by suppressing magnetically ordered states. In addition, recent theoretical work (*5*, *6*) indicates that the competition between correlation and delocalization energies is critically controlled by the degeneracy of the orbitals (*7*) carrying the active electrons, but this cannot be investigated in d-electron–based superconductors because their low-symmetry crystal structures remove the degeneracy.

An ideal material for understanding the interactions producing superconductivity in such structurally and chemically complex correlated electron systems would allow the isolation of the influence of purely electronic factors without the complications of disorder, structural transitions, and low dimensionality, while maintaining the site symmetry required for orbital degeneracy in all the potentially competing electronic ground states. The threefold degeneracy of the t_{1u} lowest unoccupied molecular orbital (LUMO) of the C_{60} molecule is maintained in the superconducting face-centered cubic (fcc) A_3C_{60} alkali metal fullerides (*8*), which have electronic structures arising from weak overlap of the s/p-derived frontier orbitals of molecular anions. However, the properties of this family—in particular, the monotonic increase of the superconducting T_c to 33 K (*9*) with interfullerene separation—can be well explained by BCS-like theories where T_c is controlled by the increase in density of states at the Fermi level, $N(E_F)$, with expansion; an anomalous decrease of T_c at high interfullerene separations is only observed in heavily disordered fcc systems superconducting at ambient pressure (*10*). There is thus no definitive experimental evidence for a non-BCS origin for superconductivity, where correlation or orbital degeneracy would play a role, as no usefully comparable competing insulating state from which superconductivity emerges has been identified.

All of the fcc A_3C_{60} fullerides are superconducting at ambient pressure, but the recently isolated (*2*) Cs_3C_{60} (*11*, *12*), which adopts the so-called A15 structure based on body-centered cubic (bcc) packing of the C_{60}^{3-} anions (Fig. 1A), is not. Cs_3C_{60} is the most expanded binary A_3C_{60} system yet reported (*2*) and thus offers the opportunity to identify the electronic ground state that competes with superconductivity in the orbitally degenerate cubic fullerides. We used magnetization, optical reflectivity, muon spin relaxation (μSR), and ^{13}C and ^{133}Cs nuclear magnetic resonance (NMR) measurements, coupled with ultrahigh-resolution synchrotron x-ray diffraction under variable pressure and temperature, to identify the ambient-pressure nonsuperconducting electronic ground state of bcc-based Cs_3C_{60} and investigate how it transforms into the superconducting state with the application of pressure.

High-resolution diffraction data (*2*) show that the cubic symmetry of A15 Cs_3C_{60}, and thus the point symmetry producing the t_{1u} orbital degeneracy, is maintained to the lowest temperatures at ambient pressure, so we undertook magnetization measurements to reveal the electronic ground state in competition with superconductivity. The temperature dependence of the paramagnetic susceptibility χ [also measured via the high-field slope of field-dependent magnetization, $M(H)$ isotherms] of a representative A15-rich Cs_3C_{60} sample (*13*) [which also contains the body-centered orthorhombic (bco) $Cs_{3+x}C_{60}$ and the fcc Cs_3C_{60} polymorphs (*2*)] is shown in Fig. 1C. These data reveal a well-defined cusp in $\chi(T)$ at 46 K; at higher temperatures, the susceptibility obeys the Curie-Weiss law with a negative Weiss temperature, consistent with antiferromagnetic correlations.

Field-cooled (FC) measurements in low applied fields (Fig. 1D) reveal a sharp increase in the magnetization $M(T)$ at 46 K, exactly the same temperature at which the cusp in the susceptibility, $\chi(T)$, occurs. The spontaneous magnetic moment approaches a value of 5.5 emu Oe mol^{-1} at 2 K, corresponding to a very small moment per C_{60} of ~0.001 Bohr magneton (μ_B). These data suggest a transition to an antiferromagnetically ordered state below the Néel temperature $T_N = 46$ K, with a small spin canting between the two magnetic sublattices giving rise to weak ferromagnetism. Systematic FC magnetization measurements on a

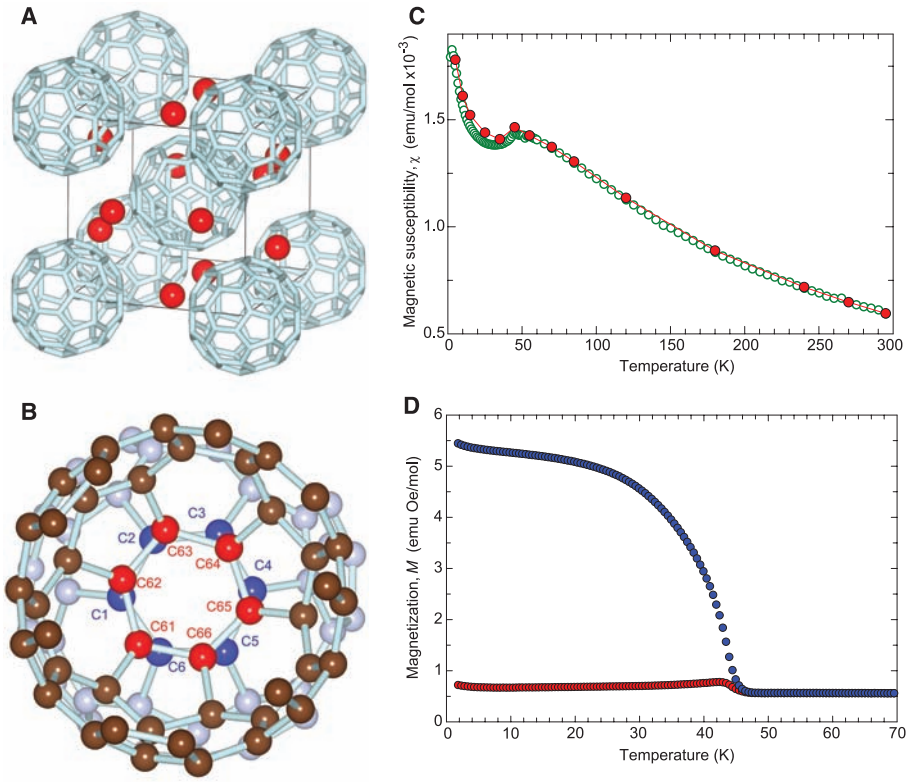

Fig. 1. (**A**) Crystal structure of A15 Cs_3C_{60} (space group $Pm\bar{3}n$) based on bcc anion packing with orientationally ordered C_{60}^{3-} anions. Cs cations are shown in red. (**B**) Intermolecular hexagon-hexagon-facing C_{60}^{3-}–C_{60}^{3-} nearest-neighbor contacts viewed along the molecule center–molecule center directions for the A15 structure. Note the absence of a center of inversion in the contact region that leads to a small misalignment of the neighboring hexagonal faces (C2-C62-C63 angle = 86°, C2-C63-C64 angle = 96°). (**C**) Temperature dependence of the magnetic susceptibility, χ, of Cs_3C_{60} at ambient pressure. Green open circles show $\chi(T)$ as obtained from the difference of the values measured at applied fields of 5 and 3 T in order to remove the influence of adventitious ferromagnetic impurities. Red solid circles show $\chi(T)$ as extracted from the high-field slope of $M(H)$ isotherms in the field range 0 to 5 T. Between 150 and 300 K, $\chi(T)$ follows the Curie-Weiss law, yielding an effective moment $\mu_{eff} = 1.32 \pm 0.01\ \mu_B/C_{60}$ (consistent with $S = ½$ in the majority C_{60}^{3-} phase and diamagnetism from the bco impurity) with a Weiss temperature $\Theta = -68 \pm 1$ K. (**D**) Temperature dependence of the magnetization, M, of Cs_3C_{60} measured in an applied field of 100 Oe (red circles, ZFC protocol; blue circles, FC protocol). T_N is defined as the temperature at which M begins to increase.

[1]Department of Chemistry, University of Durham, Durham DH1 3LE, UK. [2]Department of Chemistry, University of Liverpool, Liverpool L69 7ZD, UK. [3]Institute Jožef Stefan, Jamova 39, 1000 Ljubljana, Slovenia. [4]Faculty of Mathematics and Physics, University of Ljubljana, Jadranska 19, 1000 Ljubljana, Slovenia. [5]Institute for Materials Research, Tohoku University, Sendai 980-8577, Japan. [6]Japan Synchrotron Radiation Research Institute, SPring-8, Hyogo 679-5198, Japan. [7]RIKEN SPring-8 Center, Hyogo 679-5148, Japan. [8]Nanoelectronics Research Institute, National Institute of Advanced Industrial Science and Technology, Tsukuba, Ibaraki 305-8562, Japan.

*These authors contributed equally to this work.
†To whom correspondence should be addressed. E-mail: k.prassides@durham.ac.uk (K.P.); m.j.rosseinsky@liverpool.ac.uk (M.J.R.)

series of Cs_3C_{60} samples further reveal that the spontaneous magnetic moment scales with the fraction of the A15 phase present in the measured samples (fig. S1) (*13*). In addition, pure bco $Cs_{3+x}C_{60}$ samples show no magnetic transitions (fig. S1), and both the cusp in $\chi(T)$ and the sharp increase in $M(T)$ at 46 K are completely lost when the air-sensitive materials are exposed to air, ruling out adventitious contamination by metal oxide or metal particles as the origin of the magnetic transitions observed. Therefore, we attribute the antiferromagnetic response to the A15 Cs_3C_{60} polymorph.

An even more definitive association of this magnetic behavior in the bulk sample with the A15 Cs_3C_{60} phase that produces superconductivity upon application of pressure requires the use of a local probe to isolate the behavior of the A15 phase. The ^{13}C and ^{133}Cs nuclei in NMR studies are suitable probes because they allow direct identification of the component phases via their chemical shifts and site symmetries. In particular, the ^{133}Cs NMR resonance, when recorded with the solid echo pulse sequence, is suppressed for the two high-symmetry (8*c*) (¼,¼,¼) and (4*b*) (½,½,½) Cs sites in the fcc structure, as they have no electric field gradient (*14*). This approach isolates the resonance from the Cs cations in the lower-symmetry (6*c*) (¼,½,0) sites within the A15 structure, which allow quadrupolar interactions to be present. [See (*13*) for details of the NMR measurements; a key point is that the cation sites in the bco phase also have lower than axial symmetry, which suppresses their signal amplitudes in these experiments by lineshape broadening.] The temperature dependence of the ^{133}Cs NMR spectra of the A15 Cs_3C_{60} polymorph reveals substantial line broadening below 46 K (Fig. 2A), which demonstrates that the $M(T)$ and $\chi(T)$ features observed by magnetometry measurements indeed arise from antiferromagnetic ordering in this bcc-based phase. The lineshape broadening and the associated increase in the ^{133}Cs NMR second moment M_2 (Fig. 2B) arise from the onset of large dipolar fields of the C_{60}^{3-} anions at the ^{133}Cs sites in the antiferromagnetic phase. If we define $M_2 = M_2^Q + M_2^e$—where M_2^Q is the second moment associated with the nearly temperature-independent quadrupole interaction ($\sqrt{M_2^Q} \approx 30$ kHz) and M_2^e is the electron-nuclear dipolar broadening—the dipolar coupling between the antiferromagnetically ordered moments of the C_{60}^{3-} anions and the Cs cations ($\sqrt{M_2^e} \approx 50$ kHz) then allows an estimate of the ordered moment as ~1 μ_B per anion (*13*). The lineshape change and broadening of the ^{13}C spectra at the same temperature (fig. S2) (*13*) also confirm this interpretation. The ^{13}C spin-lattice relaxation time T_1 (Fig. 2C) is temperature-independent over the range 100 to 400 K, in contrast to the behavior of fcc A_3C_{60} metallic fullerides, in which T_1 follows the Korringa relation (*15*, *16*).

We conclude that the A15 Cs_3C_{60} phase is an insulator at ambient pressure, as also confirmed by infrared reflectivity data (Fig. 2D). Below

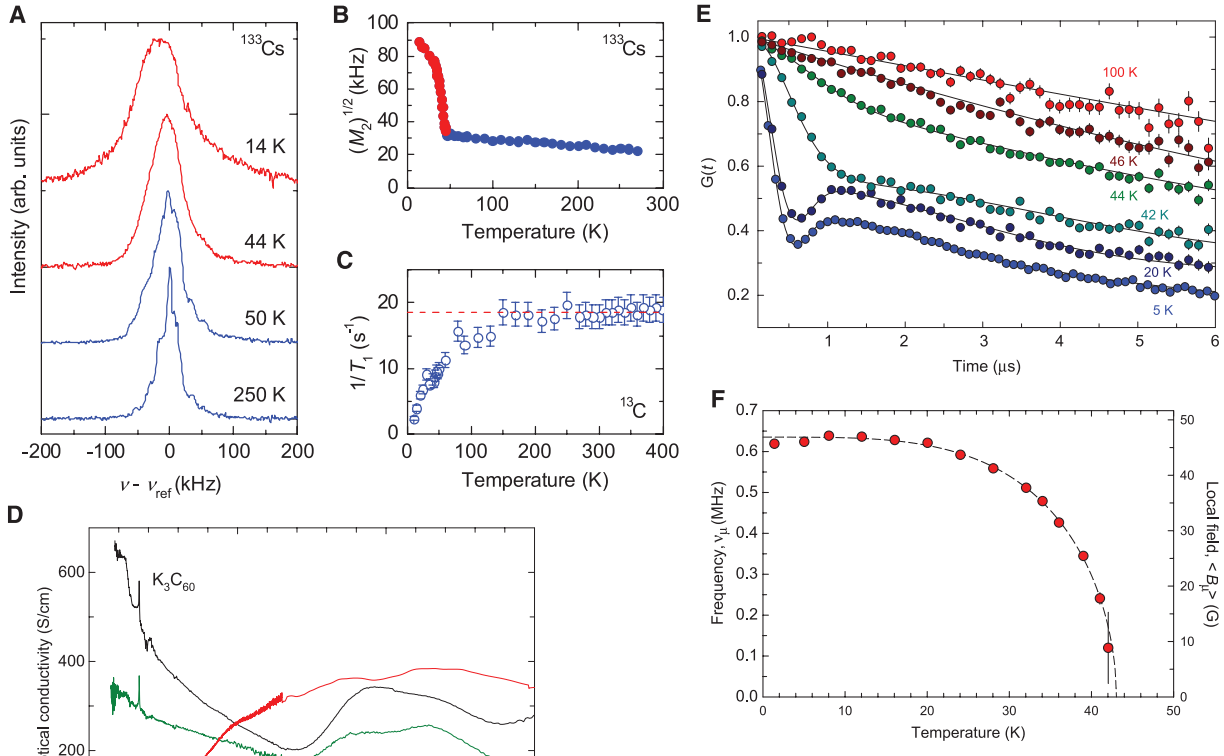

Fig. 2. (**A**) Temperature evolution of the ^{133}Cs NMR spectra of Cs_3C_{60} through the antiferromagnetic transition at $T_N = 46$ K. The characteristic powdered quadrupole lineshape (which can be simulated with an axially symmetric Cs site and is thus incompatible with those in the bco phase; the solid-echo pulse sequence used suppresses the signal for the fcc phase) at high temperatures (e.g., 250 K, blue spectra) changes to a very broad featureless lineshape below T_N (e.g., 14 K, red spectra). (**B**) Temperature dependence of the square root of the second moment, $\sqrt{M_2}$, of the ^{133}Cs NMR spectra, which reveals line broadening at T_N. (**C**) Temperature dependence of the ^{13}C spin lattice relaxation rate, $1/T_1$. The dashed line marks the average temperature-independent value of $1/T_1 = 18.5 \pm 0.5$ s^{-1} at high temperatures ($T_1 = 54 \pm 2$ ms). (**D**) Optical conductivity spectra for the trivalent cubic fullerides K_3C_{60}, Rb_3C_{60}, and Cs_3C_{60}, calculated from the reflectivity spectra at room temperature. In contrast to the Drude-type spectra characteristic of the metallic state of the ambient-pressure superconductors K_3C_{60} and Rb_3C_{60} (*28*), Cs_3C_{60} displays conductivity that decreases with photon energy, providing direct evidence for the insulating state. (**E**) Temperature evolution of $G_\mu(t)$, the ZF μ^+ spin relaxation function of Cs_3C_{60}. At temperatures higher than 46 K, the μ^+SR spectra are characteristic of the presence of weak static nuclear dipole moments together with an additional slow relaxation arising from fluctuating electronic moments. Below the 46 K freezing temperature, the μ^+SR spectra are dominated by a short-lived heavily damped oscillating signal whose depolarization gradually increases with decreasing temperature. (**F**) Temperature dependence of the ZF muon spin precession frequency, ν_μ, and of the local field at the muon site, $\langle B_\mu \rangle$. The line through the data points is a guide to the eye. All data shown were recorded at ambient pressure.

~100 K, $1/T_1$ suddenly begins to decrease and shows nearly activated behavior, implying the opening of a spin gap at temperatures well above T_N. The onset of antiferromagnetic long-range order is also confirmed by complementary zero-field muon spin relaxation (ZF-μ^+SR) measurements. A heavily damped spontaneous muon precession present below 46 K (Fig. 2E) demonstrates coherent ordering of the C_{60}^{3-} electronic moments. The quasi-static nature of the local magnetic field is confirmed by the complete recovery of the asymmetry in a longitudinal field of 250 Oe (fig. S3) (*13*). The μ^+ Larmor frequency ν_μ is 0.624 ± 0.002 MHz at 5 K and corresponds to a static internal field at the muon site, $\langle B_\mu \rangle = 46.0 \pm 0.2$ G (Fig. 2F); ν_μ is comparable to the value of 0.64 ± 0.01 MHz observed for the $(NH_3)K_3C_{60}$ antiferromagnet (*17*), which has a magnetic moment of ~1 μ_B/C_{60}. Thus, all of these experimental results indicate the presence of $S = ½$ moments localized on the fulleride anions in the insulating A15 Cs_3C_{60} phase at ambient pressure and ordering to form the AFI phase at 46 K, thereby demonstrating the key role played by

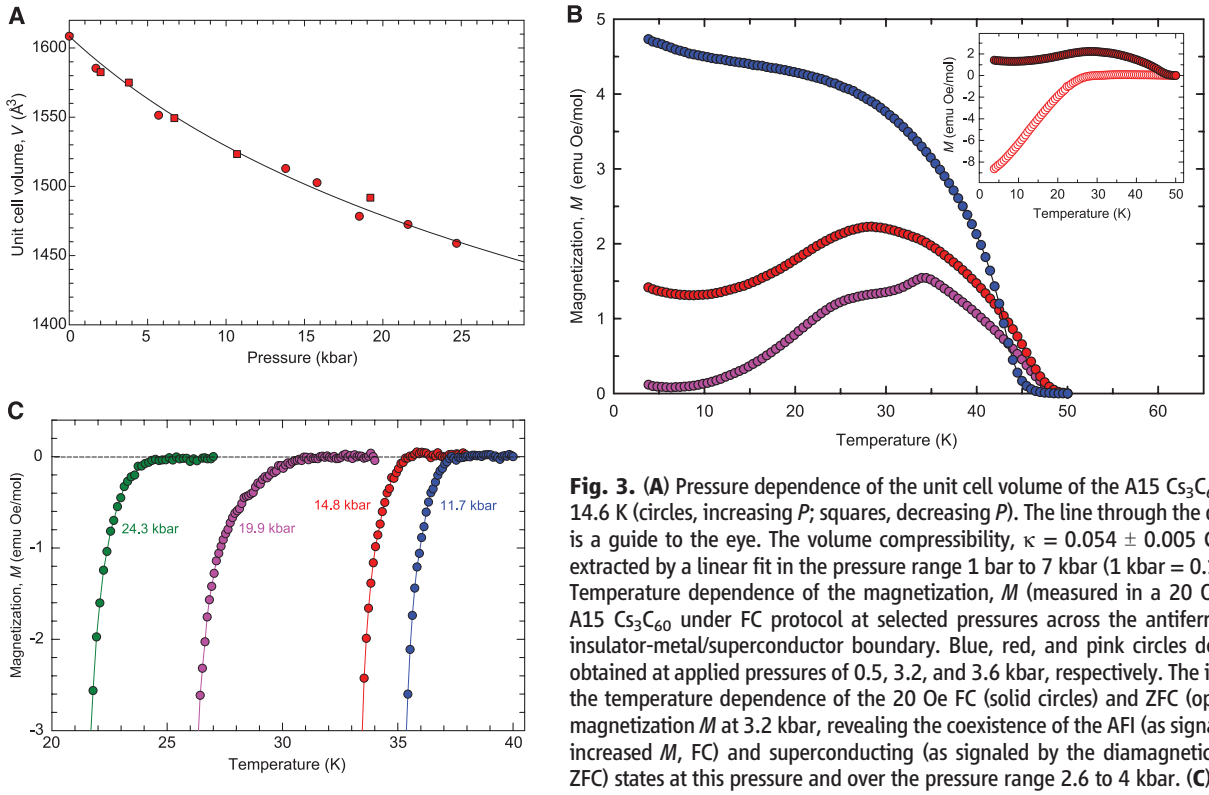

Fig. 3. (**A**) Pressure dependence of the unit cell volume of the A15 Cs_3C_{60} phase at 14.6 K (circles, increasing *P*; squares, decreasing *P*). The line through the data points is a guide to the eye. The volume compressibility, $\kappa = 0.054 \pm 0.005$ GPa^{-1}, was extracted by a linear fit in the pressure range 1 bar to 7 kbar (1 kbar = 0.1 GPa). (**B**) Temperature dependence of the magnetization, *M* (measured in a 20 Oe field) in A15 Cs_3C_{60} under FC protocol at selected pressures across the antiferromagnetic insulator-metal/superconductor boundary. Blue, red, and pink circles denote data obtained at applied pressures of 0.5, 3.2, and 3.6 kbar, respectively. The inset shows the temperature dependence of the 20 Oe FC (solid circles) and ZFC (open circles) magnetization *M* at 3.2 kbar, revealing the coexistence of the AFI (as signaled by the increased *M*, FC) and superconducting (as signaled by the diamagnetic response, ZFC) states at this pressure and over the pressure range 2.6 to 4 kbar. (**C**) Expanded view of the temperature dependence of the magnetization *M* (ZFC protocol, 10 Oe) near the onset of the transition to the superconducting state T_c at selected pressures in the range 11.7 to 24.3 kbar. T_c is defined as the temperature at which *M* begins to decrease; T_N is defined as the temperature at which *M* begins to increase.

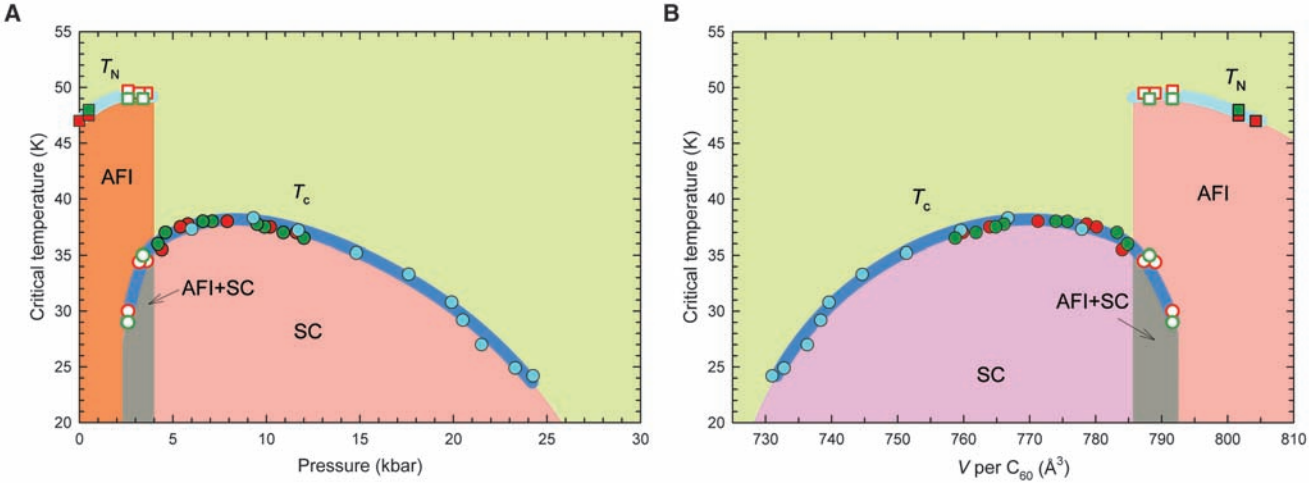

Fig. 4. Electronic phase diagram of A15 Cs_3C_{60} showing the evolution of the Néel temperature T_N (squares) and the superconducting transition temperature T_c (circles), and thus the isosymmetric transition from the ambient-pressure AFI state to the high-pressure superconducting state, (**A**) with change in pressure and (**B**) as a function of volume occupied per fulleride anion, *V*, at 14.6 K for A15 Cs_3C_{60}. Different symbol colors represent data obtained for different sample batches. Open symbols represent data in the AFI-superconductor coexistence regime. T_N is defined as the temperature at which the 20 Oe FC temperature-dependent magnetization *M* begins to increase; T_c is defined as the temperature at which the 20 Oe ZFC temperature-dependent *M* begins to decrease.

electron correlation in the fulleride superconductor systems.

High-resolution synchrotron x-ray powder diffraction at 14.6 K shows that the application of hydrostatic pressure to the cubic-localized electron $S = ½$ C_{60}^{3-} AFI with the bcc-derived A15 structure (space group $Pm\bar{3}n$) produces no structural change over the range 1 bar to 25 kbar (fig. S4) (*13*). The effect of increased pressure is thus solely to decrease the interfullerene contact distances isotropically (Fig. 3A), thereby increasing the overlap between t_{1u} orbitals on neighboring C_{60}^{3-} anions and thus the bandwidth W, which favors electron delocalization. Initially, at pressures $P \leq 3.6$ kbar, the AFI state is retained with T_N (signaled by the onset of weak ferromagnetism measured in the FC magnetization), increasing with pressure to a maximum of 49.5 K (Fig. 3B). This is consistent with the t_{1u} electrons remaining localized with enhanced exchange coupling caused by the closer intermolecular contacts.

However, in the pressure range 2.6 to 4 kbar, concurrent zero field–cooled (ZFC) magnetization measurements reveal that the antiferromagnetic state coexists in the sample with superconductivity, consistent with a first-order transition from the AFI state to superconductivity without intervening electronic states (Fig. 3B, inset). Superconductivity (with a broad diamagnetic response at the trace level of ~0.1%) is initially observed to coexist with the AFI state at 29 K at 2.6 kbar; T_c increases rapidly to 35 K at 3.6 kbar with an associated increase in shielding fraction (to ~1%). The fraction of the AFI phase decreases in this coexistence regime, as evidenced by the decrease in the FC spontaneous magnetization with increasing P (Fig. 3B). At 4.2 kbar, the signal of the AFI state in the magnetization is suppressed. However, the superconducting T_c continues to increase with P to a broad maximum of 38 K near ~7 kbar (*2*). Upon further pressure increase, the trend is reversed (Fig. 3C) and T_c now decreases monotonically with increasing P to the highest pressure of the present experiments, 24.3 kbar (Fig. 4A). T_c is insensitive to cooling rate, consistent with the absence of orientational disorder in the A15 Cs_3C_{60} superconductor that was apparent from the structural analysis.

These experimental data demonstrate the localized electron AFI state that is the decisive signature of the importance of correlation in the superconducting A_3C_{60} fullerides. Observation of this state is essential in understanding the non-BCS behavior of the superconducting state that emerges directly from the AFI state with application of pressure. The observation of localized electron magnetism indicates that in cubic A15 Cs_3C_{60} at ambient pressure, the electrons occupying the degenerate t_{1u} orbitals lie on the insulating side of the Mott-Hubbard transition, because the electron correlations quantified by the Hubbard U (the on-site interelectron repulsion) overcome the kinetic energy favoring electron delocalization quantified by the bandwidth W. Density functional theory (DFT) calculations show that despite the reduced anion packing density, the value of W in A15 Cs_3C_{60} is comparable to that in metallic fcc K_3C_{60} because of the more favorable intermolecular contact geometry (Fig. 1B) (*18*). The value of U is greater than that of W in all the fcc A_3C_{60} phases, but the metallic state is stabilized over the insulator by two key factors. One of these, the threefold frontier orbital degeneracy of the high-symmetry C_{60}^{3-} anion [which enhances intermolecular hopping relative to the singly degenerate case (*19*)], is retained in the case of AFI A15 Cs_3C_{60} because cubic symmetry is observed under all conditions corresponding to the measurements reported here. The absence of the second key feature of the fcc materials, geometrical lattice frustration (*19*), in the bcc-based A15 Cs_3C_{60} results in the observation of the localized electron AFI state, an electronic ground state not accessible in the fcc A_3C_{60} family; A15 Cs_3C_{60} has the point and lattice symmetry to allow the electronic state directly competing with superconductivity in fullerides to be identified.

The "low-spin" $S = ½$ state shows the dominant energy for the $(t_{1u})^3$ electrons localized on the C_{60}^{3-} anion by U; the vibronic Jahn-Teller coupling overcomes the intramolecular Hund's rule electron repulsion to stabilize one of the three t_{1u} orbitals, which is preferentially occupied by two electrons. The observed cubic metric symmetry of the AFI state shows that this Jahn-Teller distortion producing the $S = ½$ state must be dynamic, with the molecular distortion axis fluctuating among the three possible directions, and demonstrates that the long-range structure does not suppress the orbital degeneracy. The antiferromagnetic exchange (*20*) between neighboring C_{60}^{3-} anions is produced by dynamic orbital order (*21*) with locally favored ferrodistortive intersite arrangement of distortion axes (*22*). The weak ferromagnetic component seen at low field may then arise either from an antiferrodistortive contribution to the local dynamical coupling of Jahn-Teller distortion axes (which will give ferromagnetic exchange) or from the Dzyaloshinskii-Moriya coupling arising from the absence of an inversion center (Fig. 1B) on the direct exchange pathway (*23*) between neighboring anions in the $Pm\bar{3}n$ space group of the A15 phase.

The AFI state is suppressed in favor of the superconducting state purely by the application of pressure without any complicating influence of disorder or change in crystal structure, and thus with the preservation of t_{1u} orbital degeneracy. This symmetry retention is crucial to the stabilization of the metallic and superconducting state with increasing P; at the same volume per C_{60}^{3-} anion (*24*, *25*) found at ~13 and 10.5 kbar for superconducting A15 Cs_3C_{60}, orthorhombic $(NH_3)K_3C_{60}$ and $(CH_3NH_2)K_3C_{60}$, respectively, are antiferromagnetic insulators (*17*, *26*, *27*) because the lower point symmetry in these noncubic materials lifts the t_{1u} degeneracy and allows U to localize the electrons. The orbitally degenerate cubic superconducting phase, formed by the suppression of the AFI state upon application of pressure and initially coexisting with it, has a T_c that initially increases with decreasing interfullerene separation to a maximum of 38 K (Fig. 4B). This is the clear signature of non-BCS behavior in the superconducting state emerging directly from the AFI state as the bare density of states in A15 Cs_3C_{60} smoothly decreases with increasing P across this region, according to DFT calculations (*18*) based on the experimentally determined structures; this same effect would drive a decrease in T_c in the BCS-related models where $N(E_F)$ controls T_c exponentially. This experimental behavior is in stark contrast to the fcc A_3C_{60} systems, where the decrease of T_c with increasing pressure is driven by the accompanying decrease of $N(E_F)$ as the interanion orbital overlap increases, and has its origin in the dominance of correlations in the parent AFI state.

The high symmetry of the C_{60} building unit imposes a robust cubic three-dimensional structure on A15 Cs_3C_{60} free of positional, chemical, or orientational disorder, with a fixed charge state in which magnetism is transformed into superconductivity solely by changing an electronic parameter: the extent of overlap between the outer wave functions of the constituent anions. The pressure-induced transition in A15 Cs_3C_{60} from a localized electron AFI state to a superconducting state with two distinct dependences of T_c on packing density is purely electronic in nature, driven by increased overlap between the C_{60}^{3-} anions and the associated enhanced tendency to delocalize the t_{1u} electrons. The unconventional nature of the superconducting state that emerges from the AFI state can be associated with its proximity to the metal-insulator transition where conventional Fermi liquid theories are not expected to be valid, and quasi-localized effects produced by electronic correlation enhancing the role of intramolecular Jahn-Teller (electron-phonon) and Hund's rule (electron-electron) coupling are directly controlled by the persistent orbital degeneracy in both the insulating and superconducting states, clearly traceable to the molecular origin of the electron states. The observed maximum in the dependence of T_c on P is consistent with modern theoretical treatments (*5*–*7*) that explicitly take into account the orbital degeneracy and the repulsion between the electrons as well as the classical electron-phonon coupling. These effects are not seen in the conventional fcc A_3C_{60} systems, which are too far from the metal-insulator transition for differences from the conventional BCS predictions of the dependence of T_c on $N(E_F)$ to become apparent. A15 Cs_3C_{60} is an ideal material for understanding the interactions producing superconductivity in structurally and chemically complex correlated electron systems such as the cuprates and oxyarsenides, as it allows the isolation of the influence of only electronic factors (including orbital degeneracy) without any other complications.

References and Notes

1. N. W. Ashcroft, N. D. Mermin, *Solid State Physics* (Brooks Cole, New York, 1976).
2. A. Y. Ganin *et al.*, *Nat. Mater.* **7**, 367 (2008).
3. M. S. Nam, A. Ardavan, S. J. Blundell, J. A. Schlueter, *Nature* **449**, 584 (2007).
4. A. Comanac, L. De'Medici, M. Capone, A. J. Millis, *Nat. Phys.* **4**, 287 (2008).
5. M. Capone, M. Fabrizio, C. Castellani, E. Tosatti, *Rev. Mod. Phys.*, in press; http://arxiv.org/abs/0809.0910 (2008).
6. M. Capone, M. Fabrizio, C. Castellani, E. Tosatti, *Science* **296**, 2364 (2002).
7. O. Gunnarsson, E. Koch, R. M. Martin, *Phys. Rev. B* **54**, R11026 (1996).
8. O. Gunnarsson, *Rev. Mod. Phys.* **69**, 575 (1997).
9. K. Tanigaki *et al.*, *Nature* **352**, 222 (1991).
10. P. Dahlke, M. S. Denning, P. F. Henry, M. J. Rosseinsky, *J. Am. Chem. Soc.* **122**, 12352 (2000).
11. T. T. M. Palstra *et al.*, *Solid State Commun.* **93**, 323 (1995).
12. S. Saito, K. Umemoto, S. G. Louie, M. L. Cohen, *Solid State Commun.* **130**, 335 (2004).
13. See supporting material on *Science* Online.
14. C. P. Schlicter, *Principles of Magnetic Resonance* (Springer, Heidelberg, 1990).
15. C. H. Pennington, V. A. Stenger, *Rev. Mod. Phys.* **68**, 855 (1996).
16. N. Sato *et al.*, *Phys. Rev. B* **58**, 12433 (1998).
17. K. Prassides *et al.*, *J. Am. Chem. Soc.* **121**, 11227 (1999).
18. G. R. Darling, A. Y. Ganin, M. J. Rosseinsky, Y. Takabayashi, K. Prassides, *Phys. Rev. Lett.* **101**, 136404 (2008).
19. O. Gunnarsson, J. E. Han, E. Koch, V. H. Crespi, *Struct. Bonding* **114**, 71 (2005).
20. T. Kambe, K. Kajiyoshi, M. Fujiwara, K. Oshima, *Phys. Rev. Lett.* **99**, 177205 (2007).
21. L. F. Chibotaru, *J. Mol. Struct.* **838**, 53 (2007).
22. T. Kawamoto, *Solid State Commun.* **101**, 231 (1997).
23. J. Curely, *Monatsh. Chem.* **136**, 987 (2005).
24. S. Margadonna, K. Prassides, H. Shimoda, T. Takenobu, Y. Iwasa, *Phys. Rev. B* **64**, 132414 (2001).
25. A. Y. Ganin *et al.*, *J. Am. Chem. Soc.* **128**, 14784 (2006).
26. Y. Takabayashi, A. Y. Ganin, M. J. Rosseinsky, K. Prassides, *Chem. Commun.* **2007**, 870 (2007).
27. Y. Iwasa, T. Takenobu, *J. Phys. Condens. Matter* **15**, R495 (2003).
28. Y. Iwasa, T. Kaneyasu, *Phys. Rev. B* **51**, 3678 (1995).

29. We thank the UK Engineering and Physical Sciences Research Council for funding under EP/C511794 and GR/S77820 and for access to the synchrotron x-ray facilities at the European Synchrotron Radiation Facility (where we thank A. N. Fitch for assistance on beamline ID31) and to the muon facilities at ISIS (where we thank S. R. Giblin for assistance on the MuSR instrument). We also thank SPring-8 for access to the synchrotron x-ray facilities.

Supporting Online Material

www.sciencemag.org/cgi/content/full/323/5921/1585/DC1
Materials and Methods
Figs. S1 to S4
References

1 December 2008; accepted 2 February 2009
10.1126/science.1169163

Omnidirectional Printing of Flexible, Stretchable, and Spanning Silver Microelectrodes

Bok Y. Ahn,[1,2] Eric B. Duoss,[1,2] Michael J. Motala,[1,3] Xiaoying Guo,[1,2] Sang-Il Park,[1,2] Yujie Xiong,[1,2] Jongseung Yoon,[1,2] Ralph G. Nuzzo,[1,3] John A. Rogers,[1,2,3] Jennifer A. Lewis[1,2]*

Flexible, stretchable, and spanning microelectrodes that carry signals from one circuit element to another are needed for many emerging forms of electronic and optoelectronic devices. We have patterned silver microelectrodes by omnidirectional printing of concentrated nanoparticle inks in both uniform and high–aspect ratio motifs with minimum widths of approximately 2 micrometers onto semiconductor, plastic, and glass substrates. The patterned microelectrodes can withstand repeated bending and stretching to large levels of strain with minimal degradation of their electrical properties. With this approach, wire bonding to fragile three-dimensional devices and spanning interconnects for solar cell and light-emitting diode arrays are demonstrated.

Printed electronics offer an attractive alternative to conventional technologies by enabling the creation of large-area, flexible devices at low cost (*1*). Although there are options available for electronic materials—including conducting polymers (*2*, *3*), inorganic semiconductors (*4*, *5*) and carbon nanotubes (*6*, *7*)—the ability to print low-resistance electrodes with fine resolution in high–aspect ratio layouts, and possibly spanning three dimensions, is a technologically important goal. Many applications, including solar cell metallization (*8*), flexible displays (*9*), radio frequency identification tags (*10*), and antennas (*11*), would benefit from this capability. Conventional approaches, such as screen-printing (*12*) and inkjet printing (*13*), produce low–aspect ratio features that must be supported by the underlying substrate or device, making it impossible to pattern spanning elements in- or out-of-plane.

Direct ink writing offers an attractive alternative for meeting the demanding design rules and form factors required for metallic electrodes in printed electronic and optoelectronic devices. In this filamentary printing approach, a concentrated ink is extruded through a tapered cylindrical nozzle that is translated using a three-axis, motion-controlled stage with nanoscale precision (Fig. 1A) (*14*). Yet, several limitations remain to be overcome. To date, the minimum feature size obtained with the use of nanoparticle inks is 100 μm (*15*). In addition, the inks had to be deposited in a non-wetting oil reservoir to avoid nozzle clogging. Finally, ink deposition has been confined solely to the *xy* plane, such that three-dimensional (3D) structures are assembled in a layerwise sequence. We report the omnidirectional printing of flexible, stretchable, and spanning microelectrodes using concentrated silver nanoparticle inks that readily flow through micronozzles in air.

Metallic nanoparticles are typically synthesized in solution by the reduction of metal precursors in the presence of surface capping agents (*16*–*19*). Through a multistep approach (fig. S1), we prepared highly concentrated silver nanoparticle inks using an aqueous system that contains silver nitrate as the silver precursor, poly(acrylic acid) (PAA) as the capping agent, and diethanolamine as the reducing agent (*20*, *21*). The components are first mixed under ambient conditions to create a population of very fine (~5-nm) silver nanoparticles. This particle

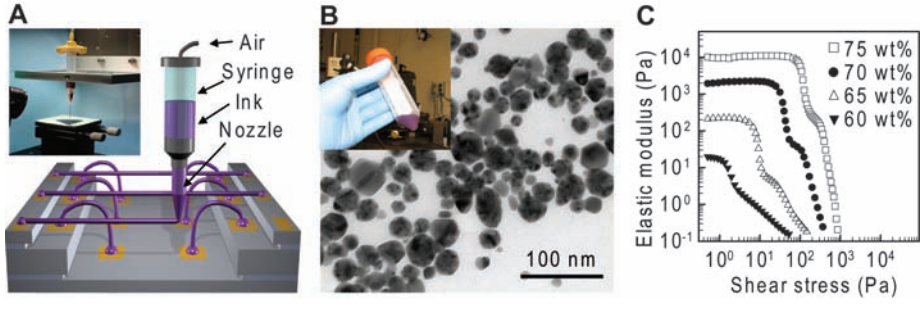

Fig. 1. (**A**) Schematic diagram illustrating omnidirectional printing and optical image of apparatus used (inset). (**B**) Transmission electron microscopy image of the synthesized silver nanoparticles and optical image of the concentrated ink (inset). (**C**) Shear elastic modulus as a function of shear stress for silver nanoparticle inks of varying solids loading.

[1]Frederick Seitz Materials Research Laboratory, University of Illinois at Urbana-Champaign, Urbana, IL 61801, USA. [2]Department of Materials Science and Engineering, University of Illinois at Urbana-Champaign, Urbana, IL 61801, USA. [3]Department of Chemistry, University of Illinois at Urbana-Champaign, Urbana, IL 61801, USA.

*To whom correspondence should be addressed. E-mail: jalewis@illinois.edu

population is ripened by heating the solution to 60°C (Fig. 1B). Ethanol, a poor solvent for the PAA-coated nanoparticles, is added to induce rapid particle coagulation. Next, the ink is centrifuged to achieve the desired solids loading [≥70 weight percent (wt %) silver nanoparticles], as shown in the inset of Fig. 1B. Finally, ethylene glycol is added as a humectant, which allows the ink to be patterned in air without clogging.

We have synthesized a broad range of silver nanoparticle inks and found that those with a solids loading between 70 and 85 wt %, a mean particle size of 20 ± 5 nm, and a particle size distribution between 5 and 50 nm exhibited both optimal flow behavior through fine deposition nozzles (1 to 30 μm) and low resistivity at modest annealing temperatures (≥200°C). Figure 1C shows the elastic modulus (G') as a function of shear stress for silver nanoparticle inks of varying solids loading. In the linear viscoelastic region, G' rises nearly three orders of magnitude as the nanoparticle content increases from 60 to 75 wt %. A minimum G' of 2000 Pa is required to produce spanning features, which occurs at a silver nanoparticle concentration of ~70 wt %. These highly concentrated inks can be stored under ambient conditions for weeks without any noticeable change in printing behavior (fig. S2).

To demonstrate the printing technique, we have patterned planar microelectrode arrays onto a silicon wafer by depositing silver nanoparticle ink (71–wt % solids) through 1-, 5-, and 10-μm cylindrical nozzles (Fig. 2A). Printed features with aspect ratios (h/w, where h is height and w is width) of ~0.7 are obtained in a single-pass, and a minimum width of ~2 μm is achieved with the use of a 1-μm nozzle. In addition, high–aspect ratio features are patterned in a layerwise manner, and their width and height are defined solely by the nozzle diameter and number of printed layers, respectively (Fig. 2, B and C).

The microstructural evolution of the printed silver microelectrodes as a function of annealing temperature is shown in Fig. 2D. As the temperature increases from 150° to 550°C, the microelectrodes undergo simultaneous loss of organics, grain growth, and densification. Thermogravimetic analysis reveals that the organic species are removed by ~400°C (fig. S1), whereas scanning electron microscopy (SEM) shows that their average grain size increases from ~180 nm at 150°C to 3 μm at 550°C, as a total volumetric shrinkage of ~30% occurs. Concomitantly, their electrical resistivity, ρ, decreases sharply over this temperature range (Fig. 2E). Upon annealing at 250°C for short times (≤30 min), the patterned microelectrodes exhibit an electrical resistivity of 5.2×10^{-5} ohm·cm, approaching the value of bulk silver (10^{-6} ohm·cm). In contrast, microelectrodes annealed at 150°C require several hours (≥25 hours) to reach $\rho \sim 10^{-3}$ ohm·cm, a value comparable to that observed for doped poly(3,4-ethylenedioxythiopene)/poly(styrenesulfonate), a widely used organic conductor (*22*, *23*).

To demonstrate the flexibility of the printed features, we patterned a series of interdigitated microelectrode arrays on a polyimide substrate. Figure 3A shows optical and SEM images of the printed silver microelectrodes after annealing at 200°C for 3 hours, followed by wrapping the patterned substrate around a scintillation vial with a bending radius of 14 mm. Solid contact pads (1 by 1 mm) connected to linear electrode features are formed with a 30-μm nozzle, to which interdigitated features are patterned with a 5-μm nozzle (Fig. 3A, top right). These elaborate structures require the initiation and cessation of ink flow multiple times during the printing process (Fig. 3A, bottom right).

To investigate the effects of mechanical bending on electrical performance, we used a custom-built mechanical stage coupled to a micropositioner to carry out bend tests (fig. S3A). For this experiment, a linear array of 10 silver microelectrodes (w = 23 μm, h = 12 μm, and length l = 1 cm) spaced 0.5 mm apart are printed on a 25-μm-thick polyimide sheet and annealed at 200°C for 3 hours in air before mechanical testing. Their electrical resistivity is measured as a function of bending radius from ±11 mm to ±5 mm, and the reported ρ values are averaged from 10 electrodes. In the first bend cycle, ρ is found to be 6.23 ± 4.40×10^{-4}, $2.11 \pm 0.91 \times 10^{-4}$, and $2.00 \pm 1.11 \times 10^{-4}$ ohm·cm in tension (convex), unstrained (flat), and compression (concave), respectively (Fig. 3B). An approximately twofold change in electrical resistivity is observed after 1000 bend cycles at the smallest radius of ±5 mm (Fig. 3C), where $(\rho_{1000} - \rho_0)/\rho_0$ is 2.17, 1.66, and 1.67 for the tensile, unstrained, and compressive states, respectively, and ρ_0 is the initial value measured in the unstrained state. The microelectrodes exhibited robust response for at least 750 bending cycles.

Ultrathin (~20 nm) metal films deposited onto prestrained, stretchable substrates can form wavy buckles and arches upon relaxation of the substrate (*24*). These configurations are even observed in brittle semiconductor materials, such as silicon, because of the differences in mechanical behavior between ultrathin and bulk materials (*25*). The built-in slack enables mechanical stretching while preserving the desired electronic properties. Stretchable, wavy, and arched architectures can also be created out of nonbrittle materials that are not ultrathin, particularly for ductile metals. Figure 3D shows stretchable silver arches formed by printing a spanning silver microelec-

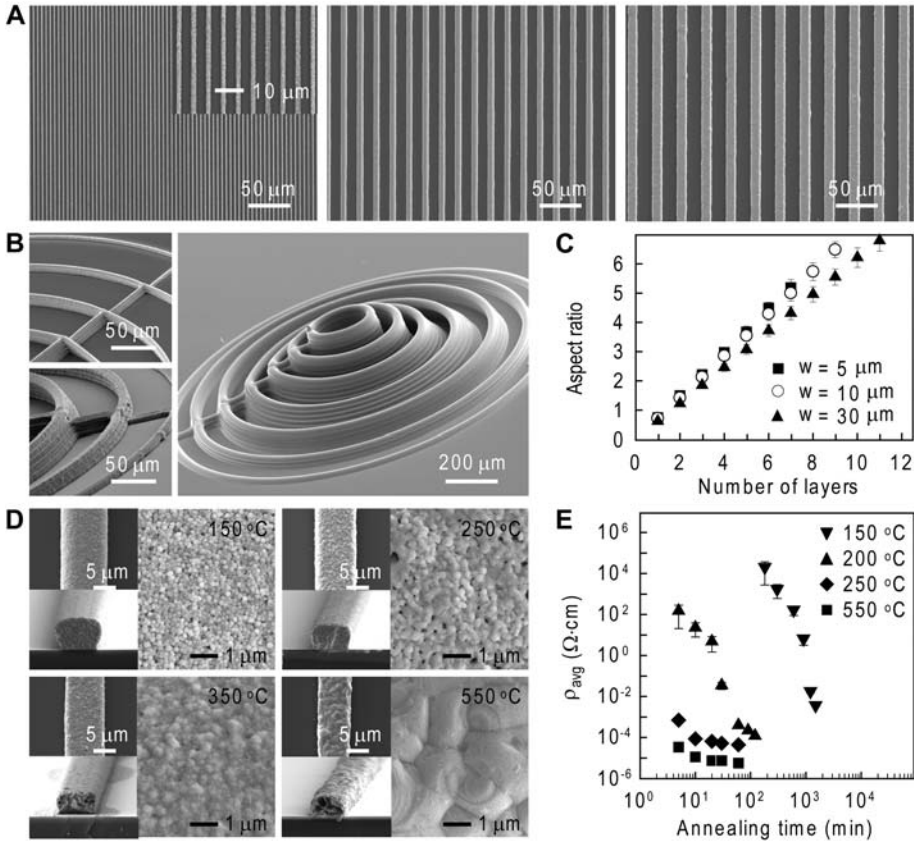

Fig. 2. (**A**) SEM images of planar arrays of silver microelectrodes patterned with 1- (left), 5- (center), and 10-μm (right) nozzles. (**B**) SEM images of multilayer silver microelectrodes patterned with 5- (top left), 10- (bottom left), and 30-μm (right) nozzles. (**C**) Aspect ratio as a function of number of printed layers for the silver microelectrodes shown in Fig. 2B. (**D**) SEM images of silver microelectrodes patterned with a 15-μm nozzle as a function of annealing temperature. (**E**) Electrical resistivity of silver microelectrodes as a function of annealing temperature and time. Error bars indicate the SD measured from three electrodes.

trode onto a prestrained spring (inset) that is then released to form the desired arches. The specimens are annealed at varying temperatures, and a silicone adhesive is subsequently printed onto the spring at the microelectrode contact points to ensure good adhesion and accurate resistivity measurements. The electrical resistivity of the silver microelectrode arches annealed at different temperatures is plotted as a function of strain $[(L - L_0)/L_0 \times 100\%]$ in Fig. 3E. The maximum strain increases with increasing annealing temperature from 8% at 200°C to 25% at 550°C, as the microelectrodes transform to a bulklike ductility. Straining these microelectrodes up to 200 cycles does not result in fatigue-induced failure at the contact points (Fig. 3F).

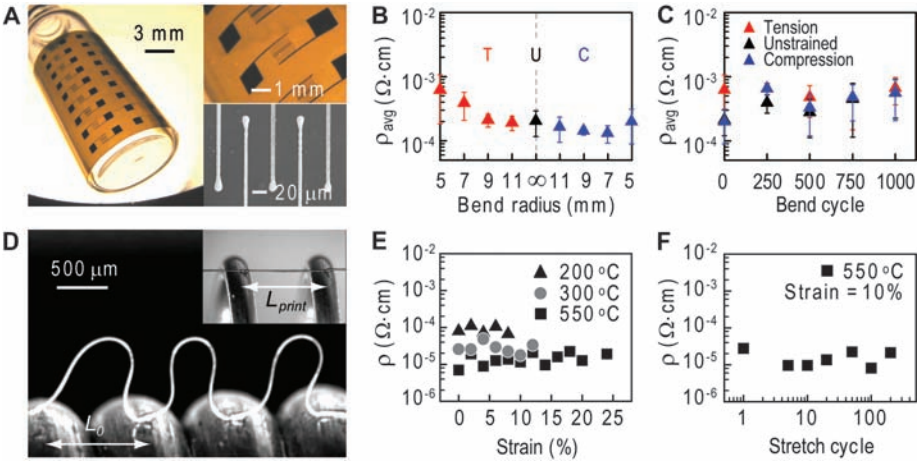

Fig. 3. (**A**) Optical and SEM images of silver microelectrodes patterned on a polyimide substrate with a bend radius of 14 mm. (**B**) Electrical resistivity of the silver microelectrodes as a function of bend radius under tension (T), unstrained (U), and compression (C). (**C**) Electrical resistivity of the silver microelectrodes as a function of bend cycle at a bend radius of ±5 mm. (**D**) Optical image of stretchable silver arches printed onto a spring. (**E**) Electrical resistivity of the stretchable silver microelectrode arches as a function of strain and annealing temperature. (**F**) Electrical resistivity of the stretchable silver microelectrode arches as a function of strain cycle. Error bars indicate the SD measured from 10 electrodes.

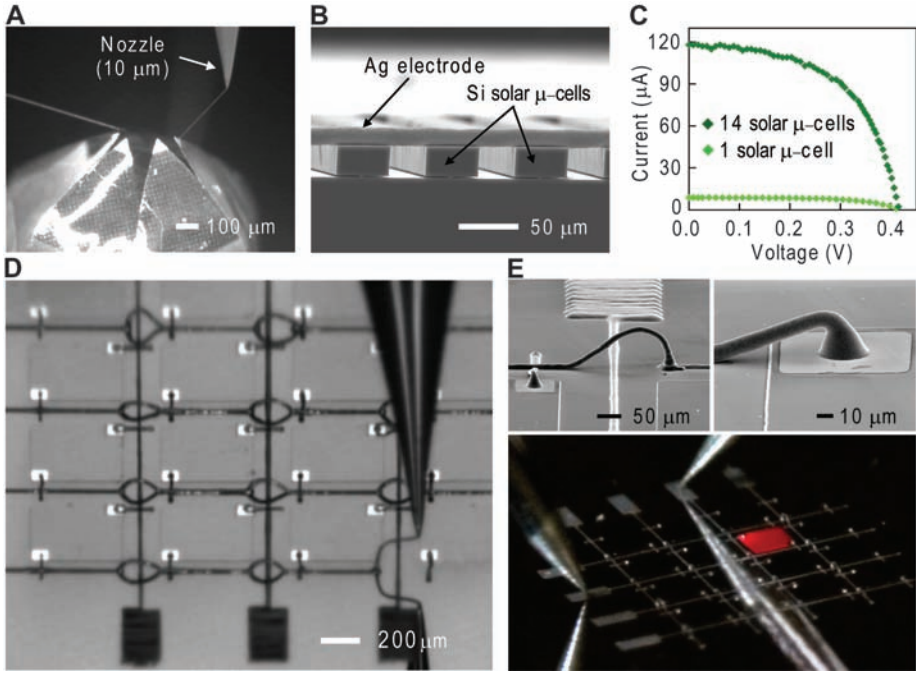

Fig. 4. (**A**) Optical image obtained during wire bonding onto a thin (2-μm) silicon spherical shell using a 10-μm nozzle. (**B**) Optical image of a spanning silver microelectrode printed onto an unplanarized, silicon solar microcell array. (**C**) Current (*I*)–voltage (*V*) response of an individual silicon solar microcell and a 14-microcell array connected by silver microelectrodes. (**D**) Optical image acquired during patterning of silver interconnects on a gallium arsenide–based, 4-by-4 LED chip array. (**E**) A silver interconnect arch printed over an electrode junction (top left) and on a gold contact pad (80 by 80 μm) (top right) and an optical image of light emission from a single LED pixel in the $y = 2$, $x = 3$ position within the array under an applied voltage (bottom).

We have provided a few examples of conductive features that can be patterned across unsupported regions in three dimensions. It is possible to vertically print microelectrodes with arbitrary height and angle (fig. S4). Figure 4A shows wire bonding of silver microelectrodes onto the surface of a thin silicon spherical shell assembled by lithographically patterning, releasing, and folding a 2-μm silicon layer in the desired 3D form (fig. S5). Unlike conventional techniques (*26*), our approach allows fine silver microwires (~10 μm) to be bonded with minimal contact pressure on both flat and curved surfaces, which is highly advantageous for delicate devices.

When combined with other processes (for instance, photolithography and transfer printing), our ink writing technique enables the heterogeneous integration of dissimilar materials (*8*, *27*). To further highlight this capability, we have patterned interconnects for both solar microcell and light-emitting diode (LED) arrays. As a first example, we patterned silver microelectrodes (w = 15 μm, h = 13 μm) onto a silicon solar microcell (w = 45 μm, h = 26 μm, and l = 2 mm) array, in which each photovoltaic element is separated by a 33-μm gap (fig S6). Figure 4B shows that the silver microelectrodes span the unsupported regions between each solar microcell without deformation. We also find that these inks can span unsupported gaps that are extraordinarily wide, up to 1.0 cm across (fig. S7). The current (*I*)–voltage (*V*) response from an individual silicon solar microcell and 14 interconnected microcells under a simulated air mass 1.5 illumination condition of 1000 W·m^{-2} is shown in Fig. 4C. Because of their fine lateral dimensions, these conductive tracks can be spaced closely together, thereby blocking less incoming light and allowing more current to be drawn from each solar cell (*28*).

As a final demonstration, we exploited omnidirectional printing to create interconnects for the gallium arsenide–based LED array (4-by-4 pixels, where each pixel is 500 by 500 by 2.5 μm and spaced 200 μm apart) shown in Fig. 4D. The ability to print out-of-plane enables the microelectrodes to directly cross pre-existing patterned features through the formation of spanning arches (Fig. 4E, top left). Typically, insulating layers or bypass electrode arrays are required in conventional layouts. Figure 4E (top right) shows silver micro-arches printed on a gold pad (80 by 80 μm) on a LED pixel. Figure 4E (bottom) displays the LED array, emitting uniform red light under an applied bias of 6 V from a single pixel, after annealing at 200°C for 3 hours. The utility of this approach is further established by printing spanning arches onto commercially available gallium nitride LED chips (fig. S8).

In summary, we have demonstrated the omnidirectional printing of flexible, stretchable, and spanning microelectrodes with the use of tailored silver nanoparticle inks. By carefully controlling

the silver nanoparticle concentration, size, and distribution, we have produced inks with high solids loading (≥70 wt %) that are ideally suited for direct-write assembly. We have shown that self-supporting microelectrodes in either planar or 3D forms of arbitrary complexity can be patterned on a wide variety of substrates. Using this technique, we have further demonstrated the feasibility of wire bonding to fragile devices and patterning complex interconnects for solar cell and LED arrays.

References and Notes

1. D. B. Chrisey, *Science* **289**, 879 (2000).
2. H. Sirringhaus *et al.*, *Science* **290**, 2123 (2000).
3. S. R. Forrest, *Nature* **428**, 911 (2004).
4. Y. Sun, J. A. Rogers, *Adv. Mater.* **19**, 1897 (2007).
5. E. Menard *et al.*, *Chem. Rev.* **107**, 1117 (2007).
6. M. C. LeMieux *et al.*, *Science* **321**, 101 (2008).
7. Q. Cao *et al.*, *Nature* **454**, 495 (2008).
8. J. Yoon *et al.*, *Nat. Mater.* **7**, 907 (2008).
9. J. A. Rogers *et al.*, *Proc. Natl. Acad. Sci. U.S.A.* **98**, 4835 (2001).
10. V. Subramanian *et al.*, *Proc. IEEE* **93**, 1330 (2005).
11. R. A. Potyrailo, W. G. Morris, *Anal. Chem.* **79**, 45 (2007).
12. M. Hosokawa, K. Nogi, M. Naito, T. Yokoyama, *Nanoparticle Technology Handbook* (Elsevier, Oxford, ed. 1, 2007).
13. T. H. J. van Osch, J. Perelaer, A. W. M. de Laat, U. S. Schubert, *Adv. Mater.* **20**, 343 (2008).
14. J. E. Smay, J. Cesarano III, J. A. Lewis, *Langmuir* **18**, 5429 (2002).
15. Q. Li, J. A. Lewis, *Adv. Mater.* **15**, 1639 (2003).
16. Y. Sun, Y. Xia, *Science* **298**, 2176 (2002).
17. B. Wiley, Y. Sun, Y. Xia, *Acc. Chem. Res.* **40**, 1067 (2007).
18. M. Yamamoto, Y. Kashiwagi, M. Nakamoto, *Langmuir* **22**, 8581 (2006).
19. A. Pyatenko, M. Yamaguchi, M. Suzuki, *J. Phys. Chem. C* **111**, 7910 (2007).
20. B.-H. Ryu *et al.*, *Colloids Surf. A Physicochem. Eng. Asp.* **270–271**, 345 (2005).
21. Materials and methods are available as supporting material on *Science* Online.
22. M. Dobbelin *et al.*, *Chem. Mater.* **19**, 2147 (2007).
23. J. Ouyang *et al.*, *Polymer* **45**, 8443 (2004).
24. T. Li, Z. Huang, Z. Suo, S. P. Lacour, S. Wagner, *Appl. Phys. Lett.* **85**, 3435 (2004).
25. D.-Y. Khang, H. Jiang, Y. Huang, J. A. Rogers, *Science* **311**, 208 (2006); published online 14 December 2005 (10.1126/science.1121401).
26. G. G. Harman, *Wire Bonding in Microelectronics: Process, Reliability, and Yield* (McGraw-Hill Professional, New York, 1997).
27. J.-H. Ahn *et al.*, *Science* **314**, 1754 (2006).
28. S. Ashley, *Sci. Am.* **299**, 32 (2008).

29. This material is based on work supported by the U.S. Department of Energy, Materials Sciences and Engineering Division under award no. DEFG-02-07ER46471, through the Frederick Seitz Materials Research Laboratory (FSMRL) at the University of Illinois. The authors gratefully acknowledge use of the FSMRL Central Facilities, including Center for Microanalysis of Materials. B.Y.A. thanks the Korean Research Foundation for the postdoctoral fellowship. We also thank C. Hansen, M. Xu, R. Shepherd, J. Bukowski, J. Carroll III, and J. Yoshikawa for useful discussions. J.A.L., B.Y.A., and E.B.D. submitted a U.S. patent application on this work entitled "Metal Nanoparticle Inks" on 3 October 2008.

Supporting Online Material

www.sciencemag.org/cgi/content/full/1168375/DC1
Materials and Methods
Figs. S1 to S9
References

11 November 2008; accepted 27 January 2009
Published online 12 February 2009;
10.1126/science.1168375
Include this information when citing this paper.

A Meta-Selective Copper-Catalyzed C–H Bond Arylation

Robert J. Phipps and Matthew J. Gaunt*

For over a century, chemical transformations of benzene derivatives have been guided by the high selectivity for electrophilic attack at the ortho/para positions in electron-rich substrates and at the meta position in electron-deficient molecules. We have developed a copper-catalyzed arylation reaction that, in contrast, selectively substitutes phenyl electrophiles at the aromatic carbon–hydrogen sites meta to an amido substituent. This previously elusive class of transformation is applicable to a broad range of aromatic compounds.

Aromatic organic compounds are ubiquitous in modern society as medicines and functionalized materials (*1*). These molecules comprise cyclic aryl cores with an often complex array of substituents on the ring carbons, which in many cases are most straightforwardly appended by electrophilic substitution (*2*). Ever since the pioneering work of Friedel and Crafts (*3*), it has been widely established that electron-donating substituents direct incoming electrophiles to the ortho and para positions, whereas electron-withdrawing groups steer to the meta position (Fig. 1A). This fundamental reactivity pattern facilitates a predictable outcome in simple cases; however, a common problem encountered in synthesis is how to access the isomer that is not anticipated by these rules. Solutions to this problem often require numerous functional group additions or manipulations in order to tailor the directing electronic properties of the precursor to furnish the desired product. Furthermore, in complex systems, where there may be more than one electronic or sterically active substituent, the competition between these directing groups may lead to mixtures of products. Although there have been some reports that indirectly address these problems (*4*–*7*), circumventing the inherent ortho/para-selectivity of electron-rich aromatic systems to generate the meta product remains a largely elusive and unmet goal for chemical synthesis.

A central theme of our research has been the development of methods to obviate reliance on complex functional group manipulations through direct metal-catalyzed C–H bond transformations (*8*, *9*). A key aspect of this goal is the ability to control the site selectivity of these transformations under mild conditions; a challenge that is further complicated by the ubiquitous nature of the C–H bond in organic molecules (*10*–*15*). The three mechanisms that usually rationalize the majority of selective metal-catalyzed C–H bond activation methods involve electrophilic aromatic substitution with electron-rich, π-nucleophilic arenes (*16*), concerted metalation-deprotonation with simple and electron-deficient benzenes (*17*–*19*), and directed cyclometalation (*20*–*26*). These mechanistic pathways most commonly form the ortho-substitution product, and as a result there is a paucity of methods for metal-catalyzed C–H bond activation at the meta position of a substituted benzene ring (*27*, *28*).

Here we describe the development of a reactivity concept for a metal-catalyzed aromatic C–H bond functionalization strategy that selectively generates the elusive meta isomer. The outcome is not predicted by the conventional rules associated with electronic factors, directing groups, or steric effects, and provides direct access to the meta isomer on highly versatile electron-rich aromatic structures. The process is simple, proceeds under mild conditions, uses inexpensive copper catalysts, and forms valuable products that would be difficult to synthesize by other methods (Fig. 1B). Furthermore, the reactivity and selectivity of this process should be compatible with other arene and C–H bond transformations and will streamline synthetic strategy for the assembly of medicines, natural products, and industrially relevant aromatic molecules.

We previously identified a copper catalysis system, based on electrophilic metalation, that enables site-selective C–H bond arylation on the indole skeleton (Fig. 2A) (*10*). We speculated that a Cu(I) catalyst is oxidized to a Cu(III)-aryl intermediate (*29*), a highly electrophilic d^8-configured metal species, that undergoes Friedel-Crafts–type metalation and arylation at the C3 position of the indole (Fig. 2B). We see C3 arylation when using our copper catalyst, whereas an almost identical process using Pd(II)-salts delivers the C2 isomer (*30*). Although the origin of this dichotomy remains unclear, it led us to speculate that use of our copper catalyst might enable us to reverse the established selectivity of other electrophilic Pd(II)-catalyzed transformations. For example, many Pd(II)-catalyzed reactions are ortho-selective and have been routinely developed by virtue of the coordinat-

Department of Chemistry, University of Cambridge, Lensfield Road, Cambridge CB2 1EW, UK.

*To whom correspondence should be addressed. E-mail: mjg32@cam.ac.uk

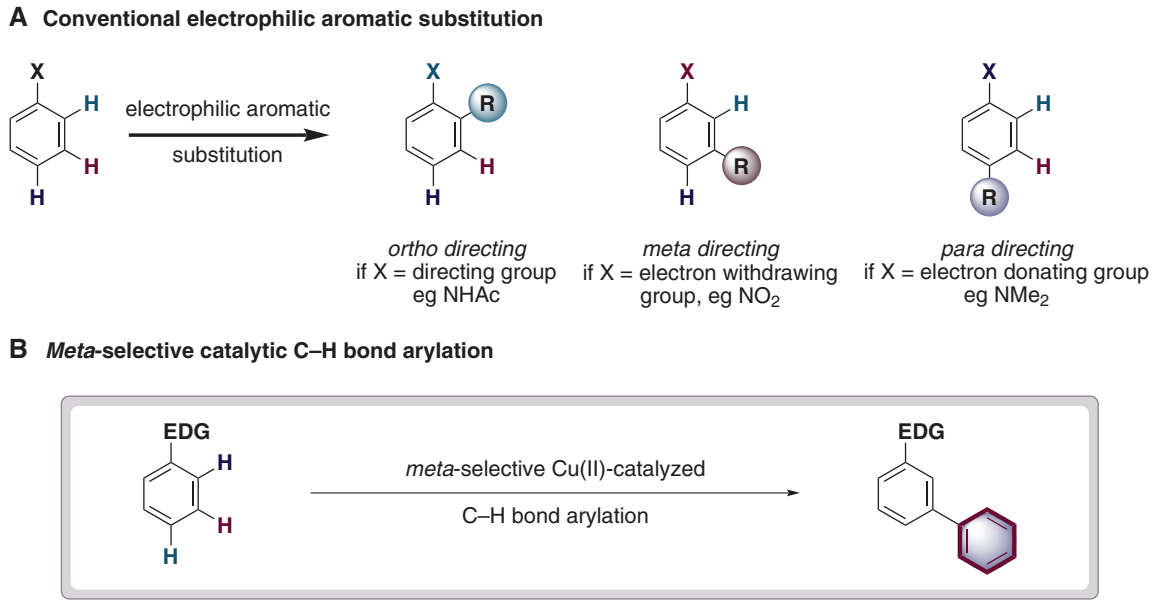

Fig. 1. (**A**) Conventional reactivity trends in electrophilic aromatic substitution. (**B**) Meta-selective catalytic C–H bond arylation. EDG, electron-donating group; Me, methyl; Ac, acetyl.

ing effect of directing groups (*20*–*26*). We reasoned that a highly electrophilic Cu(III)-aryl species could react through a different pathway with molecules such as acetanilides, potentially leading to a positional isomer not observed in conventional aromatic substitution reactions (Fig. 2C). The acetanilides are an important class of aromatic molecule that already undergoes a plethora of transformations leading to ortho/para products (*20*). Furthermore, the acetamide group is a versatile motif that can be readily transformed into a range of other functionalities through conventional synthetic procedures.

To test this hypothesis, we treated acetanilide **1a** with Ph_2IOTf (the arylating agent; Ph, phenyl; Tf, triflate) in the presence of 10 mole % $Cu(OTf)_2$ (catalyst) in 1,2-dichloroethane solvent at 70°C (*31*). Arylation occurred at the meta position to afford **2a**, albeit in low isolated yield (Table 1, entry 1); and in line with our blueprint, no products arising from monoarylation at the ortho or para position were observed (determined by ^1H nuclear magnetic resonance analysis, <5%). Furthermore, no arylation was observed with compounds that do not possess an amide group (*31*). The same exclusive meta-selectivity was observed with 2-methylacetanilide **1b**, to form the meta product **2b**, in improved 43% yield. These outcomes are in contrast to the similar Pd(II)-catalyzed C–H arylation of acetanilide that delivered the ortho-substituted product (*32*). Only the elegant iridium-catalyzed C–H borylation, developed independently by Smith-Maleczka and Hartwig-Miyuara-Ishiyama, can achieve such selectivity in certain cases (*27*, *28*). The C–H borylation reaction is mainly influenced by the steric effects on the aromatic molecule and leads to functionalization at a position that is not adjacent to any other group. In cases such as **1b**, however, the borylation reaction would be expected to afford a mixture of meta and para isomers.

Encouraged by these initial results, we next addressed reaction optimization with 2-methylanilides as our model system. We found that changing the nature of the acyl group had a large effect on the yield of the reaction without compromising the meta-selectivity (Table 1, entries 2 to 6). The reaction works with carbamate and urea groups (Table 1, entries 3 and 4), although the conversions are only moderate. However, benzamides and pivanilides (Table 1, entries 5 and 6) performed much better in the reaction, producing good yields of the desired biaryl products. In all cases, arylation is the result of reaction at the meta position to the amide, and no reaction occurs in the absence of the copper catalyst.

Although we cannot be certain of the precise mechanism of the reaction at this stage, a possible rationalization could involve the highly electrophilic Cu(III)-aryl species activating the aromatic ring sufficiently to permit an anti–oxy-cupration of the carbonyl group of an acetamide across the 2,3 positions on the arene ring (Fig. 2D, step 1). This dearomatizing transformation would place the Cu(III)-aryl species at the meta position, and rearomatizing deprotonation (step 2) followed by reductive elimination (step 3) would deliver the meta product (*33*).

Having identified a suitable amide moiety, we explored the substrate scope (Fig. 3A). The copper-catalyzed meta-arylation displays broad substrate capacity and is tolerant of a range of substituents in all positions of the aromatic ring (*34*). For example, ortho-substituted pivanilides readily produce the 1,2,5-trisubstituted arene system, in which arylation has taken place in the meta position to the amido group regardless of the electronic properties of the ortho substituent [**2f** to **2j** (**2f-j**)]. Although electron-deficient substrates suffer from poorer reactivity, it is notable that even in the presence of a competing meta-directing substituent (SO_2Me, **2k**), we observed exclusive arylation at the meta position to the amide group, in line with our hypothesis. When the pivanilide was substituted in the meta position, the C–H arylation afforded the 1,3,5 arene isomer, again with arylation taking place in the meta position to the nitrogen substituent (entries **2l-p**). Although the yields are a little lower than those of the corresponding ortho-substituted anilides, this is not the result of other isomeric products but of a slower reaction rate that leads to incomplete conversion of the starting material. Particularly noteworthy is the tolerance of halogen groups (**2m** and **2o**), which remain unaffected during the reaction; these examples demonstrate that the copper-catalyzed C–H arylation provides a complementary platform for further elaboration via conventional Pd(0)-catalyzed cross-coupling chemistry. The simple pivanilide system forms the meta-diarylation product (**2q**). The arylation process can also be extended to systems bearing a para substituent, and the arylation takes place in the sterically most demanding position, consistent with our meta-directing hypothesis, to form 1,3,4,5-tetrasubstituted anilides (**2r**). In these cases, the symmetrical diarylation predominates; however, it is possible to access the 1,3,4-trisubstituted monoarylated system (**2s**) by controlling the stoichiometry of the reaction.

More complex (tri- or tetrasubstituted) anilide starting materials are also compatible in this reaction, leading to highly functionalized products (**2t-u**) in reasonable to good yields. A hexasubstituted arene (**2v**) can be synthesized in moderate yield by this process, and versatile heterocyclic motifs such as the indoline system (**2w**) can be selectively arylated to form useful products that would be difficult to access by other methods. Moreover, the nature of the aryl coupling partner can be varied in the reaction, thereby extending the utility of this process. A range of steric, electronic,

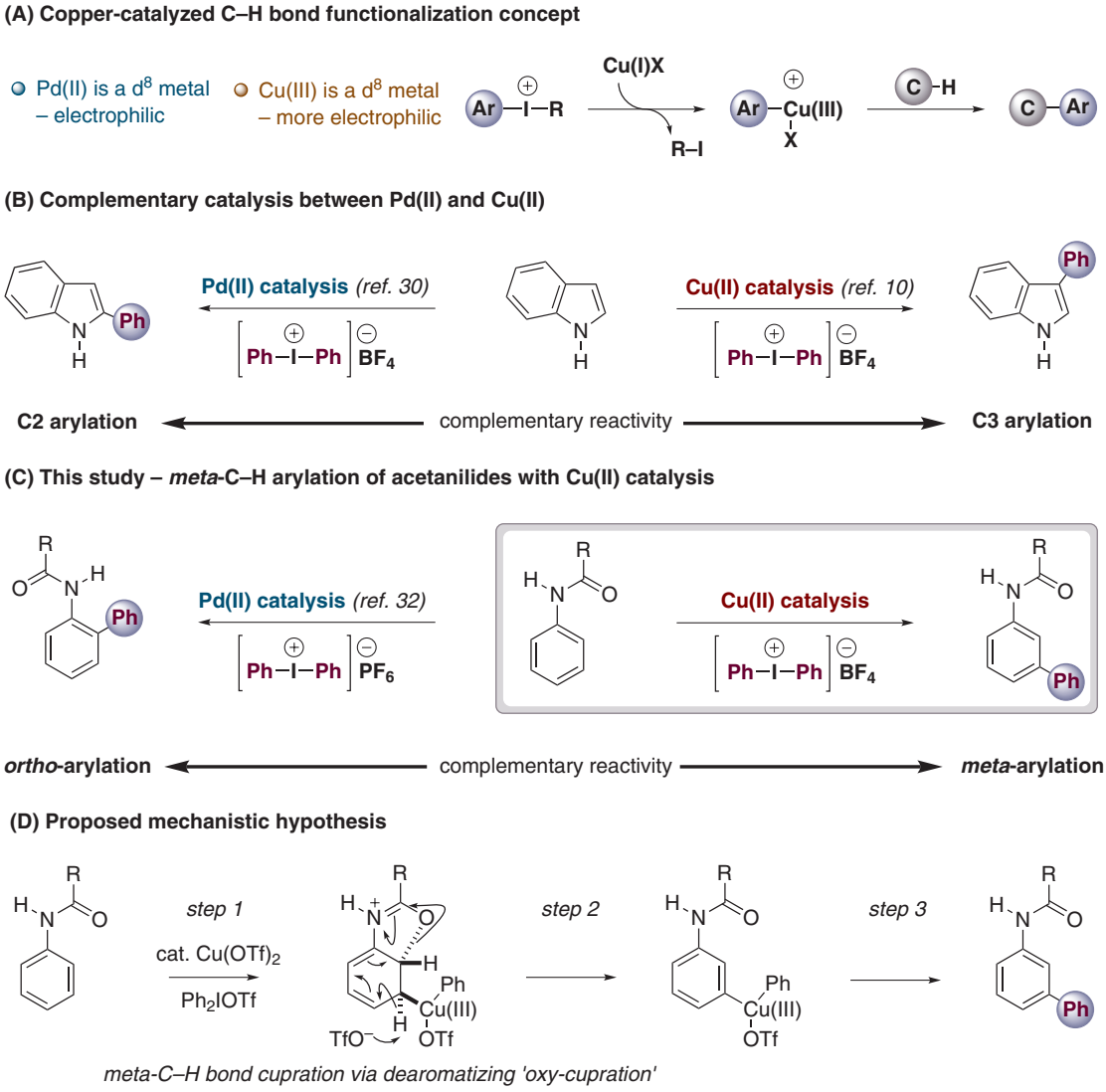

Fig. 2. Design blueprint for meta-selective copper-catalyzed C–H bond arylation (**A** to **D**). Ar, general aryl group; Ph, phenyl; Tf, triflate; R, general hydrocarbon group.

Table 1. Optimization studies for meta-selective Cu(II)-catalyzed C–H bond arylation. DCE, 1,2-dichloroethane.

Reaction optimization

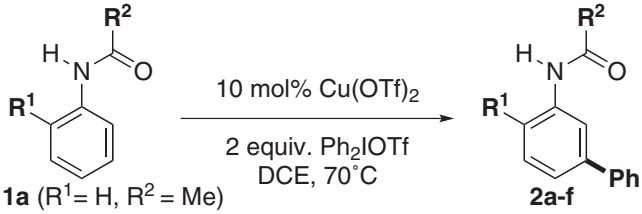

1a (R^1 = H, R^2 = Me)
1b (R^1 = Me, R^2 = Me)

entry	R^1	R^2	product	yield %
1	H	Me	**2a**	14
2	Me	Me	**2b**	43
3	Me	OMe	**2c**	45
4	Me	NEt_2	**2d**	31
5	Me	Ph	**2e**	73
6	Me	CMe_3	**2f**	79

and functionally diverse aryl groups can be transferred via the unsymmetrical iodonium salts (*35*) in good yields (Fig. 3B). In these cases, the large size of the mesityl group precludes its transfer in the coupling step, facilitating the formation of a range of functionalized biaryl products (*10*, *30*).

The meta-selectivity of this arylating transformation can be controllably overridden in certain cases, providing further access to alternative isomeric products (Fig. 4). A 3-oxygenated pivanilide derivative can be tuned through simple and straightforward manipulation of the oxygen-protecting group to afford either the 1,3,5- or 1,3,6-trisubstituted arene product. For example, a moderately electron-withdrawing 3-OTs group (Ts, tosylate) facilitates reaction in the meta position to the amide motif, in line with our model, to afford the 1,3,5-functionalization pattern (**2x**). However, if the more electron-donating 3-OMe group is incorporated, then the arylation is steered to the 6-position (ortho to the amido group and para to the methoxy) to give **2y** in good yield. This controllable switch in regioselectivity is

indicative of potential versatility in this arylation method.

A broad range of substrates is compatible with this operationally simple and mild copper-catalyzed arylation process. The method is best suited to more electron-donating substitutents on the anilide ring, but still tolerates electron-withdrawing groups, producing the meta isomer with exquisite selectivity. In certain cases the meta-selectivity can be overridden by strongly electron-donating substituents that provide a further platform for exploring the reaction parameters.

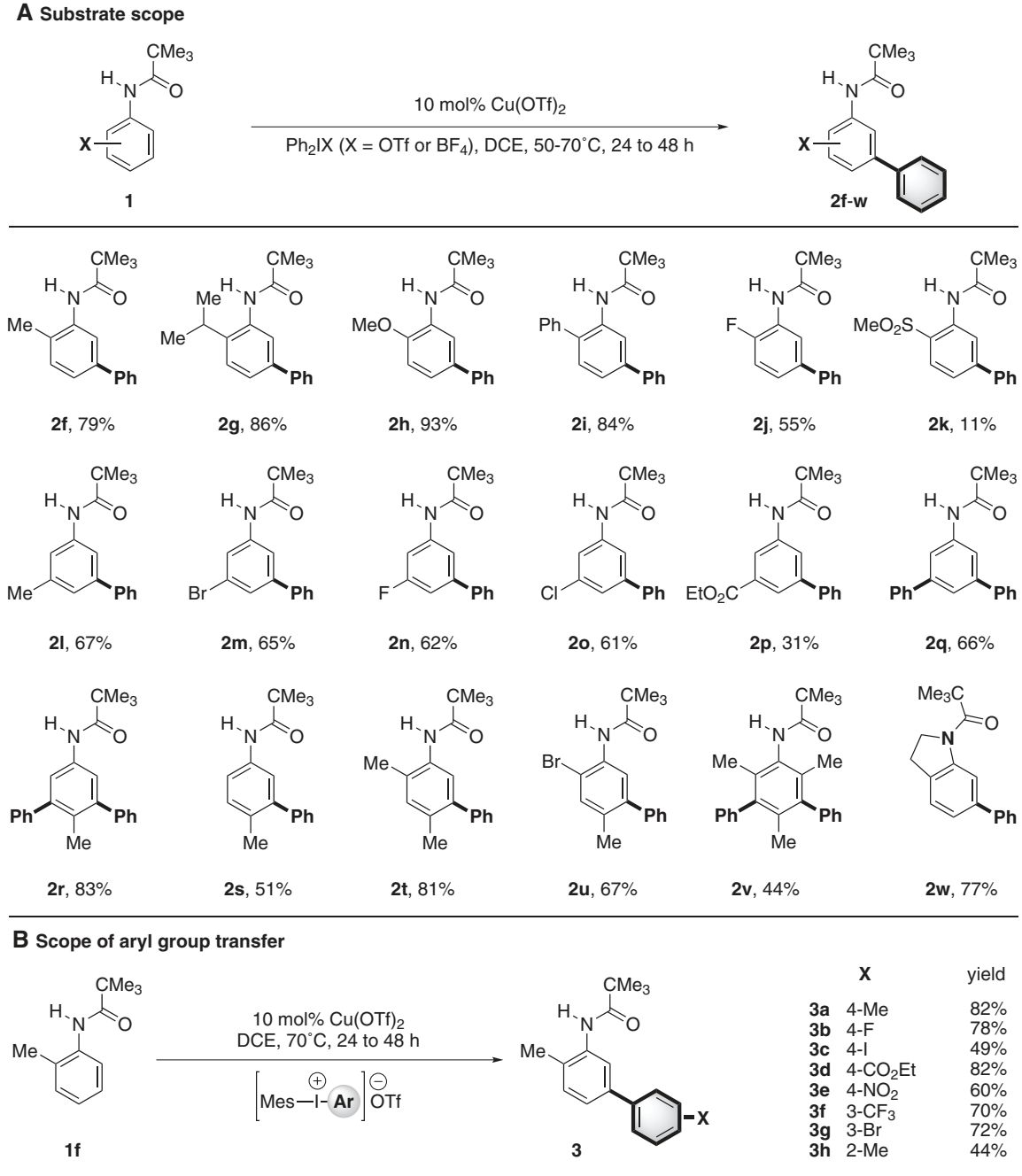

Fig. 3. Scope of anilide (**A**) and arylating (**B**) groups in the Cu(II)-catalyzed C–H bond arylation reaction; Mes, 2,4,6-trimethylphenyl; Et, ethyl. For **2s**, two equivalents of pivanilide were used.

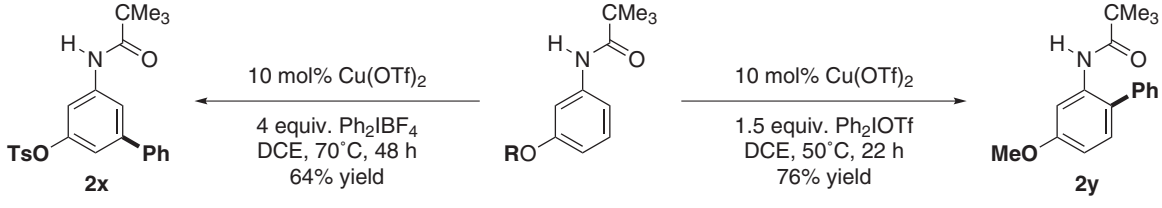

Fig. 4. Controlling the site selectivity of the C–H arylation reaction; Ts, tosylate.

We anticipate that this general copper-catalyzed meta-C–H bond functionalization reaction will provide direct access to the elusive positional isomers in aromatic chemistry and have a major impact on the way that complex molecules, pharmaceuticals, and functionalized materials are synthesized.

References and Notes

1. J. Hassan, M. Sevignon, C. Gozzi, E. Schulz, M. Lemaire, *Chem. Rev.* **102**, 1359 (2002).
2. G. A. Olah, *Friedel-Crafts and Related Reactions* (Wiley, New York, 1963).
3. C. Friedel, J. M. Crafts, *Comptes Rendus* **84**, 1392 (1877).
4. C. J. Rohbogner, G. C. Clososki, P. Knochel, *Angew. Chem. Int. Ed.* **47**, 1503 (2008).
5. J. P. Flemming, M. B. Berry, J. M. Brown, *Org. Biomol. Chem.* **6**, 1215 (2008).
6. R. E. Mulvey, F. Mongin, M. Uchiyama, Y. Kondo, *Angew. Chem. Int. Ed.* **46**, 3802 (2007).
7. V. Snieckus, *Chem. Rev.* **90**, 879 (1990).
8. D. Alberico, M. E. Scott, M. Lautens, *Chem. Rev.* **107**, 174 (2007).
9. K. Godula, D. Sames, *Science* **312**, 67 (2006).
10. R. J. Phipps, N. P. Grimster, M. J. Gaunt, *J. Am. Chem. Soc.* **130**, 8172 (2008) and references therein.
11. N. P. Grimster, C. Gauntlett, C. R. A. Godfrey, M. J. Gaunt, *Angew. Chem. Int. Ed.* **44**, 3125 (2005).
12. E. M. Beck, N. P. Grimster, R. Hatley, M. J. Gaunt, *J. Am. Chem. Soc.* **128**, 2528 (2006).
13. D. R. Stuart, K. Fagnou, *Science* **316**, 1172 (2007).
14. D. R. Stuart, E. Villemure, K. Fagnou, *J. Am. Chem. Soc.* **129**, 12072 (2007).
15. L.-C. Campeau, D. J. Schipper, K. Fagnou, *J. Am. Chem. Soc.* **130**, 3266 (2008).
16. C. Jia, T. Kitamura, Y. Fujiwara, *Acc. Chem. Res.* **34**, 633 (2001) and references therein.
17. M. Lafrance, K. Fagnou, *J. Am. Chem. Soc.* **128**, 16496 (2006).
18. D. Garcia-Cuadrado, A. A. C. Braga, F. Maseras, A. M. Echavarren, *J. Am. Chem. Soc.* **128**, 1066 (2006).
19. D. L. Davies, S. M. A. Donald, S. A. Macgregor, *J. Am. Chem. Soc.* **127**, 13754 (2005).
20. For an overview of C–H bond functionalization on acetanilides, see (*21*, *36*).
21. G. Brasche, J. Garcia-Fortanet, S. L. Buchwald, *Org. Lett.* **10**, 2207 (2008).
22. For an example of pyridine directed ortho–C–H arylation, see (*37*).
23. For Cu(II)-catalyzed, pyridine-directed, C–H bond functionalization, see (*38*).
24. For a recent example of carboxylate directed ortho–C–H bond arylation, see (*39*).
25. For imine-directed C–H bond functionalization, see (*40*).
26. For ketone-directed C–H bond functionalization, see (*41*).
27. J.-Y. Cho, M. K. Tse, D. Holmes, R. E. Maleczka Jr., M. R. Smith III, *Science* **295**, 305 (2002).
28. J. M. Murphy, X. Liao, J. F. Hartwig, *J. Am. Chem. Soc.* **129**, 15434 (2007) and references therein.
29. D. H. R. Barton, J. P. Finet, J. Khamsi, *Tetrahedron Lett.* **28**, 887 (1987).
30. N. R. Deprez, D. Kalyani, A. Krause, M. S. Sanford, *J. Am. Chem. Soc.* **128**, 4972 (2006).
31. Materials and methods are available as supporting material on *Science* Online.
32. O. Daugulis, V. G. Zaitsev, *Angew. Chem. Int. Ed.* **44**, 4046 (2005).
33. We cannot rule out coordination of the Cu(III) species at the ortho position, followed by a migration to the meta site and arylation. However, we do not see any sign of ortho-arylation that may be expected through this pathway. For example, see (*42*).
34. The pivaloyl amide moiety in **2f** can be cleaved to the corresponding amine (95% yield) on treatment with HCl-EtOH at 100°C (see supporting online material).
35. M. Bielawski, M. Zhu, B. Olofsson, *Adv. Synth. Catal.* **349**, 2610 (2007).
36. B.-J. Li, S.-D. Yang, Z.-J. Shi, *Synlett* **2008**, 949 (2008) and references therein.
37. L. V. Desai, K. J. Stowers, M. S. Sanford, *J. Am. Chem. Soc.* **130**, 13285 (2008).
38. X. Chen, X.-S. Hao, C. E. Goodhue, J.-Q. Yu, *J. Am. Chem. Soc.* **128**, 6790 (2006).
39. D.-H. Wang, T.-S. Mei, J.-Q. Yu, *J. Am. Chem. Soc.* **130**, 14082 (2008).
40. R. K. Thalji, J. A. Ellman, R. G. Bergman, *J. Am. Chem. Soc.* **126**, 7172 (2004).
41. S. Murai *et al.*, *Nature* **366**, 529 (1993).
42. G. Evindar, R. A. Batey, *J. Org. Chem.* **71**, 1802 (2006).

43. We gratefully acknowledge the Biotechnology and Biological Sciences Research Council and GlaxoSmithKline for an Industrial Case Award to R.J.P., the Royal Society for a University Research Fellowship to M.J.G., and Philip and Patricia Brown for a Next Generation Fellowship to M.J.G. We also thank S. Peace (GSK Medicines Research Center, UK) for useful discussion.

Supporting Online Material

www.sciencemag.org/cgi/content/full/323/5921/1593/DC1
Materials and Methods
References
Spectral Data

18 December 2008; accepted 2 February 2009
10.1126/science.1169975

The Burgess Shale Anomalocaridid *Hurdia* and Its Significance for Early Euarthropod Evolution

Allison C. Daley,[1]* Graham E. Budd,[1] Jean-Bernard Caron,[2] Gregory D. Edgecombe,[3] Desmond Collins[4]

As the largest predators of the Cambrian seas, the anomalocaridids had an important impact in structuring the first complex marine animal communities, but many aspects of anomalocaridid morphology, diversity, ecology, and affinity remain unclear owing to a paucity of specimens. Here we describe the anomalocaridid *Hurdia*, based on several hundred specimens from the Burgess Shale in Canada. *Hurdia* possesses a general body architecture similar to those of *Anomalocaris* and *Laggania*, including the presence of exceptionally well-preserved gills, but differs from those anomalocaridids by possessing a prominent anterior carapace structure. These features amplify and clarify the diversity of known anomalocaridid morphology and provide insight into the origins of important arthropod features, such as the head shield and respiratory exites.

Like other anomalocaridids (*1*), *Hurdia* has a complex history. The mouthparts (*2*), frontal appendages (*3*–*5*), body (*6*), and frontal carapaces (*7*, *8*) were all first described in isolation as separate animals with disparate affinities, including medusoids, holothurians, and various arthropods (*1*). When research in the 1980s revealed that many of these taxa were in fact different parts of the same animal, two anomalocaridid genera were defined (*9*), and several specimens here identified as *Hurdia* were assigned to either *Anomalocaris* or *Laggania*. These genera possess stalked eyes, frontal appendages, a circular toothed mouth structure, and a body bearing gills in association with lateral flaps. Later, Collins (*10*, *11*) informally recognized that a third undescribed anomalocaridid exhibits all these features, as well as a prominent anterior carapace composed of a triangular element, the *Hurdia* carapace (*7*), together with the purported phyllopod carapace *Proboscicaris* (*8*).

Access to important new material at the Royal Ontario Museum and restudy of older collections (*12*) identified parts of the *Hurdia* animal scattered through at least eight Cambrian taxa. This realization clarifies the systematics and complex morphology of Burgess Shale anomalocaridids, revealing that previous reconstructions of *Anomalocaris* and *Laggania* have been partially misled by the inclusion of *Hurdia* material. For clarity, generic names previously applied to anomalocaridid body parts are referred to as follows: "Hurdia" (*7*) is referred to as the H-element, "Proboscicaris" (*8*) as the P-element (with both together as the frontal carapace), "Peytoia" (*2*) as the mouthpart, and "appendage F" (*3*–*5*) as frontal appendage.

Systemic paleontology. Stem Euarthropoda, Class Dinocarida, Order Radiodonta, Genus *Hurdia* Walcott, 1912. **Synonymy and taphonomy.** See supporting online material (SOM) text. **Type species.** *Hurdia victoria* Walcott, 1912. **Revised diagnosis.** Anomalocaridid with body divided into two components of subequal length: anterior with a nonmineralized reticulated frontal carapace and posterior consisting of a trunk with seven to nine lightly cuticularized segments. The frontal carapace includes a triangular H-element attached dorsally and a pair of lateral P-elements.

[1]Department of Earth Sciences, Palaeobiology, Uppsala University, Villavägen 16, Uppsala SE-752 36, Sweden. [2]Department of Natural History, Royal Ontario Museum, 100 Queen's Park, Toronto M5S 2C6, Canada. [3]Department of Palaeontology, Natural History Museum, Cromwell Road, London SW7 5BD, UK. [4]437 Roncesvalles Avenue, Toronto M6R 3B9, Canada.

*To whom correspondence should be addressed. E-mail: allison.daley@geo.uu.se

Posterior to the frontal carapace is a pair of dorsolateral oval eyes on short annulated stalks. The anteroventral mouthparts consist of an outer radial arrangement of 32 broadly elliptical plates (similar to *Laggania* and *Anomalocaris*) forming a domed structure, within which is found a maximum of five inner rows of teeth (lacking in *Laggania* and *Anomalocaris*). A pair of appendages is located on either side of the mouthparts, consisting of 9 or 11 podomeres each, bearing short dorsal spines and long spiniferous ventral spines. The posterior half of the body consists of seven to nine reversely imbricated lateral flaps bearing a series of wide lanceolate gill-like blades. The body lacks a posterior tapering outline and tail fan (in contrast to *Laggania* and *Anomalocaris*), and the terminal body segment has two small lobe-shaped outgrowths. **Holotype of the type species.** U.S. National Museum of Natural History (USNM) specimen no. 57718, Washington, DC, USA. **Paratypes.** USNM 274159 and counterpart in two pieces (274155 and 274158). Royal Ontario Museum (ROM) 59252, 49930, 59254, and 59255, Toronto, Canada. **Other material.** At least 732 *Hurdia* specimens (*12*) from the ROM; National Museum of Natural History (NMNH); Geological Survey of Canada (GSC), Ottawa; and Museum of Comparative Zoology (MCZ), Harvard University (table S1). **Horizons and localities.** Middle Cambrian Burgess Shale Formation (*13*) (Fossil Ridge, Mount Field, and Mount Stephen); Yoho National Park; and Middle Cambrian Stephen Shale Formation (Stanley Glacier), Kootenay National Park, British Columbia, Canada.

Description. Specimens are up to 200 mm in length (table S2), with the frontal carapace making up approximately half of the total body length (Fig. 1). The P-elements (Fig. 2F) lie beneath the lateral margins of the dorsal H-element (Fig. 2G) and were attached at their anteriorly pointing narrow protrusions beneath the H-element's rostral point (Fig. 3). H- and P-elements have a polygonal pattern (fig. S1D) formed by thin walls between outer cuticle layers (SOM text). Short annulated stalks bearing oval eyes protruded through posterior notches in the frontal carapace (Figs. 1, A and B, and 3).

Mouthparts consist of a circlet of 32 plates, each bearing two or three small teeth, with four larger plates arranged perpendicularly and separated by seven smaller plates (Fig. 2D and fig. S1, D and E). The outer margins of these plates curve downward, conferring a domed shape to the structure best seen in lateral view (fig. S1A). Within the square central opening are situated five imbricated rows of teeth bearing as many as 11 sharp spines (Fig. 2D and fig. S2, D and E). All domed mouth parts with inner teeth belong to *Hurdia* (SOM text).

The frontal appendages of *Hurdia* specimens consist either of 11 robust podomeres with one dorsal spine, three lateral spines, and five elongated ventral spines (Fig. 2B and fig. S2E), or they have nine thinner podomeres with single dorsal spines, no lateral spines, and seven elongated ventral spines (Fig. 2C and fig. S2C). Both appendage types are unquestionably associated with definite *Hurdia* elements, suggesting the existence of two morphs or species.

The trunk of the *Hurdia* body consists of seven to nine poorly delimited segments of roughly equal width (Figs. 1 and 2). Each segment bore a pair of lateral flaps covered by smooth cuticle (Fig. 3), which were overlain by thin lanceolate structures arranged in series (Fig. 2E and fig. S2, C and H), interpreted to be gills. The lanceolate structures were attached to the anterior margins of the lateral flaps and were free-hanging posteriorly (fig. S2, C and H). Lateral flaps and gills are arranged in reverse imbrication. Four pairs of smaller lanceolate structures surround the mouthparts and frontal appendages (Figs. 1, A and B, and 3).

Discussion. *Hurdia* is the most common anomalocaridid in at least the Walcott Quarry. It occurs in six Burgess Shale localities in the Canadian Rockies, representing six members and two formations (table S1), as well as in Utah (*14*), Bohemia (*15*), and possibly Nevada (*16*) and China (*17*), suggesting that *Hurdia* was a generalist adapted to a range of environmental conditions (*18*). Its cephalic carapace structure is unique in its composition and anterior position relative to the rest of the body. Such a complex anterior structure finds no convincing analogs in any living or fossil arthropod. This position of the frontal carapace is probably original and not the product of postmortem displacement or moult configurations (SOM text). Like other anomalocaridids (*9*), *Hurdia* was likely an active nektobenthic animal, probably a predator or scavenger. The less robust morphology of the frontal appendages of *Hurdia* suggests that it may have been exploiting different prey sources than *Anomalocaris*.

Anomalocaridids have been variously regarded as stem- (*19*, *20*) or crown- (*21*, *22*) group

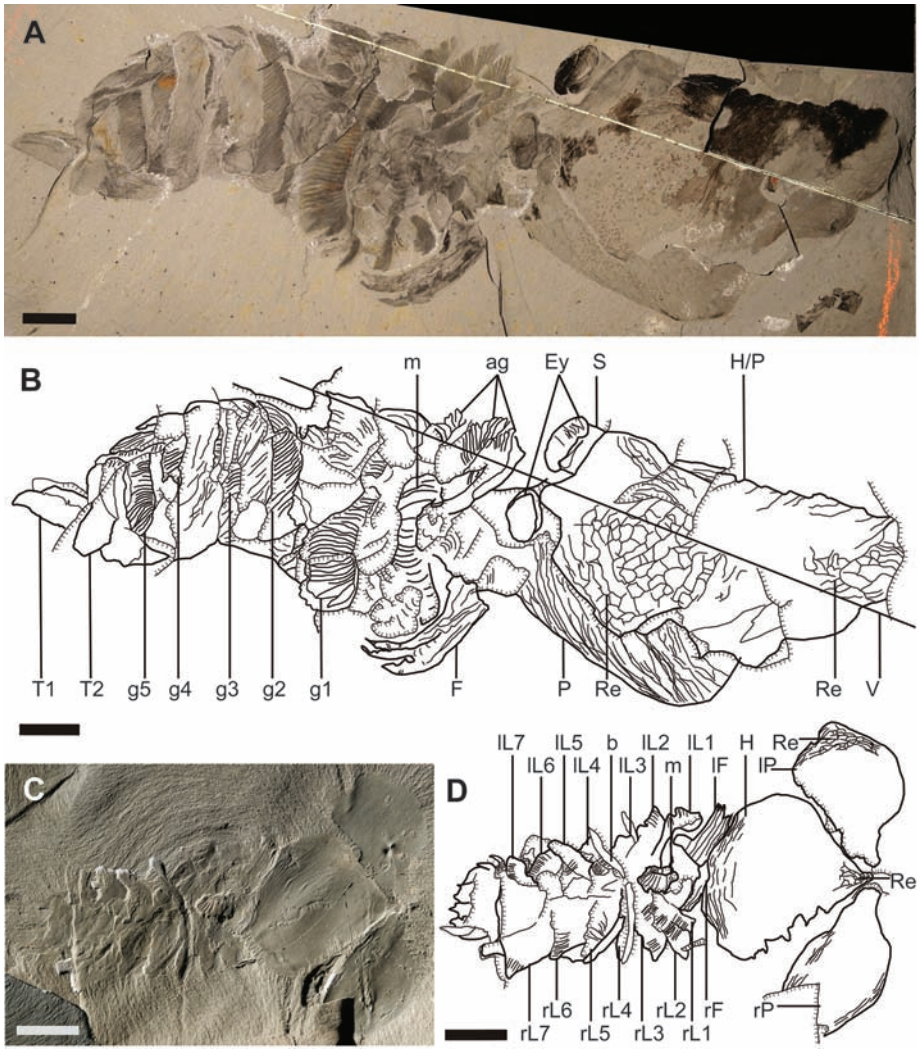

Fig. 1. *H. victoria* from the Burgess Shale, paratype specimens. (**A**) USNM 274159, dorsolateral specimen previously described as *Emeraldella brocki* (*6*) and *Anomalocaris nathorsti* (*9*). (**B**) Camera lucida drawing of USNM 274159. (**C**) ROM 59252, specimen is in dorsal view. (**D**) Camera lucida drawing of ROM 59252. Scale bars, 1 cm. ag, anterior gills; b, burrow; m, mouthparts; Ey, eye; F, frontal appendage; g, gill; H, H-element; l, left; L, lateral flap and associated gill; r, right; Re, reticulated structure; P, P-element; S, eye stalk; T, tail lobe; V, mineral vein.

euarthropods, as a sister group to arthropods in the broad sense (*23*, *24*), or within the cycloneuralian worms (*25*). The phylogenetic analysis (*12*) we conducted places *Hurdia* as sister to a group composed of *Anomalocaris* and *Laggania*, with these three taxa forming a clade in the stem group of the euarthropods (Fig. 4). Although *Anomalocaris* and *Laggania* have similar trunk morphology and number of cephalic segments, the latter taxon also shares traits with *Hurdia*, notably similar frontal appendages, weakly sclerotized anterior carapace elements, and the position of the stalked eyes directly posterior to the frontal carapace (*9*) (fig. S2, A and B). The frontal appendage of *Hurdia* was previously assigned to *Laggania* (*9*) [appendage F of *A. nathorsti* (*9*)], and although *Laggania*'s frontal appendages are similar in general morphology to the more robust of the two *Hurdia* appendage types [compare figure 7.2 of (*1*) to Fig. 2B], inadequate preservation of *Laggania* specimens prevents a more detailed comparison. The phylogenetic analysis suggests that the frontal appendages and anterior carapaces of *Hurdia* and *Laggania* are plesiomorphic for the anomalocaridids, making *Anomalocaris* the most derived member of the clade, because it secondarily lost or modified these structures. If the carapace is homologous with the euarthropod cephalic shield, this head covering may have originated before the last common ancestor of the anomalocaridids and higher euarthropods.

We regard the lanceolate structures reported here from *Hurdia* as being respiratory in function, based on their morphology and arrangement. They closely resemble and clarify the structure of those identified as present in *Anomalocaris*, *Laggania* (fig. S2I), and in some (*26*, *27*) but not all (*28*) interpretations of *Opabinia* (fig. S2G). In *Hurdia*, the insertion points of the gills (Fig. 2E and fig. S2, C and H) bear some resemblance to the "transverse rods" (*9*, *27*) of *Laggania* (fig. S2, A and B, and D to F), with both having a regularly spaced, beaded morphology and darkening associated with sclerotization. If these structures are homologous, this adds evidence to the theory that the annuli of the transverse rods are the points of origin for the blades (*27*). The morphology of the gills of *Hurdia* reveals more clearly than before that presumed anomalocaridid respiratory structures, like those of *Opabinia* (*28*), closely resemble the setae commonly associated with outer branches of Cambrian arthropod limbs (*29*). Both structures consist of a series of free-hanging filamentous gills attached to a supporting structure (the lateral lobe in anomalocaridids and the outer branch of Cambrian arthropod limbs). This homology is in accordance with the suggestion that such branches are homologous to respiratory exites of extant crustaceans and chelicerates, and not to the outer branch of the modern biramous limb (*30*). The modern biramous limb forms by division of the main limb axis (*30*), in contrast to the Cambrian limb, which may be formed by the fusion of a uniramous limb with a respiratory exite. The presence of the respiratory exite in *Hurdia*

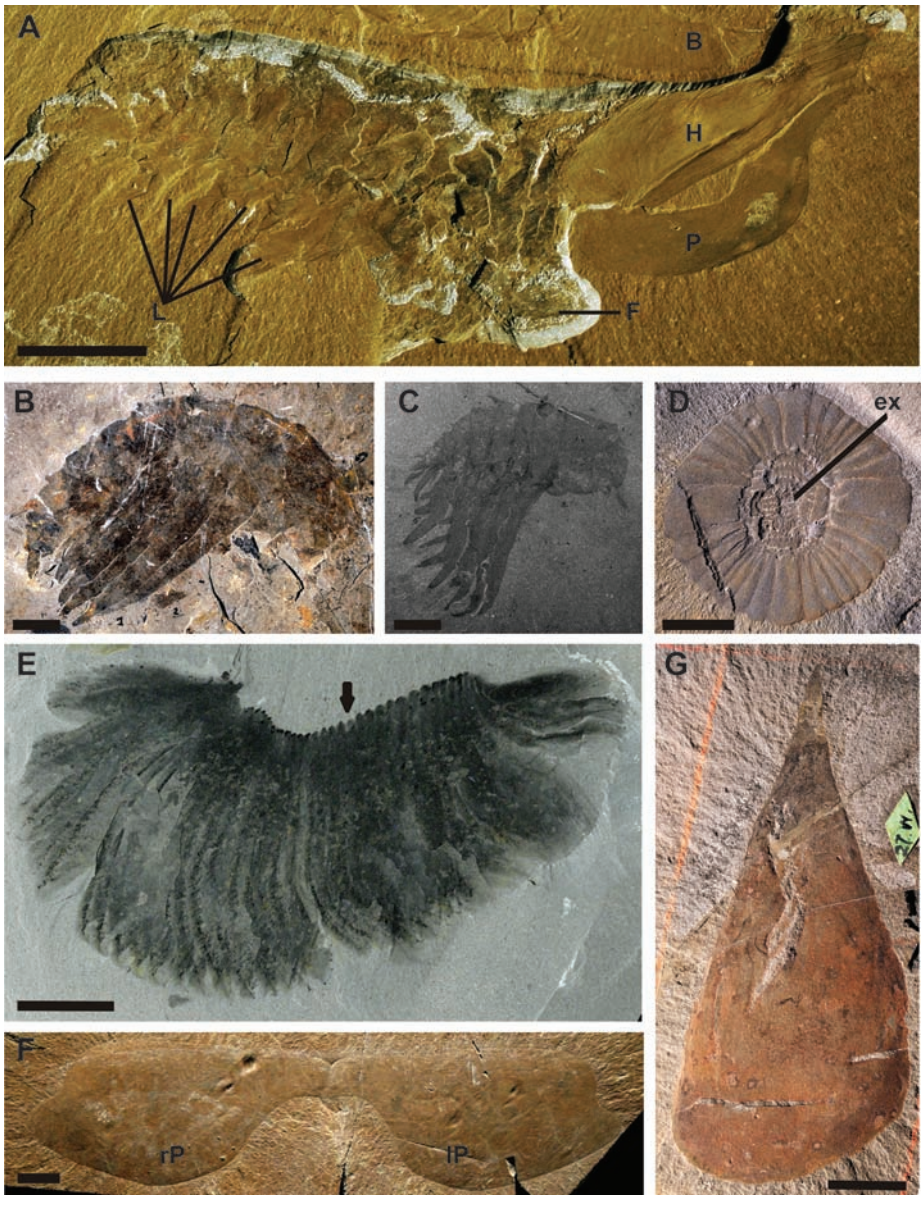

Fig. 2. Paratype specimen and isolated components of *H. victoria*. (**A**) ROM 49930, paratype, lateral view showing lateral flaps. (**B**) ROM 59258, frontal appendage morph A. (**C**) ROM 59259, frontal appendage morph B. (**D**) ROM 59260, mouthpart with extra teeth rows. (**E**) ROM 59261, lanceolate gill blades showing attachment at one end (arrow). (**F**) ROM 59262, paired P-elements. (**G**) USNM 57718, holotype of *H. victoria*. Scale bars, 1 cm. Abbreviations are as in Fig. 1. B, *Banffia*; ex, extra teeth rows.

Fig. 3. Reconstruction of *H. victoria*. [Drawing by M. Collins, 2008 © ROM/J. B. Caron]

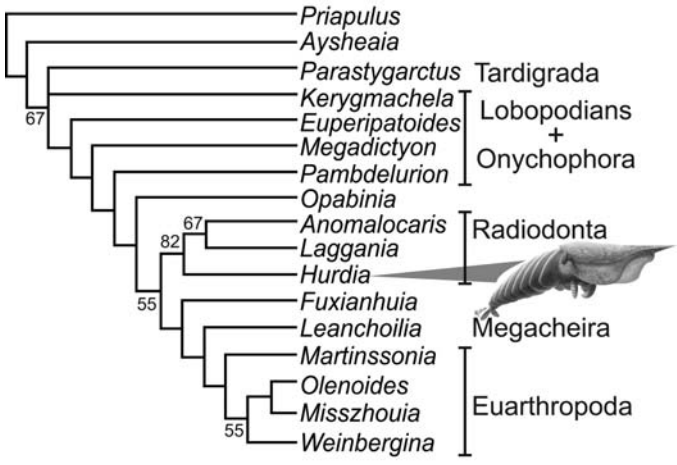

Fig. 4. Cladistic analysis (*12*) of selected stem- and crown-group arthropods (SOM text, fig. S3, and table S3). This is a strict consensus of three trees found using branch and bound search under implied weights [concavity constant (*k*) = 2]. Tree length, 53.89; rescaled consistency index, 0.76. Jackknife supports are shown at the nodes when over 50%.

pushes the origin of this structure deep into the euarthropod stem group.

Note added in proof: The recently described *Schinderhannes bartelsi* (*31*) has been placed between *Anomalocaris* and the upper stem group arthropods in a cladogram consistent with the analysis here. It has biramous trunk limbs with filamentous exites, an anomalocaridid-like radial mouthpart, and frontal appendages remarkably similar to those of *Hurdia* morph B. Presence of these features in an animal that lacks lateral lobes and gills adds evidence to the theory that Cambrian biramous limbs formed by fusion of these structures.

References and Notes

1. D. Collins, *J. Paleontol.* **70**, 280 (1996).
2. C. D. Walcott, *Smithson. Misc. Coll.* **57**, 41 (1911).
3. J. F. Whiteaves, *Can. Rec. Sci.* **5**, 205 (1892).
4. C. D. Walcott, *Smithson. Misc. Coll.* **57**, 17 (1911).
5. D. E. G. Briggs, *Palaeontology* **22**, 631 (1979).
6. A. M. Simonetta, L. Della Cave, *Palaeotogr. Ital.* **69**, 1 (1975).
7. C. D. Walcott, *Smithson. Misc. Coll.* **57**, 145 (1912).
8. W. D. I. Rolfe, *Breviora* **160**, 1 (1962).
9. H. B. Whittington, D. E. G. Briggs, *Philos. Trans. R. Soc. London Ser. B* **309**, 569 (1985).
10. D. Collins, in *North American Paleontological Convention, Chicago, Abstracts with Programs*, S. Lidgard, P. R. Crane, Eds. (The Paleontological Society, Special Publication 6, Chicago, IL, 1992), p. 66.
11. D. Collins, *Rotunda* **32**, 25 (1999).
12. Materials and methods are available as supporting material on *Science* Online.
13. T. P. Fletcher, D. H. Collins, *Can. J. Earth Sci.* **35**, 413 (1998).
14. D. E. G. Briggs, B. S. Lieberman, J. R. Hendricks, S. L. Halgedahl, R. D. Jarrard, *J. Paleontol.* **82**, 238 (2008).
15. I. Chlupáč, V. Kordule, *Bull. Czech. Geol. Surv.* **77**, 167 (2002).
16. B. S. Lieberman, *J. Paleontol.* **77**, 674 (2003).
17. Z. Cui, S. Huo, *Acta Palaeont. Sinica* **29**, 328 (1990).
18. J.-B. Caron, D. A. Jackson, *Palaeogeogr. Palaeoclimatol. Palaeoecol.* **258**, 222 (2008).
19. R. A. Dewel, W. C. Dewel, in *Arthropod Relationships*, R. A. Fortey, R. A. R. H. Thomas, Eds. (Chapman & Hall, London, 1998), pp. 109–123.
20. G. E. Budd, *Nature* **417**, 271 (2002).
21. A. Maas *et al*., *Prog. Nat. Sci.* **14**, 158 (2004).
22. J. Chen, D. Waloszek, A. Maas, *Lethaia* **37**, 3 (2004).
23. M. A. Wills, D. E. G. Briggs, R. A. Fortey, M. Wilkinson, P. H. A. Sneath, in *Arthropod Fossil and Phylogeny*, G. D. Edgecombe, Ed. (Columbia Univ. Press, New York, 1998), pp. 33–105.
24. X. Hou, J. Bergström, J. Yang, *Geol. J.* **41**, 259 (2006).
25. X. Hou, J. Bergström, P. Ahlberg, *GFF* **117**, 163 (1995).
26. G. E. Budd, *Lethaia* **29**, 1 (1996).
27. J. Bergström, *Lethaia* **20**, 187 (1987).
28. X. Zhang, D. E. G. Briggs, *Lethaia* **40**, 161 (2007).
29. G. A. Boxshall, *Biol. Rev. Camb. Philos. Soc.* **79**, 253 (2004).
30. C. Wolff, G. Scholtz, *Proc. R. Soc. London Ser. B* **275**, 1023 (2008).
31. G. Kühl, D. E. G. Briggs, J. Rust, *Science* **323**, 771 (2009).

32. We thank J. Bergström for discussion. Comments from D. E. G. Briggs, B. S. Lieberman, and anonymous reviewers improved the manuscript. J. Dougherty and F. Collier provided access to specimens at GSC and MCZ, respectively, and D. Erwin and J. Thompson provided access to specimens at NMNH. Permission to collect Burgess Shale specimens was given by Parks Canada to D.C. Funding was provided by European Union Marie Curie Research Training Network ZOONET (grant MRTN-CT-2004-005624) to G.E.B. and A.C.D. and the Swedish Research Council (Vetenskapsrådet) to G.E.B. This is ROM Burgess Shale Project number 8.

Supporting Online Material

www.sciencemag.org/cgi/content/full/323/5921/1597/DC1
Materials and Methods
SOM Text
Figs. S1 to S3
Tables S1 to S3
References

9 December 2008; accepted 2 February 2009
10.1126/science.1169514

A Role for RNAi in the Selective Correction of DNA Methylation Defects

Felipe Karam Teixeira,[1,2] Fabiana Heredia,[1] Alexis Sarazin,[2] François Roudier,[1,2] Martine Boccara,[1,2] Constance Ciaudo,[3,4] Corinne Cruaud,[5] Julie Poulain,[5] Maria Berdasco,[6] Mario F. Fraga,[6]* Olivier Voinnet,[3] Patrick Wincker,[5] Manel Esteller,[6] Vincent Colot[1,2]†

DNA methylation is essential for silencing transposable elements and some genes in higher eukaryotes, which suggests that this modification must be tightly controlled. However, accidental changes in DNA methylation can be transmitted through mitosis (as in cancer) or meiosis, leading to epiallelic variation. We demonstrated the existence of an efficient mechanism that protects against transgenerational loss of DNA methylation in *Arabidopsis*. Remethylation is specific to the subset of heavily methylated repeats that are targeted by the RNA interference (RNAi) machinery. This process does not spread into flanking regions, is usually progressive over several generations, and faithfully restores wild-type methylation over target sequences in an RNAi-dependent manner. Our findings suggest an important role for RNAi in protecting genomes against long-term epigenetic defects.

Cytosine methylation in plant genomes occurs predominantly at CG sites but also at CHG and CHH sites (where H is A, T, or C). Genetic analysis in *Arabidopsis* has uncovered an interplay between "maintenance" and "de novo" DNA methyltransferases (MTases), DNA demethylases, histone-modifying or remodeling enzymes, and RNA interference (RNAi) components (*1*, *2*). Among many mutants identified, those in the MTase gene *MET1* and the adenosine triphosphatase chromatin remodeler gene *DDM1* lead to the most severe loss (>70%) of DNA methylation overall (*3*–*6*). This loss persists in F_1 plants obtained in crosses

[1]Unité de Recherche en Génomique Végétale, CNRS UMR 8114, Institut National de la Recherche Argonomique UMR 1165, Université d'Evry Val d'Essonne, 91057 Evry Cedex, France. [2]CNRS UMR 8186, Département de Biologie, Ecole Normale Supérieure, 75230 Paris Cedex 05, France. [3]Institut de Biologie Moléculaire des Plantes, CNRS Unité Propre de Recherche 2357, 67084 Strasbourg Cedex, France. [4]CNRS UMR 218, Institut Curie, 75248 Paris Cedex 05, France. [5]Génoscope, Commissariat à L'Energie Atomique–Institut de Génomique, 91057 Evry Cedex, France. [6]Laboratorio de Epigenética del Cáncer, Centro Nacional de Investigaciones Oncológicas, 28029 Madrid, Spain.

*Present address: Immunología y Oncología, Centro Nacional Biotecnología, Consejo Superior de Investigaciones Científicas, Cantoblanco, 28049 Madrid, Spain.
†To whom correspondence should be addressed. E-mail: colot@biologie.ens.fr

with the wild type, despite *met1* and *ddm1* mutations being recessive (*3*–*6*), as well as in subsequent generations, at least at the few loci that have been examined (*2*, *7*). These and other findings have led to the prevalent view that in plants, DNA methylation cannot be restored once it has been severely compromised (*2*, *7*, *8*). However, given the stability of DNA methylation of repeat elements across generations (*9*), mechanisms must exist that protect plant genomes against the irremediable loss of DNA methylation.

To address this issue, we examined the transgenerational stability of *ddm1*-induced hypomethylation of a large number (n = 56) of transposable elements and other repeats. Methylation was first investigated five generations after segregation of the *ddm1* mutation [the *DDM1*/*DDM1* F_5 lines were obtained through one backcross and three selfings (BC1 and S3)] (fig. S1 and table S1) by means of McrBC digestion and quantitative polymerase chain reaction (McrBC-QPCR) (*10*). Of 47 *ddm1*-hypomethylated sequences examined in the repeat-rich 500-kb-long heterochromatic knob on chromosome 4, 21 remained hypomethylated in *DDM1*/*DDM1* F_5 lines that had inherited the knob region from the *ddm1* parent (Fig. 1A and table S2). However, another 22 sequences had wild-type (WT) methylation levels, and only four showed inconsistent methylation between these lines. The interspersion of hypo- and WT methylation and the consistency of methylation patterns between lines (Fig. 1A and table S2) as well as in more

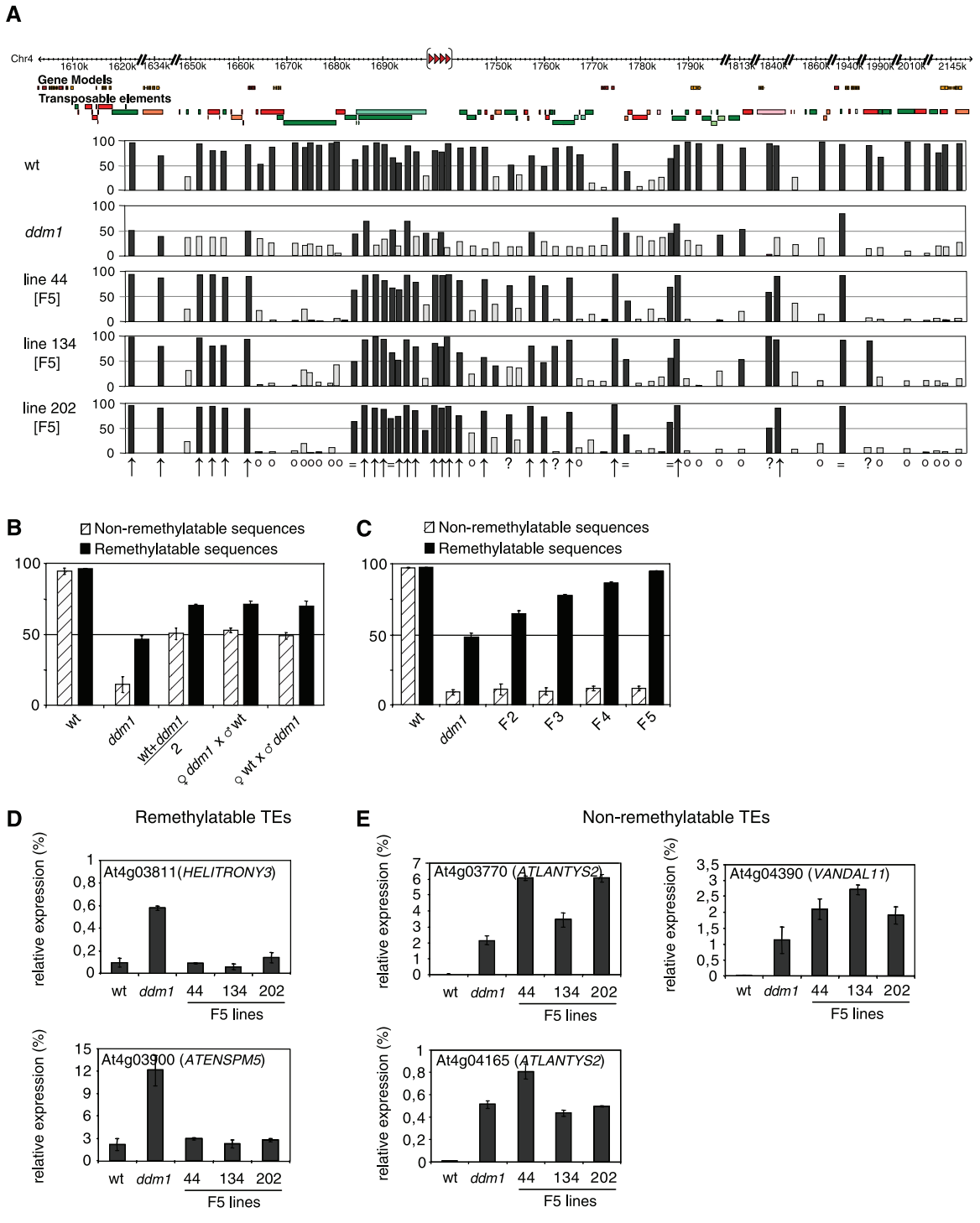

Fig. 1. DNA methylation and expression analyses in WT, *ddm1*, and progeny lines. (**A**) Annotation is at the top (red, DNA transposons; green, retro-elements). The *ATENSAT1* tandem array (22.5 copies) is depicted as four bracketed red arrowheads. Vertical bars indicate methylation levels (light gray indicates <30% methylation). (Bottom) Remethylated sequences are marked by arrows and nonremethylated sequences by open circles; sequences that were equally methylated in WT and *ddm1* are indicated by an equals sign. Inconsistent DNA methylation levels (±30% or more) between the three F_5 lines are indicated by a question mark. (**B**) Average DNA methylation level of 18 nonremethylatable and 18 remethylatable sequences in WT, *ddm1*, and F_1 progeny of reciprocal crosses. The average between WT and *ddm1* is also shown. (**C**) Average DNA methylation of 8 nonremethylatable and 15 remethylatable sequences in WT, *ddm1*, and two *DDM1*/*DDM1* progeny lines followed through four selfings (F_2 to F_5). (**D**) and (**E**) reverse transcription PCR (RT-PCR) analysis of two nonremethylatable and three remethylatable transposable elements (TEs). Results are expressed as a percentage of expression relative to controls (*10*).

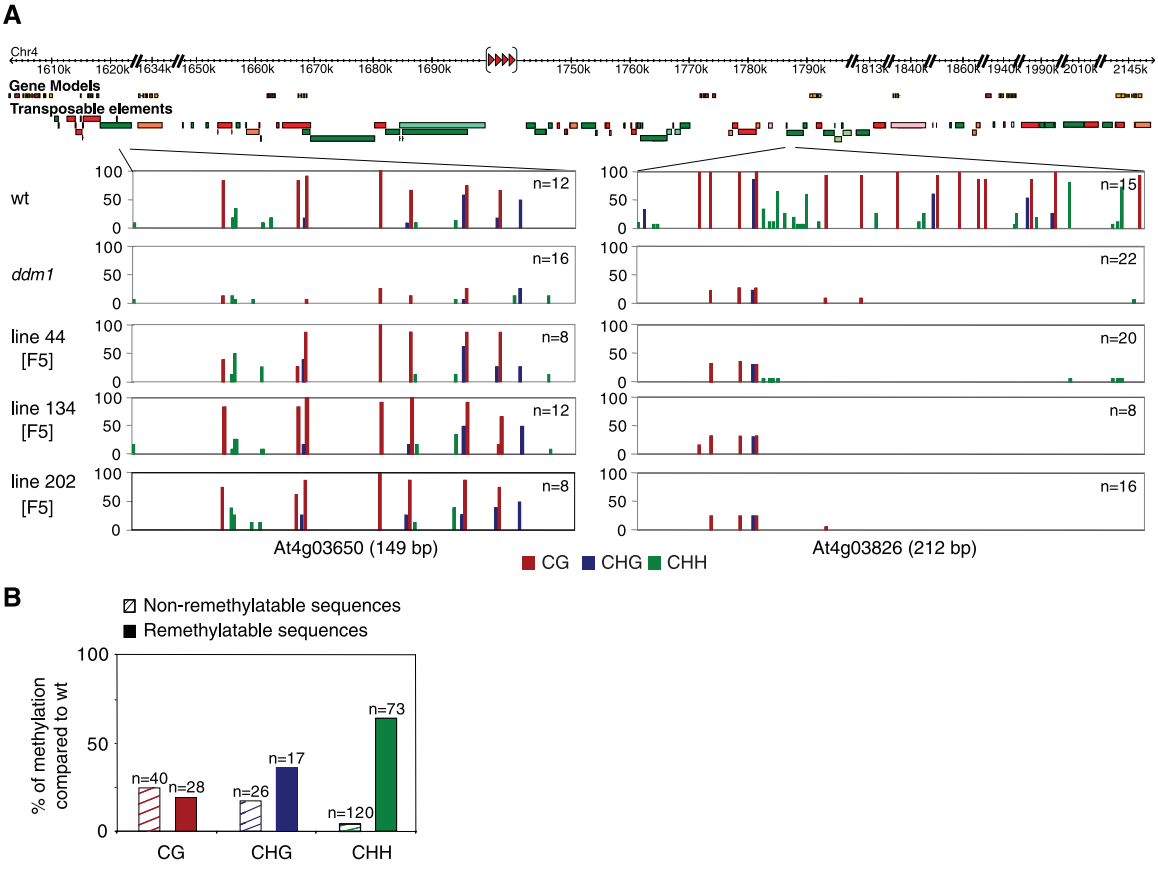

Fig. 2. Bisulfite sequencing analysis of DNA methylation in WT, *ddm1*, and progeny lines. (**A**) The locations of At4g03650 (remethylatable) and At4g03826 (nonremethylatable) are shown at the top. Vertical bars indicate the percentage of methylation for each cytosine, and *n* is the number of clones sequenced. (**B**) Percentage of CG, CHG, and CHH methylation present in *ddm1* as compared with that in WT. The total number of sites analyzed is shown above each bar. Differences were statistically significant for CHG and CHH sites (two-tailed *t* test, $P < 0.01$) but not for CG sites.

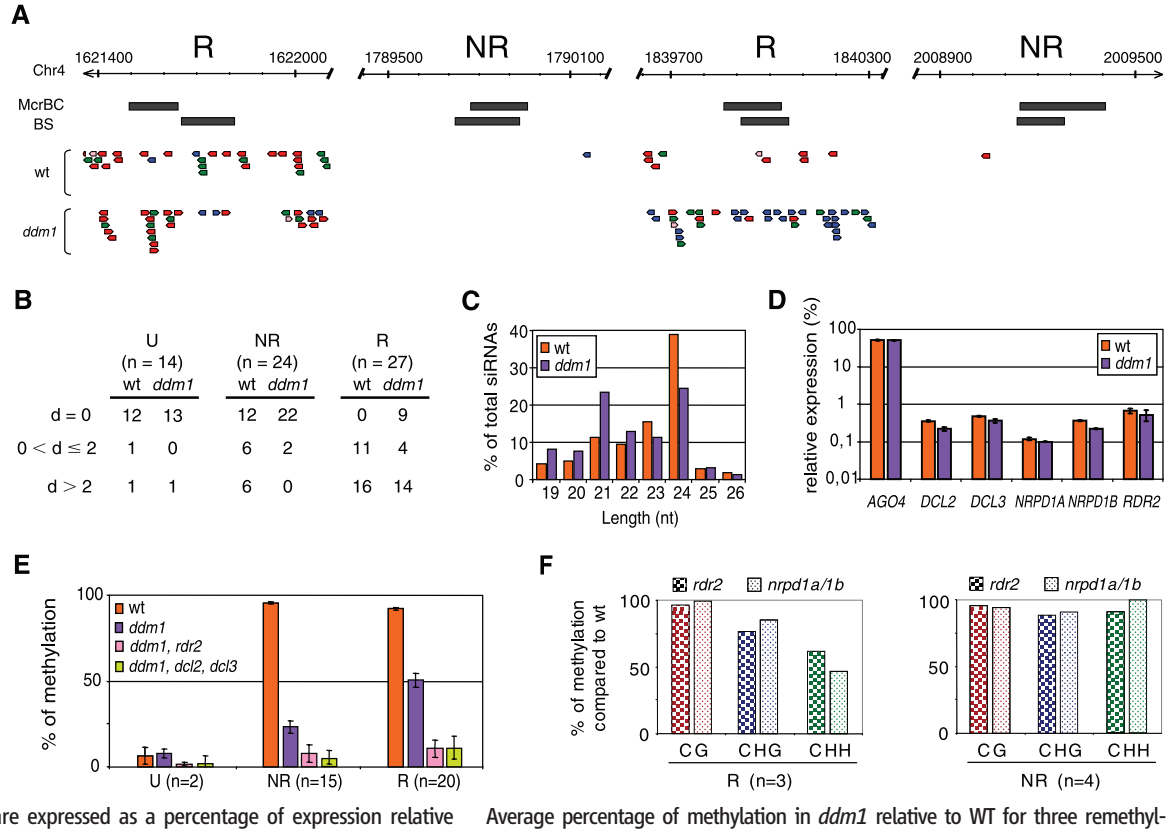

Fig. 3. Involvement of RNAi in the distinction between remethylatable and nonremethylatable sequences. (**A**) sRNAs (blue, 20 to 21 nt; green, 22 to 23 nt; red, 24 to 25 nt; pink, other sizes) matching 700–base pair (bp) regions centered on two remethylatable (R) and two nonremethylatable (NR) knob sequences, as probed by use of McrBC-QPCR and bisulfite sequencing (BS) (black bars). (**B**) Normalized density (*10*) of 24-nt RNAs for 14 unmethylated (U), 24 nonremethylatable, and 27 remethylatable sequences. Data for WT was derived from (*17*). (**C**) Frequency plot of 19- to 26-nt RNAs (minus miRNAs and tasiRNAs). (**D**) RT-PCR analysis of *ARGONAUTE 4* (*AGO4*), *DCL2*, *DCL3*, *NRPD1A*, *NRPD1B*, and *RDR2* transcripts. Results are expressed as a percentage of expression relative to controls (*10*). (**E**) Average DNA methylation of two unmethylated, 15 nonremethylatable, and 20 remethylatable sequences in different genetic backgrounds. (**F**) Average percentage of methylation in *ddm1* relative to WT for three remethylatable and four nonremethylatable sequences (figs. S5 and S6). Differential loss of CHH methylation in *ddm1* is statistically significant (two-tailed *t* test, $P < 0.01$).

advanced generations (F_6 to F_9) (figs. S2 and S3) were all indicative of a robust and targeted remethylation process. This was further illustrated by the fact that even when located close (<2.5 kb) to remethylated sequences, nonmethylated controls remained unmethylated (Fig. 1A and table S2). Remethylation was also observed for five of eight *ddm1*-hypomethylated sequences tested outside of the knob, indicating that this process acts throughout the genome (fig. S3).

To determine when remethylation occurs and whether it might be parent-of-origin–specific, we performed reciprocal crosses between wild type and *ddm1* plants. Irrespective of the direction of the cross, methylation levels were constant in the different F_1 plants and were systematically intermediate between the wild type and *ddm1*, whether "remethylatable" or "nonremethylatable" according to the initial analysis of F_5 lines (Fig. 1B, fig. S4, and table S2). These results are in agreement with global measurements of cytosine methylation (*11*) and indicate that remethylation does not occur detectably in the F_1 progeny of *ddm1*–wild type crosses. F_1 plants were selfed or reciprocally backcrossed with the wild type, and F_2 individuals of *DDM1*/*DDM1* genotype were propagated for several generations. Eight of the 21 nonremethylatable sequences originally identified (Fig. 1A) were tested, and none had regained DNA methylation in these new F_2 to F_5 lines (Fig. 1C and table S2). On the other hand, 12 of 15 remethylatable sequences had increased methylation by the F_2 and three by the F_3 (Fig. 1C and table S2). With three exceptions, remethylation was progressive and reached WT levels after one to three additional generations (Fig. 1C and table S2). Remethylation efficiencies were similar in the progeny of reciprocal backcrosses, ruling out overt parent-specific effects. Furthermore, remethylation did occur when either one or both copies of the knob were derived from the *ddm1* parent, indicating that this process differs from paramutation (*12*) or meiotic transfer of methylation (*13*), which involves a transfer of epigenetic information between alleles.

Many transposable elements are reactivated in *ddm1* (*14*, *15*), and several nonremethylatable and remethylatable sequences were of this kind. However, nonremethylatable elements remained active after the restoration of DDM1 function, whereas remethylatable elements became resilenced (Fig. 1, D and E). This suggests an important function for remethylation in protecting the genome against the deleterious effects of transposable element activity.

Three remethylatable and four nonremethylatable sequences were then analyzed by means of sequencing of bisulfite-treated DNA (*10*). These

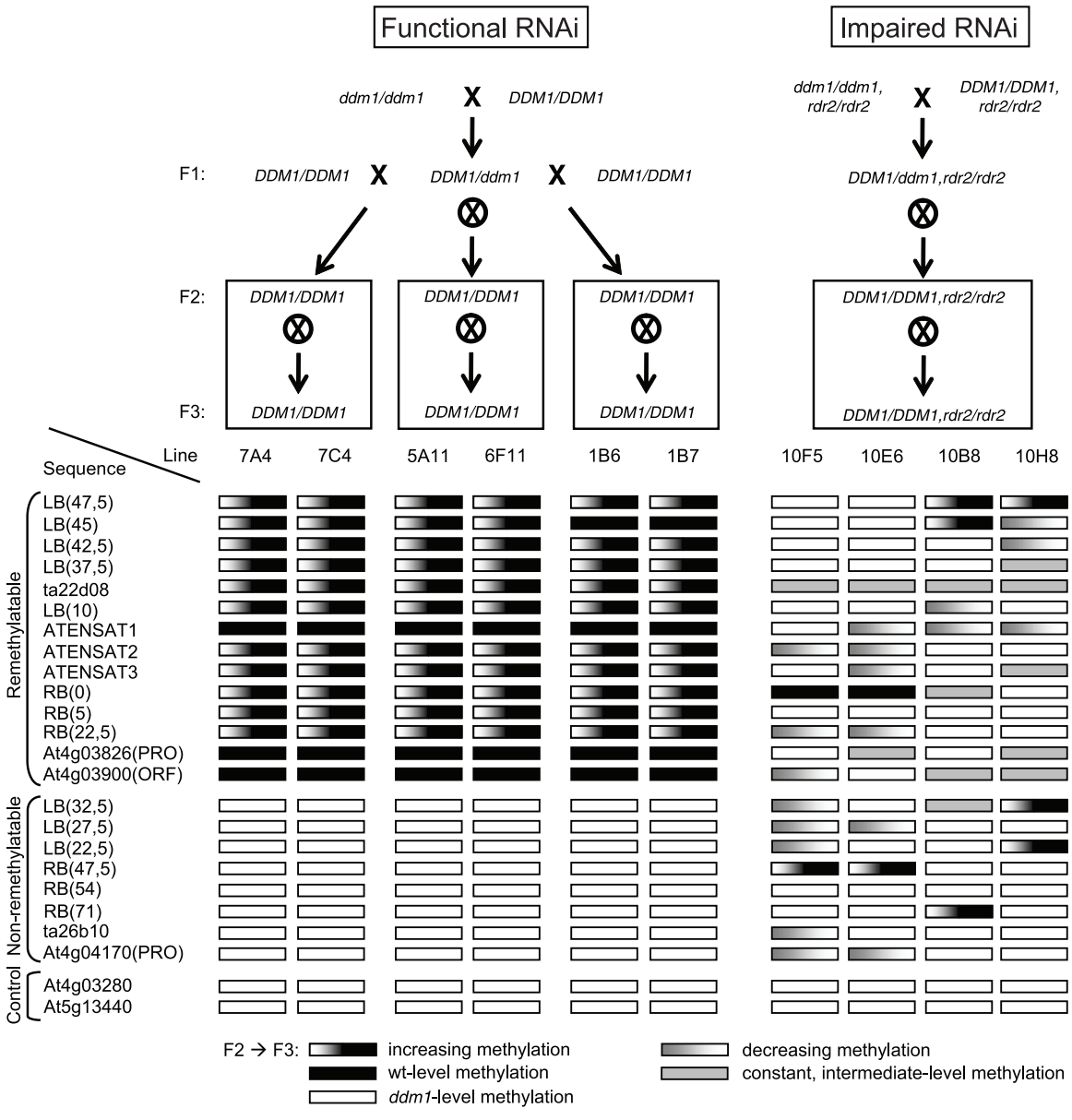

Fig. 4. Involvement of RNAi in faithful remethylation. DNA methylation was measured by means of McrBC-QPCR in F_2 and F_3 progeny lines with a *ddm1*-derived knob region. Results are summarized as illustrated.

two groups of sequences, which had comparable CG, CHG, and CHH compositions (fig. S7A), exhibited similar methylation in WT plants (Fig. 2A and fig. S7B), which is consistent with McrBC-QPCR (Fig. 1, A to C, and table S2) and genome-wide bisulphite sequencing data (fig. S7C) (*16*). In the *DDM1*/*DDM1* F_5 lines, faithful remethylation was observed at CG, CHG, and CHH sites for remethylatable sequences, whereas nonremethylatable sequences retained their *ddm1* hypomethylation profiles (Fig. 2A and figs. S5 and S6). Bisulfite sequencing also indicated that the more pronounced loss of methylation in *ddm1* over nonremethylatable sequences (Fig. 1, A to C, and table S2) was caused by differences at CHH and CHG but not CG sites (Fig. 2B and figs. S5 and S6). Indeed, although the loss of methylation in *ddm1* was severe at CG sites for the two groups of sequences (around 80%), as well as at CHG and CHH sites for nonremethylatable sequences (80 and 95%, respectively), it was less so at CHG sites and only marginal at CHH sites for remethylatable sequences (60 and 25%, respectively) (Fig. 2B and fig. S6). These results revealed a strong dependence of CHH methylation on DDM1, but only at nonremethylatable sequences.

Given the involvement of RNAi in CHH methylation (*1*, *2*), small RNA (sRNA) deep-sequencing data available for the wild type (*17*) were examined and compared with similar data obtained for *ddm1* (*10*). Contrary to nonremethylatable sequences, remethylatable sequences were characterized in WT plants by an abundance of corresponding sRNAs of mostly 24 nucleotides (nt) (Fig. 3, A and B, fig. S8, and table S1), which is consistent with genome-wide data indicating that 24-nt small interfering RNAs (siRNAs) match only a subset of methylated repeats (*18*). Analysis of the *ddm1* data revealed a change as compared with that of the wild type in the relative proportion of the different size classes of sRNAs other than known microRNAs (miRNAs) or trans-acting small interfering RNAs (tasiRNAs) (Fig. 3C). This change was mainly caused by a specific and massive accumulation of 21-nt siRNAs matching *ATHILA* elements (Fig. 3A, fig. S8, and table S1) (*10*), which is similar to that observed in *met1* mutant plants (*18*) as well as in tissue culture (*19*). Nonetheless, 18 of the 27 remethylatable sequences, including most *ATHILA* sequences, were still characterized by an abundance of matching 24-nt siRNAs (Fig. 3, A and B, fig. S8, and table S1) (*10*), which is in agreement with previous studies (*15*, *20*). This suggests that the RNAi machinery is responsible for the persistence of CHH methylation specifically at remethylatable sequences in *ddm1* and hence in their distinction from nonremethylatable sequences. Consistent with this, transcript levels of genes involved in the 24-nt siRNA production pathway (*21*–*23*), including *DICER-LIKE 3* (*DCL3*), *RNA-DEPENDENT RNA POLYMERASE 2* (*RDR2*), *NUCLEAR RNA POLYMERASE D 1A* (*NRPD1A*), and *NRPD1B*, were unchanged in *ddm1* (Fig. 3D). As anticipated from the disappearance of 24-nt siRNAs in *rdr2* and *dcl2dcl3* mutants (*22*, *23*), methylation was almost completely lost over remethylatable sequences when *ddm1* was combined with *rdr2* or *dcl2dcl3* (Fig. 3E and table S2). Reduction of methylation at nonremethylatable sequences was also observed in *ddm1rdr2* or *ddm1dcl2dlc3* mutant seedlings (Fig. 3E and table S2), suggesting a low input from the RNAi pathway in the methylation of these sequences. Although global methylation levels were unaffected in *rdr2*, *dcl2dcl3*, and *nrpd1a&1b* mutant seedlings (fig. S9 and table S2), a significant loss of CHH methylation occurred specifically over remethylatable sequences (Fig. 3F and figs. S5 and S6). These results establish a crucial role for RNAi in the distinction between remethylatable and nonremethylatable sequences.

To determine whether RNAi is causal in remethylation, *ddm1rdr2* plants were crossed with *rdr2* single mutants and the F_1 progeny was selfed to obtain F_2 and F_3 progeny with impaired RNAi but restored DDM1 function. We observed rare and nonprogressive methylation, which affected both remethylatable and nonremethylatable sequences (Fig. 4 and table S2). This mostly sporadic low-level methylation is reminiscent of that observed in mutant plants homozygous for a null allele of the maintenance MTase gene *MET1* (*8*) and suggests that when RNAi is compromised, an inefficient mechanism of compensatory methylation may come into play. This demonstrates an essential function of RNAi in robust and specific remethylation.

We have shown that contrary to the prevalent view (*2*, *7*, *8*), numerous repeat elements can efficiently regain WT methylation after a severe loss in *Arabidopsis*. This remethylation is guided by the RNAi machinery, does not spread into nearby sequences, and, in the case of reactivated transposable elements, is associated with their resilencing. Thus, two main types of methylated repeat elements may be distinguished (fig. S10A). Although methylation of some repeat elements depends almost exclusively on maintenance MTases and cannot be regained once compromised, other repeat elements are efficiently targeted in parallel by the RNAi-dependent de novo methylation machinery, which contributes marginally to their overall methylation but is critical for their faithful remethylation. A third, minor group of repeats is targeted solely by the RNAi-dependent de novo methylation machinery (*18*, *24*) and therefore remains unaffected in *ddm1* or *met1* (fig. S10B).

The progressivity of remethylation parallels that of the de novo RNA-dependent DNA methylation that is frequently observed with transgenes (*1*, *2*). This suggests that remethylation may be most effective for recently inserted transposable elements and that nonremethylatable repeats were likely to have been remethylatable when first inserted. Although the frequency with which DNA methylation can be lost in natural settings is unknown, our discovery of a corrective mechanism reveals an important role for RNAi in protecting the genome against transgenerational epigenetic defects. This mechanism also has potential adaptive and evolutionary implications (*25*) because it allows for the generation of epialleles with differences in transgenerational stability.

References and Notes

1. B. Huettel *et al.*, *Biochim. Biophys. Acta* **1769**, 358 (2007).
2. I. R. Henderson, S. E. Jacobsen, *Nature* **447**, 418 (2007).
3. A. Vongs, T. Kakutani, R. A. Martienssen, E. J. Richards, *Science* **260**, 1926 (1993).
4. H. Saze, O. M. Scheid, J. Paszkowski, *Nat. Genet.* **34**, 65 (2003).
5. M. W. Kankel *et al.*, *Genetics* **163**, 1109 (2003).
6. T. Kakutani, K. Munakata, E. J. Richards, H. Hirochika, *Genetics* **151**, 831 (1999).
7. E. J. Richards, *Nat. Rev. Genet.* **7**, 395 (2006).
8. O. Mathieu, J. Reinders, M. Caikovski, C. Smathajitt, J. Paszkowski, *Cell* **130**, 851 (2007).
9. M. W. Vaughn *et al.*, *PLoS Biol.* **5**, 1617 (2007).
10. Materials and methods are available as supporting material on *Science* Online.
11. T. Kakutani, J. A. Jeddeloh, E. J. Richards, *Nucleic Acids Res.* **23**, 130 (1995).
12. V. L. Chandler, *Cell* **128**, 641 (2007).
13. V. Colot, L. Maloisel, J. L. Rossignol, *Cell* **86**, 855 (1996).
14. A. V. Gendrel, Z. Lippman, C. Yordan, V. Colot, R. A. Martienssen, *Science* **297**, 1871 (2002).
15. Z. Lippman *et al.*, *Nature* **430**, 471 (2004).
16. S. J. Cokus *et al.*, *Nature* **452**, 215 (2008).
17. H. Rajagopalan, Vaucheret, J. Trejo, D. P. Bartel. *Genes Dev.* **20**, 3407 (2006).
18. R. Lister *et al.*, *Cell* **133**, 523 (2008).
19. M. Tanurdzic *et al.*, *PLoS Biol.* **6**, e302 (2008).
20. Z. Lippman, B. May, C. Yordan, T. Singer, R. Martienssen, *PLoS Biol.* **1**, 420 (2003).
21. X. Zhang, I. R. Henderson, C. Lu, P. J. Green, S. E. Jacobsen, *Proc. Natl. Acad. Sci. U.S.A.* **104**, 4536 (2007).
22. K. D. Kasschau *et al.*, *PLoS Biol.* **5**, 479 (2007).
23. I. R. Henderson *et al.*, *Nat. Genet.* **38**, 721 (2006).
24. B. Huettel *et al.*, *EMBO J.* **25**, 2828 (2006).
25. F. Johannes, V. Colot, R. C. Jansen, *Nat. Rev. Genet.* **9**, 883 (2008).

26. We thank P. Audigier for plant care, A. Bulski for DNA samples, R. Martienssen for sharing unpublished observations, and E. Heard for critical reading of the manuscript. F.K.T. was supported by a Ph.D. studentship (Coordenação de Aperfeiçoamento de Pessoal de Nível Superior, Brazil) and F.H. and C.C. by postdoctoral fellowships [Network of Excellence (NoE) "The Epigenome" and Fondation pour la Recherche Médicale, respectively]. Grant support was from Agence Nationale de la Recherche–Programme Blanc (PolIV), NoE "The Epigenome," Génoplante (EPIVAR), Génoscope, and CNRS (PIME). The Gene Expression Omnibus accession number for sRNA sequences is GSE13419.

Supporting Online Material

www.sciencemag.org/cgi/content/full/1165313/DC1
Materials and Methods
Figs. S1 to S10
Tables S1 to S4
References

2 September 2008; accepted 16 January 2009
Published online 29 January 2009;
10.1126/science.1165313
Include this information when citing this paper.

Genetic Incompatibility Drives Sex Allocation and Maternal Investment in a Polymorphic Finch

Sarah R. Pryke* and Simon C. Griffith

Genetic compatibility may drive individual mate choice decisions because of predictable fitness effects associated with breeding with incompatible partners. In Gouldian finches (*Erythrura gouldiae*), females paired with genetically incompatible males of alternative color morphs overproduce sons, presumably to reduce investment in inviable daughters. We also observed a reduced overall investment in clutch size, egg size, and care to offspring resulting from incompatible matings. Within-female experimental pairings demonstrate that female birds have the ability to adaptively adjust the sex of their eggs and allocate resources on the basis of partner quality. Female Gouldian finches thus make cumulative strategic allocation decisions to minimize the costs of poor-quality pairings when faced with a genetically incompatible partner.

Life-history theory predicts that females may alter reproductive investment in a particular breeding attempt according to the quality of their partner (*1*, *2*). When breeding with high-quality males is constrained, females may potentially accept incompatible mates but strategically alter their relative investment in sons and daughters to enhance the viability of their current offspring (*1*) or trade off maternal investment in lieu of future reproductive opportunities with higher quality partners (*3*). However, there is limited empirical support for adaptive maternal investment in relation to mate quality. Despite reports of sex ratio adjustment by female birds in relation to partner attractiveness (*3*, *4*), differential sex allocation as an adaptive postcopulatory mechanism in birds remains controversial (*5*–*7*). Similarly, support for differential allocation of resources by females depending on whether they are paired with high- or low-quality mates is scarce (*8*–*11*). These studies have also typically demonstrated relatively weak effects related to a single maternal variable (*8*–*11*) rather than more cumulative allocations by females, which would be expected to have greater biological importance.

The inconsistent and limited empirical support for adaptive maternal investment in vertebrates may have resulted from analyses of individual allocation decisions in the absence of theoretical frameworks (*12*, *13*) and in contexts or systems where parents are unable to precisely predict the net fitness gains from strategic adjustments. Most studies, for example, have focused on maternal allocation in the context of continuously variable male traits, such as color, environmental, or social factors, which may be quantitatively difficult for females to assess and from which the potential fitness benefits are often complex, unpredictable, and relatively weak. Theoretically, it is perhaps unrealistic to expect females to make significant responses on the basis of such variables (*6*). Indeed, most avian studies of maternal investment (*4*, *8*, *10*) have been unable to convincingly demonstrate or even predict the adaptive value to females of differential investment (*12*, *13*).

We investigated adaptive maternal investment in the Gouldian finch (*Erythrura gouldiae*), a color polymorphic bird in which we can make a priori predictions with respect to anticipated responses because of predictable sex-specific fitness effects associated with matings between genetically incompatible partners (*14*). Mate quality is signaled through head color, which is either black (70% of individuals) or red (30%) and is determined by a *Z*-linked gene; red (Z^R) is dominant to black (Z^r) (*15*). Because of the sex determination system of birds, females are homozygous for this gene, and thus phenotype matches genotype (Z^r black, Z^R red), whereas male genotypes can be homozygous Z^rZ^r (black), Z^RZ^R (red) or heterozygous Z^RZ^r (red). Heterozygous and homozygous red males are phenotypically indistinguishable (*15*). Individuals discriminate between black and red mates and demonstrate precopulatory mate preferences for their own morph type (*16*). However, up to 30% of breeding pairs in wild populations are mixed (intermorph), perhaps because of constraints on preferred mate availability in this socially monogamous species (*16*). Precopulatory mate choice is probably adaptive because postzygotic genetic incompatibilities between red and black birds (i.e., different genotypes) forced to breed in captivity results in high offspring mortality (*14*). In particular, throughout offspring development (i.e., from egg to sexual maturity, 160 days), genetically incompatible pairs have 40.2% greater mortality of sons and 83.8% greater mortality of daughters than broods produced from genetically compatible pairs (*14*). Given that females can assess the phenotype of males and that mixed-morph pairing results in fitness costs, we predict that females unable to pair preferentially with genetically compatible mates should differentially adjust their relative breeding investment accordingly.

We randomly paired 200 females (100 black, 100 red) to either a black or red male (of known morph genotype) in a visually isolated cage (*17*). To control for genetic versus parentally derived environmental effects (*18*), we conducted cross-fostering experiments involving permanent recip-

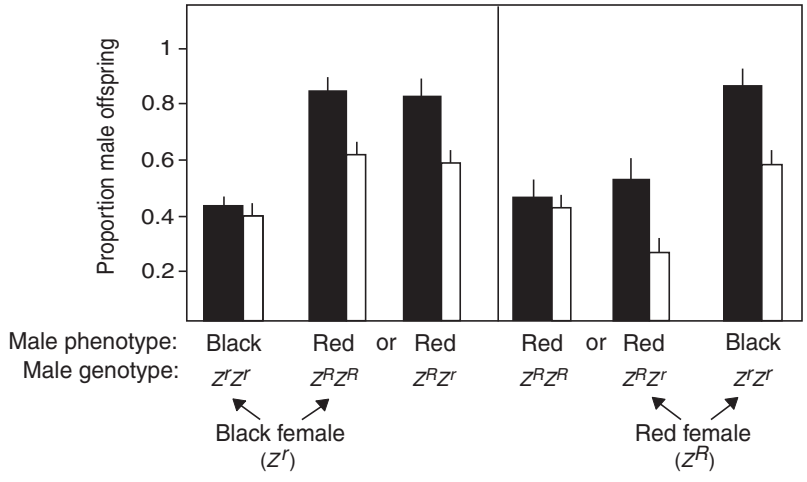

Fig. 1. Mean (±SEM) proportion of male offspring (laying to hatching) for each nest produced from within-female crosses between same (matched) and different (mixed) male morphs. Individual females given a male of a different genotype had offspring with a male-biased sex ratio (solid black bars). Even if we assume that all infertile eggs (of unknown sex) were female, a male-biased sex ratio remains (open bars). Although offspring from red females paired to heterozygous red males (i.e., genetically incompatible) suffered similar mortality rates as offspring from red-black pairings (*14*), in contrast to other incompatible mixed-morph pairs, red females in these matched pair crosses produced only a slight initial male bias (56%); if we assumed large differential female mortality in infertile eggs, these females would be predicted to produce very few male offspring.

Department of Brain, Behaviour, and Evolution, Macquarie University, Sydney, NSW 2109, Australia.

*To whom correspondence should be addressed. E-mail: sarah.pryke@mq.edu.au

rocal translocation of whole broods (hatching day 1 to 2) within and between the different treatments. Once offspring reached independence (60 days), the male and offspring were removed, and 18 days later [to discount the possibility of stored sperm (*19*)] the female was paired with a random male of the alternate morph. Each female thus bred twice, once with a male of her own morph (matched pair) and once with a different morph (mixed pair); all reported results reflect this within-female breeding design.

Because daughters are particularly susceptible to genetic viability effects from an incompatible partner genome (*14*), as expected (*20*, *21*), females in mixed pairs produced broods with male-biased primary sex ratios [82.1% males; generalized linear mixed model (GLMM), $\chi_1^2 = 14.26$, $P < 0.001$; $N = 324$ families, 1473 nestlings, and 27 dead embryos], whereas females in matched pairs produced an unbiased sex ratio (45.9% males; GLMM, $\chi_1^2 = 1.64$, $P = 0.21$; $N = 324$ families, 1473 nestlings, and 27 dead embryos) (Fig. 1). In 369 eggs (20% of all eggs produced), there were no visible signs of embryonic development (despite normal incubation), and we were unable to sex these eggs. However, even if we assume that all infertile eggs were female, we would still have observed a male-biased sex ratio in mixed-morph pairs (60.3% males; GLMM, $\chi_1^2 = 3.87$, $P = 0.04$; $N = 324$ families, 1473 nestlings, and 369 infertile eggs) (Fig. 1).

To determine whether females in mixed-morph pairs overproduce sons, independent of any intrinsic mortality effects resulting from genetically incompatible mates, we next experimentally blackened the head colors of red males before pairing them to red and black females and allowing them to breed (*17*). We found that black females paired to red males who were experimentally blackened (i.e., to resemble black males) produced a sex ratio that did not differ significantly from equality (55% males; GLMM, $\chi_1^2 = 1.06$, $P = 0.30$; $N = 18$ families, 94 chicks) despite the incompatible (red) genotype. Interestingly, this brood sex ratio was similar to the ratio of male offspring produced (56%) when red females were mated to heterozygous (genetically incompatible) red males (Fig. 1). Red females paired to experimentally blackened red males produced significantly more males (72%; GLMM, $\chi_1^2 = 13.54$, $P < 0.001$; $N = 22$ broods, 71 chicks), despite having fully compatible genotypes. These results indicate that maternal effects are most likely driven by female allocation rather than by interactions between incompatible genomes or through male coercion (*22*). These results also contrast with the prediction that females should overproduce sons when paired with attractive partners (*3*, *4*, *13*, *20*). Instead, females gain greater fitness benefits from overproducing sons when paired with a nonpreferred male morph because of the severe mortality effects on daughters in mixed-morph pairs.

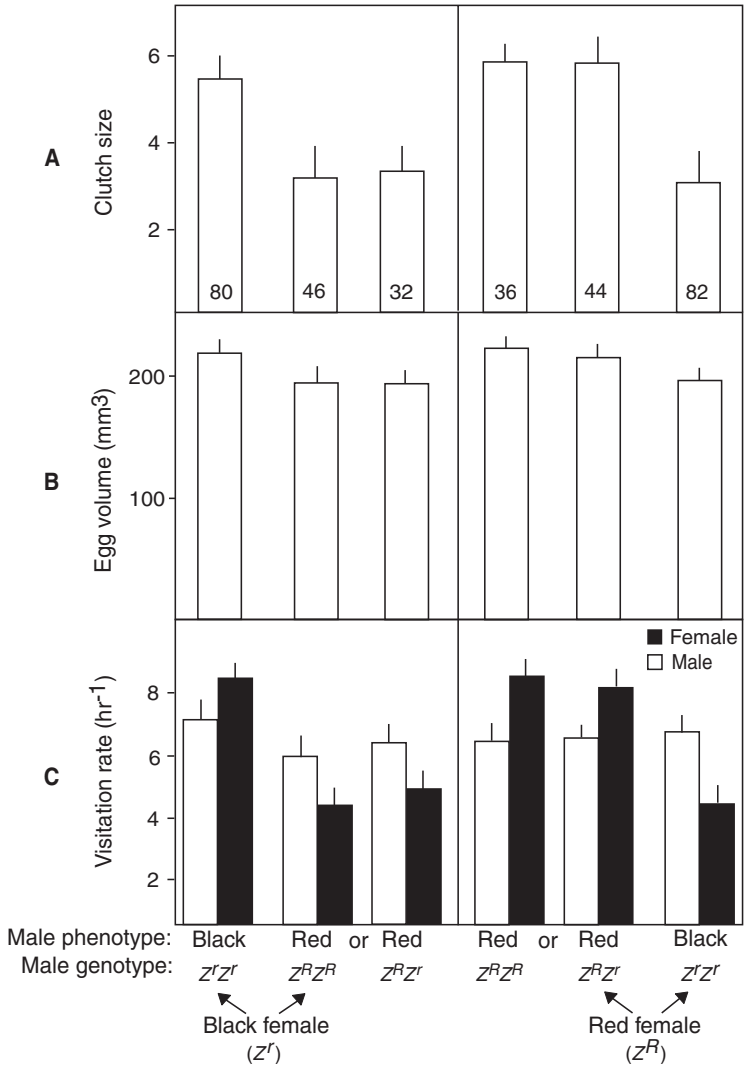

Fig. 2. Within-female differential investment when paired with the same (matched) and different (mixed) color morph. Females paired to a male of the same phenotype produced (**A**) 40.2% larger clutches, (**B**) 12.8% larger eggs, and (**C**) increased per capita provisioning of their offspring (46.1%) compared with when they were paired with a genetically incompatible male. The means ± SEM (error bars) are shown, and brood sample sizes are provided in the bars of (A).

Because of the fitness costs of breeding in mixed-morph pairs (*14*), we also examined the relative investment by females into reproduction. We found that individual females in mixed pairs produced significantly fewer eggs (3.39 ± 1.07) than when breeding in matched pairs [5.67 ± 0.89 eggs; repeated measures analysis of variance (RM-ANOVA), $F_{1,160} = 16.26$, $P < 0.001$, $r^2 = 43.3$, $N = 324$ clutches] (Fig. 2A). Females in mixed pairs also laid significantly smaller eggs (198.23 ± 14.12 mm^3) than when breeding with the same morph type (227.04 ± 12.35 mm^3; RM-ANOVA, $F_{1,159} = 14.10$, $P < 0.001$, $r^2 = 62.8$, $N = 324$ clutches) (Fig. 2B). Egg volume was unrelated to the sex of the resulting offspring (RM-ANOVA, $F_{1,160} = 0.62$, $P = 0.80$, $r^2 = 0.18$), indicating that differential egg investment was not simply due to a differential investment into sons or daughters (*23*). Egg size influences fitness in birds (*24*); in Gouldian finches, egg size was positively correlated with chick mass (measured 2 days after hatching; Pearson's correlation, $r = 0.82$, $P < 0.001$, $N = 1473$). Furthermore, after controlling for the differences in egg and brood size between matched and mixed pairs, we found that when chicks (from both mixed and matched pairs) were fostered to nests of matched pairs they grew faster than foster chicks in mixed nests (RM-ANOVA, $F_{1,158} = 7.15$, $P = 0.007$, $r^2 = 7.82$), irrespective of their genetic origin ($F_{1,158} = 0.81$, $P = 0.34$). The difference in chick mass between nests reared by foster parents of mixed and matched pairs (9.1%) appeared to be due to a per capita increase in maternal (but not paternal) provisioning to chicks in matched pairs (RM-ANOVA, female visit rate: $F_{1,159} = 87.13$, $P < 0.001$, $r^2 = 44.8$; male visit rate: $F_{1,159} = 0.04$, $P = 0.83$, $r^2 = 6.4$, $N = 324$ broods) (Fig. 2C). These effects were also apparent when males were color-manipulated; black females paired to blackened red males (i.e., genetically incompatible) significantly increased their investment into their

brood relative to genetically incompatible mismatched (black-red) pairs (clutch: $t = 5.6$; egg size: $t = 6.8$; care: $t = 8.2$; df = 86, $P < 0.001$) and instead invested similarly to genetically compatible black pairs (clutch: $t = 1.2$; egg size: $t = 0.8$; care: $t = 0.5$; df = 94, $P > 0.15$). Similarly, red females paired to blackened red males (i.e., genetically compatible) significantly reduced their investment compared with matched red morph pairs (clutch: $t = 4.4$; egg size: $t = 5.7$; care: $t = 7.3$; df = 56, $P < 0.001$), in line with red females paired to genetically incompatible black males (clutch: $t = 0.9$; egg size: $t = 1.1$; care: $t = 0.7$; df = 102, $P > 0.18$).

By controlling for individual effects (i.e., within-female) and environmental effects (i.e., controlled cage environment), we demonstrated differences in maternal investment (offspring number, quality, and sex) in a system where the fitness benefits to females from skewed allocation are large (due to genetic incompatibility) and predictable (because head color is a reliable signal of genotype). By manipulating parameters pertinent to strategic maternal investment and by preventing active precopulatory mate choice (*16*) or the ability for females to engage in extra-pair copulations with a more compatible mate to counteract the costs of a genetically incompatible social mate (*21*), we exposed extreme postcopulatory strategies. This suggests that the extent to which females can control and manipulate important life-history components of fitness may have previously been underestimated.

References and Notes

1. R. L. Trivers, D. E. Willard, *Science* **179**, 90 (1973).
2. G. C. Williams, *Am. Nat.* **100**, 687 (1966).
3. N. Burley, *Evolution* **40**, 1191 (1986).
4. B. C. Sheldon, S. Andersson, S. C. Griffith, J. Örnborg, J. Sendecka, *Nature* **402**, 874 (1999).
5. J. G. Ewen, P. Cassey, A. P. Møller, *Proc. R. Soc. London Ser. B* **271**, 1277 (2004).
6. T. W. Fawcett, B. Kuijper, I. Pen, F. J. Weissing, *Behav. Ecol.* **18**, 71 (2007).
7. J. Komdeur, I. Pen, *Philos. Trans. R. Soc. London Ser. B* **357**, 373 (2002).
8. E. Cunningham, A. Russell, *Nature* **404**, 74 (2000).
9. F. de Lope, A. P. Møller, *Evolution* **47**, 1152 (1993).
10. D. Gil, J. Graves, N. Hazon, A. Wells, *Science* **286**, 126 (1999).
11. M. Petrie, A. Williams, *Proc. R. Soc. London Ser. B* **251**, 127 (1993).
12. B. C. Sheldon, *Trends Ecol. Evol.* **15**, 397 (2000).
13. S. A. West, B. C. Sheldon, *Science* **295**, 1685 (2002).
14. S. R. Pryke, S. C. Griffith, *Evolution* **63**, 793 (2009).
15. H. N. Southern, *J. Genet.* **47**, 51 (1945).
16. S. R. Pryke, S. C. Griffith, *J. Evol. Biol.* **20**, 1512 (2007).
17. Materials and methods are available as supporting material on *Science* Online.
18. S. C. Griffith, I. P. F. Owens, T. Burke, *Nature* **400**, 358 (1999).
19. T. R. Birkhead, A. P. Møller, *Biol. J. Linn. Soc. London* **50**, 295 (1993).
20. E. L. Charnov, *The Theory of Sex Allocation* (Princeton Univ. Press, Princeton, NJ, 1982).
21. T. Veen *et al.*, *Nature* **411**, 45 (2001).
22. W. R. Rice, *Science* **256**, 1436 (1992).
23. P. J. Cordero, S. C. Griffith, J. M. Aparicio, D. T. Parkin, *Behav. Ecol. Sociobiol.* **48**, 353 (2000).
24. T. D. Williams, *Biol. Rev. Camb. Philos. Soc.* **69**, 35 (1994).

25. We thank A. Badyaev, R. Montgomerie, T. Price, A. Russell, and B. Sinervo for comments; D. Briscoe, R. Brooks, R. Bonduriansky, T. Burke, and M. Olsson for discussion; and R. Merrill, J. Brazill-Boast, and L. A. Rollins for technical help. Funded by the Australian Research Council (grants awarded to S.R.P. and S.C.G.), a New South Global Postdoctoral Fellowship (to S.R.P.), a L'Oréal For Women in Science Fellowship (to S.R.P.), and the Save The Gouldian Fund. The Animal Care and Ethics Committee of the University of New South Wales and Macquarie University approved this research.

Supporting Online Material

www.sciencemag.org/cgi/content/full/323/5921/1605/DC1
Materials and Methods
References

24 November 2008; accepted 9 February 2009
10.1126/science.1168928

The Domestication Process and Domestication Rate in Rice: Spikelet Bases from the Lower Yangtze

Dorian Q Fuller,[1]* Ling Qin,[2] Yunfei Zheng,[3] Zhijun Zhao,[4] Xugao Chen,[3] Leo Aoi Hosoya,[5] Guo-Ping Sun[3]

The process of rice domestication occurred in the Lower Yangtze region of Zhejiang, China, between 6900 and 6600 years ago. Archaeobotanical evidence from the site of Tianluoshan shows that the proportion of nonshattering domesticated rice (*Oryza sativa*) spikelet bases increased over this period from 27% to 39%. Over the same period, rice remains increased from 8% to 24% of all plant remains, which suggests an increased consumption relative to wild gathered foods. In addition, an assemblage of annual grasses, sedges, and other herbaceous plants indicates the presence of arable weeds, typical of cultivated rice, that also increased over this period.

The domestication of staple cereal crops represents the major economic and ecological transition that human societies made during the Holocene (*1*). A key change in domestication of cereals, resulting from cultivation, was the loss of natural seed dispersal, which led to domesticated cereals with dependence on humans (*2*, *3*). Direct evidence for the evolution of this trait in wheat and barley in Southwest Asia suggests that this process was slower than earlier hypothesized (*3*–*5*). Rice has been less well documented, but archaeological finds of rice grains and phytoliths indicate that it was an early crop in the Lower and Middle Yangtze region of China (*6*, *7*).

Tianluoshan is a Neolithic site of the local Hemudu Neolithic culture in Zhejiang Province, China (Fig. 1). Tianluoshan is 2 to 3 m above present-day sea level, with a high belowground water table that has preserved water-logged botanical remains in some contexts, along with charred remains throughout the site. Excavations between 2004 and 2007 revealed preserved wooden posts, boat paddles, wooden and bone tools, characteristic pottery and ground-stone axes, and animal and fish remains, as well as well-preserved plant remains (*8*). In total, 23,615 plant remains were identified from 24 systematically sieved samples, in addition to more than 12,000 hand-picked remains. More than 50 species were identified, mainly acorns (including *Lithocarpus* and *Cyclobalanopsis* types), *Trapa* water chestnuts, foxnuts (*Euryale ferox*), and rice. Probable storage pits retained acorns (*Quercus sensu lato* and *Lithocarpus*), water chestnuts (*Trapa natans sensu lato*), foxnuts, and several other edible fruit remains and seeds. One area of excavation (K3) had preserved distinct lenses of rice husks, acorn shells, *Trapa* shells, and persimmon seeds (*Diospyros* sp.).

Large quantities of rice spikelet bases, as well as a range of small seeds of wild species that may plausibly represent the arable weeds of rice cultivation, were recovered during the systematic sorting of sediment samples. Rice increased as a percentage of the total remains from sieved samples from 8% to 18% to 24% (Fig. 2). These phases were dated by direct accelerator mass spectrometry radiocarbon dates on nuts and rice grains (fig. S1) indicating a sequence for the plant samples between ~6900 and 6600 years ago, and divided into three periods (K3 midden, layers 8 and 7, and layers 6 and 5). These data suggest that rice increased in dietary importance through time. The increase in the proportion of rice supports the hypothesis that people became increasingly reliant on rice cultivation and gradually abandoned wild resources, such as acorns and *Trapa* water chestnuts.

Distinctions between wild and domestic rice are made through observations of the spikelet bases, which show key morphological differences (*9*–*12*), although in archaeological specimens this distinction can be complicated if immature specimens were harvested. We classified spikelet bases on the basis of a comparative study of spikelet bases in 140 modern populations (*13*). In domesticated rice, panicles are nonshattering, which allows most grains on the plant to reach maturity before being

[1]Institute of Archaeology, University College London, London WC1H 0PY, UK. [2]School of Archaeology and Museology, Peking University, Beijing 100871, China. [3]Zhejiang Provincial Institute of Archaeology and Cultural Relics, Hangzhou 310014, China. [4]Institute of Archaeology, Chinese Academy of Social Sciences, Beijing 100710, China. [5]Research Institute for Humanity and Nature, Kyoto 603-8047, Japan.

*To whom correspondence should be addressed. E-mail: d.fuller@ucl.ac.uk

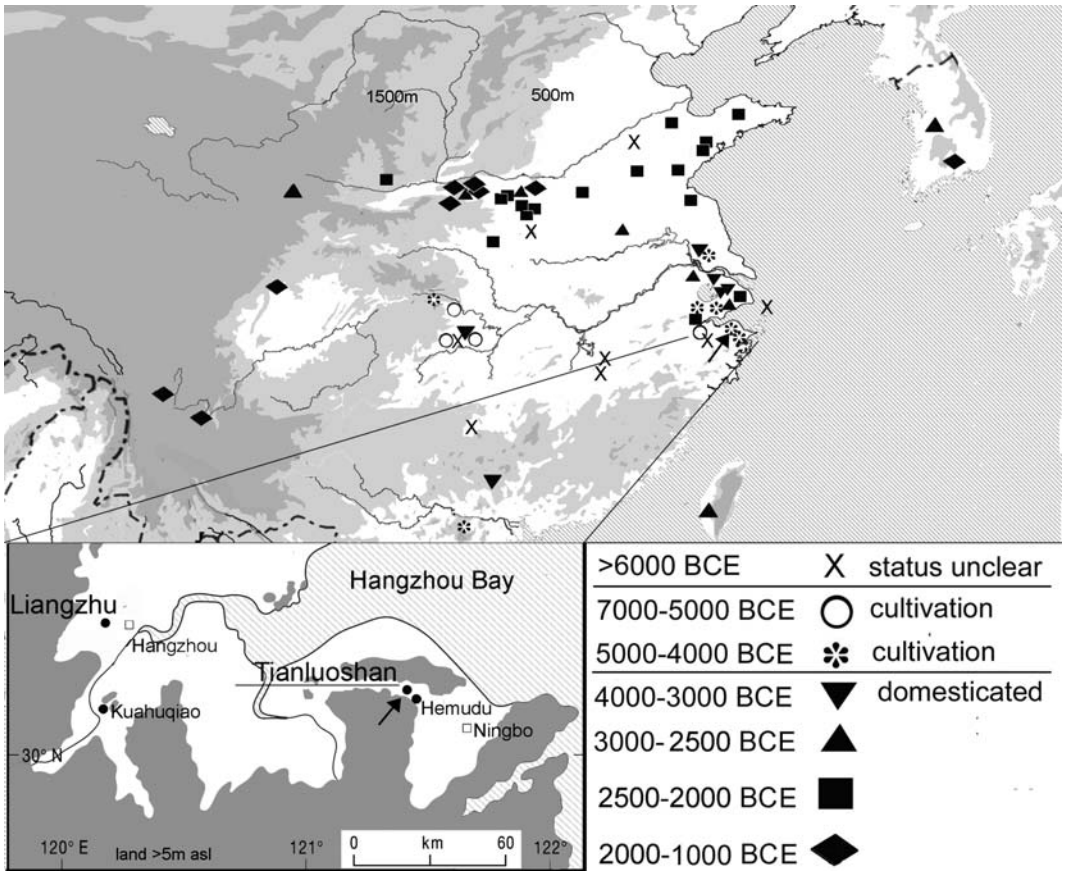

Fig. 1. Map of representative early rice finds in China, with arrow indicating Tianluoshan; the inset shows the local region of Tianluoshan and Liangzhu.

harvested. Spikelets are then separated through threshing, which causes uneven breakage at the spikelet base as well as tearing of vascular strands, resulting in a larger and more irregular pore (Fig. 3A). In addition, domesticated spikelet bases can be identified by their uneven profile, dimpled appearance, and less symmetrical scars (*10*). By contrast, wild-type rice spikelets typically have a straight profile at their bases, and shattering results in a smooth and round abscission scar and a small, distinct vascular pore (Fig. 3B). Rice harvested before maturity is expected to have protruding vascular bundles from the remnant of the attached rachilla (the fine stalk that attaches grains to the rice plant) (Fig. 3C), although this pattern is encountered in some modern domesticated varieties. To minimize the possibility of overestimating the proportion of domesticates, we classified seeds with rachilla remnants as immature.

On the basis of the above criteria, 2641 archaeological spikelet bases from Tianluoshan were divided into three categories: wild (Fig. 3, E and H), domestic (Fig. 3, D and G), and immature (Fig. 3, F and I); all three were found in all samples. When calculated by temporal period, the proportions change over time in favor of domesticated types, which increase from 27.4% to 38.8% over ~300 years, while both wild and immature types decrease (fig. S2). To test for statistical significance, we treated each sampled context with 25 or more spikelet bases as an independent sample, allowing a mean and standard deviation to be calculated for the percentages of domesticated, wild, and immature types (Fig. 4). These findings were supported by a comparison with a later domesticated population: a single sample (n = 147) available from nearby Liangzhu [~4200 years before the present (B.P.)], a quasi-urban center of a culture known for stone plough tips and sickles (*14*). Our observed domesticated types may be an underestimate, because some immature types may be domesticated (*13*). But any such underestimate is likely to be slight because wild harvests should be biased toward immature types, as inferred from grain morphometrics (*14*, *15*).

Through the three temporal phases at Tianluoshan, there is a significant increase in average proportion of domesticated types (P = 0.0048). This trend toward an increasing proportion of domesticated types through time implies that rice was under cultivation at this time and that domestication traits were under selection. However, as predicted from other lines of evidence from the region (*14*, *15*), a substantial proportion of the rice crop may have been harvested while still immature to minimize wild-type grain loss due to shattering. We also observed many small and flattened rice grains, characteristic of highly immature spikelets, present among larger, mature grain types at Tianluoshan.

Additional support for rice cultivation at Tianluoshan is provided by the accompanying species, which include many likely arable weeds. Temporal increases in domesticated rice spikelet bases were accompanied by increases in both the overall proportion of rice and these weedy taxa (Fig. 2). These include well-known wet-field rice weeds

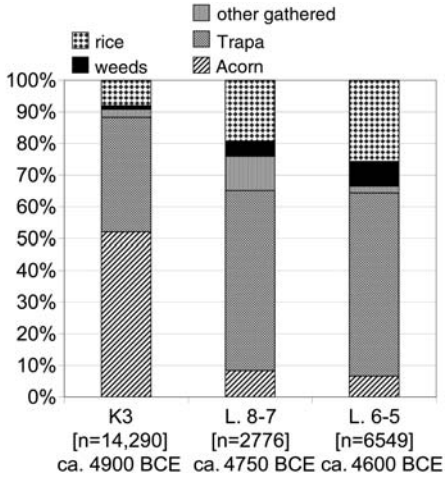

Fig. 2. Proportion of plant remains from sieved samples from the three periods, indicating percentages of rice, probable weeds of rice, acorns, *Trapa* water chestnuts, and other gathered fruits and nuts.

such as sedges (*Scirpus* spp., *Cyperus* spp., *Juncellus* spp., *Eleocharis* sp.), rushes (*Juncus* spp.), and weedy annual grasses (*Echinochloa* sp., *Eragrostis* sp., *Isachne globosa*, *Festuca* sp., *Panicum* sp., *Setaria* sp.). Several dicotyledonous weeds were also found, but with less frequency. All these species are present today as weeds in rice paddy fields (*16*–*18*).

Our data suggest that rice domestication culminated after ~6500 years B.P. This is consistent with the findings of a recent reanalysis of shifts in grain and phytolith size (*3*, *14*, *15*). The beginnings of

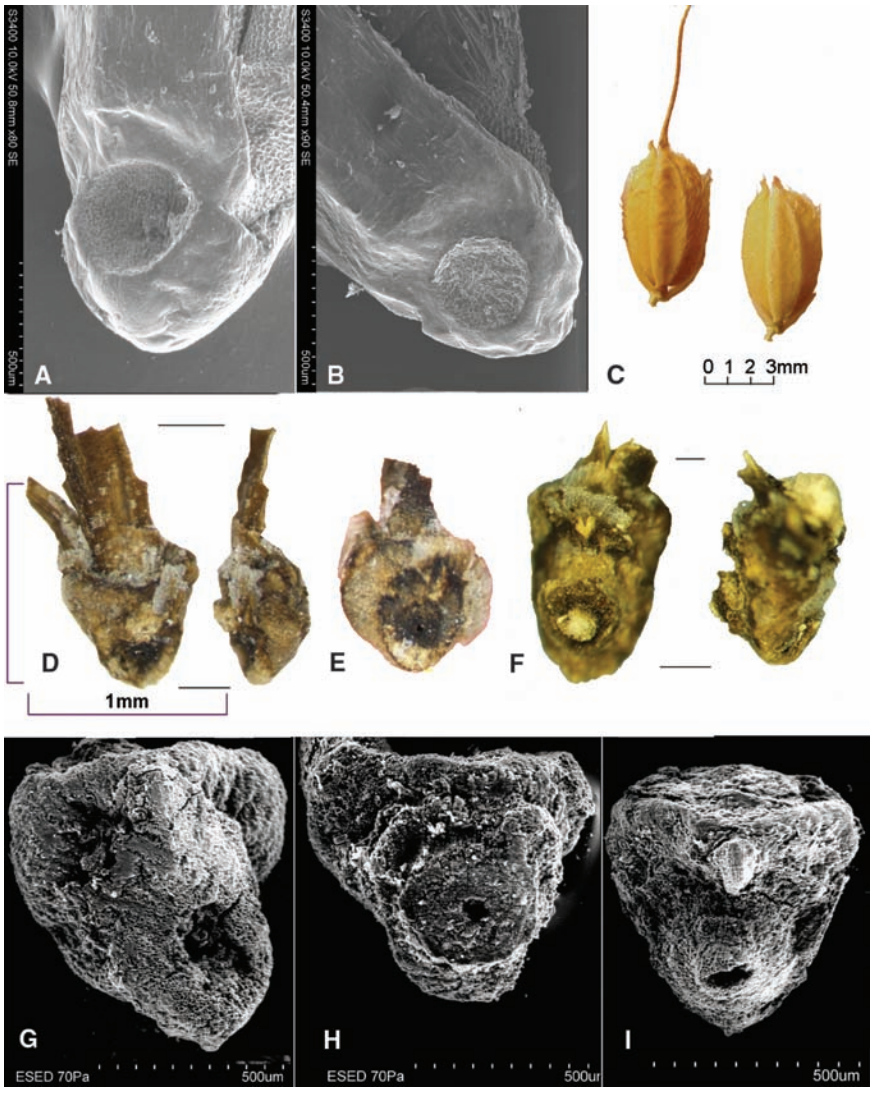

Fig. 3. Examples of modern and archaeological rice spikelet base abscission scars. (**A**) Scanning electron microscopy (SEM) image of modern *Oryza sativa* subsp. *japonica*. (**B**) SEM image of modern *Oryza rufipogon.* (**C**) Immature harvested *Oryza sativa.* (**D**) Domesticated-type spikelet base (front and profile), waterlogged, from Tianluoshan K3. (**E**) Wild type, waterlogged, from Tianluoshan K3. (**F**) Immature type (front and profile) from Tianluoshan K3. (**G**) SEM image of domesticated type, charred, from Tianluoshan H28. (**H**) SEM image of wild type, charred, from Tianluoshan H28. (**I**) SEM image of immature type, charred, from Tianluoshan H28.

Fig. 4. Proportions of wild, immature, and domesticated rice spikelet bases from three sequential periods at Tianluoshan, with later Liangzhu for comparison. Means and standard deviations are shown for the Tianluoshan periods, on the basis of all samples of 25 or more spikelet bases.

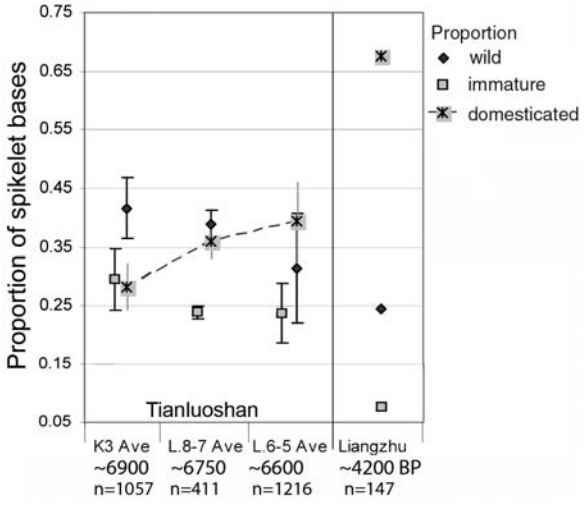

the domestication process, however, remain unclear. Early rice cultivation in China was initially a supplementary resource alongside wild nuts (*15*). Cultivation had certainly begun by 8000 to 7700 years B.P., as indicated by archaeobotanical evidence including domesticated-type spikelet bases found at Kuahuqiao (*12*). Pollen and microcharcoal data suggest that cultivation at Kuahuqiao involved water management and clearance through burning (*19*).

This evidence suggests that rice domestication was comparable in process to that of wheat and barley, in that the nonshattering phenotypes gradually became fixed in cultivated populations over at least two or three millennia (*3*, *4*). Despite higher cross-pollination rates in wild rice (*20*) relative to self-pollinating wheat and barley (*21*), pollination systems may not have had an appreciable impact on the rate of domestication. Instead, the presence of sympatric populations of both wild and domesticated cereals may have dampened selection for domestication (*22*).

Genetic studies show a deep divergence between *indica* and *japonica* rice (*23*, *24*), and it is possible that India paralleled the Chinese domestication (*25*). However, shared alleles (*26*–*28*) suggest that the domesticated Indian forms resulted from hybridization as domestic rice dispersed from China into South Asia. Additionally, the spread of rice to Southeast Asia derived from rice domesticated in the Yangtze (*1*). These new data from Tianluoshan would therefore restrict the time frame for dispersal until some centuries after ~6600 years B.P.

References and Notes

1. P. Bellwood, *First Farmers* (Blackwell, Oxford, 2005).
2. J. Harlan, J. De Wet, E. Price, *Evolution* **27**, 311 (1973).
3. D. Q. Fuller, *Ann. Bot.* **100**, 903 (2007).
4. K.-I. Tanno, G. Willcox, *Science* **311**, 1886 (2006).
5. E. Weiss, M. E. Kislev, A. Hartmann, *Science* **312**, 1608 (2006).
6. G. Crawford, in *Archaeology of Asia*, S. Stark, Ed. (Blackwell, Oxford, 2005), pp. 77–95.
7. T. L.-D. Lu, *Asian Perspect.* **45**, 129 (2006).
8. Zhejiang Provincial Institute of Archaeology *et al.*, *Wen Wu* **2007–11**, 4 (2007) (in Chinese).
9. G. B. Thompson, in *South-East Asian Archaeology 1992*, R. Ciarla, F. Rispoli, Eds. (Instituto Italiano per L'Africa e L'Orient, Rome, 1997), pp. 159–174.
10. C. Li, A. Zhou, T. Sang, *Science* **311**, 1936 (2006); published online 8 March 2006 (10.1126/science.1123604).
11. K. Onishi, K. Takagi, M. Kontani, T. Tanaka, Y. Sano, *Genome* **50**, 757 (2007).
12. Y. Zheng, G. Sun, X. Chen, *Chin. Sci. Bull.* **52**, 1654 (2007).
13. See supporting material on *Science* Online.
14. D. Q. Fuller, L. Qin, E. L. Harvey, in *Past Human Migrations in East Asia*, A. Sanchez-Mazas, R. Blench, M. D. Ross, I. Peiros, M. Lin, Eds. (Routledge, London, 2008), pp. 40–83.
15. D. Q. Fuller, E. L. Harvey, L. Qin, *Antiquity* **81**, 316 (2007).
16. Y.-H. Li, *Zhongguo Zacao Zhi* (Chinese Weed Flora) (Chinese Agriculture Press, Beijing, 1998) (in Chinese).
17. K. Moody, *Weeds Reported in Rice in South and Southeast Asia* (IRRI, Manila, 1991).
18. M. Galinato, K. Moody, C. Piggin, *Upland Rice Weeds of South and Southeast Asia* (IRRI, Manila, 1999).
19. Y. Zong *et al.*, *Nature* **449**, 459 (2007).
20. H.-I. Oka, H. Morishima, *Evolution* **21**, 249 (1967).
21. G. C. Hillman, S. Davies, *Biol. J. Linn. Soc.* **39**, 39 (1990).

22. R. G. Allaby, D. Q. Fuller, T. A. Brown, *Proc. Natl. Acad. Sci. U.S.A.* **105**, 13982 (2008).
23. A. J. Garris, T. Tai, J. Coburn, S. Kresovich, S. McCouch, *Genetics* **169**, 1631 (2005).
24. J. P. Londo, Y.-C. Chiang, K.-H. Hung, T.-Y. Chiang, B. Schaal, *Proc. Natl. Acad. Sci. U.S.A.* **103**, 9578 (2006).
25. D. Q. Fuller, *J. World Prehist.* **20**, 1 (2006).
26. T. Sang, S. Ge, *J. Integr. Plant Biol.* **49**, 760 (2007).
27. M. Sweeney, S. McCouch, *Ann. Bot.* **100**, 951 (2007).
28. D. A. Vaughan, B.-R. Lu, N. Tomooka, *Plant Sci.* **174**, 394 (2008).
29. Supported by grants from the British Academy, the Chinese Education Ministry, and the Zhejiang Provincial Institute of Archaeology and Cultural Relics. We thank S. Colledge, M. Wollstonecroft, and anonymous reviewers for helping to improve this text.

Supporting Online Material
www.sciencemag.org/cgi/content/full/323/5921/1607/DC1
Materials and Methods
Figs. S1 and S2
References

30 September 2008; accepted 4 February 2009
10.1126/science.1166605

Variants of the Antibody Herceptin That Interact with HER2 and VEGF at the Antigen Binding Site

Jenny Bostrom,[1,2] Shang-Fan Yu,[3] David Kan,[3] Brent A. Appleton,[1] Chingwei V. Lee,[1,2] Karen Billeci,[4] Wenyan Man,[1] Franklin Peale,[5] Sarajane Ross,[3] Christian Wiesmann,[1] Germaine Fuh[1,2]*

The interface between antibody and antigen is often depicted as a lock and key, suggesting that an antibody surface can accommodate only one antigen. Here, we describe an antibody with an antigen binding site that binds two distinct proteins with high affinity. We isolated a variant of Herceptin, a therapeutic monoclonal antibody that binds the human epidermal growth factor receptor 2 (HER2), on the basis of its ability to simultaneously interact with vascular endothelial growth factor (VEGF). Crystallographic and mutagenesis studies revealed that distinct amino acids of this antibody, called bH1, engage HER2 and VEGF energetically, but there is extensive overlap between the antibody surface areas contacting the two antigens. An affinity-improved version of bH1 inhibits both HER2- and VEGF-mediated cell proliferation in vitro and tumor progression in mouse models. Such "two-in-one" antibodies challenge the monoclonal antibody paradigm of one binding site, one antigen. They could also provide new opportunities for antibody-based therapy.

The binding of antibodies to specific single antigens has prompted their use for numerous targeted therapies (*1*). However, the notion of an antibody that recognizes more than one antigen is intriguing. It has been suggested that multi-specificity may evolve and play a role in the highly efficient antibody repertoire for immune protection with one antibody performing more than one task (*2*, *3*). However, the few examples of such multi-specificity are limited to antibodies that bind small haptens (*4*), and a strategy to generate a single antigen binding fragment (Fab) capable of recognizing two unrelated proteins has not yet been reported.

We set out to explore whether dual specific antibodies can be derived from a monospecific antibody with the following approach: A repertoire of Herceptin (Genentech, South San Francisco, CA) antibody variants with mutations in the light chain (LC) complementarity determining regions (CDRs) were generated, and Fabs that can bind a new protein antigen while maintaining human epidermal growth factor receptor 2 (HER2) binding were identified. The approach is based on the understanding that modifications of the LC sequence can modulate the binding specificity of antibodies (*5*, *6*). In addition, many antibodies, with Herceptin as a prime example (*7*, *8*), bind the antigens by using mainly the heavy chain (HC) CDRs, suggesting that mutations in the LC CDRs might allow preservation of the original antigen binding specificity.

The framework regions of Herceptin variable domains (V_H and V_L, the variable domain of HC and LC, respectively) belong to subtypes that are prevalent in the human antibody repertoire (V_H3, $V_L$kappa1). Thus, mutations within the antigen binding site of Herceptin that confer a second specificity may indicate a potential for a dual specific antibody to evolve from the natural repertoire. As Herceptin is a validated therapeutic for breast cancers that overexpress HER2 (*9*), recruitment of a second binding specificity to Herceptin may add to it a distinct pharmacological activity.

[1]Department of Protein Engineering, Genentech, 1 DNA Way, South San Francisco, CA 94080, USA. [2]Department of Antibody Engineering, Genentech, 1 DNA Way, South San Francisco, CA 94080, USA. [3]Department of Translational Oncology, Genentech, 1 DNA Way, South San Francisco, CA 94080, USA. [4]Department of Assay and Automation Technology, Genentech, 1 DNA Way, South San Francisco, CA 94080, USA. [5]Department of Pathology, Genentech, 1 DNA Way, South San Francisco, CA 94080, USA.

*To whom correspondence should be addressed. E-mail: gml@gene.com

Table 1. The representative antibodies from the LC library of Herceptin. Mutations from Herceptin are shown in italics. Dashes indicate positions where no residue is present. Antigen binding affinity (K_d) was determined by surface plasmon resonance using Fab. NB indicates that no binding is detected. Single-letter abbreviations for the amino acid residues are as follows: A, Ala; C, Cys; D, Asp; E, Glu; F, Phe; G, Gly; H, His; I, Ile; K, Lys; L, Leu; M, Met; N, Asn; P, Pro; Q, Gln; R, Arg; S, Ser; T, Thr; V, Val; W, Trp; and Y, Tyr.

	CDR-L1										CDR-L2				CDR-L3						Specificity		Affinity (nM)	
	28	29	30	30a	30b	30c	30d	31	32	33	50	51	52	53	91	92	93	93a	93b	94	Antigen1	Antigen2	K_d 1	K_d 2
Herceptin	D	V	N	–	–	–	–	T	A	V	S	A	S	F	H	Y	T	–	–	T	HER2	NB	0.1	NB
3-1	*N*	V	*W*	–	–	–	–	*D*	*W*	V	*P*	A	S	*S*	*G*	*W*	*Y*	*I*	–	*A*	VEGF	NB	15	NB
bH1	D	*I*	*P*	*R*	*S*	*I*	*S*	*G*	*Y*	V	*W*	*G*	S	*Y*	H	Y	T	–	–	T	HER2	VEGF	26	300
bH3	D	*I*	*G*	*L*	–	–	–	*G*	*S*	V	*W*	A	S	*Y*	H	Y	T	–	–	T	HER2	VEGF	8	19,000
bH4	D	*I*	*R*	*S*	–	–	–	*G*	*S*	V	*W*	*G*	S	*Y*	H	Y	T	–	–	T	HER2	VEGF	11	3,500
4-1	D	*I*	*W*	*N*	*R*	–	–	*R*	*A*	*L*	*E*	*G*	S	*S*	*G*	*G*	*S*	*Y*	*S*	*S*	DR5	NB	120*	NB
4-5	*N*	V	*G*	–	–	–	–	*R*	*P*	V	*G*	*G*	S	*S*	*Y*	*G*	*S*	*F*	*G*	*T*	DR5	NB	150*	NB
bD1	*N*	V	*S*	–	–	–	–	*K*	*H*	V	*W*	*G*	S	*Y*	*S*	Y	*S*	–	–	*G*	HER2	DR5	200*	14,000*
bD2	*N*	*I*	*R*	*N*	*G*	–	–	*G*	*G*	*L*	S	A	S	F	H	Y	T	–	–	T	HER2	DR5	100*	67,000*

*IgG was used to determine the K_d.

We constructed the repertoire of Herceptin LC variants by randomizing a subset of solvent exposed LC CDR positions to mimic the natural diversity in amino acid composition and length (tables S1 and S2) (*10*). Selection of the Herceptin variant library against vascular endothelial growth factor (VEGF), death receptor 5 (DR5), and the complement binding fragment of immunoglobulin G (IgG) (Fc) generated over one hundred specific clones containing 3 to 17 amino acid substitutions and/or insertions compared with Herceptin (tables S3 and S4). Some of the clones lost binding affinity for HER2 and switched binding entirely to the new antigen, whereas others maintained the ability to bind HER2 and thus were dual specific.

Representative VEGF and DR5-binding clones were expressed as Fab and IgG proteins to assess their specificity and affinity (Table 1 and fig. S1). VEGF and DR5 are therapeutic targets of known structure. Equilibrium binding affinities (K_d) of the LC library-derived monospecific antibodies ranged from 15 to 150 nM (Table 1). The dual specific antibodies bound the new antigens (i.e., VEGF or DR5) with high nanomolar to micromolar affinity while preserving HER2 binding in the low nanomolar affinity range. The antibody bH1 exhibited the highest dual affinity for the two completely different protein antigens VEGF (K_d = 300 nM) and HER2 (K_d = 26 nM).

To understand the molecular basis of the dual specificity, we determined the crystal struc-

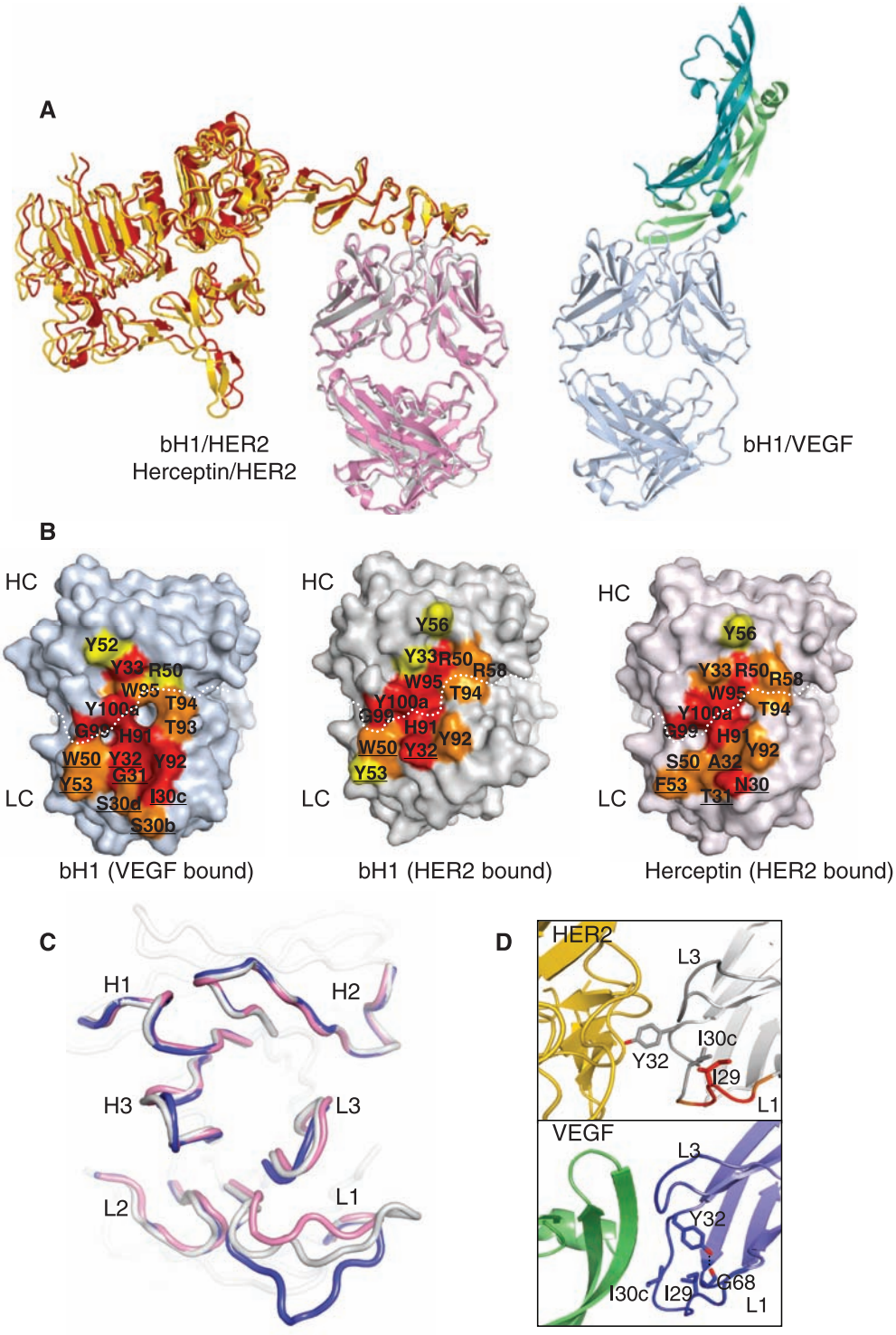

Fig. 1. The crystal structures of bH1 Fab bound to HER2 or VEGF. (**A**) The bH1 Fab (gray)/HER2 (gold) superimposed on to the Herceptin (pink)/HER2 (red) complex (left), and bH1 Fab (light blue)/VEGF (green, teal) complex (right). (**B**) Fab surface residues are colored according to the extent buried in the complex (red, >75%; orange, >50 to 75%; yellow, >25 to 50%). The underlined amino acids differ between bH1 and Herceptin. The white dotted line separates the LC and HC. (**C**) Superposition of the CDR loops of VEGF and HER2-bound bH1 (blue, gray) and HER2-bound Herceptin (pink) in the same orientation as in (B). (**D**) CDR-L1 regions of the two bH1 complexes shown in the same orientation. The residues with temperature factors higher than average are shown in red and orange. VEGF would clash with Tyr32 of bH1 in its HER2-bound conformation.

tures of the bH1 Fab bound to the extracellular domain of HER2 (residues 1 to 624) and to the VEGF receptor-binding domain (residue 8 to 109) at 2.9 and 2.6 Å resolution, respectively (Fig. 1A and table S5). The structure of the bH1/HER2 binding domains (bH1 Fv and domain IV of HER2) superimposes onto the Herceptin/HER2 complex with a root mean square deviation of 0.8 Å, showing that the Herceptin binding epitope on HER2 is retained (Fig. 1A) (*7*). The HER2 binding sites on bH1 and Herceptin differ only in the CDR-L1 and -L2 regions where the bH1 sequence differs from Herceptin (Fig. 1B).

In the structure of the bH1/VEGF complex, the Fab recognizes an epitope that overlaps with the binding sites of the VEGF receptors and other VEGF binding antibodies (*11*–*13*). Consistent with this observation, bH1 blocks the interaction between VEGF and its receptors (fig. S2).

Comparison of the bH1/VEGF and the bH1/HER2 complexes shows an extensive overlap of the VEGF and HER2 binding sites on bH1 (Fig. 1B and table S6); 11 out of the 13 bH1 residues that are in close contact with HER2 also make contact with VEGF. In the HER2 complex, the LC and HC CDRs contribute approximately equal antigen contact area (53% and 47%, respectively), whereas in the VEGF complex, the LC CDRs constitute nearly 70% of the buried surface (fig. S3).

With the exception of CDR-L1, the CDR conformations of the bH1 Fab bound to VEGF are markedly similar to those observed in bH1 or Herceptin bound to HER2 (Fig. 1C). The capability of CDR-L1 to rearrange appears to be necessary for the dual specificity of bH1 (Fig. 1D). In the HER2 complex, CDR-L1 is minimally involved in antigen interaction, and part of the loop appears to be flexible, as evidenced by poorly defined electron density (Fig. 1D). In contrast, in the VEGF complex, this loop is well structured and forms extensive contacts with VEGF. Similar conformational flexibility of CDR-L1 has been reported to play a role in antigen recognition of natural antibodies (*14*, *15*).

Next, we performed shotgun scanning mutagenesis studies to assess the energetic contributions of individual CDR residues to VEGF and HER2 binding (S11 and S12 in the supporting online material) (*10*). We determined the change in free energy ($\Delta\Delta G$) as a result of mutation to alanine (alanine scan) or a homologous residue (homolog scan) (table S7), revealing the CDR residues that make up the functional paratopes of the Fab in the two complexes (Fig. 2A).

In contrast to the extensive overlap between buried surfaces in the interfaces of bH1 bound to either VEGF or HER2, the two functional paratopes show only limited overlap (Fig. 2B and fig. S4). Energetically, the VEGF binding interaction is mediated primarily by the LC CDRs, whereas HER2 binding is dominated by HC CDRs. Compared to Herceptin, bH1 maintains the same core hotspot residues for HER2 binding (Arg50, Trp95, and Tyr100a of HC) (fig. S4).

The structural and functional studies show that the interactions between bH1 and the two entirely unrelated large proteins are distinct (Fig. 2 and fig. S5) and are characterized by conformational adaptation of the antigen binding site (table S8) and differential engagement of V_L and V_H (Fig. 2). The molecular versatility observed in the dual specific bH1 is reminiscent of other antibodies binding multiple small haptens or peptides (*4*, *16*) or of an antibody binding its

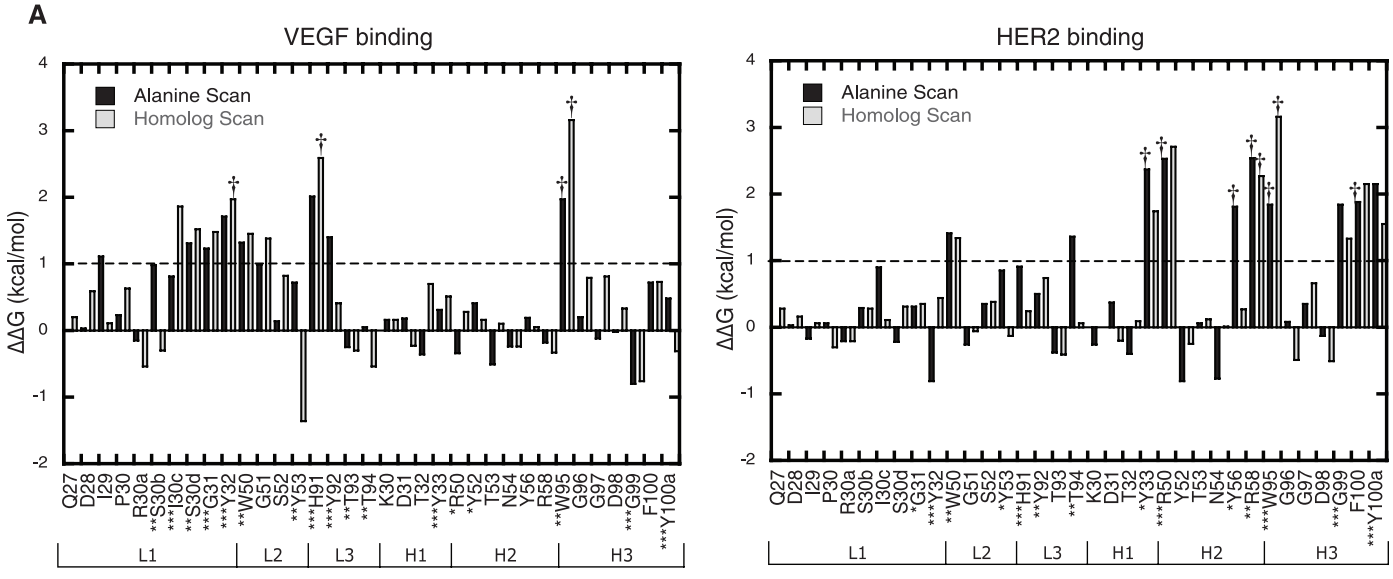

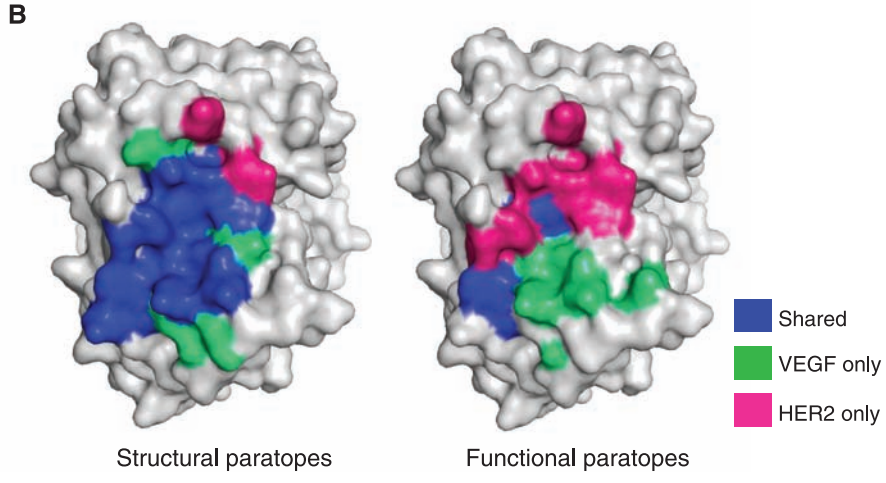

Fig. 2. The distinct interactions of bH1 with HER2 and VEGF. (**A**) The $\Delta\Delta G$ values (*y* axis, kilocalories per mole) of each mutation to alanine (black) or a homologous amino acid (white) for VEGF or HER2 binding based on shotgun scanning mutagenesis (*10*). The extent of the bH1 residues buried upon VEGF or HER2 complex formation is indicated (single asterisk, >25 to 50% buried; double asterisk, >50 to 75%; triple asterisk, >75%). The dagger symbol represents a lower limit (table S7). (**B**) The residues that make structural contacts (>25% buried) or energetic interaction ($\Delta\Delta G$ > 10% total binding energy) with HER2 (pink), VEGF (green), or both (shared, blue) are mapped on the surface of HER2-bound bH1.

cognate antigen and an anti-idiotype antibody (*17*, *18*). Further, the differential engagement of residues within a common binding site also echoes the plasticity observed in other protein-protein interactions, such as the recognition of distinct antigens (major histocompatability complex–bound peptides) by T cell receptors (*19*) or growth factor binding to different receptors (*20*).

We further examined whether the dual binding specificity can translate into dual activity in vivo. To facilitate the investigation of the in vivo activity of bH1, we generated versions of bH1 with high affinity and specificity for HER2 and VEGF (figs. S1, S2, S6, S7, and S8 and table S9). bH1, the affinity-improved bH1-81 (K_d = 58/6 nM VEGF/HER2), and bH1-44 (K_d = 3/0.2nM VEGF/HER2) inhibit VEGF-induced proliferation of human umbilical vein endothelial cells (HUVECs) and the growth of the HER2 overexpressing breast cancer cell line, BT474 (Fig. 3A). The potencies of the bH1 variants correlate with their relative affinities. The bH1-44 variant inhibits the growth of HUVEC and BT474 cells with potencies similar to bevacizumab or Herceptin, respectively.

To examine the two unique activities of bH1-44 in vivo, we studied mouse xenograft tumor models known to be responsive to treatment by anti-VEGF antibodies (Colo205, a human colorectal cancer cell line) or Herceptin (BT474M1, human breast cancer cell line). We compared the bH1-44 treated groups with those treated with anti-VEGF (B20-4.1) (*21*), Herceptin, or the combination (Herceptin + anti-VEGF) (table S10) (*10*). The results of the Colo205 model demonstrate that the VEGF binding component of bH1-44 is inhibiting tumor growth ($P < 0.0001$, $n = 10$ mice, compared with the control IgG treated group), as Herceptin alone has no effect ($P = 0.12$, $n = 10$). The BT474M1 model indicates that the HER2 binding component of bH1-44 is active ($P < 0.0001$, $n = 7$), because the effect observed with the anti-VEGF control antibody is not significant ($P = 0.6$, $n = 7$) (Fig. 3B).

Hence, bH1-44 appears to have the pharmacological activity of a VEGF blocking antibody and a Herceptin-like antibody, although we do not yet know whether bH1-44 is as effective as Herceptin or anti-VEGF administered separately or in combination. Whether there is a therapeutic benefit to co-targeting the tumor cell proliferation mediated by HER2 and tumor angiogenesis mediated by VEGF is a question currently being evaluated in clinical trials combining Herceptin and bevacizumab in breast cancer patients (*22*–*24*). If the drug combination is found to be beneficial, then dual specific antibodies like bH1-44 may merit further exploration as potential therapeutics.

Various bi-targeting antibody formats that assemble two distinct antibody fragments into one

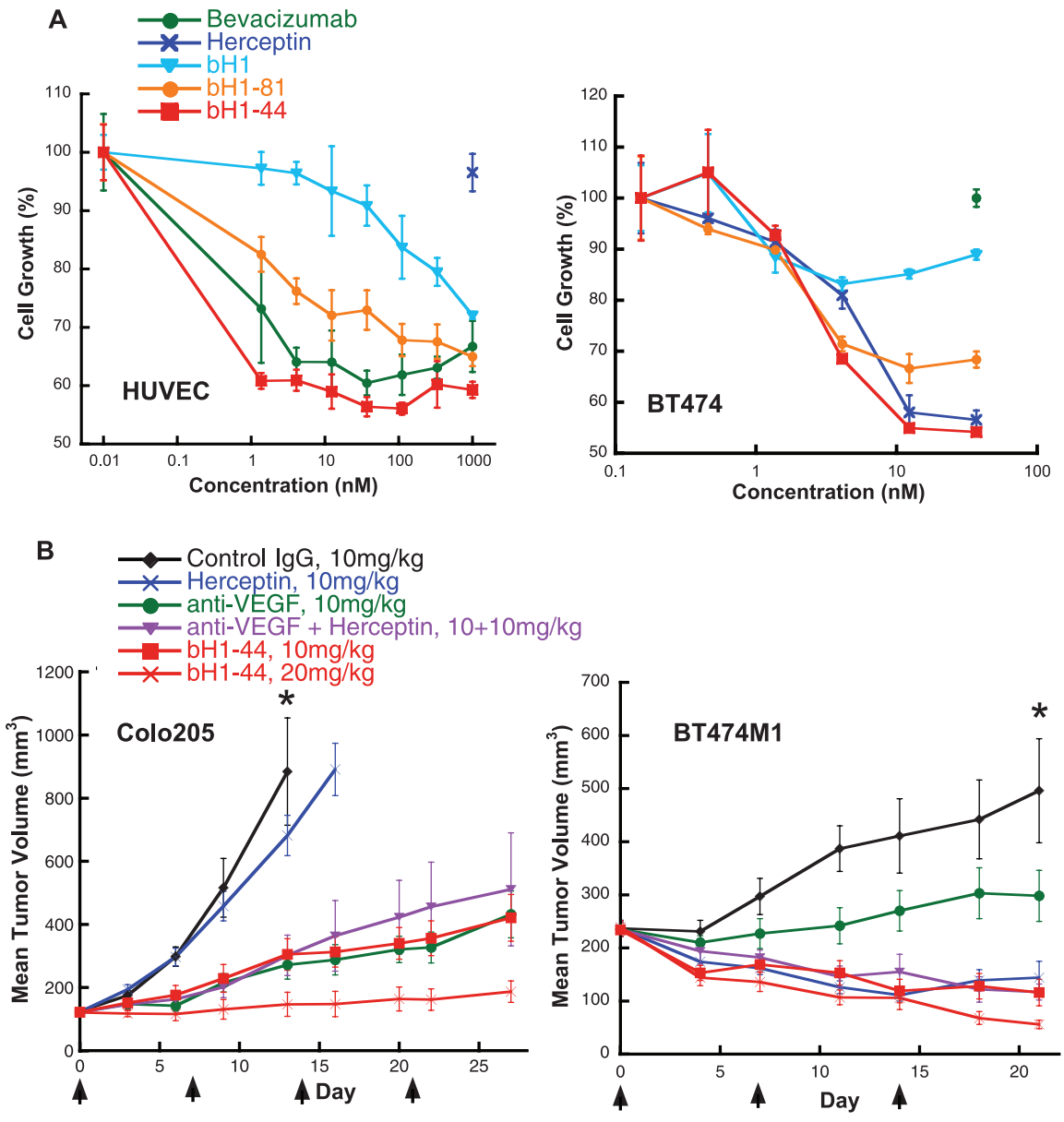

Fig. 3. Inhibition of VEGF and HER2 function in vitro and in vivo. (**A**) bH1 and the affinity improved variants bH1-81 and bH1-44 as IgGs inhibit VEGF-stimulated proliferation of HUVECs and human breast cancer cell BT474 in a dose-dependent manner. Herceptin and bevacizumab (anti-VEGF) were used as controls. Error bars represent the average deviation of triplicates ($n = 3$). (**B**) Tumor growth inhibitions of bH1-44 in Colo205 and BT474M1 xenografts in immunocompromised mice. The graph shows tumor volume as a function of time. The arrows indicate the time points for antibody (human IgG) administration. Error bars indicate SEM (*10*). An asterisk indicates the time at which the effects on tumor growth inhibition were compared. For the statistical analysis, we used one-way analysis and Student's *t* tests. For BT474M1, 5 out of the 8 mice (5/8) dosed with bH1-44 at 10 mg/kg had partial responses (PR, 50 to 99% regression from initial volume), similar to Herceptin (PR = 6/8) or the anti-VEGF/Herceptin combination (PR = 5/8). Anti-VEGF treatment alone did not yield any partial response in this model.

molecule have previously been described (*25*, *26*). In contrast to these bispecific formats, the dual specific "two-in-one" antibody we describe has the molecular structure of a regular IgG (or Fab). It has all the favorable attributes of an IgG for therapeutic development, such as predictable pharmacokinetic properties, well established manufacturing protocols, choice of Fc-mediated effector functions, and bi- or mono-valencies (*25*).

In summary, we have demonstrated that an antigen binding site is capable of interacting with two unrelated protein antigens with high affinity. The dual specific antibodies reported here are derived from a monospecific antibody through mutations in the periphery of the antigen binding site in the LC CDRs. This strategy is a general one and can be applied to create dual specific antibodies against two distinct antigens. The mutational analysis of bH1 and bH1-44 (Fig. 2 and fig. S8) suggested that the dual specificity could be switched to monospecific binding to either antigen (*10*). Indeed, bH1-44 lost binding to VEGF but retained HER2 binding when mutating two LC residues. Similarly, two alanine mutations in the HC drastically reduced the affinity for HER2 while preserving tight binding for VEGF (fig. S9). This finding highlights how a limited number of mutations in the antigen binding site can alter specificity or add a distinct specificity. During development of the natural antibody repertoire, the antigen binding sites often undergo diversification by exchanging the V_L that pairs with a V_H (*6*). Somatic mutations also occur frequently, in particular among the residues in the periphery of the antigen binding site (*27*–*30*). Our studies reveal a mechanism by which one antibody can diverge into many antibodies with distinct specificity profiles. This mechanism may contribute to the large capacity of the natural antibody repertoire for diverse antigen recognition.

References and Notes

1. J. M. Reichert, C. J. Rosensweig, L. B. Faden, M. C. Dewitz, *Nat. Biotechnol.* **23**, 1073 (2005).
2. L. Pauling, *J. Am. Chem. Soc.* **62**, 2643 (1940).
3. J. Foote, *Science* **299**, 1327 (2003).
4. L. C. James, P. Roversi, D. S. Tawfik, *Science* **299**, 1362 (2003).
5. B. M. Senn *et al.*, *Eur. J. Immunol.* **33**, 950 (2003).
6. D. Nemazee, *Nat. Rev. Immunol.* **6**, 728 (2006).
7. H. S. Cho *et al.*, *Nature* **421**, 756 (2003).
8. R. F. Kelley, M. P. O'Connell, *Biochemistry* **32**, 6828 (1993).
9. J. Baselga, L. Norton, J. Albanell, Y. M. Kim, J. Mendelsohn, *Cancer Res.* **58**, 2825 (1998).
10. Materials and methods are available as supporting material on *Science* Online.
11. C. Wiesmann *et al.*, *Cell* **91**, 695 (1997).
12. Y. A. Muller *et al.*, *Proc. Natl. Acad. Sci. U.S.A.* **94**, 7192 (1997).
13. G. Fuh *et al.*, *J. Biol. Chem.* **281**, 6625 (2006).
14. R. Jimenez, G. Salazar, K. K. Baldridge, F. E. Romesberg, *Proc. Natl. Acad. Sci. U.S.A.* **100**, 92 (2003).
15. S. E. Mylvaganam, Y. Paterson, E. D. Getzoff, *J. Mol. Biol.* **281**, 301 (1998).
16. D. K. Sethi, A. Agarwal, V. Manivel, K. V. Rao, D. M. Salunke, *Immunity* **24**, 429 (2006).
17. W. Dall'Acqua, E. R. Goldman, E. Eisenstein, R. A. Mariuzza, *Biochemistry* **35**, 9667 (1996).
18. B. A. Fields, F. A. Goldbaum, X. Ysern, R. J. Poljak, R. A. Mariuzza, *Nature* **374**, 739 (1995).
19. L. A. Colf *et al.*, *Cell* **129**, 135 (2007).
20. J. A. Wells *et al.*, *Recent Prog. Horm. Res.* **48**, 253 (1993).
21. W. C. Liang *et al.*, *J. Biol. Chem.* **281**, 951 (2006).
22. See identification numbers *NCT00625898*, *NCT00364611*, and *NCT00670982* on www.clinicaltrials.gov.
23. M. D. Pegram, D. M. Reese, *Semin. Oncol.* **29**, 29 (2002).
24. C. Bernard-Marty, F. Lebrun, A. Awada, M. J. Piccart, *Drugs* **66**, 1577 (2006).
25. P. J. Carter, *Nat. Rev. Immunol.* **6**, 343 (2006).
26. P. Kufer, R. Lutterbuse, P. A. Baeuerle, *Trends Biotechnol.* **22**, 238 (2004).
27. M. S. Neuberger, *Immunol. Cell Biol.* **86**, 124 (2008).
28. M. S. Neuberger, C. Milstein, *Curr. Opin. Immunol.* **7**, 248 (1995).
29. L. A. Clark, S. Ganesan, S. Papp, H. W. van Vlijmen, *J. Immunol.* **177**, 333 (2006).
30. I. M. Tomlinson *et al.*, *J. Mol. Biol.* **256**, 813 (1996).

31. We thank the Protein Engineering structure group, L. Haber, and D. McMahon for technical consultation and C. Eigenbrot for helpful advice. We also thank members of the DNA synthesis, DNA sequencing, in vivo cell culture, and protein chemistry groups at Genentech. We are grateful for the support of R. Neutze and Chalmers University of Technology, Sweden. The Advanced Light Source is supported by the Director, Office of Science, Office of Basic Energy Sciences, of the U.S. Department of Energy under contract no. DE-AC02-05CH11231. The atomic coordinates of the bH1/HER2 and bH1/VEGF were deposited in the Protein Data Bank with accession numbers 3BDY and 3BE1, respectively. G.F. and J.B. are inventors of the patent application "Multispecific Antibodies" (Pub. App. No. 20080069820), which relates to this work. All authors are or were under the employment of Genentech and declare competing financial interests.

Supporting Online Material

www.sciencemag.org/cgi/content/full/323/5921/1610/DC1
Materials and Methods
Figs. S1 to S9
Tables S1 to S10
References

3 September 2008; accepted 10 February 2009
10.1126/science.1165480

Ankyrin-G Promotes Cyclic Nucleotide–Gated Channel Transport to Rod Photoreceptor Sensory Cilia

Krishnakumar Kizhatil,[1] Sheila A. Baker,[2] Vadim Y. Arshavsky,[2] Vann Bennett[1]*

Cyclic nucleotide–gated (CNG) channels localize exclusively to the plasma membrane of photosensitive outer segments of rod photoreceptors where they generate the electrical response to light. Here, we report the finding that targeting of CNG channels to the rod outer segment required their interaction with ankyrin-G. Ankyrin-G localized exclusively to rod outer segments, coimmunoprecipitated with the CNG channel, and bound to the C-terminal domain of the channel β1 subunit. Ankyrin-G depletion in neonatal mouse retinas markedly reduced CNG channel expression. Transgenic expression of CNG channel β-subunit mutants in *Xenopus* rods showed that ankyrin-G binding was necessary and sufficient for targeting of the β1 subunit to outer segments. Thus, ankyrin-G is required for transport of CNG channels to the plasma membrane of rod outer segments.

Cyclic nucleotide–gated (CNG) channels initiate the electrical responses to light in photoreceptors and to chemical stimuli in olfactory neurons (*1*). CNG channels are segregated to sensory cilia, where visual and olfactory signal transduction takes place. This precise intracellular localization is dependent on the channel's β subunit (CNG-β1, CNGB1) in both classes of neurons (*2*–*4*). However, the molecular mechanism(s) of CNG channel targeting to the plasma membrane of sensory cilia, where this channel normally functions, are unclear.

Ankyrin-G is a versatile membrane adaptor involved in the formation and maintenance of diverse specialized membrane domains (*5*–*9*). Ankyrin-G is localized exclusively to rod outer segments (ROSs), where it was found along with CNG channels that have been localized to the ROS plasma membrane (*10*, *11*) (Fig. 1, A and B). In contrast, the plasma membrane of the inner segment was lined with ankyrin-B, which is required for the coordinated expression of the Na^+- and K^+-dependent adenosine triphosphatase (ATPase), Na^+ and Ca^+ exchanger, and β2-spectrin (*12*) (Fig. 1A). Localization of ankyrin-G to the plasma membrane was evident in isolated mouse ROSs, but was better demonstrated in frog ROSs, which are three to four times as large in diameter (Fig. 1B). Ankyrin-G also localized in the olfactory sensory cilia and the principal piece of sperm flagella, together with CNG-β1 (*4*, *13*) (fig. S1). We treated isolated bovine ROSs with a cleavable cross-linker, solubilized them in 0.1% SDS, and used ankyrin- or CNG-β1–specific antibodies for immunoprecipitation. We observed the reciprocal coimmunoprecipitation of CNG-β1 and ankyrin-G (Fig. 1C). The interaction with ankyrin-G was specific, because CNG-β1 was not precipitated by nonimmune or ankyrin-B–specific antibodies,

[1]Department of Cell Biology, Duke University Medical Center, Durham, NC 27710, USA. [2]Department of Ophthalmology, Duke University Medical Center, Durham, NC 27710, USA.

*To whom correspondence should be addressed. E-mail: benne012@mc.duke.edu

and the major ROS-specific protein, rhodopsin, was not precipitated in either case (Fig. 1C).

The CNG channel binding to ankyrin-G was further evaluated using a HEK 293 cell–based assay for detecting ankyrin–membrane protein interactions (*14*). In this assay, overexpressed exogenous ankyrin-G fused to the C terminus of green fluorescent protein (GFP) (ankyrin-G–GFP), which is normally localized to the cytoplasm, is recruited to the plasma membrane when ankyrin binding partners, such as neurofascin, are coexpressed. CNG-α1 expressed in HEK 293 cells localized to the plasma membrane but did not recruit ankyrin-G–GFP (Fig. 1D), whereas CNG-β1 failed to localize to the plasma membrane of these cells when expressed by itself (fig. S2). Coexpression of CNG-α and CNG-β does yield functional heterotetrameric channels in the plasma membrane of HEK 293 cells (*15*). Such coexpression also resulted in efficient plasma membrane recruitment of ankyrin-G–GFP (Fig. 1E); complete recruitment was observed in 65% of cells coexpressing the three proteins ($n = 50$). Ankyrin-B–GFP was not recruited to the plasma membrane under similar conditions (Fig. 1E), which indicated that CNG-β1 interacts with ankyrin-G.

We next sought to evaluate whether ankyrin-G is required for localization of CNG channels to ROSs in vivo, using short hairpin RNA (shRNA) to deplete (knockdown) ankyrin-G expression in neonatal mouse retinas. We injected a mixture of a plasmid encoding shRNA targeting mouse ankyrin-G in 10-fold excess over a plasmid encoding GFP into the eyes of newborn pups followed by electroporation (*16*). Under these conditions, rods expressing GFP are typically co-transfected with the shRNA plasmid. Two weeks post injection, photoreceptors transfected with control shRNA expressed GFP, displayed normal morphology, and were robustly immunostained with ankyrin-G (Fig. 2). In contrast, photoreceptors transfected with ankyrin-G shRNA (GFP^+) displayed a major reduction in the ankyrin-G immunofluorescence in ROSs [20 to 30% of control, based on immunofluorescence intensity of samples on the same slide (fig. S3)], and their ROSs were significantly shortened [average length of 4.7 μm versus 15.5 μm in control rods ($n = 25$); compare rhodopsin-labeled sections]. The immunofluorescence levels of both CNG-β1 and CNG-α1 were also markedly reduced, to a degree comparable with the ankyrin-G reduction (Fig. 2 and fig. S3). In contrast, rhodopsin levels estimated by fluorescence intensities of samples on the same slide were similar for control ROSs and ROSs expressing ankyrin-G shRNA (Fig. 2 and fig. S3). The shortened ROS phenotype in ankyrin-G–depleted retina was more severe than reported for mice lacking the CNG-β1 subunit (*2*). Thus, ankyrin-G plays role(s) in either assembly and/or maintenance of ROSs in addition to localization of the CNG channel. This result is similar to the requirement of ankyrin-G for biogenesis of the lateral membrane in cultured columnar epithelial cells (*17*).

The reduction in CNG channel expression in ankyrin-G–depleted rods could be explained by a requirement for ankyrin-G in targeting the channel to ROS plasma membrane from the endoplasmic reticulum or Golgi located in the inner segment. Indeed, ankyrin-G is required for both post-Golgi transport and immobilization of its binding partner E-cadherin in epithelial cells (*6*). To test this hypothesis, we needed to identify CNG-β1 mutants lacking ankyrin-G binding. We first determined

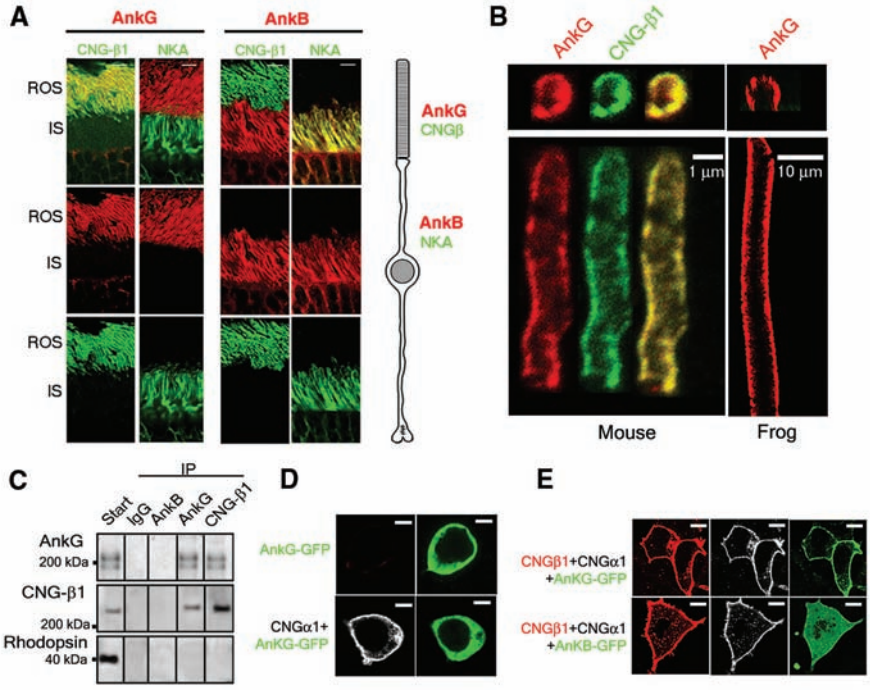

Fig. 1. Ankyrin-G is restricted to photoreceptor outer segments and binds the rod CNG channel. (**A**) Colocalization of ankyrin-G (AnkG, red, left two columns) with CNG channel (CNG-β1, green) in ROSs and colocalization of ankyrin-B (AnkB, red, right two columns) with Na^+- and K^+-dependent ATPase (NKA) (green) in inner segments (IS). A schematic of a rod cell is shown to the right. (**B**) Ankyrin-G (red) localizes to the plasma membrane of isolated mouse and frog ROSs labeled with CNG-β1–specific antibody (green). ROS tangential sections are shown (top) and longitudinal sections (bottom). (**C**) Coimmunoprecipitation of ankyrin-G with CNG-β1 channels from bovine ROS extracts. Antibodies used for precipitations are indicated on the top (immunoglobulin G, IgG), antibodies used for protein detection are indicated on the left. (**D**) CNG-α1 (white) alone does not recruit ankyrin-G–GFP (green) to the plasma membrane of HEK 293 cells. (**E**) Ankyrin-G–GFP (green) is recruited to the plasma membrane of HEK 293 cells coexpressing CNG-β1 (red) and CNG-α1 (white). Scale bars: 5 μm in (A), 10 μm in (D) and (E).

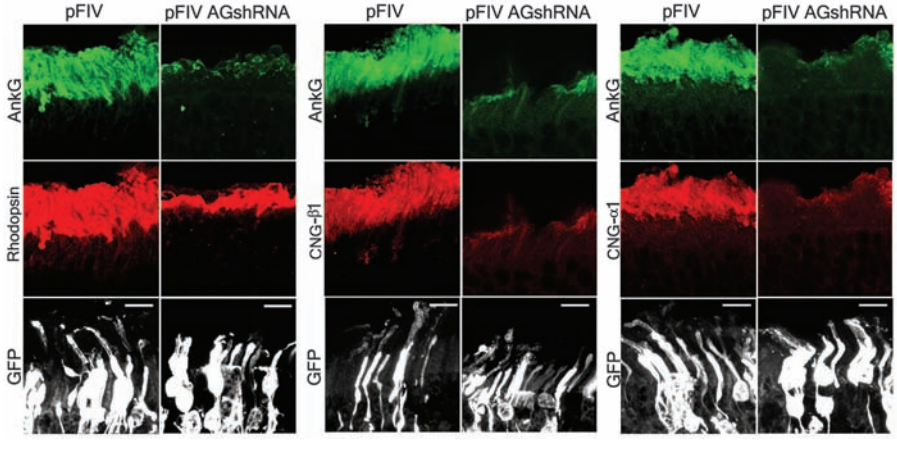

Fig. 2. Ankyrin-G is required for ROS morphogenesis. Retinas of newborn mice were electroporated with either ankyrin-G shRNA or control pFIV (3 μg/μl) plasmid, each mixed with pCAGGS-GFP (0.3 μg/μl) (*11*). Ankyrin-G (AnkG) staining is shown in green. The staining of rhodopsin (**left**), CNG-β1 (**center**), and CNG-α1 (**right**) is shown in red. GFP staining is shown in white. Scale bars, 10 μm.

whether ankyrin-G bound to either the N- or C-terminal cytoplasmic domain of CNG-β1 (Fig. 3A). Ankyrin-G–GFP was coexpressed with protein constructs in which the ankyrin-binding domain of neurofascin was replaced with either the entire cytoplasmic N or C terminus of human CNG-β1 [NF-CNG-βN (amino acids 1 to 654) and NF-CNG-βC (amino acids 1041 to 1251), respectively (Fig. 3A)]. Ankyrin-G interacted only with the C-terminal domain of CNG-β1, both in the HEK 293–based plasma membrane recruitment assay (fig. S4) and coimmunoprecipitation experiments (Fig. 3B). Immunoprecipitation experiments in HEK cells were performed in the absence of a cross-linking reagent.

A truncation of the C-terminal 28 residues of CNG-β1 is associated with retinitis pigmentosa (RP; hCNG-βΔ28) (Fig. 3A) (*18*). Indeed, neurofascin fused to the CNG-β1 C-terminal domain bearing this deletion failed to recruit or to coimmunoprecipitate ankyrin-G–GFP (fig. S2A and Fig. 3B). Additional deletion mutagenesis (hCNG-βC1243 and hCNG-βC1236, Fig. 3C) (*19*) narrowed the interaction site to a seven–amino acid stretch in this region (Fig. 3C, underlined, and fig. S4B), and alanine-scanning mutagenesis revealed that the highly conserved residues Ile[1237] and Leu[1238] were essential for ankyrin-G binding (fig. S4B and Fig. 3C). Mutant CNG-β1 (RP deletion or IL1237AA mutation, in which alanine (A) replaced isoleucine (I) and leucine (L) at positions 1237 and 1238, respectively) coexpressed with CNG-α1 in HEK 293 cells failed to bind ankyrin-G without affecting the normal CNG-α1 and CNG-β1 association (Fig. 3D).

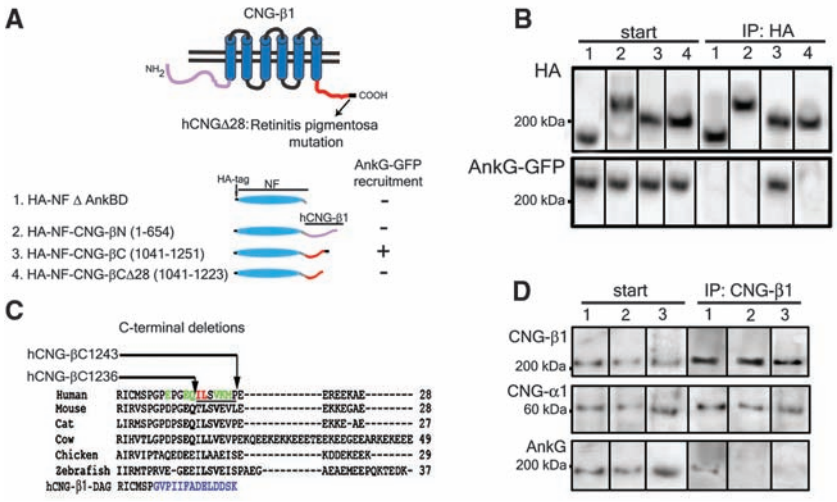

Fig. 3. The ankyrin-G–binding site resides in a C-terminal motif of CNG-β1. (**A**) Schematic diagrams of rod CNG-β1 (top) and HA-tagged neurofascin (HA-NF) chimeras with CNG-β1 (bottom). Numbers within parentheses indicate the amino acid ranges of the CNG-β1 polypeptide fused to neurofascin. The abilities of chimeras to recruit ankyrin-G–GFP to plasma membrane of HEK 293 cells is indicated by + or − (AnkBD, ankyrin-binding domain). (**B**) Ankyrin-G–GFP was coexpressed in HEK 293 cells with the chimeras shown in (A), cells were lysed, and proteins were immunoprecipitated by HA-specific antibodies. Immunoblots of samples from the starting material (left) and precipitated proteins (right) were probed with HA- or GFP-specific antibodies. Lane numbers correspond to the numbered chimeras in (A). (**C**) Sequence of the 28 C-terminal amino acids of human CNG-β1 and homologous regions from other vertebrates (*19*). Arrows indicate sites of C-terminal deletions hCNG-βC1243 and hCNG-βC1236 used to identify residues critical for ankyrin-G binding. Colored residues were mutated to alanine; those in red were critical for ankyrin-G binding and those in green were neutral. The human CNG-β1–β-dystroglycan chimera (hCNGβ-DAG) is shown at the bottom with the dystroglycan sequences marked in blue. (**D**) CNG-β1 (lane 1) CNG-βΔ 28 (lane 2) and CNG-β1 IL1237AA (lane 3) were coexpressed with CNG-α1 in HEK 293 cells and immunoprecipitated using the CNG-β1–specific antibodies. Each CNG-β1 mutant normally coprecipitated with CNG-α1, but failed to bind endogenous ankyrin-G. Starting material is shown on the left and immunoprecipitates on the right.

To test whether ankyrin-G binding was required for delivery of the channel to outer segments, human CNG-β1, either wild type or mutants unable to interact with ankyrin-G, were expressed in the rods of transgenic *Xenopus laevis* (*20*). We used a specific antibody against human CNG-β1 (*21*) to distinguish it from the endogenous *Xenopus* CNG-β1 (Fig. 4). Wild-type human CNG-β1 (WT) was found in ROSs in a distinctive pattern consistent with its plasma membrane localization (Fig. 4). In marked contrast, both the RP (Δ28) and IL1237AA mutants were confined to perinuclear sites within rod cell bodies and were completely absent from ROSs (Fig. 4).

We next tested whether an ankyrin-G–binding site from an unrelated protein was sufficient for targeting CNG-β1 to ROSs. The native site in CNG-β1 required for interaction with ankyrin-G was replaced with 14 amino acids from β-dystroglycan, which binds ankyrin-G directly (*5*) and has little sequence similarity with the CNG-β1 motif (Fig. 3C). The CNG-β1–dystroglycan (CNG-β–DAG) chimera associated with ankyrin-G when coexpressed with CNG-α in HEK 293 cells (fig. S5). When expressed in transgenic *Xenopus*, this chimera was targeted to the ROSs plasma membrane; however, the mutant CNG-β–DAG IIF/AAA chimera lacking the ankyrin-binding site (fig. S5) (*5*) was retained in the photoreceptor cell body (Fig. 4). Because there is no retrograde movement of membrane proteins from ROSs back into the cell body (*22*), we conclude that ankyrin-G binding is both necessary and sufficient for trafficking CNG-β1 to the outer segment. The ankyrin-G pathway could intersect with the microtubule motor Kif17/osm3, which is found in ROSs (*23*) and is required for ciliary transport of olfactory CNG channels when expressed in MDCK cells (*3*). Another question relates to the specific β-spectrin partner of ankyrin-G in ROSs. Ankyrins partner with β-spectrins in performing their scaffolding roles in the membrane cytoskeleton and in mediating post-Golgi transport through interactions with phospholipids and motor proteins (*24*–*27*). β2-Spectrin found in inner segments (*28*) is reduced in the retina with or without ankyrin-B (*12*) and thus is a likely partner for ankyrin-B there. β4-Spectrin is associated with ankyrin-G in axon initial segments and is present in rod inner and outer segments (fig. S4), where its presence makes it a plausible ankyrin-G partner in ROSs.

Ankyrin-G accomplishes two critical functions in photoreceptors: It is required for transport of CNG-β1 from its site of synthesis and the assembly and/or maintenance of ROSs. This

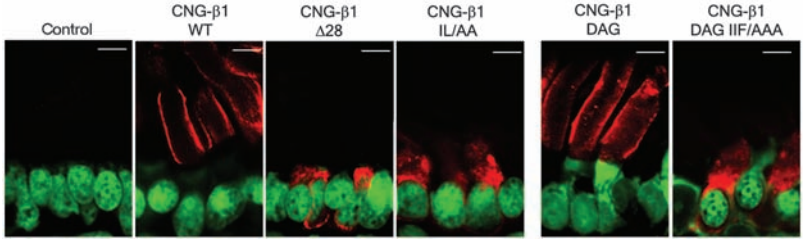

Fig. 4. Ankyrin-G binding is necessary and sufficient for CNG-β1 transport to ROSs of transgenic *Xenopus*. Retina sections in each panel are stained with CNG-β1–specific antibody (red) and TOTO-3 to label the nuclei. Nontransgenic tadpole control on the left demonstrates that this antibody does not recognize the endogenous channel. Other panels depict the localization of wild-type (WT) human CNG-β1 or its mutants (indicated above each panel; see results for abbreviations). Scale bar, 5 μm.

resembles the role of ankyrin-G in axon initial segments, where it binds to and coordinates the localization of three proteins required for the initiation and regulation of action potentials (Nav1.6, KCNQ2 and 3 channels, and 186-kD neurofascin) (*29*, *30*). Without ankyrin-G, axon initial segments lose these proteins and express dendritic markers (*31*). In epithelial cells, ankyrin-G is required both for targeting E-cadherin to the plasma membrane and for biogenesis of the lateral membrane (*6*, *17*). We hypothesize that, in addition to targeting the CNG channel, ankyrin-G can interact with other ROS membrane proteins, as well as proteins required for their ROS trafficking, and these interactions are essential for ROS morphogenesis. A conserved ankyrin-G–based mechanism may thus be shared by photoreceptors, neurons, and epithelial cells that accomplishes both the targeting of membrane-spanning proteins to specialized plasma membrane domains as well as assembly and/or maintenance of these domains.

References and Notes

1. K. Matulef, W. N. Zagotta, *Annu. Rev. Cell Dev. Biol.* **19**, 23 (2003).
2. S. Huttl *et al.*, *J. Neurosci.* **25**, 130 (2005).
3. P. M. Jenkins *et al.*, *Curr. Biol.* **16**, 1211 (2006).
4. S. Michalakis *et al.*, *J. Biol. Chem.* **281**, 35156 (2006).
5. G. Ayalon, J. Q. Davis, P. B. Scotland, V. Bennett, *Cell* **135**, 1189 (2008).
6. K. Kizhatil *et al.*, *J. Biol. Chem.* **282**, 26552 (2007).
7. J. S. Lowe *et al.*, *J. Cell Biol.* **180**, 173 (2008).
8. P. J. Mohler *et al.*, *Proc. Natl. Acad. Sci. U.S.A.* **101**, 17533 (2004).
9. D. Zhou *et al.*, *J. Cell Biol.* **143**, 1295 (1998).
10. P. Wohlfart, W. Haase, R. S. Molday, N. J. Cook, *J. Biol. Chem.* **267**, 644 (1992).
11. Materials and methods are available as supporting material on *Science* Online.
12. K. Kizhatil, N. K. Sandhu, N. S. Peachey, V. Bennett, *Exp. Eye Res.* **88**, 57 (2009).
13. B. Wiesner *et al.*, *J. Cell Biol.* **142**, 473 (1998).
14. X. Zhang, J. Q. Davis, S. Carpenter, V. Bennett, *J. Biol. Chem.* **273**, 30785 (1998).
15. T. Y. Chen *et al.*, *Nature* **362**, 764 (1993).
16. T. Matsuda, C. L. Cepko, *Proc. Natl. Acad. Sci. U.S.A.* **101**, 16 (2004).
17. K. Kizhatil, V. Bennett, *J. Biol. Chem.* **279**, 16706 (2004).
18. H. Kondo *et al.*, *Invest. Ophthalmol. Vis. Sci.* **45**, 4433 (2004).
19. Single-letter abbreviations for the amino acid residues are as follows: A, Ala; C, Cys; D, Asp; E, Glu; F, Phe; G, Gly; H, His; I, Ile; K, Lys; L, Leu; M, Met; N, Asn; P, Pro; Q, Gln; R, Arg; S, Ser; T, Thr; V, Val; W, Trp; and Y, Tyr.
20. S. A. Baker *et al.*, *J. Cell Biol.* **183**, 485 (2008).
21. A. Poetsch, L. L. Molday, R. S. Molday, *J. Biol. Chem.* **276**, 48009 (2001).
22. J. Nguyen-Legros, D. Hicks, *Int. Rev. Cytol.* **196**, 245 (2000).
23. C. Insinna, N. Pathak, B. Perkins, I. Drummond, J. C. Besharse, *Dev. Biol.* **316**, 160 (2008).
24. V. Bennett, J. Healy, *Trends Mol. Med.* **14**, 28 (2008).
25. K. Kizhatil *et al.*, *J. Biol. Chem.* **282**, 2029 (2007).
26. P. J. Mohler, W. Yoon, V. Bennett, *J. Biol. Chem.* **279**, 40185 (2004).
27. V. Muresan *et al.*, *Mol. Cell* **7**, 173 (2001).
28. S. A. Madreperla, M. Edidin, R. Adler, *J. Cell Biol.* **109**, 1483 (1989).
29. S. M. Jenkins, V. Bennett, *J. Cell Biol.* **155**, 739 (2001).
30. Z. Pan *et al.*, *J. Neurosci.* **26**, 2599 (2006).
31. K. L. Hedstrom, Y. Ogawa, M. N. Rasband, *J. Cell Biol.* **183**, 635 (2008).

32. We thank J. Hoffman for constructing the plasmids used in the study. V.Y.A. was funded by NIH grant EY12859. V.B. is an investigator of Howard Hughes Medical Institute (HHMI) and was funded by HHMI.

Supporting Online Material

www.sciencemag.org/cgi/content/full/323/5921/1614/DC1
Materials and Methods
Figs. S1 to S6
References

15 December 2008; accepted 2 February 2009
10.1126/science.1169789

The Surprising Power of Neighborly Advice

Daniel T. Gilbert,[1]* Matthew A. Killingsworth,[1] Rebecca N. Eyre,[1] Timothy D. Wilson[2]

Two experiments revealed that (i) people can more accurately predict their affective reactions to a future event when they know how a neighbor in their social network reacted to the event than when they know about the event itself and (ii) people do not believe this. Undergraduates made more accurate predictions about their affective reactions to a 5-minute speed date (n = 25) and to a peer evaluation (n = 88) when they knew only how another undergraduate had reacted to these events than when they had information about the events themselves. Both participants and independent judges mistakenly believed that predictions based on information about the event would be more accurate than predictions based on information about how another person had reacted to it.

People make systematic errors when attempting to predict their affective reactions to future events, and these errors have social (*1*–*3*), economic (*4*–*8*), legal (*9*, *10*), and medical (*11*–*22*) consequences. For example, people have been shown to overestimate how unhappy they will be after receiving bad test results (*23*), becoming disabled (*14*, *19*–*21*), or being denied a promotion (*24*), and to overestimate how happy they will be after winning a prize (*6*), initiating a romantic relationship (*24*), or taking revenge against those who have harmed them (*3*). Research suggests that the main reason people mispredict their affective reactions to future events is that they imagine those events inaccurately (*25*). For example, people tend to imagine the essential features of future events but not the incidental features (*26*–*28*), the early moments of future events but not the later moments (*17*, *24*), and so on. When mental simulations of events are inaccurate, the affective forecasts that are based on them tend to be inaccurate as well.

Attempts to improve the accuracy of affective forecasting have generally concentrated on improving the accuracy of mental simulation, and the results have been disappointing (*29*–*33*). Some interventions have failed (*16*), and those that have successfully reduced forecasting errors in one situation have typically failed to reduce them in others (*27*, *29*). But mental simulation is not the only way to make an affective forecast. The 17th century writer François de La Rochefoucauld suggested that rather than mentally simulating a future event, people should consult those who have experienced it. "Before we set our hearts too much upon anything," he wrote, "let us first examine how happy those are who already possess it" (*34*). La Rochefoucauld was essentially suggesting that forecasters should use other people as surrogates for themselves, and the advantages of his "surrogation strategy" are clear: Because surrogation does not rely on mental simulation, it is immune to the many errors that inaccurate simulations produce.

The disadvantages of surrogation are also clear: Individuals differ, and thus, one person's affective reaction is almost certainly an imperfect predictor of another's. But there are at least two reasons to suspect that affective reactions are not as different as people may believe. First, affective reactions are produced in large part by physiological mechanisms that are evolutionarily ancient, which is why people the world over have very different beliefs and opinions but very similar affective reactions to a wide range of stimuli (*35*), preferring warm to cold, satiety to hunger, friends to enemies, winning to losing, and so on. An alien who knew all the likes and dislikes of a single human being would know a great deal about the entire species. Second, people tend to marry, befriend, work with, and live near those who share their preferences and personality traits (*36*, *37*), and thus the people from whom they are especially likely to receive surrogation information—the neighbors in their social networks—are especially likely to share their affective reactions. In short, there is little disagreement among people about the sources of pleasure and pain, and even less disagreement among neighbors. These facts suggest that surrogation may be more powerful than people realize.

[1]Department of Psychology, Harvard University, Cambridge, MA 02138, USA. [2]Department of Psychology, University of Virginia, Charlottesville, VA 22904, USA.

*To whom correspondence should be addressed. E-mail: gilbert@wjh.harvard.edu

We tested this hypothesis in two experiments. The events we studied were (i) speed dating, in which undergraduate women predicted how much they would enjoy a 5-min speed date with an undergraduate man, and (ii) peer-evaluation, in which undergraduates predicted how they would feel after being evaluated by a peer (*38*). In both experiments, we gave participants either information that allowed them to simulate the future event (simulation information) or information about the affective reaction of a fellow undergraduate who had experienced the same event in the past (surrogation information). We predicted that participants would make more accurate affective forecasts when they knew nothing about the future event and knew only how someone in their social network had reacted to it.

In experiment 1, we created a speed-dating service in which undergraduate men and women had brief "getting acquainted" conversations. We included 8 men and 33 women who were undergraduates at Harvard University, unmarried, and self-identified as heterosexual. There were eight speed-dating sessions, each of which included one of the eight men and between two and eight of the women. No one participated in more than one session. In each session, the man was first escorted to the speed-dating room, where he completed a short personal profile listing his name, age, height, hometown, and residence, as well as his favorite movie, sport, book, song, food, hangout, and college class. His photograph was taken and printed. Next, a woman was escorted to the speed-dating room and left to have a 5-min private conversation with the man. Next, the experimenter escorted the woman to another room where she reported how much she had enjoyed the speed date by marking a 100-mm continuous "enjoyment scale" whose end points were marked not at all and very much. This report is hereinafter referred to as her affective report.

Next, a second woman was given one of two kinds of information: simulation information (which consisted of the man's personal profile and photograph) or surrogation information (which consisted of the affective report provided by the first woman). The second woman was then asked to predict (on the enjoyment scale) how much she would enjoy her speed date with the man. This prediction is hereinafter referred to as her affective forecast.

After making her prediction, the second woman was shown the kind of information (simulation or surrogation) that she had not already received. We did this to ensure that each woman had the same information about the man before the actual speed date. The only difference between the two conditions, then, was whether the second woman had surrogation information or simulation information when she made her forecast.

Next, the second woman was escorted to the dating room, had a speed date, and then reported how much she enjoyed it (on the enjoyment scale). This report is hereinafter referred to as her affective report. The second woman also reported whether she believed that simulation information or surrogation information would have allowed her to make the more accurate prediction about the speed date she had and about a speed date that she might have in the future. This process was repeated in an alternating pattern for each additional woman until the session ended. [For a full description of the procedure, see (*39*)].

Affective forecasting error was calculated by taking the absolute difference between the affective forecast and affective report of each woman (except the first woman, who made no affective forecast). Raw data may be seen in fig. S1, a and b. Women were considerably more accurate when they used surrogation information (mean ± SD, 11.42 ± 8.70 mm) than when they used simulation information (22.38 ± 10.79 mm) [$t(23) = 2.78$, $P = 0.01$]. Relative to simulation, surrogation reduced the size of the affective forecasting error by 49%. Ironically, 75% of the women believed that simulation information would have allowed them to make a more accurate forecast about their date with the man they met, and 84% believed that simulation information would allow them to make a more accurate forecast about a future date with a different man.

One potential concern about these results is that the simulation information (which was provided by the men) may not have been entirely accurate, and its inaccuracy may have contributed to the inaccuracy of the forecasts that were based on it. The data do not support this suggestion. If men portrayed themselves as better than they actually were, then women who used simulation information should have overestimated how much they would enjoy the date. In fact, women underestimated how much they would enjoy the date (see supporting online text). Nonetheless, we conducted a second experiment in which simulation information was completely accurate. In addition, we collected data on the perceived utility of simulation and surrogation from an independent panel of judges rather than from the participants themselves.

Experiment 2 had three parts. In part one, 17 women and 8 men who were undergraduates at Harvard University served as surrogates. Surrogates were told that they would write a story and that a peer in an adjoining room would evaluate the story and use it to classify them as one of three personality types. In fact, there was no peer. Surrogates read detailed descriptions of the type A, type B, and type C personalities. The description of the type A personality was positive, the description of the type B personality was neutral, and the description of the type C personality was negative. For example, people with type C personalities were said to "sacrifice their beliefs because they seek contentment rather than challenge" and "when long-term relationships end it is usually because the person's partner has found a more suitable alternative." Previous studies have shown that few people classify themselves as type C, and most feel unhappy when they are so classified by a peer (*24*, *40*). Surrogates then wrote stories that were ostensibly given to their peer in the adjoining room. Ten minutes later, the experimenter informed the surrogates that they had been classified as type C by their peer. Ten minutes later, surrogates reported their current affective state by marking a continuous 100-mm "feeling scale" whose end points were labeled very bad and very good. These reports are hereinafter referred to as the surrogates' affective reports.

In part two, 28 men and 60 women who were undergraduates at Harvard University served as forecasters. Forecasters were also told that they would write a story and that a peer would evaluate the story and then classify them as one of three personality types. Half the forecasters were randomly assigned to receive simulation information. These forecasters were shown complete descriptions of the three personality types and were asked to predict (on the feeling scale) how they would feel if their peer classified them as each of the three types. These forecasters, therefore, had complete and accurate information about the upcoming event.

The remaining forecasters were assigned to receive surrogation information. Instead of being shown the descriptions of the three personality types, these forecasters were shown the affective report of one randomly selected surrogate from part one who had been classified as a type C, and they were asked to predict how they would feel if their peer classified them as each of the three types. These predictions are hereinafter referred to as the forecasters' affective forecasts. After making these forecasts, forecasters in the surrogation condition were shown the descriptions of the three personality types.

All forecasters then wrote a story, were told that their peer had classified them as a type C, and reported how they felt (on the feeling scale). These reports are hereinafter referred to as the forecasters' affective reports.

Affective forecasting error was calculated by taking the absolute value of the difference between each forecaster's affective forecast and affective report. (Raw data may be seen in fig. S2, a and b). As in experiment 1, forecasters were considerably more accurate when they used surrogation information (12.50 ± 14.10 mm) than when they used simulation information (33.75 ± 22.01 mm) [$t(86) = 5.38$, $P < 0.001$]. Relative to simulation, surrogation reduced the size of the affective forecasting error by 63%.

In part three, 23 men and 40 women who were undergraduates at Harvard University served as judges. The judges were told about the procedure for part one and were asked to rank several pieces of information based on how useful each piece would be in allowing them to estimate the affective response of a participant. These included simulation information (complete descriptions of each of the three personality types) and surrogation information (the affective report of another randomly selected participant). Judges

believed that simulation information would be more useful (rank, mean ± SD, 1.45 ± 0.694) than surrogation information (2.1 ± 0.718) [$t(61) = 4.18$, $P < 0.001$].

In two experiments, participants more accurately predicted their affective reactions to a future event when they knew how a neighbor in their social network had reacted to it than when they knew about the event itself. Women made more accurate predictions about how much they would enjoy a date with a man when they knew how much another woman in their social network enjoyed dating the man than when they read the man's personal profile and saw his photograph. Men and women made more accurate predictions about how they would feel after being evaluated by a peer when they knew how another person in their social network had felt after being evaluated than when they previewed the evaluation itself. Although surrogation trumped simulation, both participants and independent judges had precisely the opposite intuition (*41*). By a wide margin, they believed that simulation was more likely than surrogation to produce accurate affective forecasts.

Two points are worthy of note. First, surrogation is by definition superior to simulation when individual differences are relatively small and simulations errors are relatively large, and it is inferior to simulation when the opposite is true. Although there is no way to know which of these is more typical in everyday life, the situations we studied—dating and peer-evaluation—are by no means exotic. Furthermore, our experiments provided an especially conservative test of the power of surrogation because participants received surrogation information from a person who happened to attend the same university as they did but with whom they had no personal relationship. In everyday life, people are likely to receive surrogation information from those with whom they affiliate, and because people affiliate with those who are similar, their surrogates are even more likely to share their preferences and predilections. This suggests that the potential utility of surrogation information may be greater in vivo than our experiments suggest.

Second, although our experiments demonstrate the power of surrogation, they also suggest that people may not normally take advantage of this power. Our participants mistakenly believed that simulation was the superior strategy even after it had failed them, which suggests that people may be reluctant to engage in surrogation if they have the opportunity to do otherwise. Participants in the surrogation conditions of our experiments were unable to engage in mental simulation because they knew little or nothing about the future event and thus had no choice but to rely on the surrogation information we provided. But given people's mistaken beliefs about the relative ineffectiveness of surrogation and their misplaced confidence in the accuracy of their own mental simulations (*39*), it seems likely that in everyday life, La Rochefoucauld's advice—like the advice of good neighbors—is more often than not ignored. When we want to know our emotional futures, it is difficult to believe that a neighbor's experience can provide greater insight than our own best guess.

References and Notes

1. K. Kawakami, E. Dunn, F. Karmali, J. F. Dovidio, *Science* **323**, 276 (2009).
2. T. D. Wilson, D. B. Centerbar, D. A. Kermer, D. T. Gilbert, *J. Pers. Soc. Psychol.* **88**, 5 (2005).
3. K. M. Carlsmith, T. D. Wilson, D. T. Gilbert, *J. Pers. Soc. Psychol.* **95**, 1316 (2008).
4. D. T. Gilbert, J. E. J. Ebert, *J. Pers. Soc. Psychol.* **82**, 503 (2002).
5. S. L. Wood, J. R. Bettman, *J. Consum. Psychol.* **17**, 188 (2007).
6. D. A. Kermer, E. Driver-Linn, T. D. Wilson, D. T. Gilbert, *Psychol. Sci.* **17**, 649 (2006).
7. N. Sevdalis, N. Harvey, *Psychol. Sci.* **18**, 678 (2007).
8. K. S. Kassam, D. T. Gilbert, A. Boston, T. D. Wilson, *J. Exp. Soc. Psychol.* **44**, 1533 (2008).
9. J. A. Blumenthal, *Indiana Law J.* **80**, 155 (2005).
10. J. Bronsteen, C. Buccafusco, J. Masur, *Columbia Law Rev.* **108**, 1516 (2008).
11. R. Rhodes, J. J. Strain, *Camb. Q. Healthc. Ethics* **17**, 54 (2008).
12. D. I. Shalowitz, E. Garrett-Mayer, D. Wendler, *PLoS Med.* **4**, e35 (2007).
13. J. Baron *et al.*, *Med. Decis. Making* **23**, 422 (2003).
14. P. A. Ubel, G. Loewenstein, N. Schwarz, D. Smith, *Health Psychol.* **24**, S57 (2005).
15. P. A. Ubel, G. Loewenstein, C. Jepson, *Qual. Life Res.* **12**, 599 (2003).
16. P. A. Ubel *et al.*, *Med. Decis. Making* **21**, 190 (2001).
17. J. Riis *et al.*, *J. Exp. Psychol. Gen.* **134**, 3 (2005).
18. P. Menzel, P. Dolan, J. Richardson, J. A. Olsen, *Soc. Sci. Med.* **55**, 2149 (2002).
19. G. L. Albrecht, P. J. Devlieger, *Soc. Sci. Med.* **48**, 977 (1999).
20. N. F. Boyd, H. J. Sutherland, K. Z. Heasman, D. L. Tritchler, B. J. Cummings, *Med. Decis. Making* **10**, 58 (1990).
21. D. L. Sackett, G. W. Torrance, *J. Chronic Dis.* **31**, 697 (1978).
22. P. H. Ditto, N. A. Hawkins, *Health Psychol.* **24**, S63 (2005).
23. T. D. Wilson, T. Wheatley, J. Kurtz, E. W. Dunn, D. T. Gilbert, *Pers. Soc. Psychol. Bull.* **30**, 340 (2004).
24. D. T. Gilbert, E. C. Pinel, T. D. Wilson, S. J. Blumberg, T. P. Wheatley, *J. Pers. Soc. Psychol.* **75**, 617 (1998).
25. D. T. Gilbert, T. D. Wilson, *Science* **317**, 1351 (2007).
26. N. Liberman, Y. Trope, *Science* **322**, 1201 (2008).
27. T. D. Wilson, T. P. Wheatley, J. Meyers, D. T. Gilbert, D. Axsom, *J. Pers. Soc. Psychol.* **78**, 821 (2000).
28. E. W. Dunn, T. D. Wilson, D. T. Gilbert, *Pers. Soc. Psychol. Bull.* **29**, 1421 (2003).
29. P. A. Ubel, G. Loewenstein, C. Jepson, *J. Exp. Psychol. Appl.* **11**, 111 (2005).
30. L. J. Damschroder, B. J. Zikmund-Fisher, P. A. Ubel, *Soc. Sci. Med.* **61**, 267 (2005).
31. T. D. Wilson, J. Meyers, D. T. Gilbert, *Pers. Soc. Psychol. Bull.* **27**, 1648 (2001).
32. P. Ayton, A. Pott, N. Elwakili, *Think. Reason.* **13**, 62 (2007).
33. E. W. Dunn, M. A. Brackett, C. Ashton-James, E. Schneiderman, P. Salovey, *Pers. Soc. Psychol. Bull.* **33**, 85 (2007).
34. F. de La Rochefoucauld, *Collected Maxims and Other Reflections* (Oxford Univ. Press, Oxford, 2007), p. 354.
35. D. A. van Hemert, Y. H. Poortinga, F. J. R. van de Vijver, *Cogn. Emotion* **21**, 913 (2007).
36. M. McPherson, L. Smith-Lovin, K. Cook, *Annu. Rev. Sociol.* **27**, 415 (2001).
37. K. Lee *et al.*, *J. Pers. Soc. Psychol.* **96**, 460 (2009).
38. Materials and methods are available as supporting material on *Science* Online.
39. D. W. Griffin, D. Dunning, L. Ross, *J. Pers. Soc. Psychol.* **59**, 1128 (1990).
40. D. T. Gilbert, M. D. Lieberman, C. K. Morewedge, T. D. Wilson, *Psychol. Sci.* **15**, 14 (2004).
41. N. Epley, D. Dunning, *J. Pers. Soc. Psychol.* **79**, 861 (2000).

42. We acknowledge the support of research grant BCS-0722132 from NSF to D.T.G. and T.D.W.

Supporting Online Material

www.sciencemag.org/cgi/content/full/323/5921/1617/DC1
Materials and Methods
SOM Text
Figs. S1 and S2

30 September 2008; accepted 5 February 2009
10.1126/science.1166632

New Products

Expression Kits

QIAgenes Expression Kits provide a comprehensive set of ready-cloned plasmids with synthetic genes covering the entire human genome. The kits are designed to be an alternative to protein production using *E. coli* cells. The kits make use of synthetic cDNA with a human genome sequence optimized for expression in *E. coli,* insect, or mammalian cells. This optimized sequence increases protein yields as much as 50-fold and produces expression success rates as high as 90 percent. The kits include ready-to-go vectors, but are flexible enough to express only parts of a gene.

Qiagen
For information 240-686-7686
www.qiagen.com

ELISA Development Kits

Immunoset enzyme-linked immunosorbent assay (ELISA) kits, for assaying proteins in various matrices, contain the basic components and protocol for the development of five 96-well colorimetric enzyme immunoassays. The manufacturer plans to develop additional kits for the detection of mouse and rat heme oxygenase-1 and p53/MDM2 complexes.

Assay Designs
For information 800-833-8651
www.assaydesigns.com

Circulating Baths

Model 9112 and Model 9012 Refrigerating/Heating Circulating Baths deliver ±0.01°C temperature stability, a temperature range of -20 to 200°C, six-liter reservoir, and remote temperature control capability. They are suitable for use with Abbe refractometers. The heart of the systems is the programmable controller, which features an LCD display, multilanguage help menus, and sophisticated time and temperature programming. The controller can store up to 10, 50-step programs and offers extensive data logging capability, including communications support for Microsoft Excel, National Instruments LabView, and the Palm OS. Other standard features include user-settable high and low temperature alarms, a variable-speed pump capable of closed and open loop external circulation, and a built-in RS-232 interface. Model 9112 requires less than a square foot of bench space, and the low-profile Model 9012 fits on a shelf.

PolyScience
For information 800-229-7569
www.polyscience.com

Reversible Protein Stain

The BLOT-FastStain is for reversible protein staining on nitrocellulose and polyvinylidene fluoride (PVDF) transfer membranes. It stains only protein and leaves the background untouched and brilliant white, resulting in high band visibility. The staining procedure takes 10 minutes and has a sensitivity of 2 ng bovine serum albumin, which is higher than silver stains. The membrane can be destained simply by rinsing it in warm water for 10 minutes. Staining and destaining do not affect the biological properties of the proteins. After destaining, protein bands can be probed with protein immunoblot protocols and other analyses, including sequencing work.

G-Biosciences
For information 314-991-6034
www.GBiosciences.com

Microscopy Catalog

The 2008–2010 Electron Microscopy Sciences catalog is available on CD-ROM. This interactive catalog contains a complete collection of products for light microscopy, histology, and electron microscopy and general biological and materials research. It contains more than 12,000 products, including 2,000 new items. In addition to the product descriptions, the CD-ROM contains a library of technical documents, including datasheets that provide procedures and protocols for sample preparation, newsletters, instrument manuals, and technical tips. The catalog runs on any web browser, has bookmarks for movement between catalog sections, and includes full search capability.

Electron Microscopy Sciences
For information 215-412-8400
www.emsdiasum.com

Benchtop Freeze-Dryers

The Virtis Advantage Plus line of benchtop freeze-dryers, with up to three fluid-cooled shelves, maintain precise temperature control previously available only in pilot and production scale units. The Advantage Plus can be configured to freeze-dry bulk product or for applications in stoppered vials. Side-mounted manifold valves provide the additional flexibility to freeze-dry products in flasks. Three refrigeration choices are available for the large six-liter capacity condenser, depending on the type of product and solvents being lyophilized. The process control software provides the ability to develop a complete freeze-drying recipe together with the flexibility to program and control individual pressure and temperature settings at each step of the process.

SP Industries
For information 845-255-5000
www.spindustries.com

Direct Drive Robot

The Direct Drive Robot (DDR) makes use of configurable Z-travel technology to enable greater stacking of instruments and more functionality in a smaller footprint. The DDR offers high operational precision, reliability, and safety. It features a one-person, one-touch teaching mode for fast and easy configuration. In this mode, a teaching jig can be used to move the robot to any location. Once the desired position is reached, the user pushes a button, and a light blinks indicating the instrument has learned the position. There is no need to use a pendant to jog the arm into position, so less time is needed for repositioning and refining.

Velocity 11
For information 408-345-8044
www.velocity11.com

Electronically submit your new product description or product literature information! Go to **www.sciencemag.org/products/newproducts.dtl** for more information.

Newly offered instrumentation, apparatus, and laboratory materials of interest to researchers in all disciplines in academic, industrial, and governmental organizations are featured in this space. Emphasis is given to purpose, chief characteristics, and availabilty of products and materials. Endorsement by *Science* or AAAS of any products or materials mentioned is not implied. Additional information may be obtained from the manufacturer or supplier.

Science Careers
Classified Advertising

For full advertising details, go to **ScienceCareers.org** and click **For Advertisers**, or call one of our representatives.

UNITED STATES & CANADA
E-mail: advertise@sciencecareers.org
Fax: 202-289-6742

Joribah Able
Industry – US & Canada
Phone: 202-326-6572

Alexis Fleming
Northeast Academic
Phone: 202-326-6578

Tina Burks
Southeast Academic
Phone: 202-326-6577

Daryl Anderson
Midwest/Canada Academic
Phone: 202-326-6543

Nicholas Hintibidze
West Academic
Phone: 202-326-6533

EUROPE & INTERNATIONAL
E-mail: ads@science-int.co.uk
Fax: +44 (0) 1223 326532

Tracy Holmes
Associate Director, *Science* Careers
Phone: +44 (0) 1223 326525

Alex Palmer
Phone: +44 (0) 1223 326527

Dan Pennington
Phone: +44 (0) 1223 326517

Susanne Kharraz Tavakol
Phone: +44 (0) 1223 326529

Louise Moore
Phone: +44 (0) 1223 326528

JAPAN
Mashy Yoshikawa
Phone: +81 (0) 3 3235 5961
E-mail: myoshikawa@aaas.org

To subscribe to *Science*:
In US/Canada call 202-326-6417 or 1-800-731-4939.
In the rest of the world call +44 (0) 1223 326515.

Science makes every effort to screen its ads for offensive and/or discriminatory language in accordance with US and non-US law. Since we are an international journal, you may see ads from non-US countries that request applications from specific demographic groups. Since US law does not apply to other countries we try to accommodate recruiting practices of other countries. However, we encourage our readers to alert us to any ads that they feel are discriminatory or offensive.

Science Careers
From the journal *Science* AAAS

POSITIONS OPEN

RUTGERS
THE STATE UNIVERSITY OF NEW JERSEY

BENNETT L. SMITH ENDOWED CHAIR IN BUSINESS AND NATURAL RESOURCES

The Department of Earth and Planetary Sciences and the School of Business are seeking to fill an endowed chair at the level of **FULL PROFESSOR** or above with tenure. The successful candidate should have broad knowledge and experience in Earth sciences related to energy and climate as well as an understanding of relevant economic and business policies. A Ph.D. in Earth sciences and advanced studies in economics and business are required; experience with energy valuation models is desired. We seek to build on existing strengths: (1) the geology of energy, basin analysis, global biogeochemistry, and geophysics; (2) a growing energy institute, with interests in carbon sequestration, biofuels, photovoltaics, and wind energy; and (3) a top-ranked business school. The successful candidate will take the lead in developing research, teaching, and service in energy and the Earth. Expertise in evaluating commercial prospects of energy-oriented technologies is desired. Candidates with exemplary records in academia, government, or business are encouraged to apply.

The salary range is competitive, commensurate with experience and qualifications. Review will begin on June 1, 2009, and will continue until the position is filled. Applicants should submit a letter of interest, curriculum vitae, and the names and contact information for at least three references. All correspondence should be e-mailed to:

Michael Carr, Chair
Search Committee for Bennett L. Smith Chair
School of Arts and Sciences, Rutgers University
77 Hamilton Street, New Brunswick, NJ 08901
Telephone: 732-932-7494
E-mail: carr@rutgers.edu

Affirmative Action/Equal Employment Opportunity.

LABORATORY ASSISTANT, BIOLOGY

Manhattan College is an independent, Catholic coeducational institution in the Lasallian tradition located in the Riverdale section of New York City. We ask our faculty, administration, and staff to be knowledgeable about our mission and to make a positive contribution to that mission.

We seek a Laboratory Assistant to order supplies, keep inventory, store/dispose of materials, and coordinate laboratories for classes, including nonmajor biology laboratories and upper level microbiology and genetics. Will teach introductory laboratory for biology majors as well as laboratories for nonmajors.

Master's of Science degree required. Laboratory experience in making microbial culture media, molar solutions, and buffers recommended. Experience teaching in a laboratory setting a plus. Must work well in a team environment and have ability to work with diverse group of faculty, staff, and students. Occasional evening and weekend work required. Please submit curriculum vitae and two letters of recommendation to:

Human Resources/ Biology Search Committee
MANHATTAN COLLEGE
4513 Manhattan College Parkway
Riverdale, New York 10471
E-mail: humanresources@manhattan.edu

Electronic submission of material is encouraged. Review of applications will begin March 30, 2009.

Women and minorities are encouraged to apply. We are committed to a diverse campus community. An Affirmative Action/Equal Opportunity Employer, Minorities/Females/Persons with Disabilities/Veterans.

Two-year **POSTDOCTORAL ASSOCIATE** position available in our bovine mastitis research group. Qualifications: D.V.M./Ph.D. working in applied immunology with experience in animal models. Submit a resume with names of three references to: **Dr. Ynte Schukken, e-mail: yhs2@cornell.edu.**

Cornell University is an Affirmative Action/Equal Opportunity Employer.

POSITIONS OPEN

TEXAS A&M HEALTH SCIENCE CENTER
COLLEGE OF MEDICINE

POSTDOCTORAL POSITIONS in Cardiovascular Molecular Signaling Networks

Two NIH-funded positions are immediately available to study intracrine mechanisms of renin-angiotensin system actions in cardiac cells and animal models. Recent Ph.D. graduates in the biological sciences, with a background in immunohistochemistry, confocal imaging, intracellular trafficking, culture of neonatal and adult heart cells, RT-polymerase chain reaction, cell transfection, and small animal surgical techniques are encouraged to apply.

Please forward a cover letter, curriculum vitae, and three reference letters to **e-mail: kbaker@medicine.tamhsc.edu** or to: **Kenneth M. Baker, M.D., Division of Molecular Cardiology, Mayborn Chair in Cardiovascular Research, Texas A&M Health Science Center, College of Medicine, 1901 South First Street, Building 205, Temple, Texas 76504.**

FACULTY POSITION in Spinal Cord and Brain Injury Research Indiana University School of Medicine

The Stark Neurosciences Research Institute (SNRI) of the Indiana University School of Medicine is seeking an outstanding investigator for a tenure-track faculty position at the rank of **ASSISTANT** or **ASSOCIATE PROFESSOR** in its Spinal Cord and Brain Injury Research Group (SCBIRG). More senior candidates with outstanding credentials in research and extramural funding may also be considered. Primary faculty appointments will be in the Department of Neurological Surgery and/or the Department of Anatomy and Cell Biology, although other department affiliations are possible. Of particular interest are candidates with one or more of the following areas of expertise in spinal cord injury research: (1) molecular mechanisms underlying axonal guidance, plasticity, and regeneration, (2) cell death mechanisms and neuroprotection, (3) transplantation-mediated recovery of function, and (4) transgenic animal models in spinal cord regeneration.

Qualified applicants should have a Ph.D. and/or M.D. degree, at least several years of postdoctoral experience, and a consistent history of high-quality publications. Candidates will be expected to develop a successful, funded research program and participate in graduate and medical student training. Exceptional resources include generous startup funding, ample laboratory space in a new research building, and access to excellent core facilities including DNA array and mass spectral analyses, viral vector generation, transgenic facilities, multiphoton microscopy, and small animal functional imaging.

Interested individuals should send curriculum vitae, a cover letter stating research interests and accomplishments, a prospectus of future research plans, and names and addresses of three professional references. Please address application materials to SCBI Faculty Search Committee and submit in electronic format to **e-mail: snri@iupui.edu.** Evaluation of applications will begin upon receipt and continue until the position is filled.

Women and minority candidates are especially encouraged to apply. IU is an Equal Employment Opportunity/Affirmative Action Employer, Minorities/Females/Persons with Disabilities.

POSTDOCTORAL POSITION GERMLINE STEM CELLS

Studies include culture, differentiation, and gene activity of male germline stem cells. See *Science* **316:**404, 2007, and *J. Biol. Chem.* **282:**25842, 2007. Send curriculum vitae, names of three references, and a letter describing research experience to: **R. L. Brinster, School of Veterinary Medicine, University of Pennsylvania, e-mail: cpope@vet.upenn.edu.**

NOVARTIS: GLOBAL EXCELLENCE IN VACCINES RESEARCH

Novartis Vaccines and Diagnostics is a division of Novartis focused on the research and development of preventive treatments. Novartis Vaccines is the world's fifth-largest vaccines business and the second-largest manufacturer of influenza vaccines with important meningococcal, pediatric and travel vaccine franchises.

With its scientific expertise and high degree of technological innovation the division is a solid landmark for the international scenario in the fight against infectious diseases.

Our goals are to deliver innovative products performing high quality science. We pioneered the introduction of genomics, bioinformatics and proteomics in our field as essential components of future science and jumped into them collaborating with the best groups in the world. It is our belief that we have the right technologies and skills to play a relevant role in the vaccine field for the years to come.

The Novartis Vaccines Research Center located in Siena (Italy) with its 255 scientists is among the most esteemed vaccines research environments worldwide. It is characterized by the high quality of the science and the multicultural community that populates the center.

Rino Rappuoli, since 2005 elected foreign associate of the National Academy of Sciences, one of the most reputable American scientific institutions, heads the Novartis Vaccines research group. The group includes a research facility in Cambridge (USA). When fully up and running, the Cambridge facility will employ 150 associates and focus on the research of viral diseases such as Respiratory Syncytial Virus, Influenza, Cytomegalovirus, and HIV.

The Siena Research Center is responsible for the creation of most of those vaccines that are currently part of the Novartis pipeline. Some of the most innovative vaccines currently available on the market were conceived and developed in the Siena laboratories: ranging from the new MF59-adjuvanted seasonal and pandemic influenza vaccine to the conjugated vaccine against meningococcal type C.

Novartis is a global leader in developing and providing vaccines to protect against deadly meningococcal disease: in addition to the meningococcal serogroup C conjugate vaccine, Novartis has developed a late-stage investigational vaccine for the four other common meningococcal serogroups, A, C, W-135 and Y.

Furthermore, Novartis Vaccines scientists pioneered an innovative approach called "reverse vaccinology" (a technique that uses information from a microbe's genome to predict which of its proteins might be useful for vaccines) to develop the MenB vaccine, the first potentially broad coverage meningitis B vaccine to reach phase III clinical testing in 2008.

Novartis has also a longstanding commitment to corporate citizenship, with numerous initiatives to improve access to medicines. In 2007, it extended this objective to vaccines, creating the Novartis Vaccines Institute for Global Health (NVGH). This new institute, led by Allan Saul, leverages the research and development expertise and assets that exist within the Novartis Vaccines facilities in Siena, Italy. With NVGH's not-for-profit mission, NVGH will focus on the translational research and development of vaccines for diseases that receive inadequate attention, especially those which are particularly devastating to developing countries.

The first NVGH projects are vaccines for Salmonella and Shigella. In the future, NVGH will work on a range of viral, bacterial and parasitic diseases. NVGH offers its staff the potential to make a significant impact on some of the major global diseases, growing with a rapidly expanding organization and benefiting from the close proximity of the outstanding Novartis Vaccines & Diagnostics center of excellence in Siena.

NOVARTIS
VACCINES

Job Offers

Novartis Vaccines Research Site Head Italy

We are looking for a scientific leader with a track record of innovation, demonstrated scientific vision, and personal leadership. This person will report to the global head of Research, and will head the leading bacterial vaccine research center in the world. The Site Head will oversee a growing center of over 200 researchers involved in all aspects of vaccines research based in Siena Italy. The new Site Head will be a leader in their understanding of bacterial pathogens, and they will be familiar with all of the scientific components that make up a successful vaccine candidate. In addition they will have demonstrated the ability to lead a diverse group of scientists towards a common goal. The ideal candidate will have an extensive history of developing promising scientists into scientific leaders.

The Site Head will be responsible for overseeing the development of the next generation of bacterial vaccines, while providing leadership for a large research facility, and ensuring that Novartis Vaccines increases it scientific leadership in bacterial vaccines.

We expect that the appointee will have a:

- PhD with about 15+ years post doctoral experience in the area of infectious diseases
- Track record of attracting and developing promising new scientists
- Exceptional publication record
- Demonstrated capability to develop new vaccines
- History of strong organizational and operational leadership
- Strong network of global collaborators

Location: Siena. In addition to an attractive salary package, Novartis Vaccines & Diagnostics offers extensive relocation support.

For an application please e-mail to *applications.nvdit@novartis.com*
Quote Job Reference: NVRH001

Novartis Vaccines Academy Director

The Novartis Vaccines Academy, based in Siena Italy, is intended to be the leading center for developing new vaccines researchers, providing educational opportunities for graduate students, post-docs, and continuing education. The Academy Directory will be responsible for:

- Designing and implementing the curriculum of the academy
- Overseeing the development of the students
- Establishing contacts with academia and industry in the course of pursing its mission

The Academy Director will be a leading vaccines scientist with a broad understanding of all the components of vaccine discovery and development. Ideally, a candidate will have a background in academic and laboratory leadership with demonstrated industry interaction would be ideal. A history of developing talented students is a strong plus. Ex-dean or department chairs in appropriate sciences would be strong candidates.

In addition to broad mastery of vaccine science, academic leadership, and mentorship capabilitities we expect that the appointee will have the following:

- An PhD with 10+ years post-doctoral work experience in vaccine science and education
- Excellent analytical and communication skills
- A strong track record in working with and managing external collaborations
- Experience working with national and international health organizations

Location: Siena. In addition to an attractive salary package, Novartis Vaccines & Diagnostics offers extensive relocation support.
For an application please e-mail to *applications.nvdit@novartis.com*
Quote Job Reference: NVAD002

NVGH Exploratory Program Leader

We are looking for a dynamic scientist with potential for a major leadership role within NVGH. This person will report to the CEO, Dr Allan Saul, and will head a team assessing the potential to turn a laboratory concept into a practical vaccine. Three criteria are important:

- The technical feasibility of producing the vaccine
- The likelihood that the vaccine induces a protective immune response
- The likelihood that a successful vaccine would be used to make a significant impact on health

The person will have a sufficiently broad working knowledge of infectious diseases of developing countries in all three areas to enable him/her to direct a team of specialists in generating the detailed experimental and public health information required. In addition to directing the overall exploratory program, the appointee will directly lead a team in the laboratory work required to design a vaccine and to establish initial immune indicators of protection for a vaccine with potential for development within NVGH. Thus this person will need excellent laboratory credentials.

We expect that the appointee will have a:

- PhD with about 10 years post doctoral experience in the area of infectious diseases
- Track record of supervising postgraduate students and post-doctoral positions
- Strong publication record
- Record of successful grant applications
- Network of collaborators in the developed and developing world

Location: Siena. In addition to an attractive salary package, Novartis Vaccines & Diagnostics offers extensive relocation support.
For an application please e-mail to *applications.nvdit@novartis.com*
Quote Job Reference: NVGHEL001

NVGH Public Health Expert

This person will be responsible for evaluating vaccine projects within the Exploratory Program for their potential public health impact and will report to the head of the Business Development and Partnership Section, Mae Shieh. The key issues that will drive such evaluations include:

- Burden, including economic cost, of disease preventable by a vaccine
- Availability of alternative treatments
- Cost of vaccine and vaccine delivery
- Factors driving priorities and decision making in key individuals, national and international health organizations
- Resources available in the constrained healthcare systems of developing countries

The appointee will also play a key role in developing the investment case for vaccines at a more advanced state of development that will guide rational decision making by potential manufacturers, National Departments of Health and International Health Organizations and funding agencies.

The appointee is expected to have a sufficiently broad working knowledge the public health aspects of diseases of developing countries to enable him/her to direct or coordinate a team of specialists in generating the detailed information required and have particular expertise in at least one of the disciplines required. The appointee will directly supervise a small team within NVGH working on one or more aspects to ensure an internal center of expertise. However, most of the information required will come through collaborations with external groups.

In addition to knowledge in epidemiology, disease burden, cost analysis, etc., we expect that the appointee will have:

- An advanced degree with 10 years work experience in public health, particularly in the developing world
- Good analytical and communication skills
- A strong track record in working with and managing external collaborations
- Experience working with national and international health organizations

Location: Siena. In addition to an attractive salary package, Novartis Vaccines & Diagnostics offers extensive relocation support.
For an application please e-mail to *applications.nvdit@novartis.com*
Quote Job Reference: NVGHPE002

UC DAVIS
SCHOOL OF MEDICINE

CHAIR, Department of Biochemistry and Molecular Medicine

The University of California, Davis, School of Medicine seeks an academic leader to chair the Department of Biochemistry and Molecular Medicine. We seek candidates with a Ph.D. and/or M.D. degree and training in biochemistry, molecular-based medical research, or a related field. The successful candidate is expected to have a distinguished record in research, teaching, administration and program development, and excellent interpersonal skills. Additionally, the candidate should have the ability to foster a school-wide and university-wide synergistic research approach in both basic and translational science. The recruitment package will include multiple faculty positions, research space and fiscal resources to support program departmental development.

The Department of Biochemistry and Molecular Medicine has full-time Ph.D. and M.D./Ph.D. faculty in a variety of research areas, including eukaryotic gene expression, signal transduction, cancer biology, membrane biology, neurobiology, muscle physiology, protein structure function relationships, and human genetics.

The School of Medicine and Department have facilities both on the main Davis campus and also in the heart of Sacramento, near the state capital building (ten miles east of Davis). This is in the center of northern California, ideally located between Lake Tahoe and San Francisco and offers urban, college town or other living options. There is a diverse community, with many entertainment, cultural and outdoor activities. Interested candidates should send their curriculum vitae, a statement of interests, and teaching and administrative responsibilities to: **Donald M. Bers, PhD, Chair of the Biochemistry and Molecular Medicine Chair Search Committee, care of Megan Rott**, via e-mail at **megan.rott@ucdmc.ucdavis.edu**, or via regular mail to **Megan Rott, Office of Academic Personnel, UC Davis School of Medicine, PSSB Suite 1100, 4150 V Street, Sacramento, CA 95817**. For full consideration applications must be received by **May 31, 2009**. The position will remain open until filled.

The University of California is an Affirmative Action / Equal Opportunity Employer.

MGH 1811

Faculty Position in Immunology and Pulmonology

Massachusetts General Hospital Harvard Medical School

The Center for Immunology and Inflammatory Diseases and the Pulmonary and Critical Care Unit at the MGH are seeking an outstanding scientist to develop a rigorous independent research program to study mechanisms of immunity as it relates to the lung and pulmonary disease. The Center for Immunology and Inflammatory Diseases is a diverse, interactive group interested in basic mechanisms of immune-mediated diseases. Outstanding applicants whose programs address other areas of basic and translational immunology will also be considered. Applicants may have an MD, PhD or MD/PhD degrees. Academic appointment at the Assistant or Associate Professor level will be in the Department of Medicine at Harvard Medical School.

Applicants should submit a CV, research plan and the names of three references to **Diane Qualters**, **dqualters@partners.org**.

Women and minority applicants are particularly encouraged to apply.

A FACULTY POSITION IN PLANT AND MICROBIAL BIOLOGY

The Institute of Plant and Microbial Biology, Academia Sinica, Taipei is inviting applications for a research-focused faculty position in plant-microbe interactions, plant-related microbiology, secondary metabolites or microbial biotechnology. This position can be at the level of Assistant, Associate, or Full Research Fellow (equivalent to Assistant, Associate, or Full Professor in a university) depending on the applicant's experience. Excellent facilities and starter grants will be provided for the position.

For details of the Institute and Academia Sinica, please visit the website at **http://ipmb.sinica.edu.tw/** Applicants are expected to have a Ph.D. degree plus postdoctoral training. Chinese language skills are NOT required and international scientists are encouraged to apply. The application folder should include curriculum vitae, a statement of research accomplishments, and future research plans. The application folder and at least three letters of recommendation should be sent to Dr. Teng-Yung Feng, Chair of Search Committee, Institute of Plant and Microbial Biology, Academia Sinica, 128, Sec. 2, Academia Rd., Nankang, Taipei, Taiwan 11529 E-MAIL: **nslin2@gate.sinica.edu.tw**. FAX: (+886)2-2782-1605. The review of applications will start on May 20, 2009 and continue until the position is filled.

University at Buffalo
The State University of New York

Neurodevelopmental or Neurodegenerative Disorders

Professor and Director of Basic Sciences

Hunter J. Kelly Research Institute

The Hunter James Kelly Research Institute (**http://www.huntershope.org/research/default.asp**) and the School of Medicine and Biomedical Sciences, University at Buffalo, The State University of New York, seek an established senior investigator in the area of Neurodegenerative Disease and/or Neurodevelopmental Disorders to serve as its founding Director of Basic Sciences. The successful applicant will have a productive and well-funded program of basic research in one of these areas, particularly as related to demyelinating diseases, and will qualify for appointment as Professor in the most appropriate basic science or clinical department in the School. In addition to maintaining and expanding this research program, we seek an individual with the vision and leadership skills to effectively recruit additional faculty to the Institute, as well as playing a key role in our broader neuroscience program (**http://www.smbs.buffalo.edu/neuroscience**). Funds are available to support generous startup packages for the Director as well as future recruits, and additional funds will be available to support ongoing Institute functions in the future. State of the art laboratory space will be provided in the New York State Center of Excellence in Bioinformatics and Life Sciences, located on our downtown campus adjacent to the Roswell Park Cancer Institute. In conjunction with the Center, the School of Medicine and Biomedical Sciences supports core facilities in genomics, proteomics, microscopy and imaging, and genetically modified organisms. Expansion of the University's downtown campus to include a multi-story Clinical and Translational Research Center is underway, and will bring new clinical and basic science programs together in an exciting new interdisciplinary environment.

Applications, including CV, brief description of research orientation, accomplishments and plans, and names of at least three references, should be addressed to: Dr. Kenneth Blumenthal, Chair, Department of Biochemistry and Chair HJKRI Search Committee, School of Medicine and Biomedical Sciences, University at Buffalo, and submitted confidentially to **www.ubjobs.buffalo.edu** for posting number **0900075**. Nominations and/or inquiries should be addressed to **Dr. Blumenthal** by telephone or email at **kblumen@buffalo.edu**.

The University at Buffalo is an Affirmative Action/Equal Opportunity Employer.

DIRECTOR *KwaZulu-Natal Research Institute for TB and HIV*

The Howard Hughes Medical Institute (HHMI) and the University of KwaZulu-Natal (UKZN) have jointly established the KwaZulu-Natal Research Institute for Tuberculosis and HIV (K-RITH). Envisioned as an international center of excellence for research and training, K-RITH will be housed in a state-of-the-art BSL-3 laboratory facility on the campus of the Nelson Mandela School of Medicine in Durban, South Africa.

K-RITH scientists will be uniquely positioned to use the tools of basic science to alleviate the deadly impact of TB and HIV in the epicenter of a dual epidemic of these diseases. The Institute is also expected to play an important role in the training of future research leaders in Africa.

The Director of K-RITH will be charged with developing and leading a research program focused on the diagnosis, pathogenesis, treatment, and prevention of HIV and TB and, specifically, the interactions of these pathogens. Research collaborators will include Howard Hughes Medical Institute Investigators at Harvard Medical School and the Albert Einstein College of Medicine. The ideal candidate will be a highly accomplished scientist, as well as a recognized leader in TB or HIV research. The individual will also combine demonstrated leadership and management skills with a broad vision for developing a collaborative research environment and the capacity to realize the long-term potential for this vital enterprise.

HHMI has committed to funding core research operations at K-RITH for 10 years. The appointment of the Director will be made jointly by HHMI and UZKN. HHMI will provide generous research support to the Director.

Additional information about academic qualifications and other position requirements may be found at www.hhmi.org/k-rith. Applicants are asked to submit a three to five page vision statement for K-RITH, a two-page summary of current and future research interests, a curriculum vitae, and the names of three individuals who will act as references. Review of applications will begin after May 14, 2009. Preliminary interviews will be conducted in Durban in July 2009; final interviews will be in held Chevy Chase in September 2009.

Application materials may be sent to:

Jill Conley
Director, International Programs
Howard Hughes Medical Institute
4000 Jones Bridge Road
Chevy Chase, MD 20815 USA
Email: k-rith@hhmi.org

HHMI
HOWARD HUGHES MEDICAL INSTITUTE

UNIVERSITY OF
KWAZULU-NATAL

The Faculty of Natural Sciences offers at the **Institute for Theoretical Physics** in the Department of Physics a

W2-Professorship in Theoretical Physics

limited on five years

The Elite Network of Bavaria has established a physics degree course for top performing students with integrated doctoral college. The position offered involves teaching in this program. The applicant is expected to represent the field both in teaching and research. We are seeking a highly qualified scientist with an outstanding track record in statistical or soft condensed matter physics. The successful applicant is expected to interact with experimental and theoretical groups in the Department.

Qualifications include university undergraduate and doctoral degrees, good teaching skills, and a habilitation or equivalent other qualification, which may have been gained outside the University or within a "Juniorprofessur".

At the time of appointment the candidate must not be older than 52 years of age. The Ministry for Science, Research and Art may allow an exception in special cases, which has to be approved by the Ministry of Finance.

The University of Erlangen-Nürnberg is an equal opportunity employer. We strongly encourage women to apply in an effort to increase a female representation in research and teaching.

Applications from the severely disabled having the same suitability for appointment as other candidates will be given priority.

The position is to be filled by October 1st, 2009.

Application documents (curriculum vitae, photograph, list of publications and teaching activities, certified copies of degree certificates but no publications) and a brief statement of research interests must be sent not later than **April 30th, 2009** to: Dekan der **Naturwissenschaftlichen Fakultät** der Universität Erlangen-Nürnberg, Universitätsstr. 40, 91054 Erlangen, Germany.

Friedrich-Alexander-Universität Erlangen-Nürnberg

Grundzertifikat audit familiengerechte hochschule

www.uni-erlangen.de

复旦大学脑科学研究院

The Institute of Brain Science, Fudan University

Principal Investigator Positions

The Institute of Brain Science, Fudan University, Shanghai, China, a newly established research institution supported by the National "985" Program of the Ministry of Education, is currently recruiting principal investigators (PIs) in the field of neuroscience.

I. Senior PI

Candidates should have a Ph.D. and/or M.D. degree and possess a long-standing research experience in brain science. Independent research capacity is absolutely needed. Those who have the experience of leading a laboratory will be given a favorable consideration.

Candidates should have a systematic and impressive research record, with important papers published in peer-reviewed international journals of high reputation as a corresponding author.

Candidates must work in the Institute for more than 9 months per year, when appointed.

II. Junior PI

Candidates should have a Ph.D. and/or M.D. degree and possess at least 2-year postdoctoral experience.

Candidates should have a good research record in brain science, with substantial papers published in peer-reviewed international journals as a corresponding author or the first author.

Candidates must work in the Institute for more than 9 months per year, when appointed.

Interested individuals please contact the Institute of Brain Science (E-mail: ibs@fudan.edu.cn, Tel：+86-21-54237641) for the application form, or send a package including CV, a list of publications, reprints of 3-5 representative papers, a one page summary of the research accomplishments, and a 1-2 page research proposal, and arrange to have 3 letters of reference sent to: Ms. Rong Chen, Institute of Brain Science, Mail Box 295, Fudan University, 138 Yixueyuan Road, Shanghai 200032, China. The closing date for applications is May 15, 2009.

For more information, please visit our website: www.fudan-iobs.com

---

University of Massachusetts **UMASS** Lowell

Careers with **Mass Appeal**

Assistant/Associate Professor (Tenure-Track)

Clinical Laboratory and Nutritional Science
School of Health and Environment

Clinical Laboratory and Nutritional Sciences, a department within UMass Lowell's School of Health and Environment, invites applications for a permanent, academic year, tenure-track appointment.

This faculty member will teach Clinical Laboratory Instrumentation, Physiological Chemistry, and Organic Reactions and Structure and coordinate their laboratories; supervise on campus student research and advise students; and develop industry relations for Clinical Sciences students and for senior research projects/internships. Interdisciplinary research in biomedical device development and/or nanomedicine desirable.

Candidates must hold an earned Doctorate in Biomedical or Clinical Chemistry or similar discipline; ASCP or NCA certification recommended. Applicants should be recognized for teaching excellence; demonstrated record of scholarly research, secured grants and publications; and capacity to work with diverse populations.

Academic Year: Fall 2009.

Application review will begin immediately and continue until position is filled.

Salary and rank are commensurate with qualifications and experience. Applicants should send a cover letter, statement of teaching and research interests, your curriculum vitae, and the names of three references to: Dr. Alease Bruce, Chairperson, Personnel Committee, School of Health and Environment, University of Massachusetts Lowell, 3 Solomont Way, Suite 4, Lowell, MA 01854 USA OR **email cover letter, statement of your teaching and research interests, your curriculum vitae, and the names of three references to search _clns09@uml.edu. Please include reference number FC02030901 in subject line of email.**

For complete job description, please visit www.uml.edu/hr/jobpostings.

The University of Massachusetts is an Equal Opportunity/Affirmative Action Title IX, H/V, ADA 1990 Employer, and Executive Order 11246, 41 CFR60-741 4, 41 CRF60-250 4, 41CRF60-1 40 and 41 CFR60-1,4 are hereby incorporated.

Associate Director
The Center for Photonics in Biology and Medicine

NORTHWESTERN UNIVERSITY

Northwestern University invites exceptional candidates to apply for the position of the Associate Director of The Center for Photonics in Biology and Medicine, which is being formed by the University.

The mission of the Center is to develop novel optics technologies for the characterization and imaging of biological tissue. The focus is on the nanoscale, microscale and the molecular levels. The Center also utilizes biophotonics to gain new insights into biological systems and their response to disease. Furthermore, the Center aims to translate these technological and biological innovations into clinical practice. The Center will be supported in part by a recently awarded $7.5M grant from the NIH.

The Associate Director will work in close collaboration with the **Center Director, Professor Vadim Backman**. S/he will play a leadership role in the Center overseeing administration and ongoing research activities. In particular, the candidate will be responsible for identifying new research targets and help define the Center strategic development. The candidate is expected to help secure new research funding for the Center. The candidate will manage scientists involved in the Center projects, provide creative scientific input and coordinate the overall execution of the projects. The candidate will build relationships and coordinate external collaborations with academia and industry.

The successful candidate will have a Ph.D. and 4+ years of experience in biophotonics or a related field. The candidate will have demonstrated an outstanding record of research accomplishment and leadership documented by peer-reviewed publications and external reputation. The candidate is expected to have excellent interpersonal and writing skills.

Candidates should submit their Curriculum Vitae and the names of four referees by e-mail to the following address: **m-proenca@northwestern.edu**. Questions of scientific nature should be addressed to **Professor Vadim Backman** at **v-backman@northwestern.edu**. Applications will be accepted until the position is filled.

University of
Colorado Denver

School of Medicine

The University of Colorado Denver School of Medicine seeks applicants for the position of Chair of the Department of Pharmacology. The Department consists of 24 faculty members whose interests span neurosciences, cell biology, drugs of abuse, genomics and bioinformatics, signal transduction, lipid mediators, and structural biology. The Department occupies dramatic new laboratories and offices in twin towers of the Research Complex at the new University of Colorado Denver Anschutz Medical Campus.

The Department of Pharmacology has a large basic science research program with more than $19 million in annual research funding. The Department has won numerous awards for the teaching of medical students. Details are available at the departmental web site: **http://pharmacology.ucdenver.edu/index.shtm**.

The Chair of the Department of Pharmacology reports to the Vice-Chancellor for Health Affairs/Dean of the School of Medicine and participates with other department chairs and faculty to develop School and Department programs, curriculum, administration, and budgetary planning and implementation. The position requires excellence in teaching, demonstrated administrative ability/leadership and leadership in research and scholarly activity.

Review of applications will continue until the position is filled. Applicants should apply online at the **https://www.jobsatcu.com** website using posting number **806418**. Questions about the application process may be directed to **Jan.Bodin@ucdenver.edu**.

The University of Colorado Denver is committed to the recruitment and employment of a diverse faculty. We encourage applications from women and minorities.

NUS
National University
of Singapore

Research Centre of Excellence in Mechanobiology

50 Postdoctoral Positions

This newly established Centre at the National University of Singapore (NUS) aims to complete an integrated nanometer to tissue description of the mechanically dependent functions in cells and tissues. Through quantitative biophysical approaches, we will address major problems in biomedical sciences including pathogenesis (from bacterial to cancer), tissue regeneration and function. We are seeking outstanding candidates with strong background in molecular and cell biology, biophysics, biology-related engineering or computer sciences, and a commitment for collaborative interdisciplinary research to join research in molecular, cellular and tissue mechanics.

Faculty in the Centre are coming from many major international research universities with diverse research backgrounds. They have a common goal of training a new generation of researchers to solve important biological problems by combining the approaches of nanotechnology, bioinformatics, molecular biology, modeling and biophysics. The Centre is directed by Mike Sheetz and Paul Matsudaira. For further information on the research profiles of the team members, see website www.dbs.nus.edu.sg/mechano/index.html

Singapore is a vibrant garden city with year round tropical climate and rich multicultural heritage. Established in 1905, NUS has evolved into a top teaching and research-intensive institution, acknowledged as one of the finest universities in the Asia-Pacific. The Centre offers competitive salary package, and housing allowance.

Please submit your application (form downloadable from www.dbs.nus.edu.sg/mechano/index.html), along with curriculum vitae, research interest and names of three external referees to:

Choy L Hew, Deputy Director
RCE in Mechanobiology
National University of Singapore
14 Science Drive 4
Singapore 117543
Fax: (65) 67795671
Email: mechbio@nus.edu.sg

Founded in 1911, The University of Hong Kong is committed to the highest international standards of excellence in teaching and research, and has been at the international forefront of academic scholarship for many years. Of a number of recent indicators of the University's performance, one is its ranking at 26 among the top 200 universities in the world by the UK's Times Higher Education Supplement. The University has a comprehensive range of study programmes and research disciplines, with 20,000 undergraduate and postgraduate students from 50 countries, and a complement of 1,200 academic members of staff, many of whom are internationally renowned.

Research Assistant Professorships and Post-doctoral Fellowships

Applications are invited for a number of positions as Research Assistant Professor (RAP) (Ref.: RF-2008/2009-584) and Post-doctoral Fellow (PDF) (Ref.: RF-2008/2009-585), at the University of Hong Kong, on or before February 28, 2010. Appointments will be made for a period of 2 to 3 years.

RAP and PDF posts are created specifically to bring new impetus and vigour to the University's research enterprise. Positions are available from time to time to meet the strategic research needs identified by the University. Positions are available in the following Departments/Area of Excellence:

- Architecture
- Faculty of Dentistry
- Faculty of Education
- Civil Engineering
- Electrical and Electronic Engineering
- Mechanical Engineering
- Law
- Biochemistry
- Centre for Cancer Research
- School of Chinese Medicine
- Research Centre of Heart, Brain, Hormone and Healthy Aging
- Research Centre of Infection and Immunology
- Medicine
- Microbiology
- Orthopaedics and Traumatology
- Paediatrics and Adolescent Medicine
- Pathology
- Psychiatry
- Public Health Research Centre
- Centre for Reproduction, Development and Growth
- Area of Excellence (AoE) on Developmental Genomics and Skeletal Research
- School of Biological Sciences
- Chemistry
- Earth Sciences
- Geography
- Psychology

Research Assistant Professors

The main focus of an RAP's duty is research. RAPs can however be assigned some teaching duties, up to 50% of the normal teaching load. Applicants should be research active and have a proven publication record. A highly competitive salary commensurate with qualifications and experience will be offered, with a contract-end gratuity and University contribution to a retirement benefits scheme (totalling up to 15% of basic salary). Annual leave, and medical/dental benefits will also be offered.

Post-doctoral Fellows

PDFs are expected to devote full-time to research. Applicants should be doctoral degree holders having undertaken original research that has contributed to the body of knowledge. A highly competitive salary commensurate with qualifications and experience will be offered. Annual leave and medical benefits will also be available.

Procedures

Prospective applicants are invited to visit the following webpage <http://www.hku.hk/apptunit/> to view the full list of the research areas and their home Faculties/Departments/Schools/Centres for which RAP/PDF positions are currently available. Before preparing an application they should contact the Head of the appropriate academic unit to ascertain that their research expertise matches the research area for which a vacant RAP/PDF post is available.

Applicants must submit a completed University application form, which should clearly state **which position** they are applying for; and in which **academic discipline**. They should also provide further information such as details of their research experience, publications, research proposals, etc.

Further particulars and application forms (152/708) can be obtained at http://www.hku.hk/apptunit/; or from the Appointments Unit (Senior), Human Resource Section, Registry, The University of Hong Kong, Hong Kong (**fax**: (852) 2540 6735 or 2559 2058; **e-mail**: senrappt@hku.hk). **Closes April 17, 2009**. Candidates who are not contacted within 3 months of the closing date may consider their applications unsuccessful

The University is an equal opportunity employer and is committed to a No-Smoking Policy

POSITIONS OPEN

POSTDOCTORAL POSITIONS IN MOLECULAR AND CELLULAR BIOLOGY
The Wine Research Centre,
University of British Columbia,
Vancouver, B.C., Canada

Two Postdoctoral positions are available immediately in the Wine Research Centre **(website: http://www.landfood.ubc.ca/wine/index.html)** for a 24-month appointment with potential for extending employment. These positions are funded by large-scale Genome British Columbia wine genomics grants to characterize fermentation stress response genes in *S. cerevisiae*. Successful candidates will be responsible for establishing function of each of these 62 genes induced during wine fermentation using a systems biology approach. Outstanding research facilities are available. Salary approximately $50,000 annually, including benefits.

A Ph.D. in molecular and cellular biology is required. Experience in transcriptomics/proteomics/metabolomics will be an asset. Interested candidates should apply with curriculum vitae and names of three references to: **Dr. Hennie J. J. van Vuuren, Director, e-mail: hjjvv@interchange.ubc.ca.**

ASSISTANT/ASSOCIATE PROFESSOR
Department of Pharmaceutical Sciences
The Feik School of Pharmacy
University of The Incarnate Word
San Antonio, Texas

A 12-month, tenure-track medicinal chemistry faculty position in the Department of Pharmaceutical Sciences. Preferred start date is June 2009. Candidate for this position should have a Ph.D. in medicinal chemistry; teaching and/or postdoctoral experience is preferred. The candidate will be expected to develop and teach the medicinal chemistry section in the integrated pharmacotherapy courses in the Pharm.D. program. See our **website: http://jobs.uiw.edu** for further information.

MARKETPLACE